For Reference

NOT TO BE TAKEN FROM THIS ROOM

Ex libris
universitatis
albertaensis

QUAECUMQUE VERA

THE UNIVERSITY OF ALBERTA

RELEASE FORM

NAME OF AUTHOR Robert Hugh Hall

TITLE OF THESIS Quantitative Aspects of Atomic Emission Spectroscopy using a Fourier Transform Spectrometer.

DEGREE FOR WHICH THESIS WAS PRESENTED Ph.D.

YEAR THIS DEGREE GRANTED 1979

Permission is hereby granted to THE UNIVERSITY OF ALBERTA LIBRARY to produce single copies of this thesis and to lend or sell such copies for private, scholarly or scientific research purposes only.

The author reserves other publication rights, and neither the thesis nor extensive extracts from it may be printed or otherwise reproduced without the author's written permission.

THE UNIVERSITY OF ALBERTA

QUANTITATIVE ASPECTS OF ATOMIC EMISSION SPECTROSCOPY USING A FOURIER TRANSFORM SPECTROMETER

by

© ROBERT HUGH HALL

A THESIS

SUBMITTED TO THE FACULTY OF GRADUATE STUDIES AND RESEARCH
IN PARTIAL FULFILMENT OF THE REQUIREMENTS FOR THE DEGREE
OF DOCTOR OF PHILOSOPHY.

DEPARTMENT OF CHEMISTRY

EDMONTON, ALBERTA

FALL, 1979

THE UNIVERSITY OF ALBERTA

FACULTY OF GRADUATE STUDIES AND RESEARCH

The undersigned certify that they have read, and recommend to the Faculty of Graduate Studies and Research, for acceptance, a thesis entitled QUANTITATIVE ASPECTS OF ATOMIC EMISSION SPECTROSCOPY USING A FOURIER TRANSFORM SPECTROMETER submitted by ROBERT HUGH HALL in partial fulfilment of the requirements for the degree of Doctor of Philosophy.

ABSTRACT

The attainment of sensitive, accurate, precise, simultaneous, multielement analysis over a wide dynamic range and for a wide variety of elements, has been the goal of much research in analytical chemistry. The combination of an atomic emission source with a multiplex Michelson interferometer based detection system to achieve this goal, has been under investigation in our laboratory. In this work, the quantitative aspects of the interferometer based system in combination with three atomic emission sources, an air-acetylene flame, a nitrous oxide-acetylene flame and a radio-frequency inductively coupled argon plasma, have been studied. The interferometer's inherent dynamic range limitations and spectral noise distribution properties were of special interest, in that these aspects may determine the feasibility of the system in practical simultaneous, multielement analysis.

Preliminary investigations using the flame emission sources indicate the presence of a dynamic range limitation due to the sample matrix and/or background spectral emission. In some situations optical filtering can eliminate the problem. Similar dynamic range problems were also encountered using the plasma emission source, most notably due to the emission of hydrogen, argon and hydroxyl radical. The use of a solar blind photomultiplier tube to isolate the ultraviolet region from 240 nm to 300 nm provided a spectrally clean background emission region and shows the most promise for

elemental analysis. If not under dynamic range limitations, linear analytical curves were obtained for lithium, sodium, calcium in the air-acetylene flame and manganese and magnesium in the argon plasma. A linear dynamic range covering three orders of magnitude was obtainable in most cases.

The spectral noise distribution property of the interferometer based system was found to be similar to that of a scanning monochromator based system; that is, the peak localization of noise was found to be present. This is in direct opposition to the uniform spectral frequency distribution of noise predicted by multiplex theory.

A portion of the study was also devoted to the correlation processing of interferogram domain spectral information. Correlation processing was found to produce statistically equivalent analytical results, when compared with the FFT technique, dependent upon the proper selection of the mask interferogram. Significant advantages in spectral selectivity of the information processed, and in the case of software implementation for long interferograms, were noted over the FFT technique.

In spite of the inherent limitations of the interferometer based system, advantages in the areas of resolution potential, wavelength accuracy and precision in the spectral domain, and its simultaneous multielement detection capability over a wide spectral range, make the multiplex interferometer based atomic emission system a technique with great potential.

ACKNOWLEDGEMENT

I would like to acknowledge the guidance and assistance given by Dr. Gary Horlick.

Table of Contents

Chapter Page

I Information Decoding in Atomic Emission Spectroscopy 1

A. Currently Available Techniques in Optical Spectroscopy 2

B. Decoding Systems for Atomic Emission Spectroscopy 6

1. Dispersion Based Measurement Systems 6

2. Multiplex Based Measurement Systems 11

C. Spectral Information Decoding: Multiplex vs. Dispersive 15

1. Frequency Information Decoding 15

2. Intensity Information Decoding 25

3. Spatial Information Decoding 34

4. Temporal Information Decoding 37

D. Conclusions 39

II Instrumentation: Description and Modifications 41

A. The Interferometer System 41

B. Modifications 41

1. Changes in the Electronic Control Circuitry 41

2. Changes in the Detector Circuitry 47

C. The Minicomputer Data Acquisition System 52

Chapter		Page
III	Interferometer Response to Hollow Cathode Lamp Atomic Emission Sources	54
	A. Introduction	54
	B. Instrumentation	54
	C. Results and Discussion	56
	D. Conclusions	70
IV	The Application of Fourier Transform Spectroscopy to Flame Atomic Emission Spectroscopy	71
	A. Introduction	71
	B. The Experimental System	72
	C. The Air Acetylene Flame Emission Source	75
	1. The Silicon Photodiode as a Detector	76
	2. Multiple Element Detection Capabilities	86
	3. The Photomultiplier Tube as a Detector	90
	D. The Nitrous Oxide-Acetylene Flame Emission Source	104
	1. Introduction	104
	2. Applications with the F.T.S. System	105
	E. Conclusions	113
V	The Radio Frequency-Inductively Coupled Plasma as an Atomic Emission Source for the Interferometer	116
	A. Introduction	116
	B. Instrumentation	117

Chapter | Page

C. Results and Discussion 120
1. The 1P28 Photomultiplier Tube as a Detector 120
2. The Solar Blind P.M.T. as a Detector 141
3. The Silicon Photodiode as a Detector 164
D. Conclusions 167

VI Correlation: A Parallel Method to the Fourier Transform Processing of Interferograms 168
A. Introduction 168
B. The Fourier Transform Process 169
1. Mathematical Definition 169
2. Historical Aspects of Interferogram Processing 171
3. Implementation of the FFT 175
C. The Correlation Operation 177
1. Correlation and the Fourier Transformation 177
2. Applications of Correlation to Interferometry 181
3. Experimental Results and Discussion 186
D. Future Correlation Applications 203
E. Conclusions 206

VII Summary 207

Page

Bibliography	210
Appendix A	217
Appendix B	220
Appendix C	222
Appendix D	225

List of Tables

Table	Description	Page
I	Aliasing regions present in the U.V.-VIS. spectral region.	22
II	Major Emission lines of the Mg and Si hollow cathode lamp sources.	59
III	Major emission lines of the Cu, Pb, Zn, Sn, hollow cathode lamp source.	62
IV	Major emission lines of the Ca, Al, Mg hollow cathode lamp source.	66
V	Major emission lines of the Fe, Ni, Cu, Co, Cr, Mn hollow cathode lamp emission source.	69
VI	Normal Flame Operating Conditions	78
VII	Major emission lines of Fe, Ni, Cu, Cr, Mn emission in the nitrous oxide acetylene flame.	112
VIII	Normal Plasma operating conditions.	118
IX	Emission lines of H, Ar and OH in the argon plasma background.	123
X	Multielement sample emission lines in the plasma source.	133
XI	Variance study with Ca and Mg.	140
XII	Multielement sample emission lines with a solar blind detector and the plasma source.	146
XIII	Major ultraviolet emission lines of Mn, Mg and C.	151
XIV	Variance Study with Mn(290.0 nm) and Mg (280.0 nm) and 304.4 nm baseline point.	163
XV	Plasma background emission viewed with a silicon photodiode detector.	166
XVI	Regression data for Li, Ca and Na for both FFT and correlation.	192
XVII	Mn and Mg Regression analysis data.	197
XVIII	Precision study with Mn and Mg.	204

List of Figures

Figure	Description	Page
1.	The optical spectroscopic experiment in block diagram form.	3
2.	Dispersive based spectral information decoding systems.	9
3.	A multiplex based spectral decoding system.	14
4.	Typical interferometer resolutions at various wavelengths in the spectral domain.	24
5.	Schematic of the current Michelson Interferometer.	42
6.	The current interferometer system in block diagram form.	43
7.	Electronic control circuit diagram.	44
8.	A spectrum showing the presence of satellite peaks.	48
9.	The same spectrum without satellite peaks present.	49
10.	Schematic of the modified 1P28 dynode chain.	51
11.	Silicon hollow cathode lamp emission spectrum.	57
12.	Magnesium hollow cathode lamp emission spectrum.	58
13.	Cu, Pb, Zn, Sn hollow cathode lamp emission spectrum.	61
14.	Ca, Al, Mg hollow cathode lamp emission spectrum	64
15.	Ca, Al, Mg hollow cathode lamp emission spectrum with a Corning 7-51 optical filter employed.	65
16.	Expansion of the Ca, Al, Mg spectrum of Figure 15.	67

Figure	Description	Page
17.	Fe, Ni, Cr, Co, Cu hollow cathode lamp emission spectrum.	68
18.	Spectrum of the air-acetylene flame background emission using a silicon photodiode detector.	77
19.	The emission spectrum of a 30.0 ppm aqueous LiCl solution.	79
20.	Air acetylene flame emission spectra of (A) 30.0 ppm LiCl (b) 1.0 ppm LiCl (C) 0.03 ppm LiCl.	81
21.	The analytical curve obtained for Li flame emission.	82
22.	Standard deviation studies of Li flame emission.	83
23.	Baseline amplitude study of Li flame emission.	85
24.	Multielement flame emission of Li, Na, K in the air-acetylene flame.	88
25.	Analytical curves for the simultaneous determination of Na and K.	89
26.	Air-acetylene flame background emission with a 1P28 P.M.T. detector.	92
27.	Emission spectrum of a 1000 ppm Ca aqueous solution.	93
28.	Ca(OH) at 555.0 nm analytical curve.	95
29.	CaI at 422.6 nm analytical curve.	96
30.	Standard deviation study with Ca flame emission.	97
31.	Air acetylene flame emission spectrum of a 1.0 ppm aqueous NaCl solution.	99
32.	Air acetylene flame emission spectra of (A) 30.0 ppm Na (B) 1.0 ppm Na (C) 0.01 ppm Na.	100

Figure	Description	Page
33.	Analytical curve for Na 30.0 ppm to 0.01 ppm.	101
34.	A plot of standard deviation vs. Na peak amplitude (A) Na peak standard deviation (B) Baseline standard deviation	102
35.	A plot of mean baseline amplitude vs. Na peak amplitude.	103
36.	Nitrous oxide acetylene flame emission background.	107
37.	Cu, Mn, Cr nitrous oxide acetylene flame emission spectrum.	110
38.	Multielement emission spectrum in a nitrous oxide acetylene flame.	111
39.	Emission spectrum of a 1.0 ppm Ca solution in a nitrous oxide acetylene flame.	114
40.	Argon plasma background emission spectrum, water aspirating.	122
41.	Argon plasma background emission spectrum, no water aspirating.	124
42.	Expansion of the plasma emission near 400 nm.	125
43.	Plasma emission spectrum of 1.0 ppm $Ca(NO_3)_2$.	127
44.	Plasma emission spectrum of 0.3 ppm $Ca(NO_3)_2$.	128
45.	Ca emission (A) air-acetylene flame (B) nitrous oxide acetylene flame (C) argon I.C.P.	130
46.	Multielement argon plasma emission spectrum.	132
47.	Emission spectrum of Ca and Al.	135
48.	Ca (0.1 ppm) ion emission lines in the presence of 100.0 ppm Mg, unfiltered.	138
49.	Ca (0.1 ppm) ion emission lines in the presence of 100.0 ppm Mg, filtered.	139
50.	Argon plasma background emission as seen by the solar blind P.M.T.	143

Figure	Description	Page
51.	Multielement plasma emission spectrum solar blind PMT detector.	144
52.	Expansion of spectrum in Figure 51.	148
53.	Plasma emission spectrum of Mn and Mg (C impurity present).	150
54.	Plasma emission spectrum of a 4.4 ppm aqueous $MnCl_2$ solution.	152
55.	Analytical curve for Mg plasma emission.	154
56.	Analytical curve for Mn plasma emission.	155
57.	Standard deviation study on Mg emission data.	156
58.	Baseline amplitude study on Mg emission data.	158
59.	Plasma emission spectrum of 100.0 ppm Mg and 4.4 ppm Mn aqueous solution.	160
60.	Noise distribution study using Mn 290.0 nm emission triplet and Mg.	161
61.	Plasma background emission spectrum as seen by a silicon photodiode detector.	165
62.	The FT illustrated graphically.	174
63.	Correlation illustrated graphically.	182
64.	Comparison of Li analytical curves, correlation vs. FFT.	187
65.	Comparison of Na analytical curves, correlation vs. FFT.	189
66.	Comparison of Ca analytical curves, correlation vs. FFT.	191
67.	Comparison of Mg analytical curves, correlation vs. FFT.	194
68.	Comparison of Mn analytical curves, correlation vs. FFT.	195
69.	Analytical curve for Mn and Mg simultaneously detected and decoded.	202

CHAPTER I

INFORMATION DECODING IN ATOMIC EMISSION SPECTROSCOPY

The development of highly sensitive techniques to accurately, precisely and rapidly determine the elemental composition of a sample has been the object of much research in analytical chemistry. Various analytical techniques including electrochemistry, chromatography, chemical complexation, x-ray fluorescence, activation analysis, mass spectroscopy and optical spectroscopy are currently used for elemental analysis in a wide range of laboratories. Each technique offers specific advantages whether they lie in the areas of sample preparation, sensitivity, multielement capability, selectivity or economy. The recent trend in all methods has been for the development of a highly sensitive, simultaneous multielement analysis. Due to the already high popularity of optical spectroscopic techniques, a great deal of research has been involved in the extension of optical methods in the above areas. One such extension currently under investigation in our laboratory, involves the combination of atomic emission spectroscopy and a multiplex interferometer based detection system. The experiments carried out for this thesis attempt to gain further insight into the quantitative aspects of such a system. Before entering into a detailed discussion of the experimental results, let us delve into a general discussion of the optical spectroscopic technique.

A. Currently Available Techniques in Optical Spectroscopy

A block diagram of the optical spectroscopic experiment is presented in Figure 1. In order to obtain analytical information about the sample through optical techniques, the information must first be encoded in some form of electromagnetic radiation. The encoding step may take the form of emission, absorption, fluorescence, scattering or reflection of electromagnetic radiation. In order to place the analytical information in an interpretable form, a decoding step involving the four information domains, frequency, intensity, spatial and temporal, must be employed. The combination of a highly efficient encoding and decoding stage provides the analyst with the maximum amount of information about the sample.

Let us consider the three most commonly used atomic spectroscopic techniques for elemental analysis, emission, absorption and fluorescence. The emission technique encodes information in the radiation emitted as an atomic species falls from an excited state to a ground state. Atomic absorption involves the absorption of light as an atomic species changes from a ground state to an excited state. Atomic fluorescence is more complex in that it involves both the absorption of light to reach an excited state and the reemission of light at the same frequency as it returns to the ground state. This is termed resonance line atomic fluorescence. In all three techniques the concentration of the atomic species present

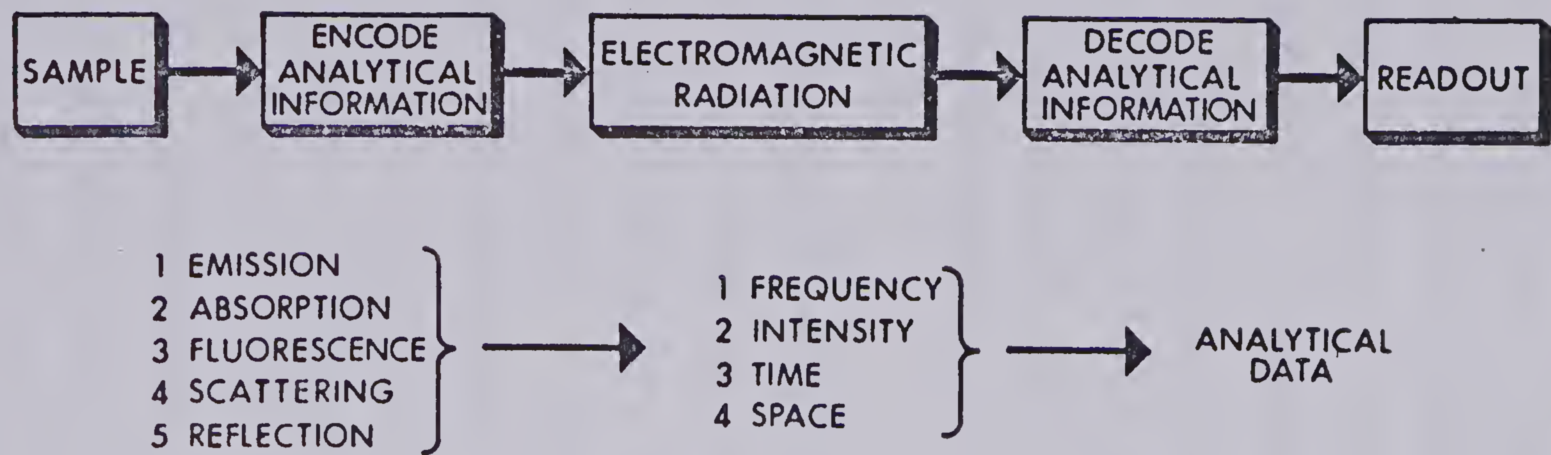

FIGURE 1. The spectroscopic experiment in block diagram form.

is related directly to the intensity of the light absorbed, in atomic absorbance, or emitted, in atomic emission and fluorescence. The need for simultaneous multiple element analysis has severely limited the use of atomic fluorescence and atomic absorbance techniques in samples where a large number of elements are to be determined. Both techniques require high intensity sources and in the latter case spectrally narrow and element specific. This poses a serious problem for multiple element atomic absorbance experiments. Atomic fluorescence is limited by the source intensity and the low emission levels that must be detected. Thus atomic emission appears to be the technique of choice for simultaneous multiple element analysis.

In considering the atomic emission experiment in more detail, let us first look at the excitation sources used. The vast majority of atomic emission analyses performed every year are carried out with a D.C. arc or A.C. spark excitation source. The D.C. arc provides thermal excitation of atomic species to an excited state through the formation of a high temperature, high current arc containing the sample. The A.C. spark excitation source provides the electrical excitation of an atomic species through the formation of a high voltage spark. Detailed circuits and further characteristics of these sources may be found in analytical instrumentation texts such as Strobel (1). Both the arc and spark sources due to the large amount of energy available for excitation are very good multielement emission sources for

semiquantitative elemental emission analysis. Flames composed of various gas mixtures have been used as atomic emission sources over the last several decades. The most commonly used flames today are the premixed air-acetylene flame and the premixed nitrous oxide acetylene flame. The latter operates at a temperature of about 3000°C, while the former is a cooler flame operating in the neighbourhood of 2000°C. Due to their lower temperatures when compared with the D.C. arc and A.C. spark, a narrower range of elements may be induced to emission. Under proper operating conditions flames may provide analyses for some forty elements. For a general review of flame methods, see references (2 - 5). Within the last ten years a relatively new atomic emission source has entered the analytical laboratory, the radio frequency inductively coupled argon plasma. This high energy source provides the multiple element capability of the arc or spark source coupled with higher sensitivity and much higher precision. Although the excitation process is not clearly understood, the plasma source will certainly be the atomic emission source of the future. For a general discussion of the inductively coupled plasma refer to references (6 - 8). With such high energy atomic emission sources available, the analyst must further consider the most efficient schemes available for decoding the spectroscopic information.

B. Decoding Systems for Atomic Emission Spectroscopy

The previous section very briefly described several of the currently available atomic emission sources. The decoding state of the atomic emission experiment will now be considered. The four information domains, frequency, intensity, spatial and temporal all carry information related to the behaviour of a sample as it passes through or is sampled by one of the excitation sources. Information from the frequency domain provides elemental identification, since the specific wavelengths of light emitted by an element are characteristic of that element alone. Information from the intensity domain provides a link to the amount of the element, since intensity varies directly with the concentration of the emitting species in the sample. Therefore, by decoding these two information domains the identity and quantity of the emitting species within the sample has been found. This is very often the only information required by the analyst. In order to decode the frequency and intensity information with high precision and sensitivity, the spatial and temporal behaviour of the emission source must also be fully understood. Let us further look at how each of these information domains may be decoded.

1. Dispersion Based Measurement Systems

The most commonly used instruments for atomic emission spectral information decoding are dispersive in nature; that is, the component frequencies of light entering the instrument are spatially sorted or dispersed across the

instrumental exit focal plane. These instruments are referred to as polychromators or monochromators depending on the number of frequencies that may be simultaneously observed. The dispersive element within the monochromator may be classified into two groups: those based upon refraction and those based upon a combination of diffraction and interference. First consider the refraction based elements which depend upon a change in the refractive index with wavelength, as light passes from one substrate, such as air, into a second substrate, such as quartz. A quartz prism is a prime example of a refraction based dispersive element operating in the ultraviolet-visible spectral range. Quartz works very well because of the large value of $dn/d\lambda$ (n - refractive index, λ - the wavelength of light entering the substrate) it possesses. Various parameters other than $dn/d\lambda$, such as the optical angle of the prism and the thickness of the prism base, are also critical for optimum dispersion of light into its component wavelengths as it exits the prism. The second group of dispersive elements to be considered are those based upon diffraction and interference of which the grating monochromator provides the best example. A typical grating may have on the order of one thousand rulings per millimeter, and provides, through interference and diffraction phenomena, the spatial dispersion of light into its component wavelengths. Both the prism and grating are housed in mono or polychromator assemblies that contain the appropriate auxiliary optics to

bring the dispersed light to a focal plane. The relative intensities of the various wavelengths of light may then be determined by strategically placing detectors in the focal plane.

The monochromator assembly is available in several configurations, the most common of which is the single exit slit scanning monochromator illustrated in Figure 2, in block diagram form. The scanning monochromator is characterized by the presence of a stationary entrance and exit slit and a single detector. In order to scan the various wavelengths across the detector, the dispersive element is rotated, thus changing the horizontal position of the wavelength in the focal plane. Immediate wavelength selectivity is provided by the narrow, (e.g. 100 μm wide) exit slit in front of the detector. For qualitative atomic emission work the complete ultraviolet-visible wavelength region must be slowly scanned across the exit slit. For quantitative work a single emission wavelength may be monitored for single element determination or the system may be slew scanned between different emission lines under computer control for multiple element determination. See Winefordner (9) for further details concerning the advantages and limitations of the slew scan system. The scanning monochromator whether slew scanned or not, still allows only one emission line to be monitored at a time making complex multielement analysis very tedious. The obvious solution to the problem is to place more exit slits and detectors in the instruments focal

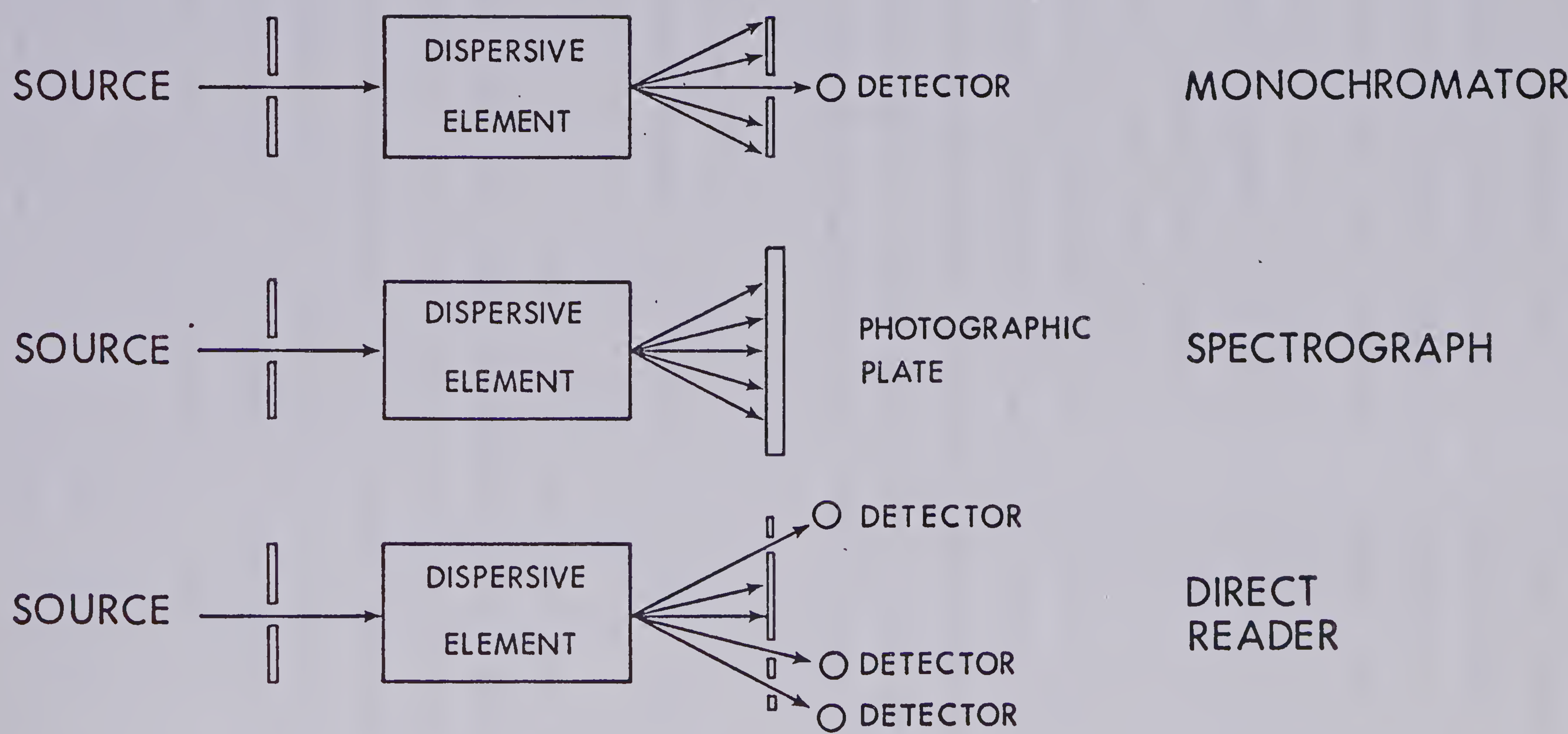

FIGURE 2. Dispersive based spectral information decoding systems

plane. This multiple exit slit, multiple detector configuration is referred to as the direct reader and is also illustrated in block diagram form in Figure 2. This system provides for simultaneous multiple line detection and the number of lines detected is limited only by the physical problems incurred in fitting the detectors into the focal plane. Systems are commercially available providing the capability for detection of 48 emission lines simultaneously. (Jarrell-Ash Corporation)(10). A third solution to the simultaneous multiple line detection problem has been offered through the use of modern image sensor technology. Two major types of image sensors have found such applications: the linear self-scanned silicon photodiode array (11) and the vidicon tube (12). The former consists of a linear one-dimensional array of small silicon photodiodes mounted on a standard sixteen pin integrated circuit chip. The total length of a 1024 element array is about one inch and has a height of up to 2.5 mm. Other array lengths are available, from 64, 128, 256, 512 and 1776 elements long. When this array is placed in the focal plane of the monochromator a spectral window of the emission lines falling on the array is provided. By varying the focal plane location of the array or scanning the monochromator, the spectral window may be centered anywhere within the diodes spectral response. For complete details on implementation and operation of such an array see Horlick (13). The vidicon tube has the added advantage of providing two-dimensional capability in the focal plane,

ideal for source profiling studies. Both the diode array and the vidicon tube provide excellent multiple line detection capability over a given spectral window. Both systems are available commercially from Princeton Applied Research as OMA Model 1410 (14). The last to be discussed, and probably the most widely used in qualitative and semi-quantitative spectroscopic work is the spectrograph configuration. The detector for this system is a photographic emulsion supported on a glass plate about 10 in. by 4 in. One or more photographic plates may be placed directly into the focal plane of the dispersive instrument, providing multiple line detection over a wide spectral range. The density of the emulsion, after exposure to the various light frequencies present in the focal plane, is indicative of their individual intensities. The spectrograph is also shown in block diagram form in Figure 2. The above decoding systems are all dispersively based, although the configuration may vary. Another broad group of spectral decoding instruments that are multiplex based will be described in the following section.

2. Multiplex Based Measurement Systems

Multiplex spectrometers form a very important second classification of instruments that may be used for spectroscopic analysis. Multiplex techniques by their definition can provide simultaneous multiple frequency analysis. A multiplex technique may be defined as a technique in which all or a selected group of the signals present are combined

or multiplexed together into a single signal to be detected by a single detector. A further mathematical processing step is then required to de-multiplex the detected signal into its component signals. Two well known examples of multiplex spectrometers are the Fourier Transform Spectrometer and the Hadamard Transform Spectrometer. The discussion in this thesis will be limited to the Michelson interferometer based Fourier Transform Spectrometer. References describing the theory and implementation of a Hadamard Transform spectrometer are readily available in the literature (15 - 18).

Let us further consider the interferometer-based multiplex spectrometer in more detail. Excellent overall reviews with respect to the Michelson interferometer are easily found in the following references (19 - 25) and the references contained therein. The specific interferometer under study has been adequately described in the literature by Horlick and Yuen (26 - 28) and in their theses (29,30). The Michelson interferometer is a two-beam optical interference technique. As light enters the interferometer it is split into two equal amplitude beams, one travelling into each arm of the interferometer, by a beamsplitter. Through the use of a flat mirror in each arm of the interferometer, the light is reflected back to a common point on the beamsplitter where optical interference occurs. The degree of interference, constructive or destructive, is dependent upon the relative optical path distances travelled by the light beams in the two arms of the interferometer. A path

difference of $n\lambda/2$ implies maximum destructive interference while a path difference of $n\lambda$ implies maximum constructive interference. The interference signal is monitored by a standard detector, such as a photomultiplier tube, TGS detector or silicon photodiode depending upon the spectral region of interest, as a function of the optical path difference between the two interferometer arms. Scanning the interferometer, varying the optical path difference, is most easily accomplished by maintaining one of the mirrors stationary and accurately displacing the other mirror. Refer to Horlick and Yuen (27) for details on how this is accomplished in our system. The interference signal detected is in fact a multiplex signal since all of the frequencies present will undergo a degree of interference at the same physical point on the beamsplitter. Therefore a single detector sees all of the information present all of the time providing simultaneous multiple frequency detection. The interferogram, a function of optical interference signal amplitude with time or mirror distance travelled, may be decoded into the standard spectral domain, amplitude or intensity versus frequency, through the use of Fourier Transform mathematics. Refer to Figure 3 for an interferometer-based multiplex spectrometer system and compare it to the dispersive based systems in the previous Figures The important concept to stress is that through the use of optical interference a single detector simultaneously responds to all frequencies within its bandwidth. Such a system would

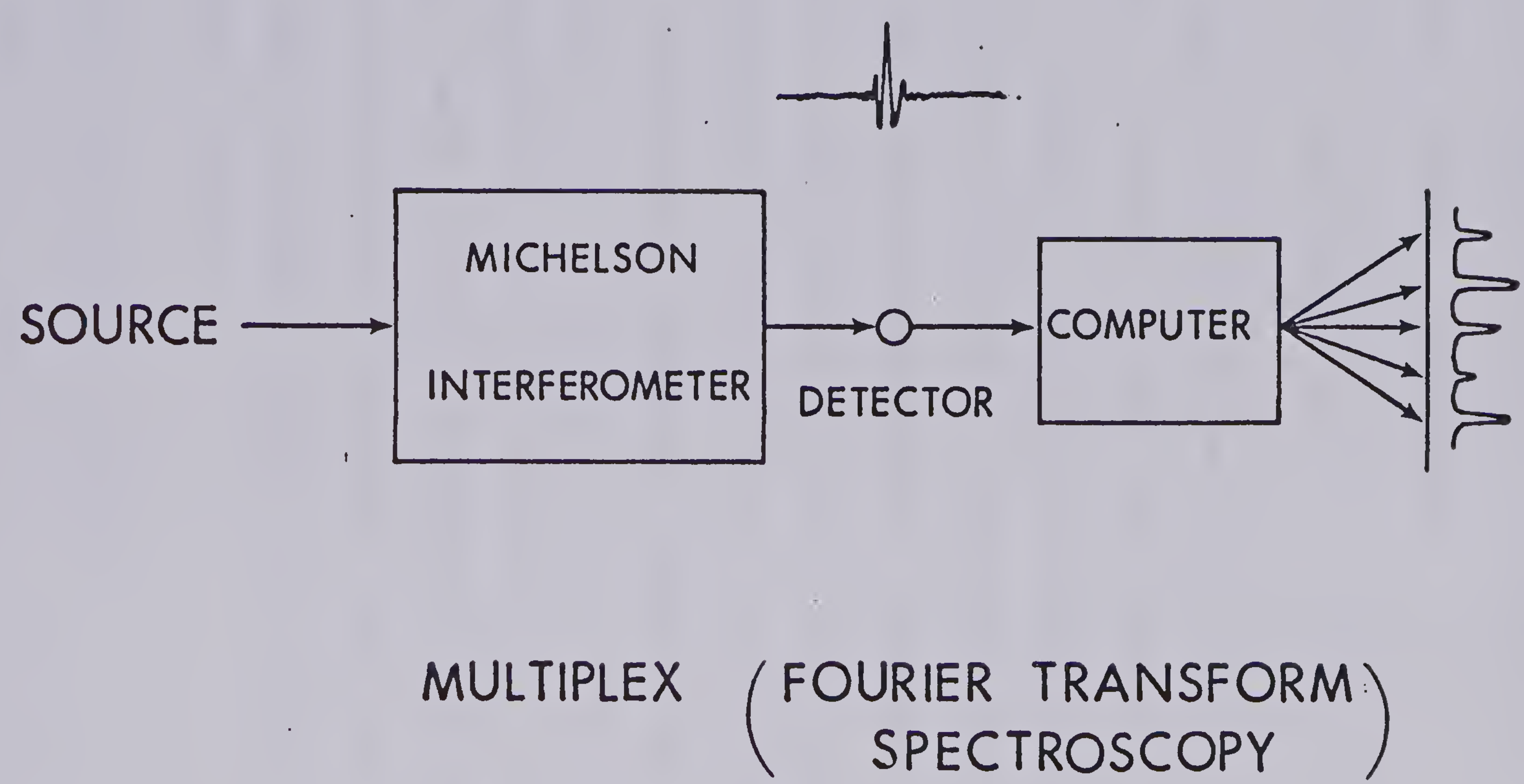

FIGURE 3. Block diagram of a multiplex spectrometer

be ideal, in theory, for use in atomic emission spectroscopy as a spectral decoding system. In the following section the interferometer based multiplex spectrometer will be compared in detail with the commonly used dispersive-based spectrometers with regard to their performances as atomic emission spectroscopy decoding techniques.

C. Spectral Information Decoding: Multiplex vs. Dispersive

The spectroscopic information from the atomic emission experiment is encoded in the four information domains of Figure 1 , frequency, intensity, spatial and temporal. Each of the decoding instruments, just described in the previous section, has unique strengths and weaknesses in spectral decoding. In this section a qualitative comparison of each of the instruments' capabilities in each domain will be offered. Griffiths, Sloane and Hannah (31) have provided a similar comparison, restricting their considerations to the infrared spectral range and commercially available instruments. Many of their comments may be extrapolated for the current interferometer system operating in the ultraviolet-visible spectral range. Refer also further to the references of Griffiths (21,23).

1. Frequency Information Decoding

In order to provide accurate identification of the elements undergoing emission in the source, the frequency of the emitted light must be accurately and precisely determined. The accuracy of a dispersive-based instrument is often dependent

upon the completion of a wavelength position calibration with a known line emission system, such as iron. Any changes in the grating, or exit slit, or detector position will require a recalibration of the wavelength positions. In contrast, the high wavelength accuracy of the interferometer-based system is inherent in the instrument design (30). The wavelength axis accuracy is directly related to the accuracy and stability of the wavelength assigned to the helium neon laser used as a source in an internal reference interferometer. The output of this internal reference interferometer serves as a data acquisition clock for the main sample channel interferometer signal. It is therefore essential to know the wavelength of the helium-neon laser emission with high accuracy, in order to correctly assign the wavelengths present in the main interferometer channel. The laser emission wavelength is tabulated in several sources (32). The precision of the wavelength axis is directly related to the stability of the helium-neon laser emission wavelength and to the reproducibility of the data acquisition sampling system. Thus the wavelength precision of the interferometer-based system is very high. The precision of the dispersive-based systems differ depending upon the configuration. For example, the scanning monochromator's precision is limited mechanically since it depends solely upon the ability of a sine bar drive that rotates the grating to reproducibly do so, with respect to a focal plane position, time and time again. Mechanical specifications just cannot match the high optical precision requirements. This is a very serious problem for the slew

scanned monochromator systems of Winefordner and Malmstadt (33,34). It is very difficult to accurately rotate the grating to a previous setting without the benefit of a reference emission line. The wavelength precision of the direct reader is also limited mechanically since only a shift in position of the grating or slits or detector will effect the emission line alignment. The spectrograph is also limited mechanically through plate alignment from series to series, but the wavelength precision within a plate is very high and can be easily monitored with internal standard emission lines. The photodiode array system is highly precise once placed in the exit focal plane, but, it too will suffer in wavelength precision from any mechanical changes or movements affecting the array or grating. Thus only the interferometer system exhibits both high inherent accuracy and precision with respect to emission line wavelength assignment. All of the dispersive systems require initial and periodic calibrations to ensure the wavelength axis accuracy.

After the frequency of the emitted light has been accurately and precisely assigned, one must consider the range limitations imposed on the frequencies. Over what spectral range can the decoding system detect the emitted light? Apart from the transmittance reflectance properties of the monochromator optics and grating, the spectral range detected is normally imposed by the detector's response

characteristics. For a scanning monochromator or direct reader configurations, 1P28 photomultiplier tubes are often used as detectors. These detectors have a response range from 180 nm to 650 nm. It must be remembered that in the scanning monochromator configuration only one spectral line at a time can be monitored. Similarly for the direct reader configuration, only one line may be monitored per detector. In addition to the spectral response range as defined by the detector, the number of emission lines detected simultaneously across that complete range is important. In both the scanning monochromator and direct reader situation a great deal of information is lost even though it falls within the system's spectral response range. In the photodiode array configuration, the simultaneous spectral response range is defined by the spectral window chosen in the focal plane of the monochromator, and by the 200 nm to 1000 nm spectral response of the silicon photodiode. The spectral information outside these bounds is lost as in the previous cases. The photographic emulsion detector of the spectrograph provides a wide spectral window over which many emission lines may be simultaneously monitored. The limiting factor for most spectrographs so far as simultaneous spectral coverage, is the spectral resonse of the emulsion or in some cases the physical positioning of multiple photographic plates. For a variety of reasons the dispersive instruments provide very drastic differences in the simultaneous wavelength coverage available. Let us now

examine the capabilities of the interferometer-based spectrometer.

The simultaneous wavelength coverage available with a Fourier Transform spectrometer is not as easy to demonstrate as with dispersive-based instruments. Excluding the transmittance-reflectance-absorbance properties of the mirrors, beamsplitter and other associated optics, the simultaneous spectral response range of the interferometer based system is limited solely by the spectral response of the detector. The situation is made complex by the phenomenon of aliasing that occurs during the data acquisition stage. For a complete discussion of aliasing and its effects in atomic emission analysis refer to Yuen (30) and the references contained therein. Aliasing by definition results from the incorrect sampling of a high frequency signal resulting in the appearance of this high frequency signal at a lower frequency. For example, a 160 Hz frequency is sampled correctly, according to the Nyquist theory, by 400 Hz clock frequency. If the clock frequency now changes to 200 Hz in frequency, the 160 Hz signal now appears aliased at the 40 Hz frequency. In no way can this 40 Hz signal be distinguished from an aliased 160 Hz signal without redoing the experiment at a different clocking frequency and looking for a shift in frequency of the observed signal. If a shift occurs, the signal was aliased from a higher frequency. The possibility of multiple aliasing occurs; that is, signals from sampling regions not immediately above the primary sampling region.

For example the 40 Hz signal may have resulted from an aliased signal of any of the following frequencies for a 200 Hz clocking rate: 160 Hz, 240 Hz, 360 Hz, 440 Hz, 560 Hz, 640 Hz. Let us examine in greater detail how aliasing manifests itself in the Fourier Transform spectrometer.

Our Michelson interferometer system, and most commercially available FT spectrometers, are actually composed of three interferometers, a main sample interferometer, a white light zero path difference reference interferometer and a He-Ne laser clock reference interferometer. All three interferometers share the same mirror drive mechanism and in our case they share the same mirror, providing an exact internal reference. The output of the laser interferometer is a cosine wave that is used directly as a sampling clock for the main signal channel. The frequency of this clock is determined by the following relationship:

$$f_M = 2.V.\bar{v}$$

where V = the mirror drive velocity, $\bar{v}$ is the emission line wavenumber (15,802.8 cm^{-1} for the He-Ne laser) and f_M is the modulation frequency that is observed. The same expression naturally holds for the sample channel interferometer. Therefore, with regard to the correct non-aliased sampling of the main signal channel interferometer, only those emissions below 7901.4 cm^{-1} will be correctly sampled. This implies that only a 7901.4 cm^{-1} spectral window may be

uniquely defined. How does this affect work in the U.V.-VIS spectral range? The aliasing regions present are listed in Table I. Consider for example an emission line at 250.0 nm detected by the interferometer system. With the current laser interferometer clock, this line could be interpreted as 250.0 nm or 256.3 nm or 413.27 nm or 430.83 nm due to aliasing. Thus, even though a wide spectral range may be detected by a photomultiplier tube, only a 7901.4 cm^{-1} range is uniquely defined. This aliasing overlapping very often leads to difficulty in unique line emission assignments.

None of the decoding systems offer the simultaneous, complete spectral coverage of the ultraviolet-visible spectral range although the interferometer system closely approaches that goal. Through the use of selected spectral windows the dispersive based instruments can provide a high degree of simultaneous wavelength coverage.

Thus far the accuracy, precision and simultaneous wavelength coverage have been considered, leaving only the ability to resolve two emission frequencies unanswered. This is very important in the case of atomic emission spectroscopy due to the narrow line width atomic emission lines that must be analysed. It is of even greater importance in the interferometer-based system in that the high resolution may be able to help sort out the aliasing problem. The greater the resolution, the easier it may be to determine if an overlapping peak is actually an aliased signal from another spectral region or the presence of a rather broad correctly sampled

Table I

Aliasing Regions in the Ultraviolet-Visible Spectral Range

Region (cm^{-1})	Region (nm)
16802.8 → 7901.4	632.8 → 1265.6
15802.8 → 23704.2	632.8 → 421.9
31605.6 → 23704.2	316.4 → 421.9
31605.6 → 39507.0	316.4 → 253.1
47408.4 → 39507.0	210.9 → 253.1

emission signal. The interferometer used in this laboratory has a resolution of 7.75 cm^{-1} across the complete spectral range. The resolution may be determined by taking the inverse of the optical path difference present between the two interferometer arms. Commercially available instruments have resolutions exceeding 0.05 cm^{-1} (35). The plot in Figure 4 illustrates the wavelength resolution available for (7.75 cm^{-1}, 3.875, 1.988 and 0.994 cm^{-1}) resolution at various wavelengths in the spectral domain. The interferometer system resolution is ultimately limited by the physical distance over which the mirror may be driven, and by solid angle effects in the interferometer detector optics (23,36). An excellent discussion of the resolution limits in F.T.S. is also given by Chantry and Fleming (37).

Dispersive based instruments have their resolution limited basically by the ability of their collimating optics to collect the light from the dispersive element. Monochromators are currently available with resolution less than 0.001 nm. It is the reciprocal linear dispersion, $d\lambda/dx$ in the focal plane, that very often determines the practical resolution of a system. This is especially true for the direct reader and photodiode array based system where discrete detectors are used. The physical placement of these detectors in the focal plane limits the resolution available. Two detectors can only be placed so close together. Such detector placement limitations do not play a part in determining the resolution of the scanning monochromator or

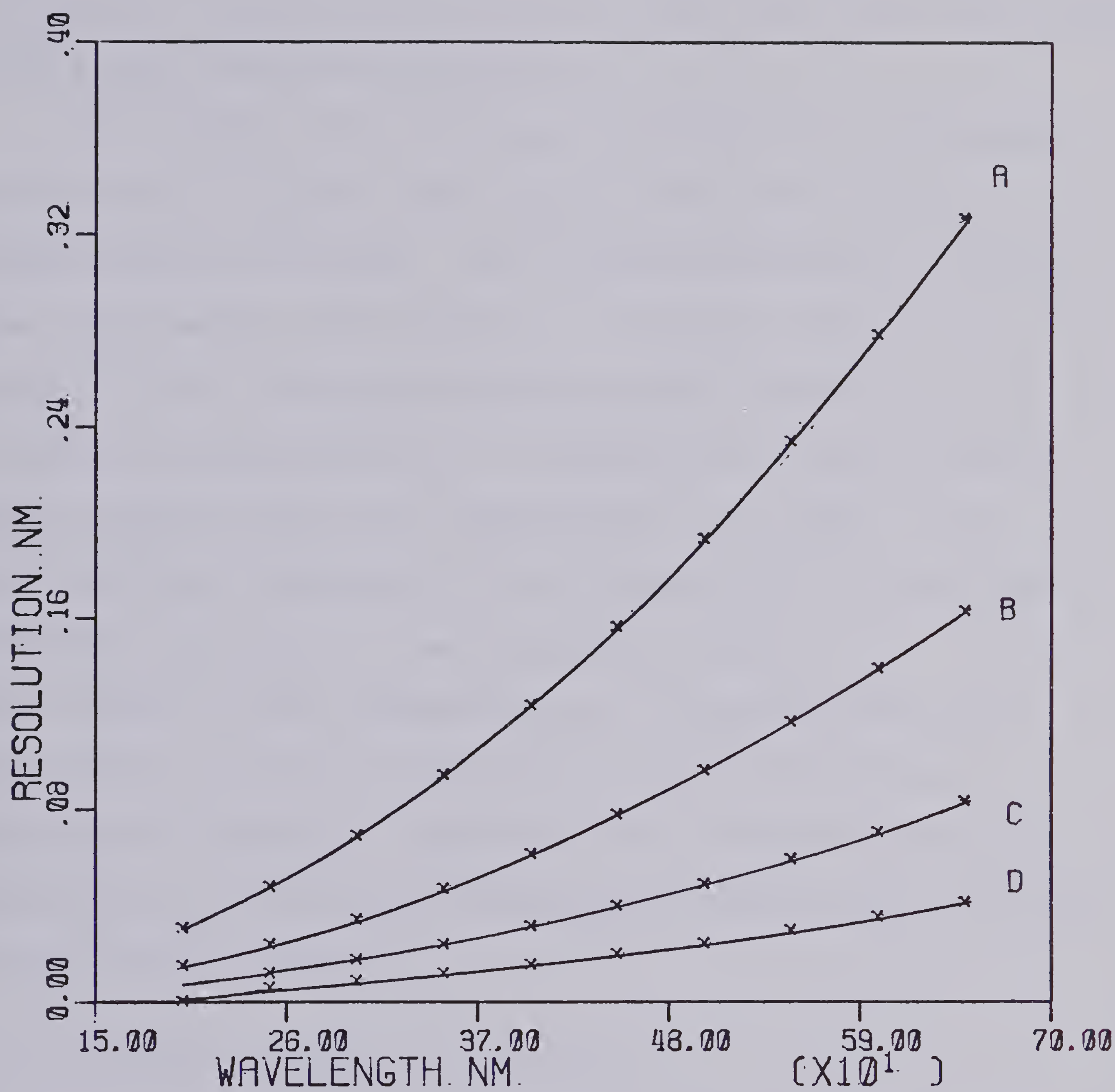

FIGURE 4. Resolution in nm at (A) 7.75 cm^{-1}
(B) 3.875 cm^{-1}
(C) 1.988 cm^{-1}
(D) 0.994 cm^{-1}
resolution

spectrograph. In the former case the resolution is very often slit width-limited while in the latter case the system optics play the determining role.

One further point of comparison should be mentioned with respect to resolution capabilities, that of the instrumental line shape. For dispersive-based instruments the instrumental line shape is ultimately determined by the nature of the grating or prism used and remains constant for a specific configuration. In contrast the interferometer-based system allows the instrumental line shape to be mathematically determined through apodization of the interferogram (38,39,30). The maximum available resolution is still limited by the instrument but with apodization an optimal line shape may be chosen for a particular situation. Lephardt (40) offers an excellent discussion of resolution enhancement capabilities available in the Fourier domain.

2. Intensity Information Decoding

Through decoding the frequency of the emitted light, the elemental identification may be achieved. The question next arises as to the quantity of the element present in the sample. The intensity of the spectral line must be interpreted by relating it to the emission intensity of a known concentration of the element in the same source, thus the need for wide dynamic range analytical curves. The discussion in this section will cover the spectral detection characteristics of each of the decoding instruments and any

advantages or disadvantages present in each. Discussion in the two general areas of linear dynamic range available and signal to noise ratio characteristics will be developed.

Let us first consider the dynamic range limitations present in either a dispersive or multiplex-based noise free spectrometer. Please note the assumption of a noise free system for this portion of the discussion. The dispersive-based spectrometers are limited in their intensity linear dynamic range by the detectors employed. The 1P28 photomultiplier tube in combination with a dispersive system can provide a linear dynamic range covering six orders of magnitude. In constrast the silicon photodiode, unless extensively cooled, can provide only three orders of magnitude in dynamic range. The effect of detector cooling may improve the linear response range to four orders of magnitude. The combination of either detector with an interferometer-based system provides similar dynamic range possibilities for the detection of a single spectral line emission. For the determination of multiple emission signals with the interferometer, the intensity linear dynamic range for each signal present changes depending upon the number of emission signals being detected. This complication is often referred to as the "Multiplex Disadvantage" of interferometers.

The multiplex disadvantage stems from the fact that in a multiplex technique all of the frequency and intensity information is present at the detector all of the time. Consider the system in this laboratory as an example. The

data acquisition unit has a 12 bit analog to digital converter allowing it to resolve 1 part in 4096. The signal voltage input dynamic range is 10 volts. Therefore the lowest voltage level detectable is 2.44 mV. Consider a single frequency emission signal of frequency f_1 and intensity I_1 that has been amplified to fill the dynamic range of the input system. It will have a linear intensity dynamic range of 4096 without the benefit of signal averaging. Consider now the case of 9 additional frequencies of intensity I_1 entering the interferometer. According to multiplex theory the maximum possible interferogram amplitude corresponds to the algebraic summation of the amplitudes of the interfering frequencies. In the Michelson interferometer, this occurs at the zero path difference between the two arms of the interferometer. Therefore the amplitude of frequency f_1 now determines only 10% of the input dynamic range. Since the bit resolution of the system has remained constant, the linear dynamic range capability for frequency f_1, as well as the other frequencies present is only 409.6. This example can be readily extrapolated to more complex systems consisting of large numbers of different intensity emission lines. The worst case occurs in the presence of large broadband emissions such as those of calcium oxide. Apart from decreasing the intensity dynamic range of the larger emission signals present, the multiplexing disadvantage may cause low intensity signals to be completely lost from the resolution capability of the analog to digital converter. Two possible solutions

exist. Either increase the bit resolution of the analog to digital converter or allow extensive signal averaging to achieve the same result. Both are limited, the former by technology, the latter by temporal effects, neither offering an absolute solution to the dynamic range problem.

The above discussion has assumed the presence of noise-free emission signals, a non-realistic assumption. Let us look in greater detail at the response of the various decoding systems to noise. In the atomic emission experiment in the ultraviolet-visible spectral range, two types of noise predominate: detector shot noise and source fluctuation noise. Both vary directly with the emission signal intensity, the former having a square root relationship, and the latter having a linear relationship. For a discussion of these and other common atomic excitation source noises see Talmi (41). How do the dispersive-based instruments deal with intensity related noise? In a scanning monochromator system such noise appears as a noisy emission peak; that is, the standard deviation of the peak maximum amplitude is greater than the standard deviation of a baseline point. The scanning monochromator detector sees the high intensity signal only as it is scanned across the exit slit. A somewhat different situation exists for the multiple detector-based systems such as the direct reader or photodiode array configurations. The noise is still peak localized on the high intensity emission signal, but it is continuously monitored. Similar arguments hold for the spectrograph. In all cases the use of signal integration over a set time

period decreases the effect of the noise on the signal amplitude determination. The important concept to realize is that the intensity related noise appears spectrally located only at the wavelength corresponding to that specific intensity emission. The noise is not spectrally distributed in any manner in a dispersive based system. This is not the case for the multiplex-based system.

The spectral distribution of shot or fluctuation noise in a multiplex spectrometer was originally discussed by Mertz in 1961 (42) and by other authors since (43,44). In theory, both intensity generated source fluctuation noise and detector shot noise have random frequency components and a Gaussian amplitude distribution about the signal mean amplitude. Due to the simultaneous detection of all frequencies, including noise, in a multiplex spectrometer, the random frequency noise appears evenly distributed across the spectral domain following Fourier Transformation. Only through complex phase analysis (39) can an elemental emission line be differentiated from a noise frequency. This is due to the random nature of the phase components of noise. In theory the standard deviation of a peak in the spectral domain should be equal to the standard deviation of a baseline point or any other spectral peak present, independent of amplitude. The standard deviation amplitude should be dependent only upon the peak emission amplitude of their

summation in the case of multiple emission peaks. The spectral noise distribution poses a second problem for the dynamic range considerations of the interferometer-based system. A small amplitude emission signal may be lost in the noise produced by a larger amplitude emission signal at a different frequency. Whether this actually occurs under experimental conditions remains to be seen. The combination of a limited dynamic range available for complex mixtures and the nature of the spectral distribution of noise may cause severe limitations for the interferometer-based detection system when applied in a practical atomic emission experiment.

The previous discussion concerning the spectral distribution of noise in a multiplex spectrometer did not give any consideration to the relative amplitudes of the signal and the noise. The inherent signal to noise ratio advantage offered by a multiplex-based spectrometer over a scanning monochromator, in a detector noise limited environment, has been well documented in the literature. The reader is referred to several review articles dealing specifically with this topic and several texts for a broader background in this area (20 - 25, 33, 43). In this section we will qualitatively consider the signal to noise ratios of the dispersive and multiplex instruments under study in this chapter. Any mathematical derivations will be included in Appendix A or the reader will be referred to an appropriate reference.

As an initial comparison let us investigate the scanning monochromator system and the multiplex system under conditions of a detector noise limited experiment. Such a system might involve a TGS detector in the mid-infrared spectral region. This situation has been well documented in the literature by Tai and Harwitt (45,46), Winefordner (43), Hirschfeld (44), Treffers (47) and Sakai (36) to name a few. All agree upon a signal to noise ratio advantage for the multiplex system that may be expressed as $(N)^{\frac{1}{2}}/E$ where N is the number of resolution elements present and E is an efficiency term related to beamsplitter and overall encoding efficiency of the interferometer. E is considered to have a value of 4, except by Treffers, and Tai and Harwitt who include an additional factor of 2 for an encoding inefficiency of the interferometer. Through the use of a cosine modulation, the interferometer, in theory, is only fifty percent efficient in the encoding process. A square wave modulation was defined as having a one hundred percent efficiency. Hirschfeld (48) disagrees with this additional factor of two loss, stating that due to detector optimization, with respect to signal to noise, both encoding modulations achieve the same efficiency. The discussion continues.

A signal independent detector noise limited situation is most commonly encountered in the infrared spectral region. The work in this thesis employs an interferometer operating in the ultraviolet-visible spectral range with a photomultiplier tube detector.

The detector noise limited criterion of the above example no longer applies since the photomultiplier detector will likely be limited by a combination of source fluctuation and detector shot noise. There may or may not be a signal to noise ratio advantage present under these conditions for a multiplex-based system over a dispersive system. The multiplex gain or signal to noise ratio advantage under such conditions was first described by Kahn in 1959 (49) and more recently by Filler in 1973 (50), Chester et al. in 1976 (51), Winefordner et al. in 1976 (43), Hirshfield in 1976 (44), Knacke in 1978 (52) and Luc and Gerstenkorn in 1978 (53). All of the authors have reached approximately the same conclusion: No signal to noise ratio advantage exists for the multiplex spectrometer operating under photon noise limited conditions, except in the case of sparse narrow linewidth emission spectra. A definite signal to noise ratio disadvantage occurs in the case of dense spectra such as would be found with broad band absorbance measurements. This, of course, assumes comparison with a scanning monochromator system, as opposed to a direct reader or photodiode array configuration. Hirshfield (44) expresses this "distributive multiplex gain" as follows:

$$\frac{SNR_{FT}(\bar{v})}{SNR_{SC}(\bar{v})} = \left[\frac{f(\bar{v})}{\dfrac{E}{\bar{v}_2-\bar{v}_1} \displaystyle\int_{\bar{v}_1}^{\bar{v}_2} f(\bar{v})\,d\bar{v}} \right]^{1/2} \tag{1}$$

where $f(\bar{v})$ is the spectral density function, $\bar{v}$ is the wavenumber of the line of interest, $\bar{v}_2-\bar{v}_1$ defines the spectral scanning range and E is a modulation efficiency factor. Refer to Appendix A for a complete derivation. From equation (1) it is readily seen that the presence of emission signals other than at wavenumber $\bar{v}$,decreases the possible signal to noise ratio advantage. But in the case of a relatively sparse line emission spectrum over a wide spectral range, a definite signal to noise ratio advantage may exist for the interferometer over the scanning monochromator. For a detailed analysis refer to Chester et al. (51) and Winefordner et al. (43).

Such a signal to noise ratio advantage as described above does not exist for the interferometer over the multichannel detection systems such as the direct reader or the diode array-based system or the spectrograph. All of these configurations also continuously monitor the emission lines,and so,any gain in signal to noise ratio will be a function of the specific detector characteristics as opposed to the basic instrument concept.

Let us briefly consider the overall consequences of noise with respect to an interferometer-based atomic emission system. Note that the noise is not solely limited to detector shot noise. Due to the distributive properties of noise,weak emission signals may be lost in the presence of high intensity signals. Due to the signal to noise ratio nature of the instrument a definite signal to noise ratio

disadvantage may be present when compared to the dispersive-based instruments. The source background emission signal, if relatively intense and distributed over a wide spectral range, may contribute to both of the above problems. This effect would have to be carefully taken into account, or if possible, eliminated through optical filtering or proper detector selection. The analysis of a complex multiple element mixture may, through the emission of its constituent elements, contribute to the above problems. This factor must also be accounted for in the interferometer-based system. In both of the above examples, the background and sample emission, the dynamic range problem may also be a factor for low level determinations. Thus, with respect to the decoding of intensity information, the interferometer-based spectrometer may indeed be much less capable than the various dispersive-based instruments.

3. Spatial Information Decoding

Spatial information may play a very important role in the interpretation of the intensity information just discussed. The optimal region for an emitting species in the emission source must be chosen to obtain the highest sensitivity and signal to noise ratio possible. The relative importance of the spatial information depends upon the emission source used for excitation. Sources such as the D.C. arc, spark and plasma are very sensitive to spatial effects while the flame sources are sensitive to lesser extents. Let us consider briefly each source with regard to spatial effects,

and then, the ability of the different decoding systems to deal with the problem.

The D.C. arc and A.C. spark excitation sources suffer from many of the same spatial problems. Both sources are subject to wandering, that is, neither source maintains a constant origin on the cathodic surface, therefore, changing the spatial window. Within the actual arc or spark itself, spatial effects are present since the maximum amount of energy available for excitation of atomic species occurs near the cathode. Different atomic species may be seen to emit at the cathode than a few millimeters away at the anode. Unless external optics take this into account and provide a wide spectral window, any of the decoding instruments described will suffer a less than optimum signal. Flame emission sources also suffer from spatial problems but to a lesser extent than the arc or spark. A great deal of experimental flame profiling has been done over the last several decades in order to fully interpret this information and allow the choice of an optimal spectral emission region for a particular species (3). The more recently available argon I.C.P. source appears extremely sensitive spatially. Factors such as nebulizer flow rate, power used, and analyte observed, determine its spatial behaviour spectroscopically (54). All emission excitation sources suffer from some degree of spatial influence.

How does each of the decoding instruments under discussion react to spatial problems? For a monochromator dispersive-based system the external imaging optics play the decisive role of determining the spatial window of the source seen

by the detector. With the choice of proper imaging of the source onto the entrance slits and proper overall system alignment, a great deal of spatial selectivity may be obtained with a monochromator based system. A caution exists in that no optimum window exists for all emitting species and a realignment may have to be done for various emission measurements. The multiplex interferometer-based system is susceptible, to a greater extent than the monochromator-based instruments, to spatial effects. This is due to the requirement that light entering the interferometer must be collimated. This collimation ensures no interference from off axis rays undergoing a greater optical retardation than on axis rays (55,56). Collimation may be accomplished in various ways two of which employ an off axis parabolic mirror or a standard quartz lens. The off axis parabolic mirror provides collimation of light emitted by the source, if the source is placed at the mirror's focal point. The light reflected on axis forms a collimated beam that may be directed to the interferometer's entrance aperture. A quartz lens may be similarly employed with the stipulation that the interferometer must be at the focal length of the lens, in distance from the lens, and on the lens' axis. Both systems have been employed with the interferometers and found to work well. The problem occurs in that the actual spatial window observed is determined in theory by the size of the focal point on the source. Since this area is extremely small the spatial window must be chosen with great

care. This leads to problems with a source such as the plasma that undergoes spatial speciation of emitting elements or, with a source such as the nitrous oxide acetylene flame that is very susceptible to source fluctuation in the form of air currents. In either case the interferometer may become severely limited in the acquisition of precise quantitative analytical data. Examples of such spatial problems will be presented in later chapters.

4. Temporal Information Decoding

The final, and by no means the least important, information domain to be considered is the temporal domain. How well can the information decoding systems under discussion respond to temporal information? Let us first look at the temporal behaviour of the atomic emission sources under study to obtain a criterion for the temporal requirements of the decoding systems. The flames and plasma emission sources do not exhibit an inherent temporal behaviour although temporal problems may exist due to external factors, such as source power modulation in the plasma. In contrast the arc and spark emission sources do exhibit an inherent temporal behaviour. The arc source undergoes selective volatilization of the sample that is dependent upon the sample matrix. Selective volatilization refers to the excitation of specific elements throughout different time periods during the life of the arc. The spark excitation source also has an inherent time behaviour in that the spark occurs once every 16 msec and has a decay period of about 50 μsec. The detection system

used for either the arc or spark source must be able to adapt to their time behaviour.

A very important facet of spectral decoding is brought to light if the analyte emission intensity varies with time. In order to obtain an indication of the analyte concentration, the spectral intensity detectors must be able to integrate the intensity over a suitable time period, such as the duration of the arc or 10000 repetitions of the spark. Simply sampling the intensity at discrete points over the time period will not give a good indication of the total analyte concentration. The addition of a simple electronic integrator on the output of the photomultiplier tube provides integration capability and is widely used in direct readers and single slit systems. It is especially advantageous in the direct reader in that the optimum integration time may be chosen for each spectral line independent of the other lines. Thus the precision of a weak intensity emission may be increased. The opposite is true in the case of the spectrograph. While the photographic emulsion is inherently an integrating detector, all of the emission line intensities must be integrated over the same exposure time. Very often the more intense emission lines will "bloom" into the surrounding areas of the emulsion, possibly overlapping onto nearby emission lines. The silicon photodiode array does not suffer from blooming problems and offers a high degree of flexibility in the available integration times (13). It is interesting to note that the photodiodes may be allowed to

saturate at strong emission lines while continuing to integrate weaker signals with no deleterious effects on either.

The FTS interferometer-based system, due to its multiplex nature, suffers greatly in the detection of a time varying analyte emission. The interferometer system is not an integrating system by nature, since data is acquired in the time domain at precisely defined intervals. The signal intensity must remain constant at least over the period of a single scan and more commonly over the period of several scans to provide a signal averaging capability for signal to noise ratio enhancement. Thus the interferometer system would not be a suitable decoding system for the D.C. arc or spark atomic emission source due to their highly time-dependent behaviour.

D. Conclusions

From the discussions and comparisons presented in this chapter, it is evident that the interferometer based multiplex spectrometer offers definite potential as a decoding system for atomic emission analysis. Although restrictions have been cited with respect to the noise and dynamic range problems, the advantage of simultaneous multiple element detection, with high wavelength accuracy and precision, under high resolution conditions, may out-weigh any disadvantages present. Such a system was in fact constructed and examined under experimental conditions in this laboratory.

The chapter following immediately will provide a description of the current design status of the interferometer, noting any changes incorporated since those of Yuen (30). Chapter III will provide an indication of the system's response using hollow cathode lamp sources of known spectral emissions. Chapters IV and V will then provide an indication of the system's performance under conditions imposed by "real" atomic emission sources commonly used, such as flames, or a radiofrequency inductively coupled argon plasma. The discussion of Chapter VI relates to the area of interferogram data processing using correlation analysis techniques. The following experiments will provide an overall indication of the interferometer's feasibility as a detection system for atomic emission spectroscopy. Let us now look more closely at the interferometer that forms the basis of this system.

CHAPTER II

INSTRUMENTATION: DESCRIPTION AND MODIFICATIONS

A. The Interferometer System

The Michelson Interferometer system used throughout this experimental work has been developed over a period of the last ten years (29,30). Currently two such interferometers exist in this laboratory, each independently equipped with optics and electronics. Both interferometer blocks were machined in the departmental shop and detailed specifications may be obtained in the references mentioned above. A schematic diagram of the interferometer assembly, as well as an overall block diagram of the system, are included in Figures 5 and 6, respectively for completeness.

B. Modifications

1. Changes in the Electronic Control Circuitry

A detailed circuit diagram of the interferometer control electronics is included in Figure 7 to illustrate two modifications, one a minor correction, and the second a major design change. Changes in the circuit diagram are indicated by dotted lines. No attempt has been made to completely redesign or update the electronics, only to optimize the present system. The minor correction made simply involves the addition of a nand gate between the clock output and the input of the modulo-N counter. The nand gate serves solely as a buffer for the TTL level signal entering

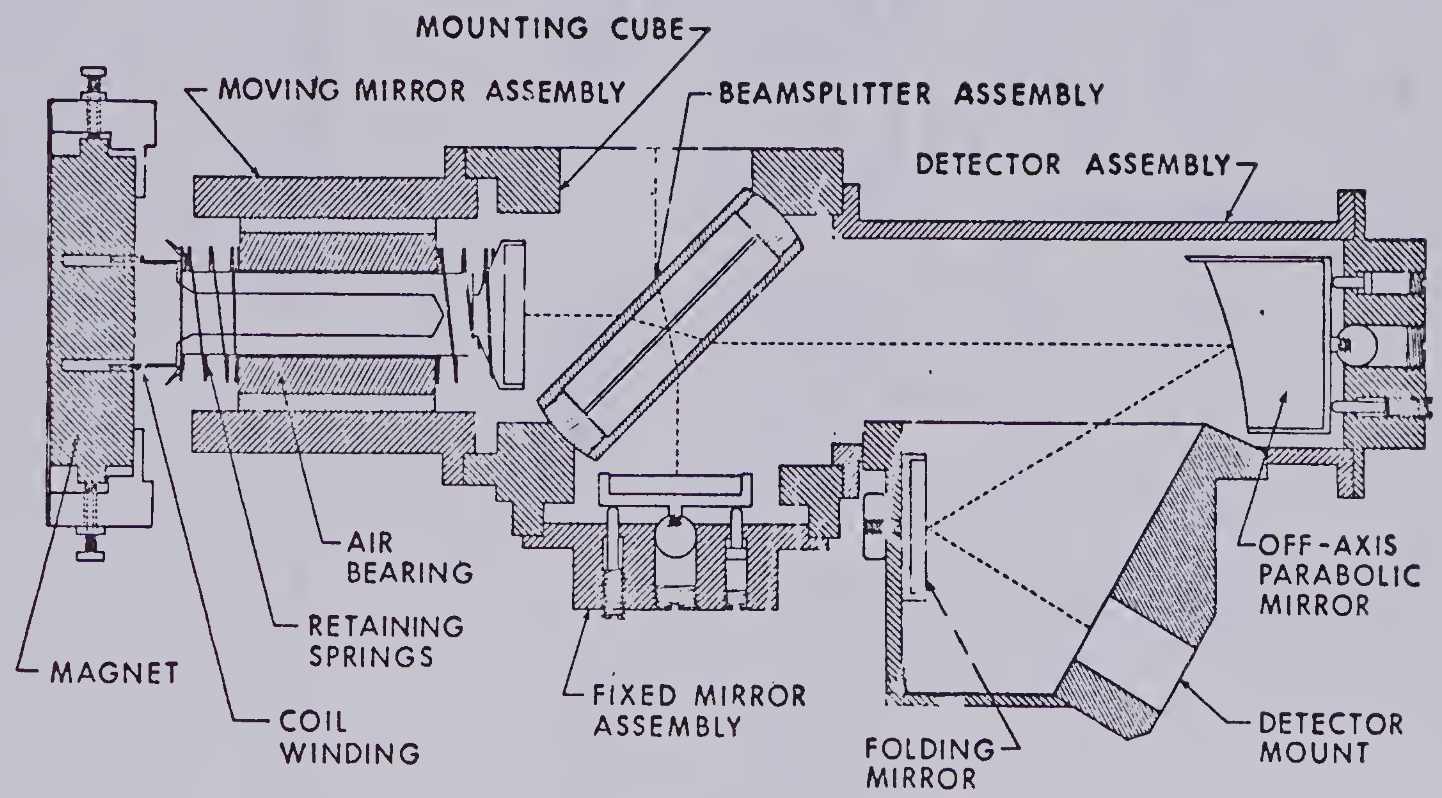

FIGURE 5. Interferometer assembly schematic

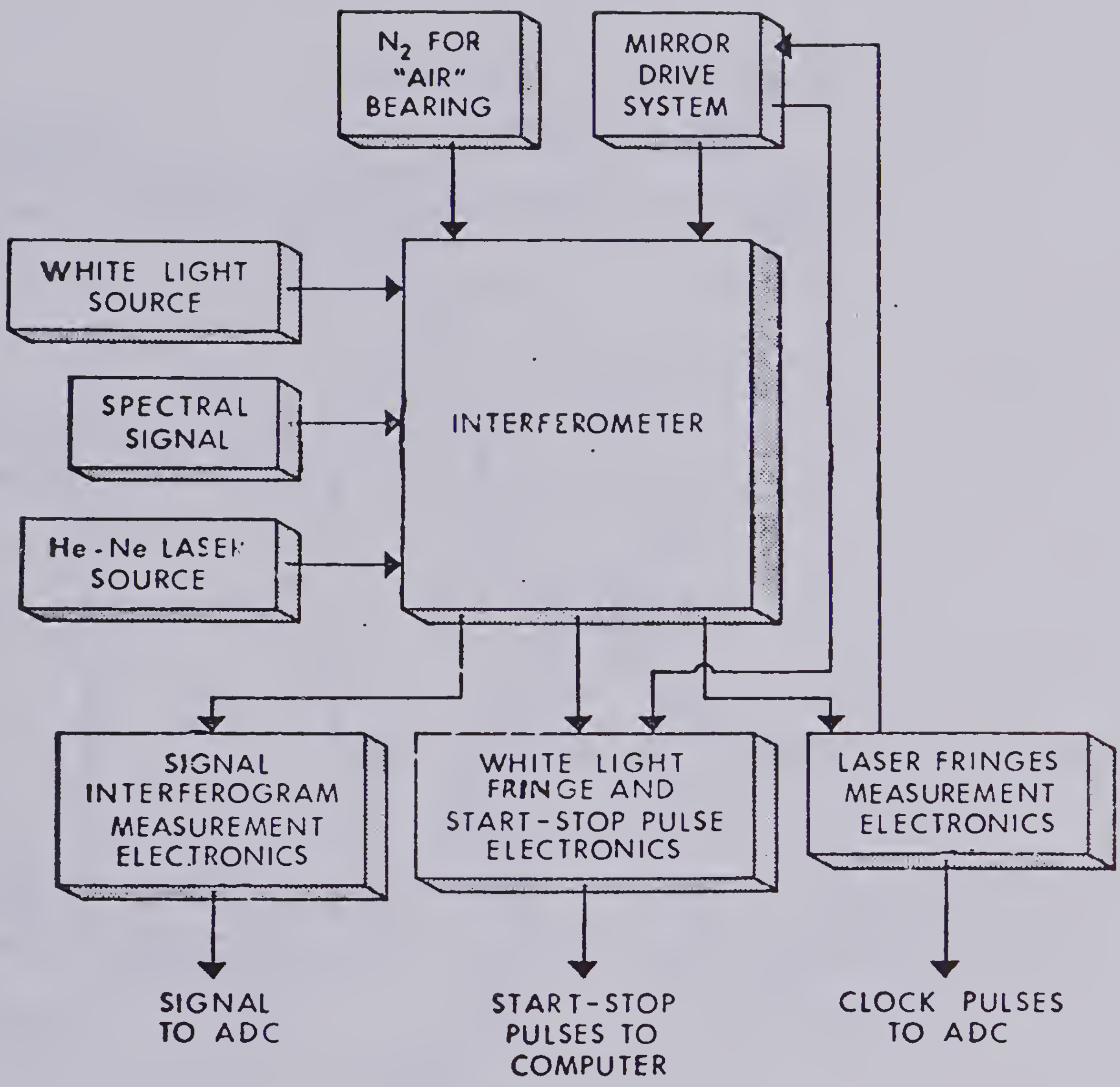

FIGURE 6.

Block diagram of the interferometer system in use

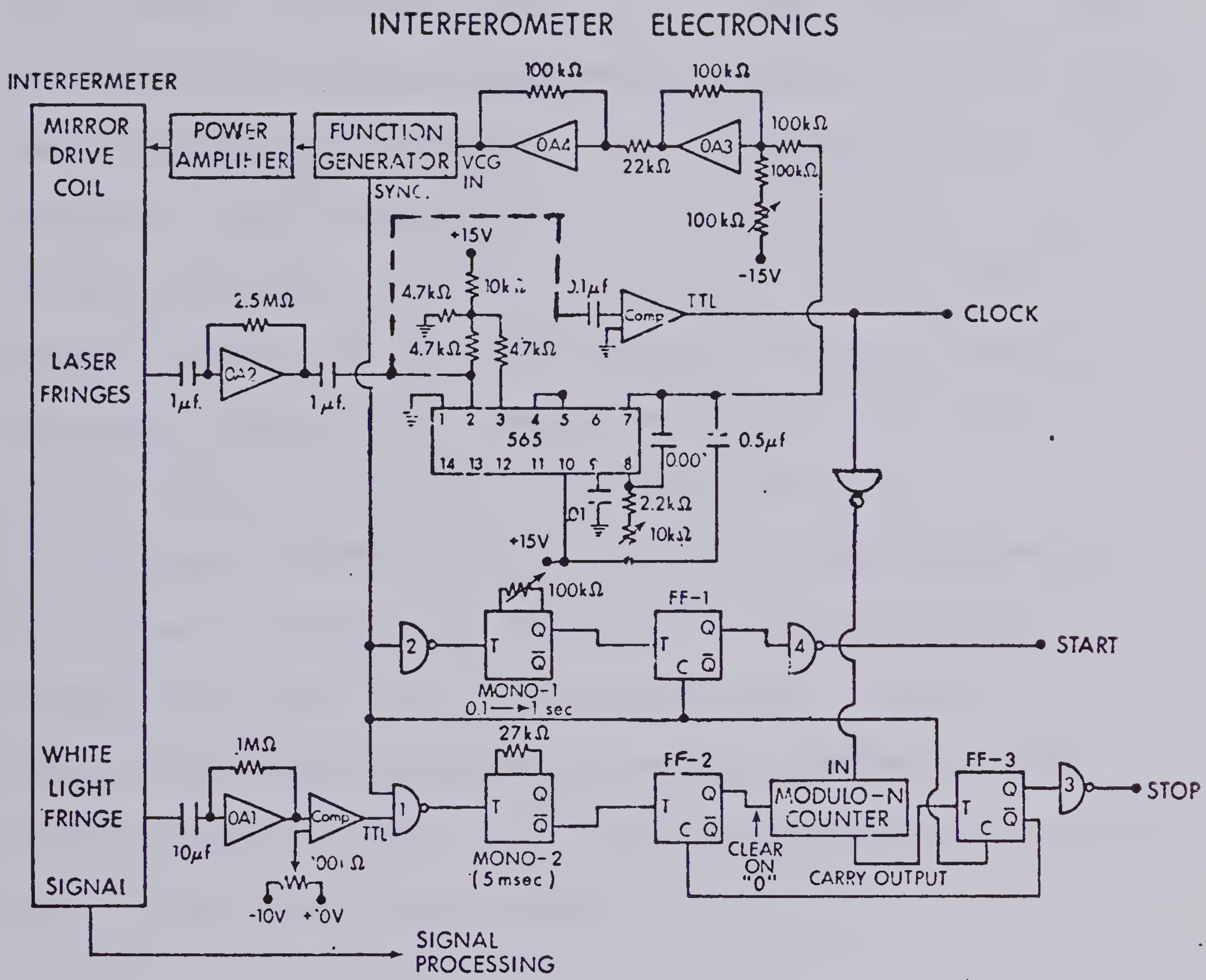

FIGURE 7. Electronic control circuit diagram

the counter and has no effect upon the system control logic.

The second modification, although subtle in nature, has rather important consequences. Consider the portion of the control circuitry generating the clocking signal used by the minicomputer for data acquisition. This refers to the portion of the circuit diagram starting at "laser fringes" and terminating at "clock". The helium-neon laser interferometer output signal is a cosine wave with a frequency of approximately 4000 Hz. This signal is amplified as it passes through OA2 and then enters the phase comparator of the phase locked loop. Previously (30), the clock signal used for data acquisition was obtained at the V.C.O. output of the phase locked loop and routed to the minicomputer. The object of the phase locked loop is to generate a correction signal in order to maintain a constant velocity mirror drive and, therefore, a constant frequency laser interferometer signal. The relationship between frequency and velocity may be expressed as follows:

$$f_M = 2.V.\bar{v}$$

where V = the velocity of the mirror drive, $\bar{v}$ = the wavenumber of the light entering the interferometer, and f_M = the frequency of modulation. Therefore if the velocity is maintained constant, the output signal of the interferometer, f_M, will be of constant frequency. This feedback system takes into account any drive non-linearities generated by non-

homogeneities in the voice coil or magnet used in driving the mirror. To operate correctly, the output of OA2 should be placed directly into the comparator input as well as into the phase comparator input of the phase locked loop. This allows the clock to be generated directly by the reference helium-neon laser interferometer signal, as it should be, in order to have exact synchronization between the laser reference interferometer and the main sample interferometer. The loss of exact synchronization produces errors in the sampling of the main interferometer signal and, depending upon the source of these errors, they will be periodic or non-periodic in nature. For example, if the clock signal is obtained from the phase locked loop, as in the previous design, the possibility of further modulation by internally generated loop frequencies exists. The interferometer main signal will then be incorrectly sampled. A periodic sampling error manifests itself in the spectral domain as symmetrical satellite peaks about the correctly sampled major peak. If the amplitude of the error frequency is large enough, a series of satellite peaks at $\bar{v} \pm n\bar{v}'$ will occur.

$\bar{v}$ = the wavenumber of the correctly sampled peak,

$\bar{v}'$= the wavenumber of the error frequency,

n = 0, 1, 2, 3 ...

The amplitude of these satellite peaks is given by $A = \pi \bar{v} B$ where B is the error signal amplitude. Thus a change in the periodic error signal frequency affects both the satellite peak location and the peak amplitude in the spectral domain.

Further mathematical details are given by Sakai (57). Example spectra with and without satellites are shown in Figures 8 and 9 respectively. By implementing the circuit changes described, the occurrence of satellite peaks in our emission spectra greatly diminished. This indicates that the phase locked loop, although not the only source of error, did contribute to the incorrect sampling of the main channel interferogram. Other sources of periodic sampling errors still exist in the system, but to a much lesser extent, and normally are not visible as satellite peaks.

2. Changes in the Detector Circuitry

A final modification to the instrumental electronics involved a change in the dynode chain of the photomultiplier tube. Previous modifications by Yuen (30) had optimized the chain for the detection of A.C. signals by the use of several coupling capacitors. The rapid A.C. signal response is very important in the case of the Michelson interferometer, since a rather large unmodulated level of light hits the photomultiplier tube. Typically the A.C. portion of the signal, the interferogram, accounts for about one third of the total light level present when working in the U.V.-VIS. For a study concerning the relative amplitudes of the A.C. and D.C. levels present in this interferometer system, please see Appendix B. In the case of a monochromator photomultiplier tube combination the photomultiplier tube need only respond to the changes in D.C. level as the wavelengths are sequentially scanned, or the emission intensity varies with analyte

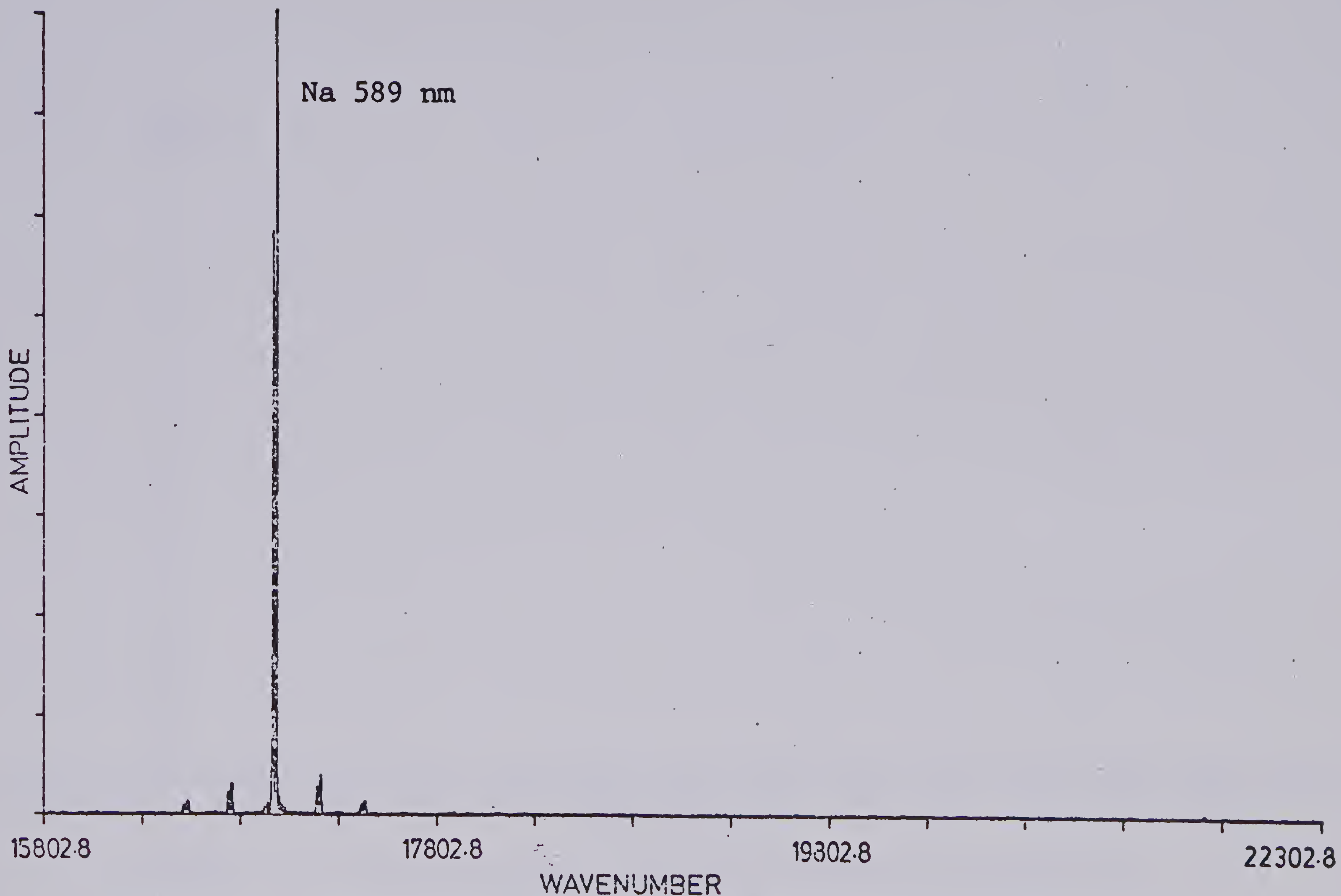

FIGURE 8. Sodium emission spectrum showing the presence of satellite peaks

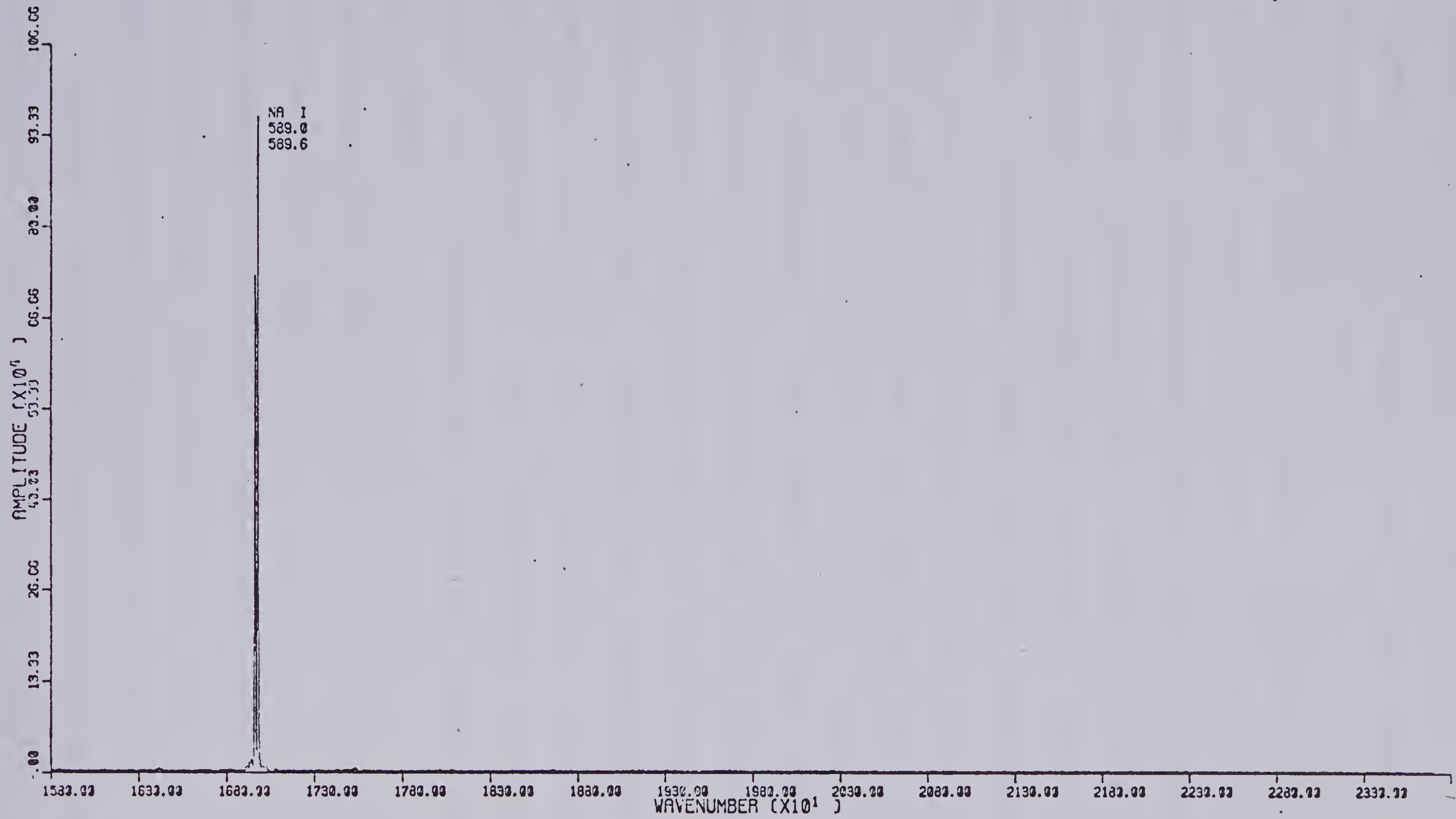

FIGURE 9. Sodium emission spectrum showing the absence of satellite peaks.

concentration. Due to the multiplex nature of the interferometer, the photocathodic surface must respond to a consistently high light level, even if A.C. optimized, since all of the intensity and frequency information is present in the optical signal all of the time. By the time this high level signal reaches the last couple of dynodes in the chain, the number of secondary emission produced electrons is enormous. A problem with such a large number of electrons exists in attempting to focus them onto the last dynodes. When operated as a linear potential difference dynode chain, a high number of electrons is simply lost from the last dynodes due to the dynode's inability to electrostatically focus the electrons. This results in a decay of signal quality even at moderate levels with the interferometer and was noted as a time domain response by Yuen (29). After about one half hour of operation the signal decayed completely. A solution to the electrostatic focussing problem was offered by E.M.I. (58) a manufacturer of photomultiplier detectors. By increasing the resistance value over the last two dynodes, a larger potential is allowed to develop, thereby increasing their electrostatic focussing capability. The changes made are illustrated in Figure 10. Discussions and implementations of similar changes are available in the literature (59,60). The signal quality now remains consistent over long periods of time, several hours at least.

No other instrumental changes were made in the control circuitry or detector electronics. An attempt was made to instrumentally produce an accurate start pulse for the data

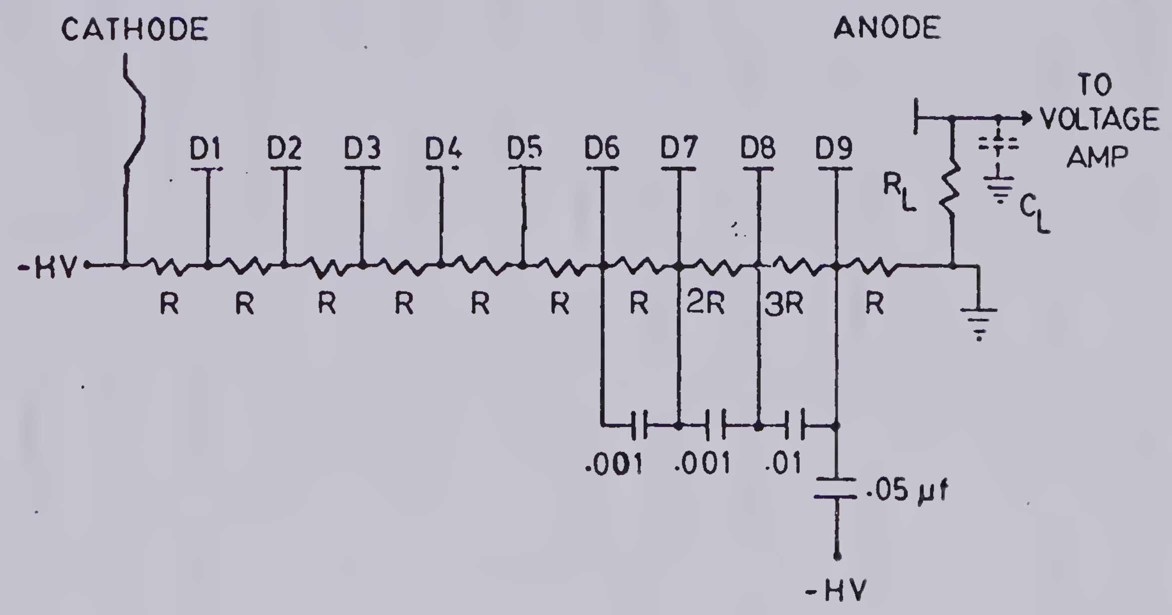

FIGURE 10. Schematic of the modified 1P28 dynode chain

acquisition system. Due to instrumental limitations discussed by Yuen (30), the only accurate reference pulse, apart from the clock, was the stop pulse. This resulted in some rather complex software and hardware control in the data acquisition system in order to provide the signal averaging capability necessary for high signal to noise ratio F T S. A complete description of the optical system used and the reasons for its failure is included in Appendix C.

C. The Minicomputer Data Acquisition System

A Digital Equipment Corporation (DEC) PDP 11/10 sixteen bit minicomputer was used for data acquisition, display, processing and storage of the interferometer data. The minicomputer operated under the RT11-02C disk based operating system with 32K words of memory available. Programming was done in both the high level Fortran O1C and assembler level Macro O1C. Data storage was available on a 2.50 megabyte RK05 single disk drive and a TA11 dual cassette drive. Data display was available in three forms, a decwriter II and a Zeta Research Corporation (61) incremental plotter for hardcopy, and a VT11 display processor in combination with a VR17 graphics display CRT for temporary display.

The data acquisition was accomplished through DEC's Laboratory Peripheral System (LPS). A complete description of the components and capabilities is available in the DEC manuals (61,62). The twelve bit analog to digital converter in

combination with three lines of digital input were used in the interferometer minicomputer interface. The analog to digital converter has a resolution of 12 bits (1:4096) and a total conversion time of 20 μsec. For a complete description of the hardware interferometer minicomputer interface see Yuen (30). The software description, including a program flow diagram and printouts with documentation, is contained in Appendix D.

CHAPTER III

INTERFEROMETER RESPONSE TO HOLLOW CATHODE LAMP ATOMIC EMISSION SOURCES

A. Introduction

The discussions in Chapters I and II have provided a conceptual and an instrumental description of an interferometer based atomic emission analysis system. In this chapter the spectral response capabilities of the interferometer system itself will be examined using hollow cathode lamps as atomic emission sources, and either a 1P28 or solar blind photomultiplier tube as a detector. These experiments will allow the spectral response limitations in terms of spectral range, resolution available, aliasing complications and wavelength accuracy to be observed under operating conditions. The multielement sources will also provide an indication of the simultaneous multielement detection capability of the system and the associated dynamic range problems that may exist. Example emission spectra from several hollow cathode lamps will be shown.

B. Instrumentation

The following hollow cathode lamps were used as atomic emission sources:

1) Si
2) Mg
3) CuZnPbSn
4) CaAlMg

5) FeCuMnCrNiCo

For lamps 1 to 3 a solar blind photomultiplier tube (R166, Hamamatsu T.V. Co. Ltd) (63) operated at a potential of 600 volts was used as a detector. This detector has a peak spectral response at 220 nm falling to 10% at 160 nm and 300 nm. For lamps 4 and 5 a standard 1P28 photomultiplier tube (R.C.A.) (64) operated at 400 volts was employed as a detector. This tube has a peak spectral response at 350 nm falling to 10% peak response at 185 nm and 650 nm. Both lamps employed the modified dynode chain outlined previously in Chapter II. The optical lamp-interferometer interface was accomplished by placing the cathode of the lamp at the focal point of a 6.6 in. focal length, 2 in. diameter, aluminum coated, off axis parabolic mirror. The axis of the mirror was aligned with the entrance aperture of the interferometer, thus providing collimation of the light. The lamps were operated in a current range from 10 ma to 20 ma depending upon the specific lamp. A Princeton Applied Research Corporation low noise preamplifier provided any amplification necessary of the detector signal before entering the data acquisition system. The frequency bandpass was set at 300 Hz and 10 KHz for lower and upper limits respectively. Double-sided interferograms, 4096 points in length, were acquired in order to minimize any phase problems present (30). A Gaussian apodization, previously found to be optimal for atomic emission spectra was employed prior to the FFT processing (30). As part of the FFT processing, one level of zero

filling was employed yielding 4096 unique spectral points (30). These will be the standard conditions under which all of the following interferograms have been processed unless otherwise stated. The only variation may lie in the number of signal averaged interferograms present in the final interferogram. For the hollow cathode lamps, there were fifty signal averaged interferograms used to obtain the final interferogram. This amounted to a total observation time of 25 seconds and a total experimental time of 2 minutes.

C. Results and Discussion

The ultraviolet spectral response region, as seen by the solar blind photomultiplier tube, was the first region to be considered. The individually acquired spectra using the silicon and magnesium hollow cathode lamp sources are shown in Figure 11 and 12 respectively. The observed and literature wavelengths are tabulated in Table II. Consider first the non-aliased spectral emission lines of the magnesium lamp. The aliasing point in this spectral region occurs at 253.12 nm, placing all of the magnesium neutral atom and ion emission lines in a non-aliased spectral region. Note that all frequencies greater than that of the helium neon laser reference interferometer used as a data acquisition clock are actually aliased, but since the detector response is limited to the ultraviolet spectral region, the spectral region of highest wavelength response is referred to as a non-aliased spectral region. This region corresponds to the range from 253.12 nm to 316.40 nm for the solar blind detector. The resolution available at 277.5 nm is 0.060 nm, quite adequate

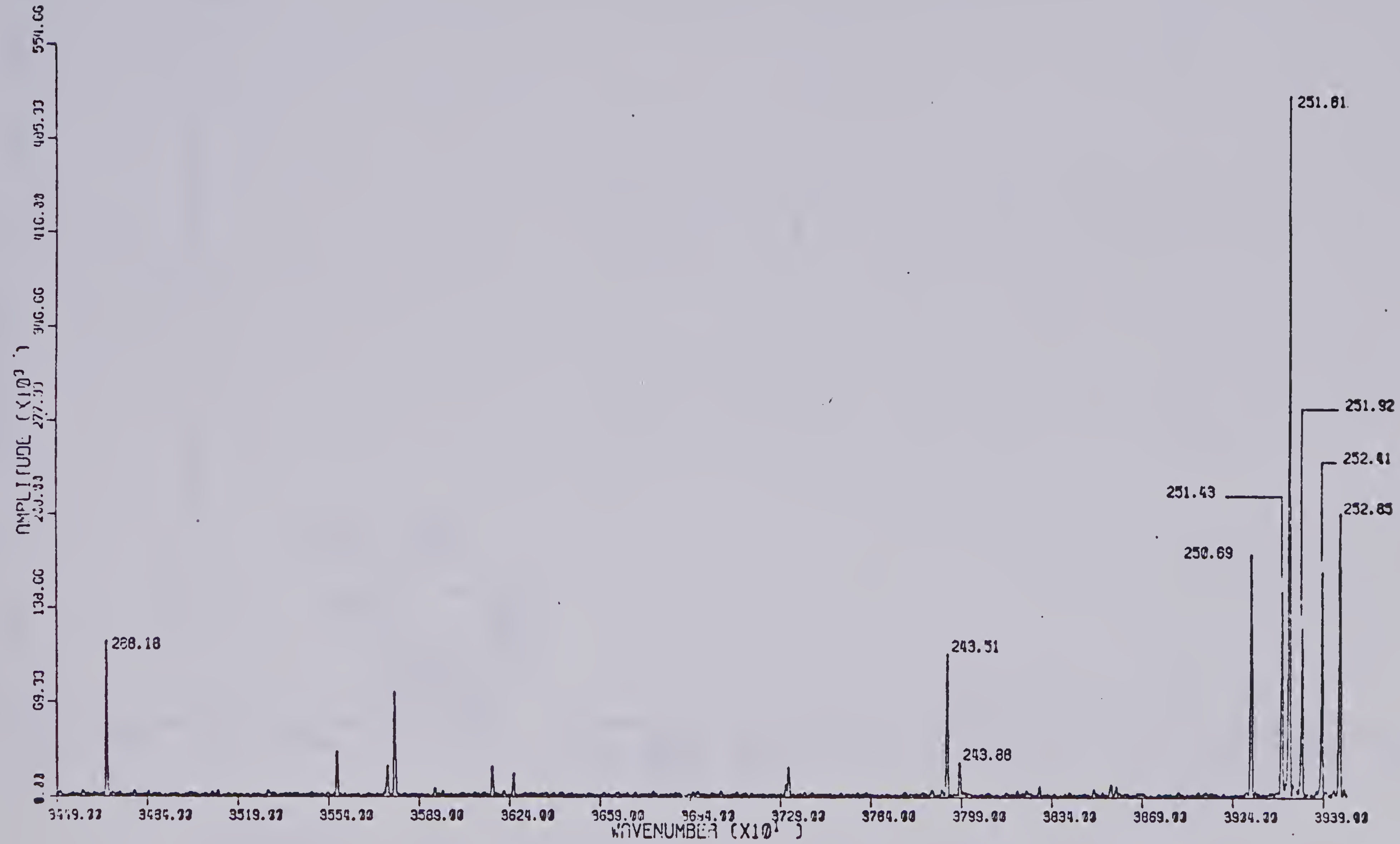

FIGURE 11. Silicon hollow cathode lamp emission spectrum

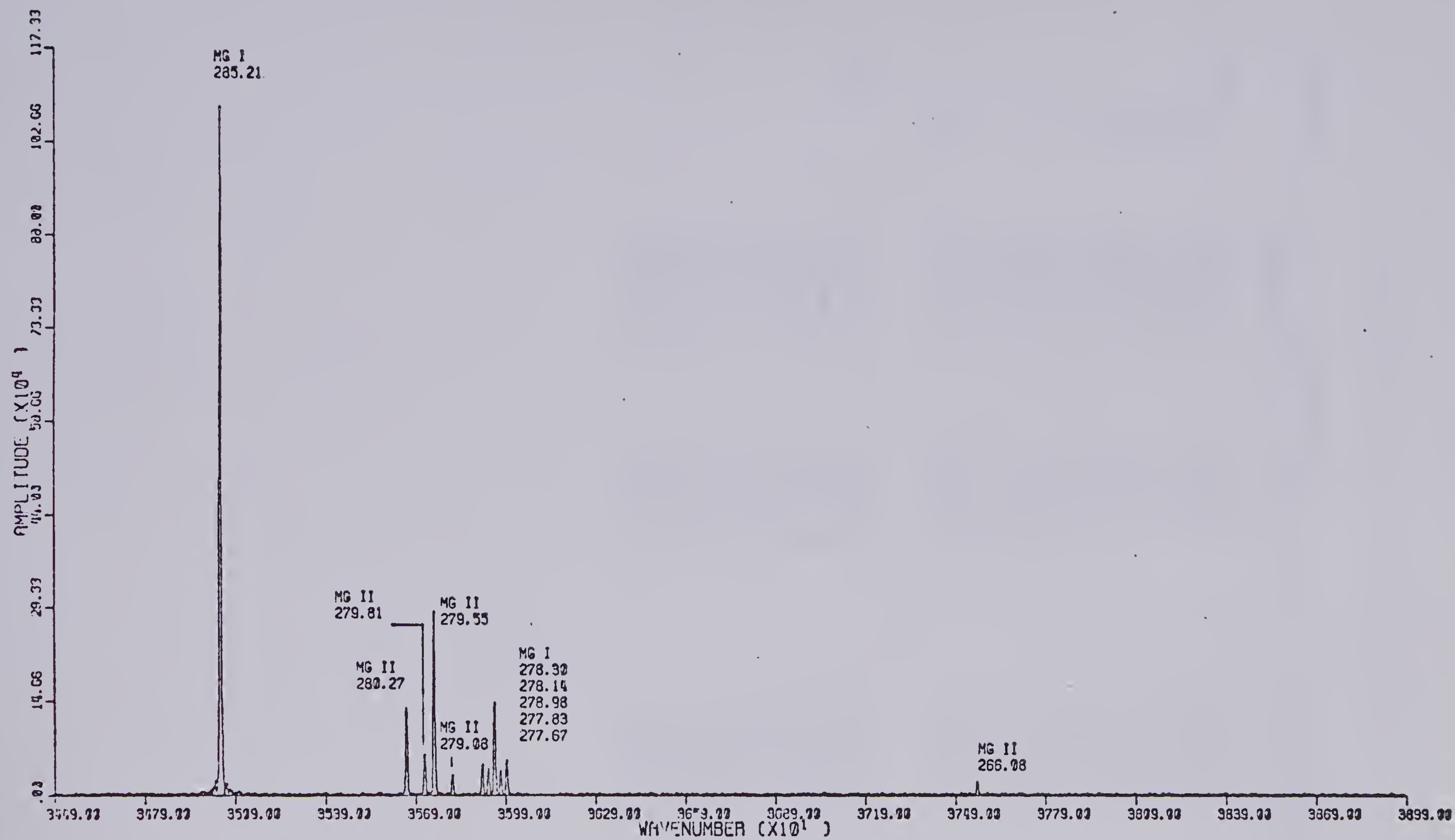

FIGURE 12. Magnesium hollow cathode lamp emission spectrum

Table II

Si and Mg H.C.L. Emission Lines

Element	Observed Wavenumber	Observed Wavelength	Literature (65) Wavelength
Mg I	35059.4	285.23	285.21
II	35777.3	280.29	280.27
II	35738.5	279.81	279.81
II	35769.2	279.57	279.55
II	35830.7	279.09	279.08
I	35931.2	278.31	278.30
I	39950.9	278.16	278.14
I	35973.4	278.98	277.98
I	35991.9	277.84	277.83
I	36014.0	277.67	277.67
II	37581.3	266.09	266.08
Si	39542.9	252.89	252.85
	39613.4	252.44	252.41
	39690.4	251.95	251.92
	39737.7	251.65	251.61
	39767.8	251.46	251.43
	39885.1	250.72	250.69
	41012.2	243.83	243.88
	41059.3	243.55	243.52
	34700.5	288.18	288.16

to resolve the neutral atom emission quintuplet at 277.8 nm. With the Mg hollow cathode lamp source, no obvious spectral limitations were observed. The second source used with the solar blind detector was the silicon hollow cathode lamp. This lamp provided a slightly more complex emission spectrum in that most of the emission lines occur at wavelengths shorter than 253.12 nm, the aliasing point. The emission line at 288 nm is the only non-aliased line present. An indication of the spectral response window available is given since according to the literature (65), one would expect to observe at least two additional silicon emission lines at 221.17 nm and 221.81 nm. These lines are not present in the spectrum even though they lie very close to the detector's peak spectral sensitivity. This implies the existence of other spectral coverage limiting factors.

The spectral emission lines from the multielement lamp, Cu, Sn, Pb, and Zn, should give additional information about the system's spectral response. The spectrum is contained in Figure 13, with the tabulations in Table III. The usually observed elemental emission lines for Cu, Sn, and Pb were found to be present, but the emission lines for Zn at 213.8 nm, 206.1 nm and 202.5 nm were noted to be absent. Also absent from the spectrum were two lead emission lines at 220.4 nm and 217.0 nm. Again an instrumental spectral response limit, other than detector imposed, is observed. This multielement spectrum does provide a good indication of the interferometer's simultaneous multielement detection

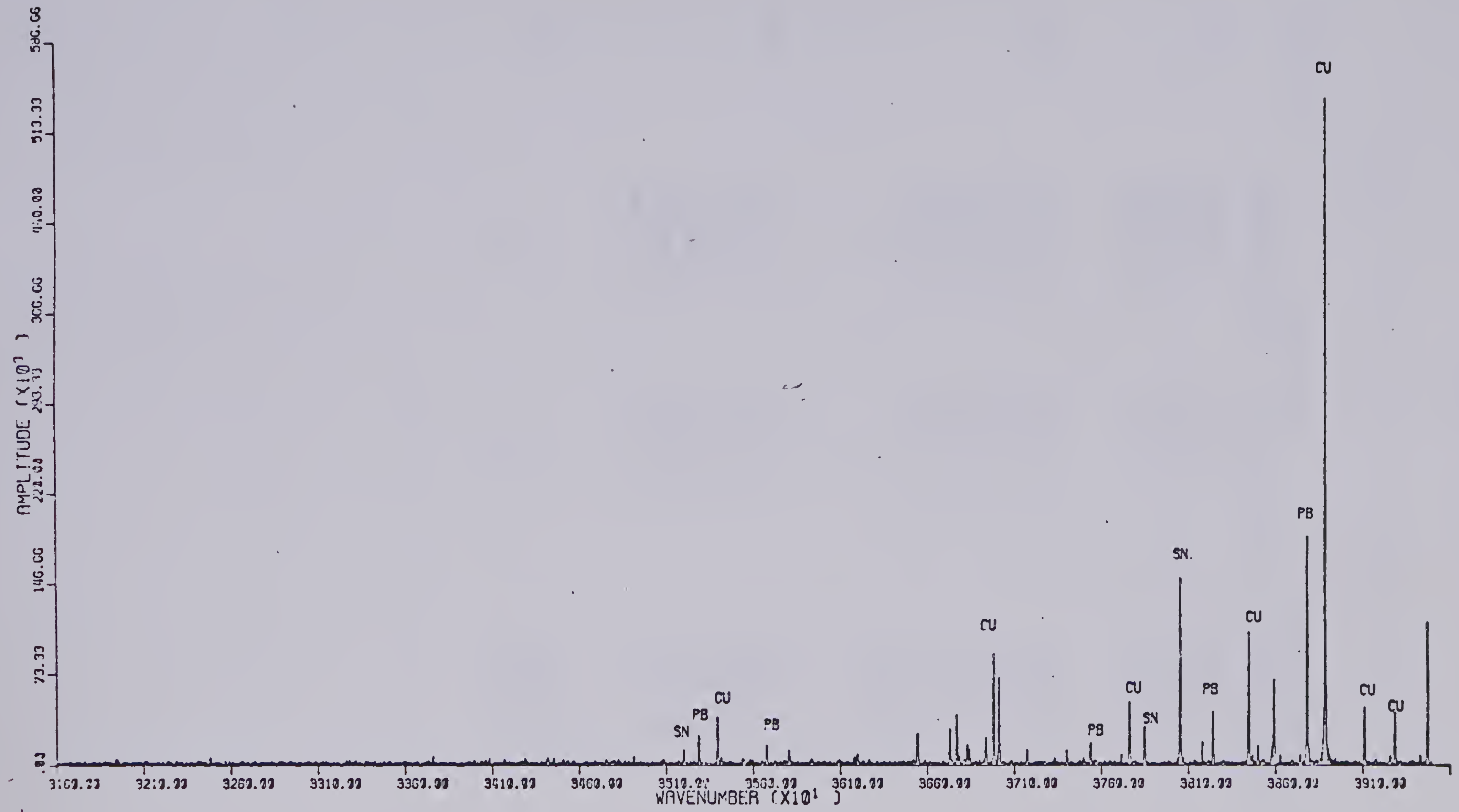

FIGURE 13. Cu, Pb, Zn, Sn hollow cathode lamp emission spectrum

Table III

Cu, Zn, Pb, Sn H.C.L. Emission Lines

Element	Observed Wavenumber	Observed Wavelength	Literature (65) Wavelength
Cu I	35403.2	282.46	282.44
I	38188.3	261.86	261.84
	40120.4	249.25	249.22
	40950.0	244.20	244.16
Pb I	35297.0	283.31	283.33
	35688.8	280.20	280.22
	37548.8	266.32	266.32
	38252.6	261.42	261.43
	38800.3	257.73	257.79
	40381.2	247.64	247.66
	--	--	220.40
	--	--	217.00
Sn I	34924.7	286.33	286.35
	35211.3	384.00	284.03
	36948.1	270.65	270.66
	38886.3	257.16	257.13
	39268.0	254.66	254.66
	40267.4	248.34	248.37
Zn	--	--	213.80
	--	--	206.10
	--	--	202.50

capability.

Fitting the interferometer with a 1P28 photomultiplier detector extends the spectral response limits to 180 nm and 650 nm. The first study with this detector involved the three elements Ca, Al, and Mg hollow cathode lamp emission source. The possible dynamic range problems became immediately evident. The hollow cathode lamps are filled with an inert gas, in this case neon, and neon possesses many intense spectral emission lines at wavelengths greater than 450 nm for example at 470.4, 470.8, 471.0, 471.1, 471.5 nm to cite a few. The emission lines of Ca, Al, and Mg were completely absent from the spectrum of Figure 14. An optical bandpass filter (Corning CS #7-51) (66) was used to isolate the spectral region from 310 nm to 420 nm approximately. The resulting filtered emission spectrum is shown in Figure 15 with tabulations in Table IV. Note that the calcium neutral atom emission line at 422.6 nm is now the dynamic range limiting factor. An expansion of this spectrum, excluding the calcium neutral atom emission line and the remaining neon emission lines, is shown in Figure 16. Note the high resolution capability present and the presence of aliasing about the 421.9 nm wavelength point.

The last hollow cathode lamp source used contained a number of components, Fe, Ni, Cr, Co, Cu and Mn, all with complex emission spectra in the 400 nm wavelength region. A spectrum is contained in Figure 17 with some of the elemental emission lines tabulated in Table V. From the spectrum, one

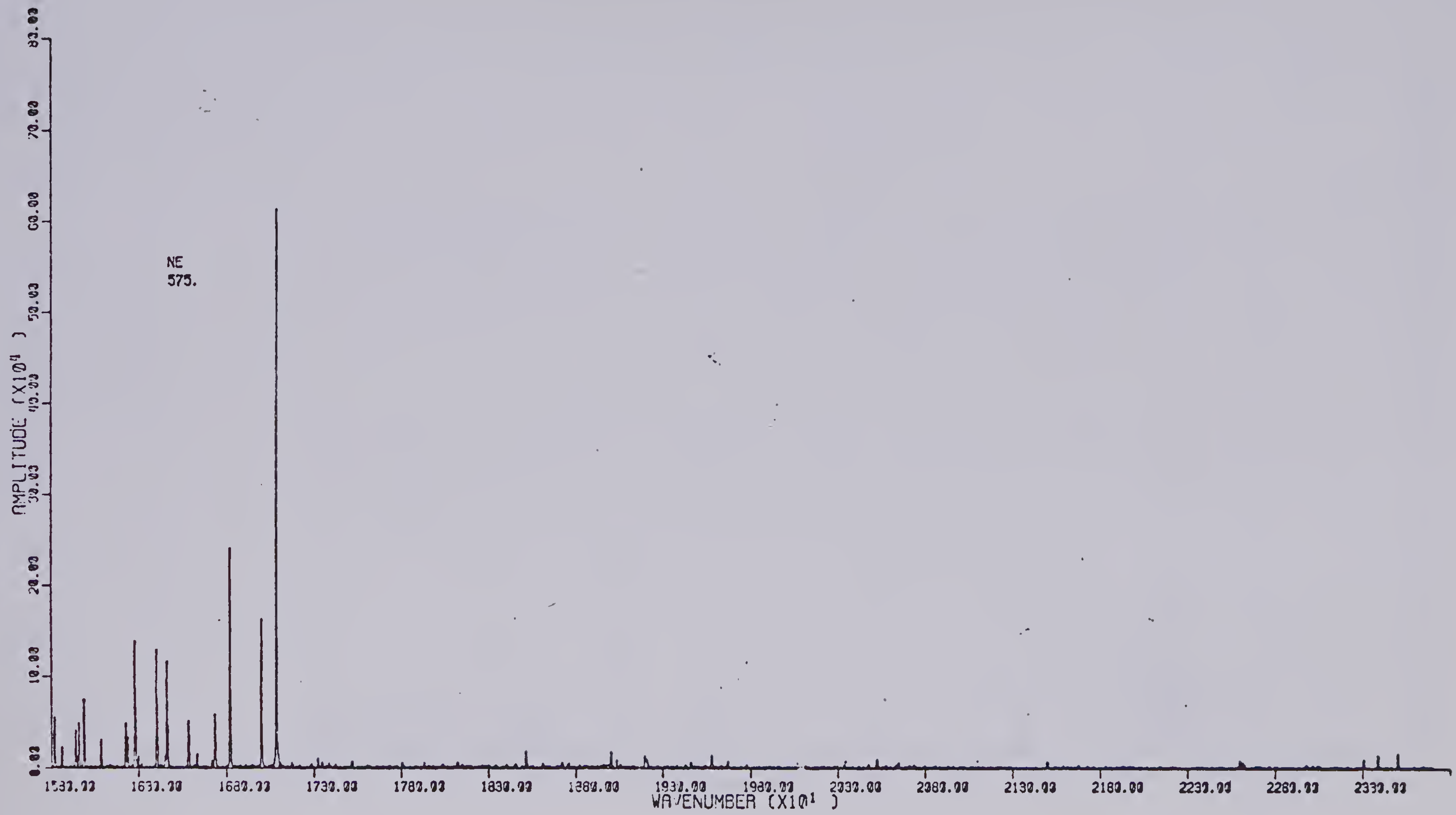

FIGURE 14. Ca, Al, Mg hollow cathode lamp emission spectrum

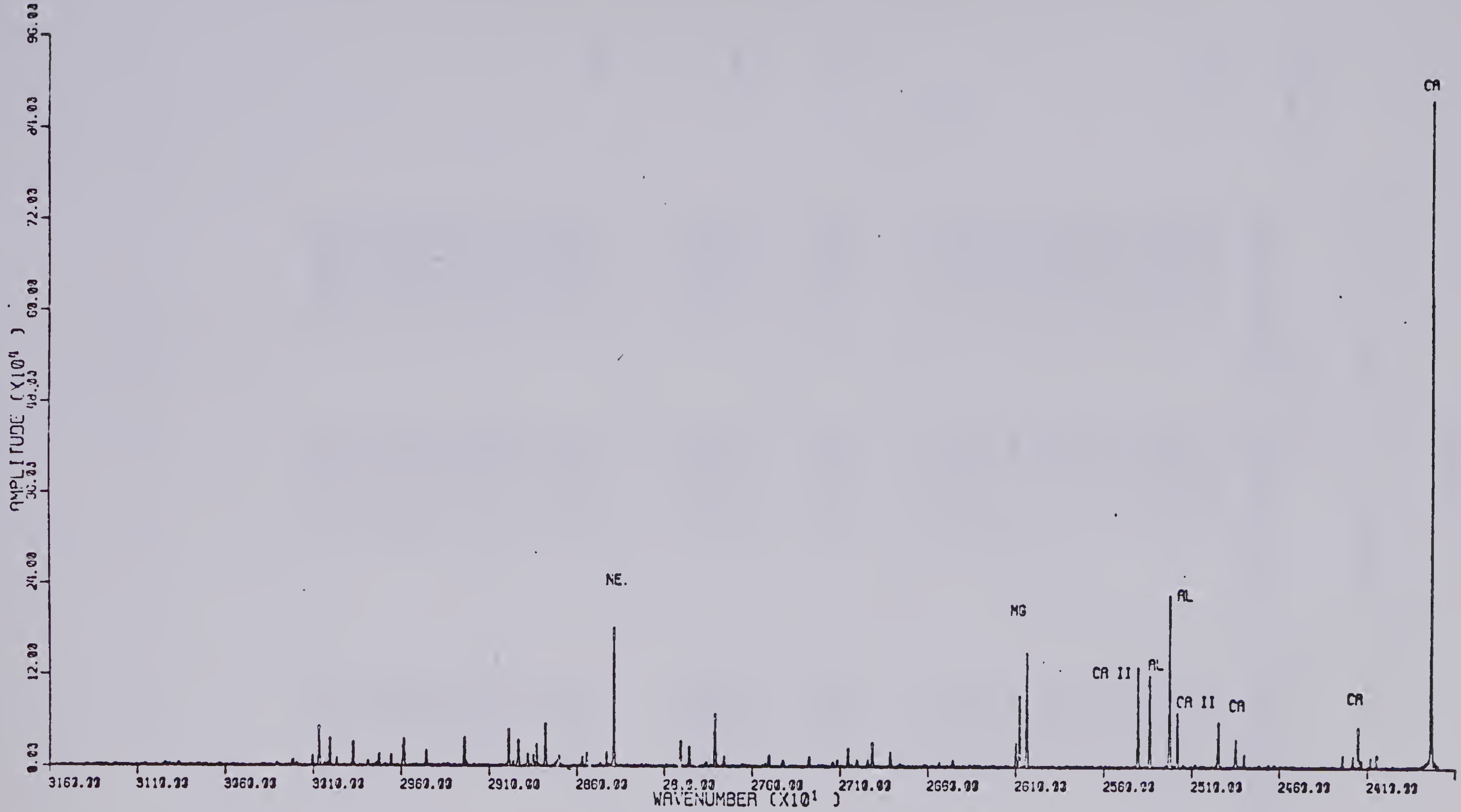

FIGURE 15. Ca, Al, Mg hollow cathode lamp emission spectrum including filter 7-51

Table IV

Ca, Al, Mg H.C.L. Emission Lines

Element	Observed Wavenumber	Observed Wavelength	Literature (65) Wavelength
Ca I	23659.8	422.66	422.67
	23347.2	428.32	428.30
	23314.4	428.92	428.94
	23243.1	430.24	430.25
	23214.1	430.77	430.77
	23156.2	431.85	431.87
	22596.7	442.54	442.54
	22548.4	443.49	443.50
	22448.1	445.47	445.48
II	22212.7	396.89	396.85
II	21990.8	393.43	393.37
Al I	25240.1	396.20	396.15
	25354.9	394.40	394.40
Mg I	26050.5	383.87	383.83
	26091.0	383.27	383.23
	26110.3	382.99	382.93
Ne	26928.4	371.36	371.31
	27067.3	369.45	369.42
	26828.1	372.74	372.71
	27289.2	366.45	366.41
	27825.6	359.38	359.35
	28402.1	352.09	352.05
	28445.1	351.56	351.52
	28794.3	347.29	347.26
	29255.4	341.82	341.77
	29672.2	337.02	336.99
	29984.8	333.50	333.49

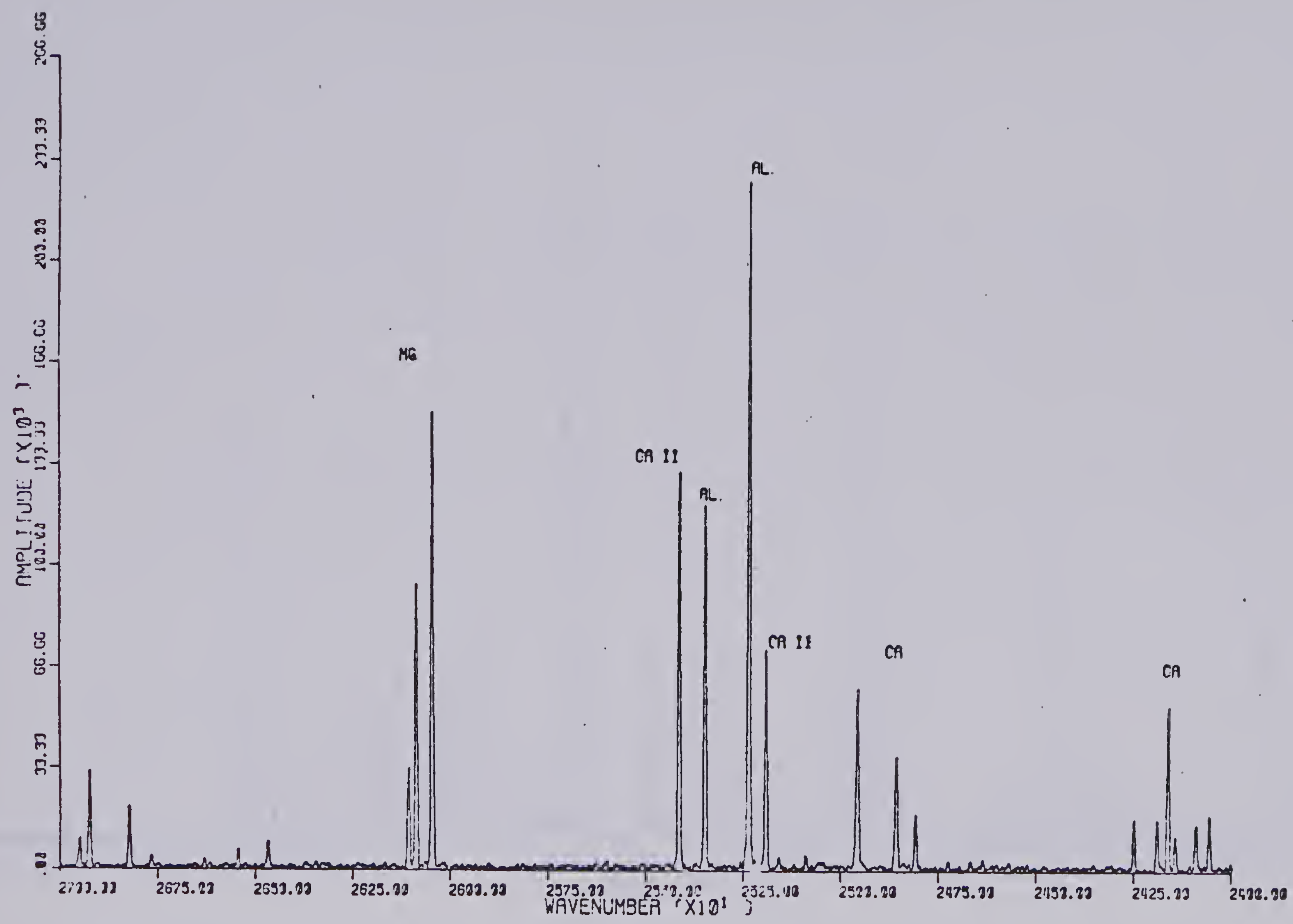

FIGURE 16. Ca, Al, Mg hollow cathode lamp spectrum expansion

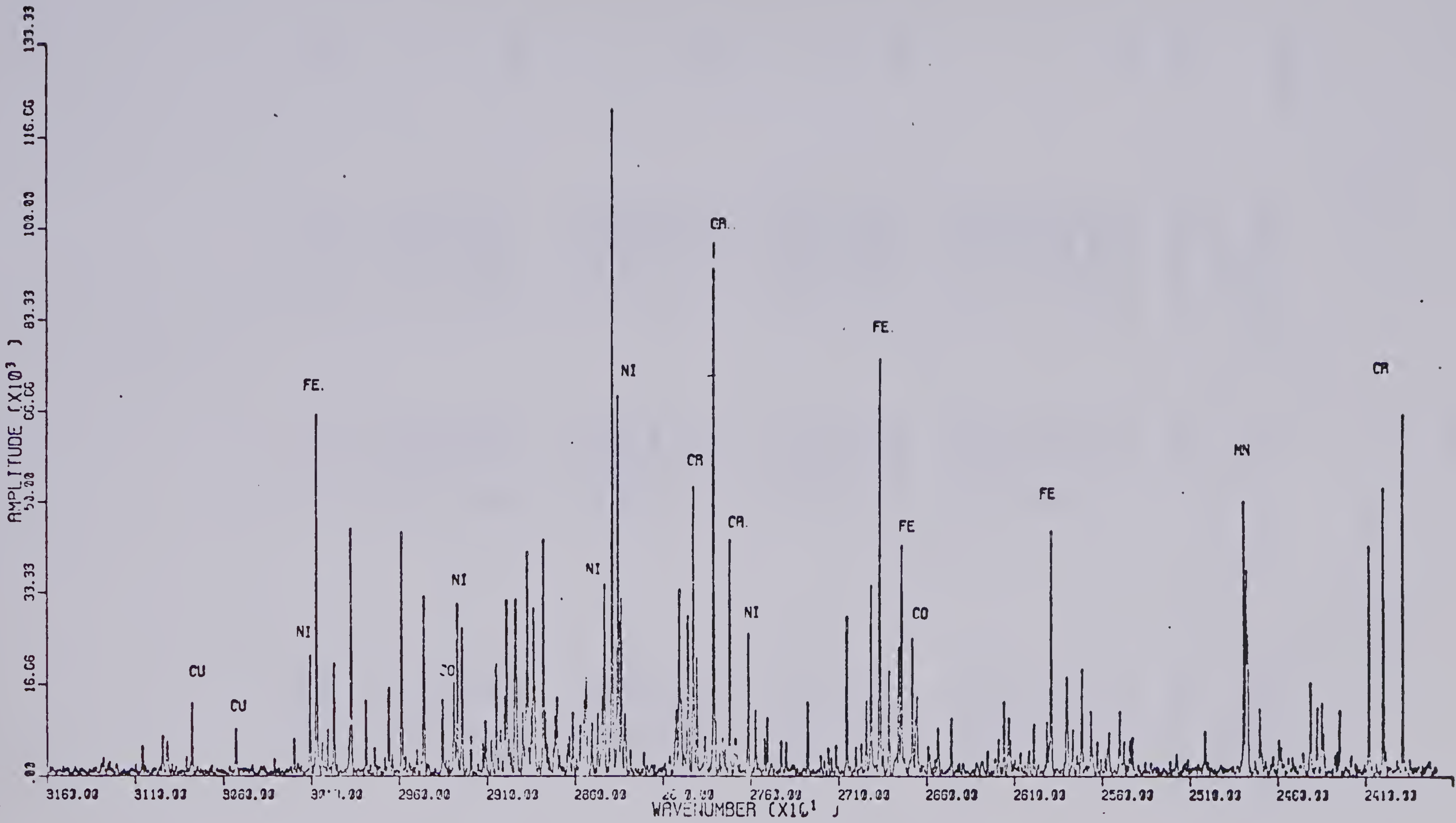

FIGURE 17. Fe, Ni, Cr, Co, Cu hollow cathode lamp emission spectrum (filtered 7-51)

Table V

Cu, Ni, Fe, Co, Cr, Mn H.C.L. Emission Lines

Element	Observed Wavenumber cm^{-1}	Observed Wavelength nm	Literature (65) Wavelength nm
Cu	30791.0	324.77	324.75
Ni	30121.4	331.99	332.03
	29284.3	341.48	341.48
	28886.7	346.18	346.16
	28628.7	349.30	349.30
	28447.1	351.53	351.50
	28371.7	352.46	352.45
	27626.6	361.97	361.94
Fe	30085.1	332.39	332.38
	29805.4	335.51	335.52
	27972.0	358.14	358.12
	26880.3	372.02	371.99
	26772.3	373.52	373.49
	26756.6	373.74	373.71
Co	29367.7	340.51	340.51
	29302.3	341.27	341.23
	28952.8	345.39	345.35
	28852.5	346.59	346.58
	28330.4	352.98	352.98
	24261.8	412.17	412.13
Cr	27941.5	357.89	357.87
	27825.7	359.38	359.35
	27734.6	360.56	360.53
	23312.7	428.95	428.97
	23393.3	427.47	427.48
	23507.3	425.40	425.43
Mn	24807.7	403.10	403.08
	24792.4	403.35	403.31

can see the vast number of lines present and, in no way, was an attempt made to assign all of the lines. The same optical filter as used in the previous section was employed again to eliminate the high intensity neon emission signals above 450 nm. The important observation to make from this spectrum is the interferometer's capability for multielement, multiple line detection capability.

D. Conclusions

The use of hollow cathode lamps as atomic emission sources definitely show the simultaneous multiline detection capability of the interferometer system. The spectra are of high resolution and high wavelength axis accuracy although aliasing complications do exist. The interferometer's dynamic range problem was well illustrated and a solution to such a problem was offered through optical filtering of the incoming signal. This may or may not be viable in all situations, depending on the proximity of the line of interest and the range limiting emission line. There appears to be a lower wavelength system sensitivity of about 240 nm. This is most likely due to the germanium beamsplitter no longer acting as a beamsplitter at these low wavelengths. Depending upon the emission wavelengths of interest this may or may not be a severe limitation. Overall the interferometer based atomic emission system appears very promising for simultaneous multielement analysis. Let us now proceed to further studies using various atomic emission sources.

CHAPTER IV

THE APPLICATION OF FOURIER TRANSFORM SPECTROSCOPY TO FLAME ATOMIC EMISSION SPECTROSCOPY

A. Introduction

Flame atomic emission methods have been used for many years in the analytical determination of a wide variety of elements due to their accuracy, precision, ease of use and economy. Although out of date with respect to instrumentation, the text "Flame Spectroscopy" by Mavrodineanu and Boiteux (3) gives an excellent overall view of flame emission spectroscopy. More recent review articles include that of Pickett and Koirtyohann (67). Many publications occur every year on varying aspects of flame emission and the reader is referred to the "Fundamental Reviews" published every two years by "Analytical Chemistry" (2).

Through the use of flame atomic emission sources for the interferometer based detection system it is hoped to evaluate the feasibility of such a system under actual operating conditions. Preliminary work was completed by Yuen and Horlick (26) with the air-acetylene flame system. The current studies involve further quantitative studies with the air-acetylene flame and the addition of a nitrous oxide-acetylene flame to the system. Overall qualitative and quantitative aspects of both flame sources will be studied with special emphasis upon the spectral distribution of noise due to the system's multiplex nature.

B. The Experimental System

The basic F.T.S. flame emission system consists of three sections: the flame nebulizer-burner support assembly, the collimating optics and interferometer, and the data acquisition and processing system. The latter two systems have been previously discussed in Chapter II and elsewhere (29). The flame system employed a Varian Techtron manual gas flow control box and a Varian Techtron nebulizer-burner support assembly, both from the model AA6 spectrophotometer. Two custom burner heads were made, one for the air-acetylene flame and one for the nitrous oxide-acetylene flame. The standard ten centimeter slotted burners could not be used due to the large amount of flicker present. The interferometer system ideally requires a stable point source of emission due to the collimated light requirements of the interferometer, as previously discussed in Chapter I. The burners used were designed after those of Aldous (68) and were manufactured in the departmental machine shop. Further discussion of the criteria for safe burner design is available in the literature (69,70) and will not be dealt with in this thesis. The air-acetylene flame burner consists of an array of approximately sixty 1.0 mm inside diameter stainless steel capillary tubes epoxied side by side into a 1.5 cm inside diameter stainless steel sleeve. The capillaries project about 5 mm above the top of the sleeve. The top surface of the capillaries was flattened. This burner actually provides a very stable array of sixty individual flames, one from each

capillary tube, of about 30 cm in height and 20 mm in diameter. For the air-acetylene flame, at normal flow rates, the flame appeared as a solid tall cone. The nitrous oxide-acetylene burner was similarly constructed with the exception of the use of smaller diameter, 0.5 mm I.D., stainless steel capillary tubes. This was necessary in order to provide the high gas flow velocity required to exceed the relatively high burning velocity of this flame. The resulting flame appeared rather exciting, about 100 cm in height and 15 mm in diameter. The characteristic red feather zone occurred at a maximum of 1.0 cm above the burner top. The individual capillary flames were actually visible with the high flow velocities used, and so the flame did not appear as a solid tall cone. The presence of these individual flames may have contributed to the somewhat imprecise results obtained for the quantitative work done with this flame.

The burner heads were also outfitted with an outer collar about 5.0 cm in total diameter and 3.5 cm in height. The top surface of the doughnut shaped collar was level with the top of the burner head, when fitted onto the burner and provided about one hundred pin hole exits for a sheathing gas to surround the flame. The sheathing gas served two purposes, one of which was to provide increased vertical stability for the flame. Both the air-acetylene and nitrous oxide-acetylene flames were very susceptible to fluctuations produced by air drafts in the immediate area. In this system a high flow rate of nitrogen sheathing gas was employed to

encircle the flame and reduce the effects of such drafts. A thorough study of the effects of flame sheathing, either with an inert gas or a quartz cylinder, on the spectral noise present has been carried out by Hieftje and Bystroff (71). They reached two conclusions: the background emission due to species entrained from the surrounding atmosphere is greatly reduced and the flame fluctuation noise is greatly minimized. Agreement was found experimentally for both conclusions in this work. The decrease in emission due to air entrainment was especially evident in the case of calcium emission in an air-acetylene flame. The sheath helped to maintain the major region of calcium emission within the central zone of the flame and it helped to reduce the amount of calcium oxide formation. These results were observed qualitatively as opposed to a detailed quantitative study. Other studies have been done on the effect of inert gas flame sheathing upon the temperature profile of the flame. These studies, carried out by Kirkbright and Vetter (72), lead to the conclusion that the temperature profile in the most analytically useful regions of the flame did not change with sheathing. No quantitative experimental work was undertaken in this current study to either confirm or disprove any of the above conclusions. In our case the flame sheath gas served another minor role, that of maintaining the burner head in a cool state. It was found that after prolonged operation, especially in the nitrous oxide-acetylene flame, the burner head became very warm, as well as the nearby

safety shield and fume hood. The nitrogen sheath also provided a shield between the 6.6" focal length off axis parabolic mirror used for light collimation and the flame. For all of the above reasons, flame sheathing was employed in all of the experiments to follow.

C. The Air-Acetylene Flame Emission Source

The air-acetylene flame is one of the most widely used flames in atomic spectroscopic analysis due to its ease of use and economy. The relatively low temperature of this flame, approximately 2000°C, offers only a limited amount of thermal energy to achieve the elevation of an atom from a ground state to an excited state. For this reason, and due to the relatively high background emission of this flame, it has been primarily used as an atomization source in atomic absorption spectroscopy. In spite of the limited excitation energy available, the neutral atom species of the alkali metals can be induced to emission as well as some of the oxides of the alkaline earth elements such as calcium. A detailed review of the emission characteristics of this flame is available in the literature (3, 5). Qualitative studies as well as a limited quantitative study, have been carried out previously with the combination of the air-acetylene flame and the Fourier Transform spectrometer (26). Therefore, the major emphasis in the work following is on the quantitative aspects of this system for atomic emission analysis. The flame was

studied with two detectors having different spectral responses: a silicon photodiode and a 1P28 photomultiplier tube.

1. The Silicon Photodiode as a Detector

The spectral window from 400.0 nm to 1000.0 nm provides the majority of the emission information available from the air-acetylene flame. It was therefore deemed appropriate to initiate the interferometer flame emission studies with a silicon photodiode detector having a peak response at 850 nm and extending to a lower limit of 400 nm and an upper limit of 1050 nm (ENL Si photodiode, type 626) (73). The background emission spectrum of the air-acetylene flame, with water aspirating into the flame, is contained in Figure 18. The instrumental settings for the work in this section are listed in Table VI. Unless otherwise stated these parameters were maintained. The characteristic band-head of the near infrared water emission is labelled in the spectrum. This band does not become a limiting factor under normal experimental conditions and is visible in the spectrum only due to a very high gain applied to the detector output. The complete emission spectrum of a 30.0 ppm LiCl aqueous solution is shown in Figure 19. Twenty-five interferograms were signal averaged and transformed to obtain the emission spectrum. The signal from the 30.0 ppm lithium emission completely filled the data acquisition system dynamic range. Corresponding portions of the emission spectrum at the same instrumental settings, of

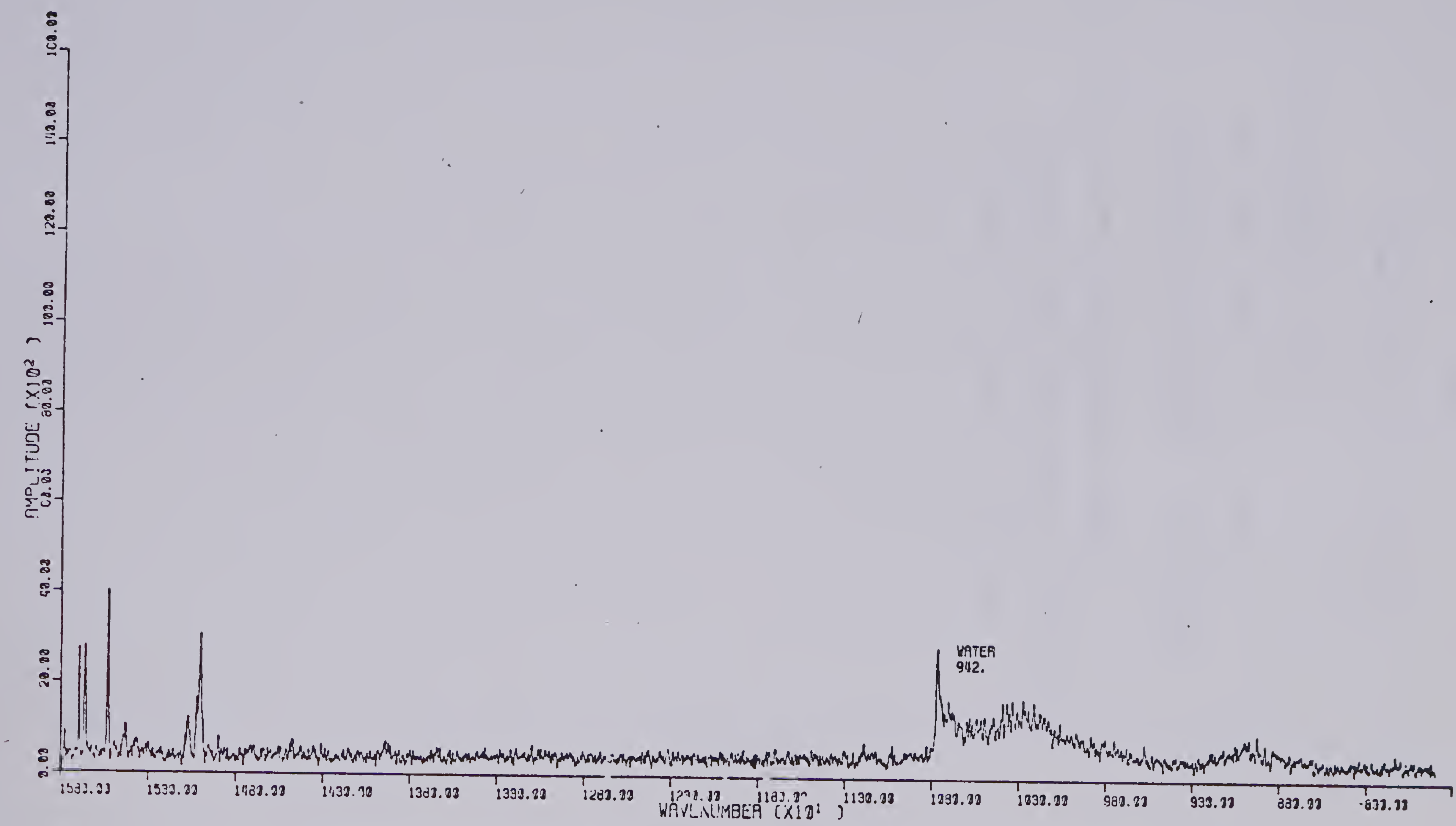

FIGURE 18. Air-acetylene flame emission background--silicon photodiode detector

Table VI

Flame Operating Conditions

1. Air-Acetylene Flame

   Air Flow Rate: ~5.0 l/min.

   Acetylene Flow Rate: ~2.4 l/min.

2. Nitrous Oxide-Acetylene Flame

   Nitrous Oxide Flow Rate: ~12. l/min.

   Acetylene Flow Rate: ~4. l/min.

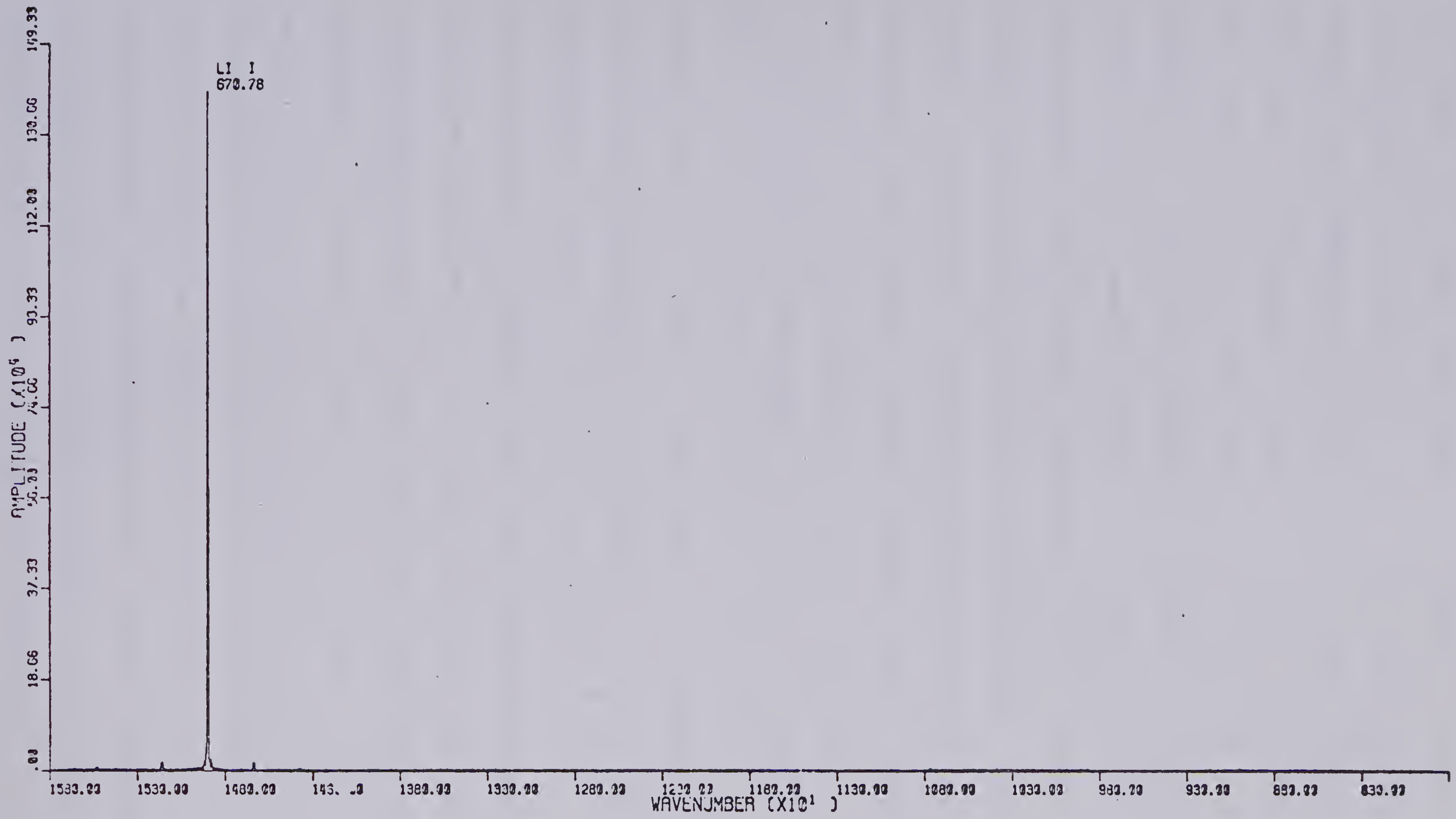

FIGURE 19. Air-acetylene flame emission of 30.0 ppm LiCl

a 30.00, 1.00, and 0.03 ppm LiCl aqueous solution are illustrated in Figure 20. Note that the spectral amplitude scales are expanded and that each of these spectra is now the spectral average of six, twenty-five scan interferograms. The complete analytical curve, based upon the lithium peak height at 670.8 nm is shown in Figure 21. Note that the linear dynamic range extends over three orders of magnitude. The arrows indicate 95% confidence levels based on the six repetitions completed at each concentration. The dynamic range is excellent considering the silicon photodiode detector alone rarely reaches such a linear dynamic range. The best fit linear equation for the curve has a slope of 1.12±0.02 and an intercept of 4.55±0.02 on the log-log plot. The overall standard deviation is 0.074 with a correlation coefficient of 0.9980. The signal to noise ratio for the 30.00 ppm lithium peak is 109, while it is 8.2 for the 0.03 ppm lithium peak. In Figure 22 a log-log plot of the lithium peak amplitude standard deviation versus the peak amplitude is shown in curve "A". It may be easily seen that a direct relationship exists between the peak amplitude and the standard deviation or noise on that peak. Curve "B" of the same plot shows the mean standard deviation values at four wavelengths, located away from the lithium emission peak, plotted versus the lithium peak amplitude. If the multiplex nature of the interferometer does indeed evenly distribute the noise across the spectral domain, there should be a definite relationship between the two curves. In fact, the

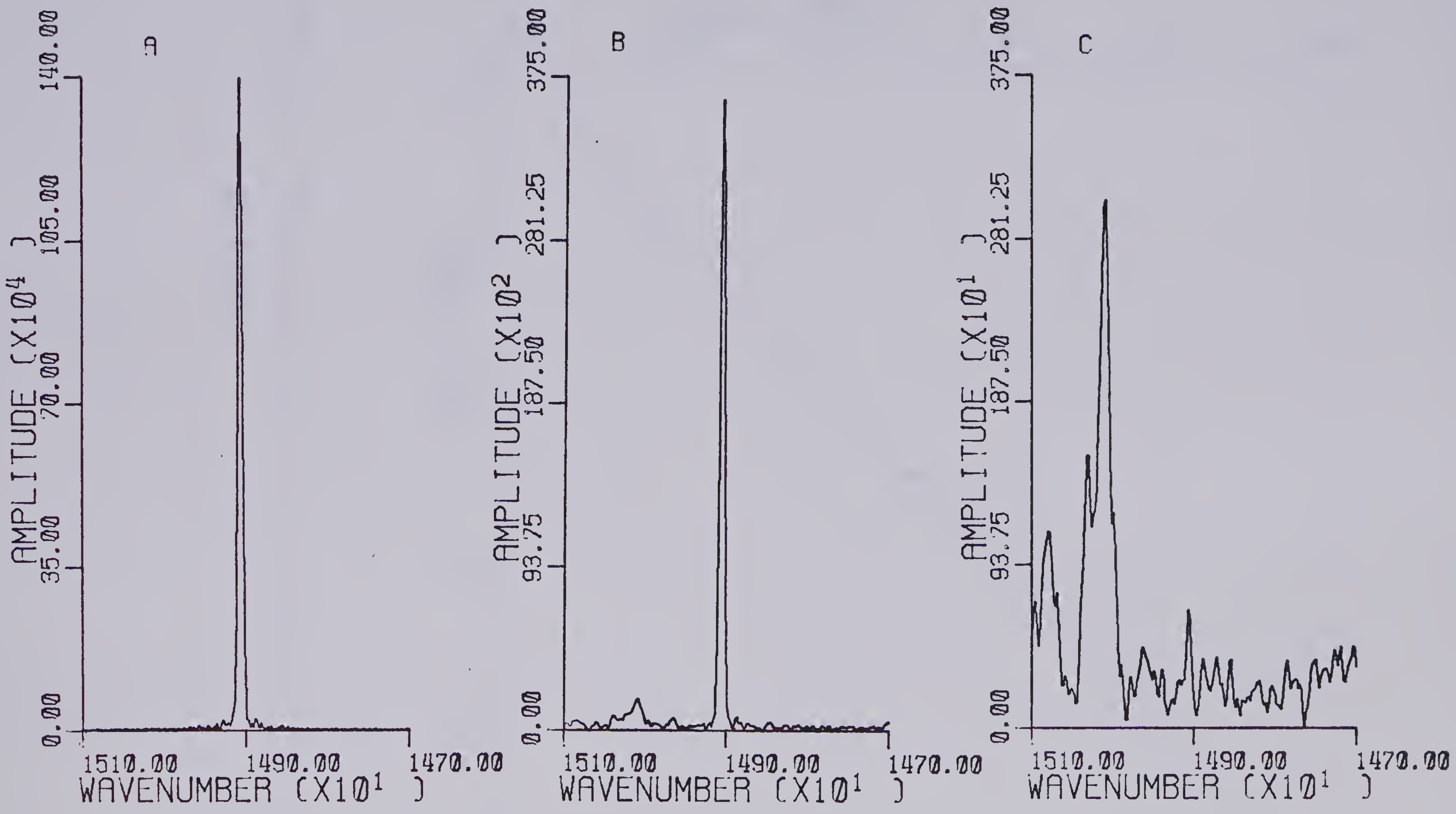

FIGURE 20. Air-acetylene flame emission of: (A) 30.0 ppm Li, (B) 1.0 ppm Li, (C) 0.03 ppm Li

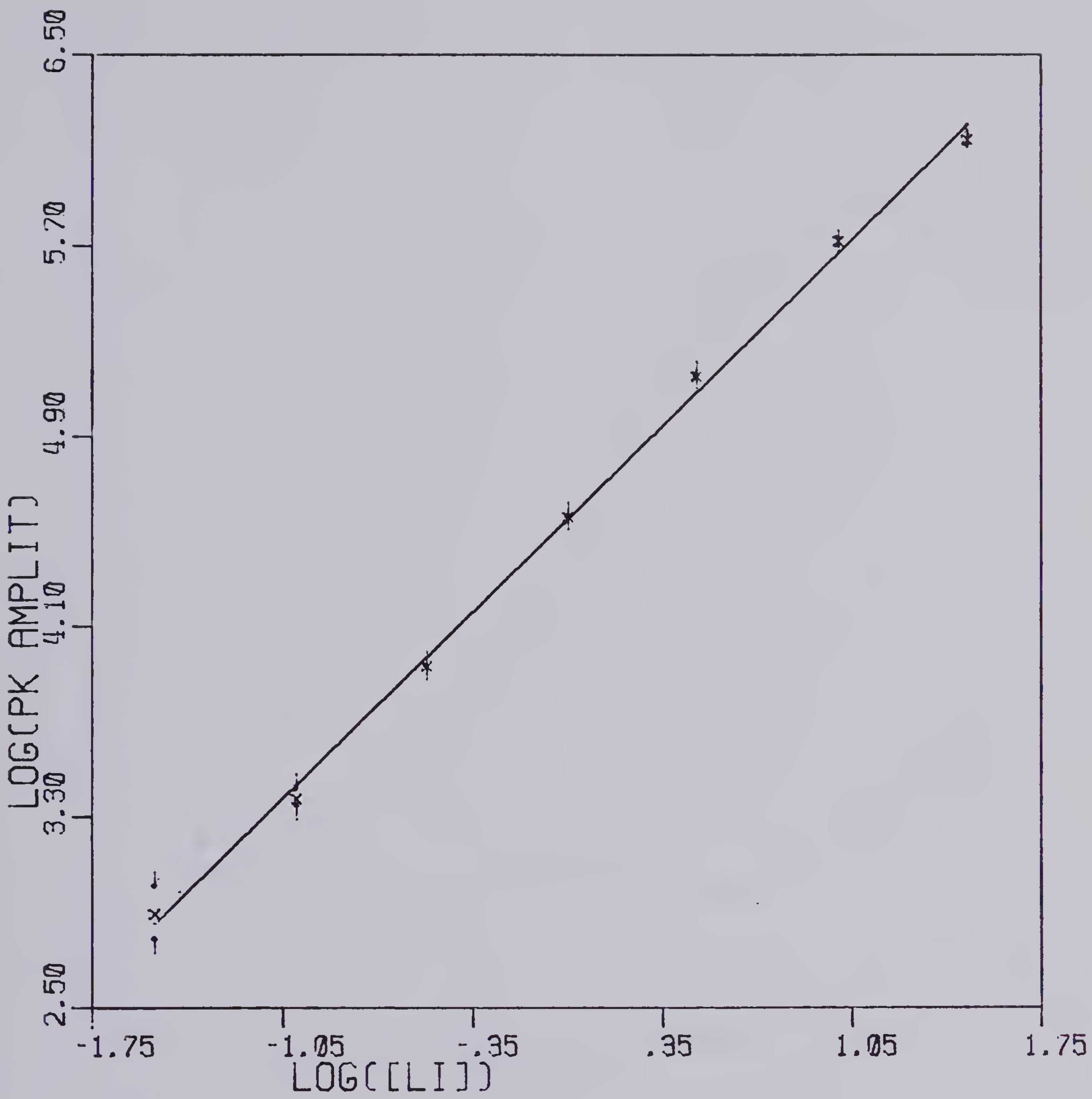

FIGURE 21. Analytical curve for Li flame emission 0.03 to 30.0 ppm

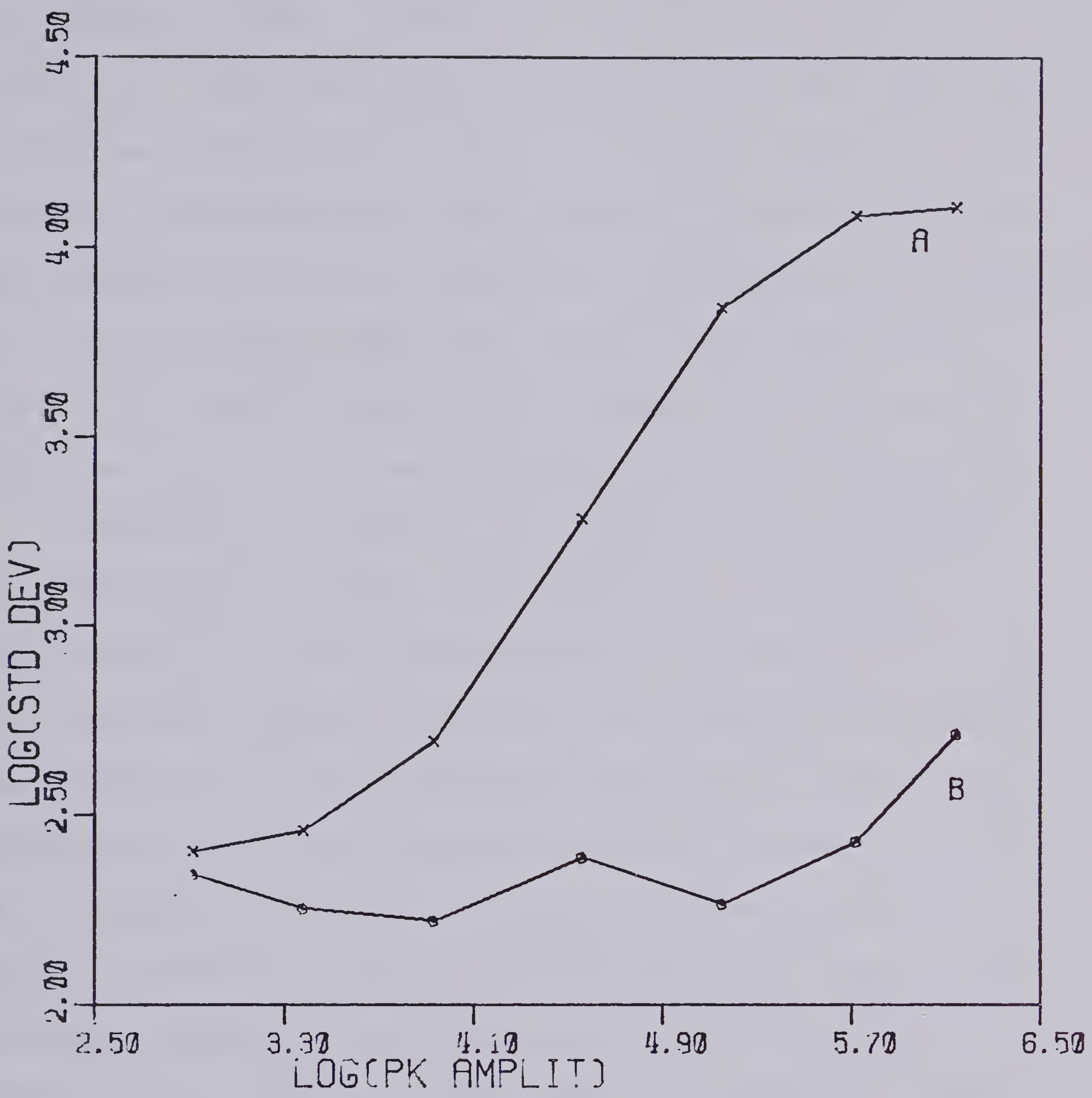

FIGURE 22. Standard deviation vs. Li peak amplitude

(A) Li peak standard deviation

(B) Baseline standard deviation

curves should be identical! Any increase or decrease in amplitude of curve "A" should at least be mirrored by curve "B". From this plot it demonstrates that noise may indeed be localized on a peak, just as in the case of a scanning monochromator-based detection system. The mean amplitude values for the same four wavelengths are plotted on a log-log plot versus the lithium peak amplitude in Figure 23, indicating no large increase in the emission baseline value as the emission peak amplitude increases.

Returning to curve "A" in Figure 22 three distinct portions become visible. The portion of the curve at low peak amplitude with a slope near zero indicates the presence of a constant level background noise probably originating in the detector or its associated electronics. The sloping portion of the curve indicates a steady increase in noise with emission intensity a situation characteristic of a source fluctuation noise limited system. At high lithium emission intensity the curve again flattens indicating the presence of a constant noise level independent of emission intensity. Photodiode saturation is not indicated since analytical curve response is still linear within this concentration range. This curve was reproducible over several experiments and no detailed explanation could be provided for its behaviour at high concentration values. For the situation of a single frequency atomic emission, such as in the lithium case, the combination of an air-acetylene flame and an interferometer equipped with a

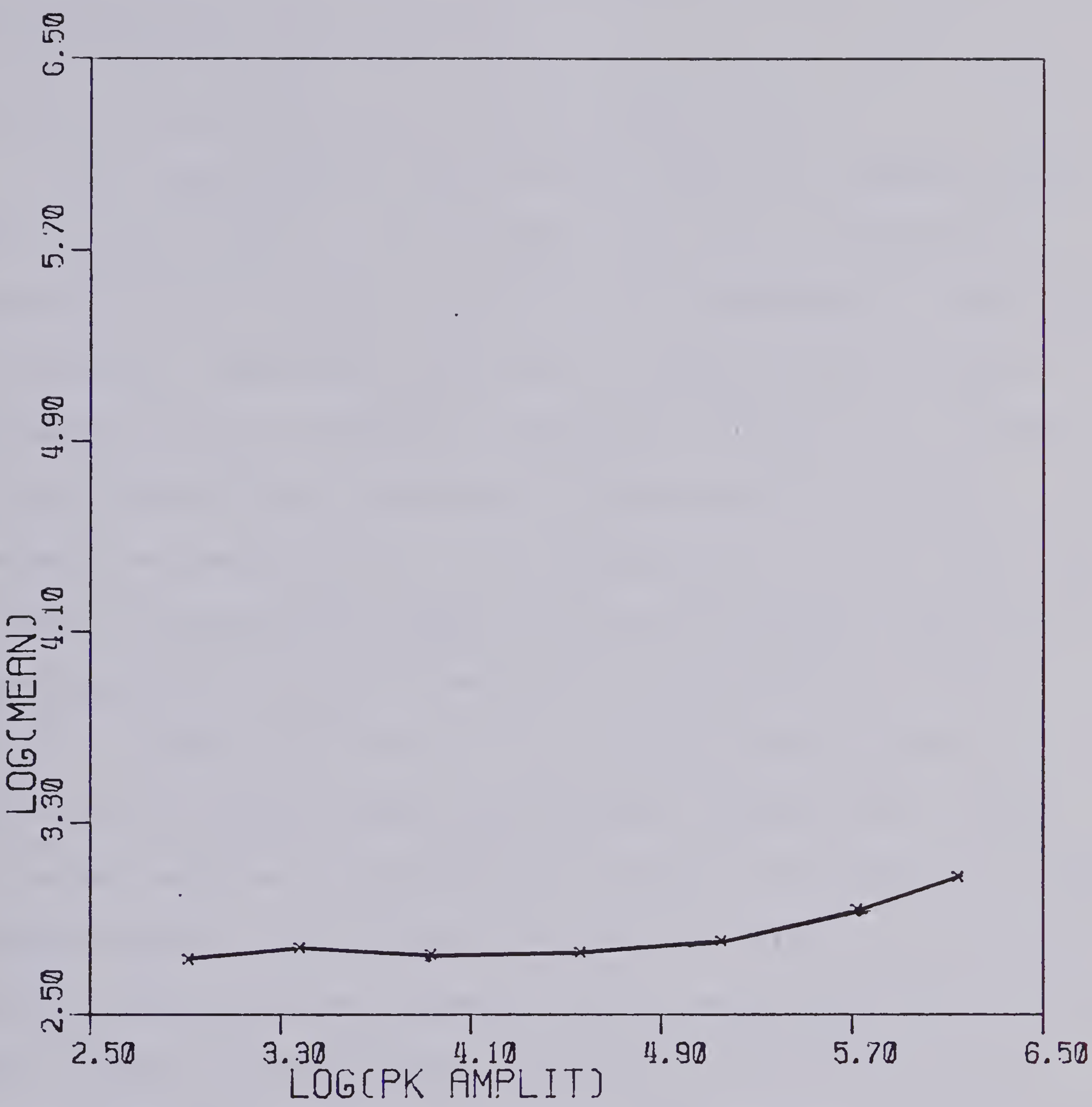

FIGURE 23. Baseline mean value at four different wavelengths vs. Li peak amplitude.

silicon photodiode detector has proved to be acceptable as a quantitative analysis unit.

2. Multiple Element Detection Capabilities

The simultaneous multielement detection capability of the interferometer system offers some very interesting possibilities in the area of clinical chemistry. Often in a clinical laboratory the serum or urine levels of many elements must be carefully monitored (74,75,76). In most laboratories this is currently accomplished with ion selective electrodes or flame photometry, neither technique offering the desired simultaneous multielement capability. Morrison has used an intensified target silicon silicon tube in combination with a flame spectrometer system to provide the simultaneous multielement capability (74,75). A second approach is available with the interferometer based spectrometer. Due to the wide spectral range covered with high resolution many elements may be monitored simultaneously. For example, an experiment was done to monitor the blood serum levels of sodium, potassium and lithium simultaneously. Normal physiological blood serum levels for sodium range from 3000 ppm to 4000 ppm and the corresponding range for potassium is 100 ppm to 300 ppm. Lithium is not normally present in blood serum, but it is used in the treatment of manic depressives in the therapeutic range of 0.01 ppm to 20.0 ppm (74). The lithium level must be carefully monitored since the serum toxic level is 25.0 ppm. The previous study in this chapter indicated that lithium, alone in solution, may be analytically determined success-

fully using an interferometer-based system. What happens to this determination if only two of the other elements present physiologically, sodium and potassium, are also present in the solution? Can all three elements be simultaneously, quantitatively determined?

An aqueous solution containing 20.0 ppm Li, 35.0 ppm Na and 2.0 ppm K was aspirated into the air-acetylene flame. A portion of the resulting spectrum is shown in Figure 24. The concentrations of sodium and potassium represent a one hundred fold dilution of the serum. Note that the level of lithium is still at a high, nearly toxic level without dilution. The interferometer system obviously cannot be used for the lithium analytical determination in the presence of sodium and potassium, at physiological levels, due to the dynamic range problem discussed in Chapter I. The addition of other commonly found elements in serum, such as calcium, would make the situation even worse. Calcium is normally present in the range of 100 ppm in blood serum.

The second question asked whether the sodium and potassium could be determined simultaneously with the flame interferometer system. The simultaneously determined analytical curves are presented in Figure 25. It must be noted that an internal standard had to be used in order to obtain reasonable linearity. The 20.0 ppm Li line was successfully used. This nicely illustrates another capability available with the interferometer-based flame system. The internal standard is automatically monitored through the

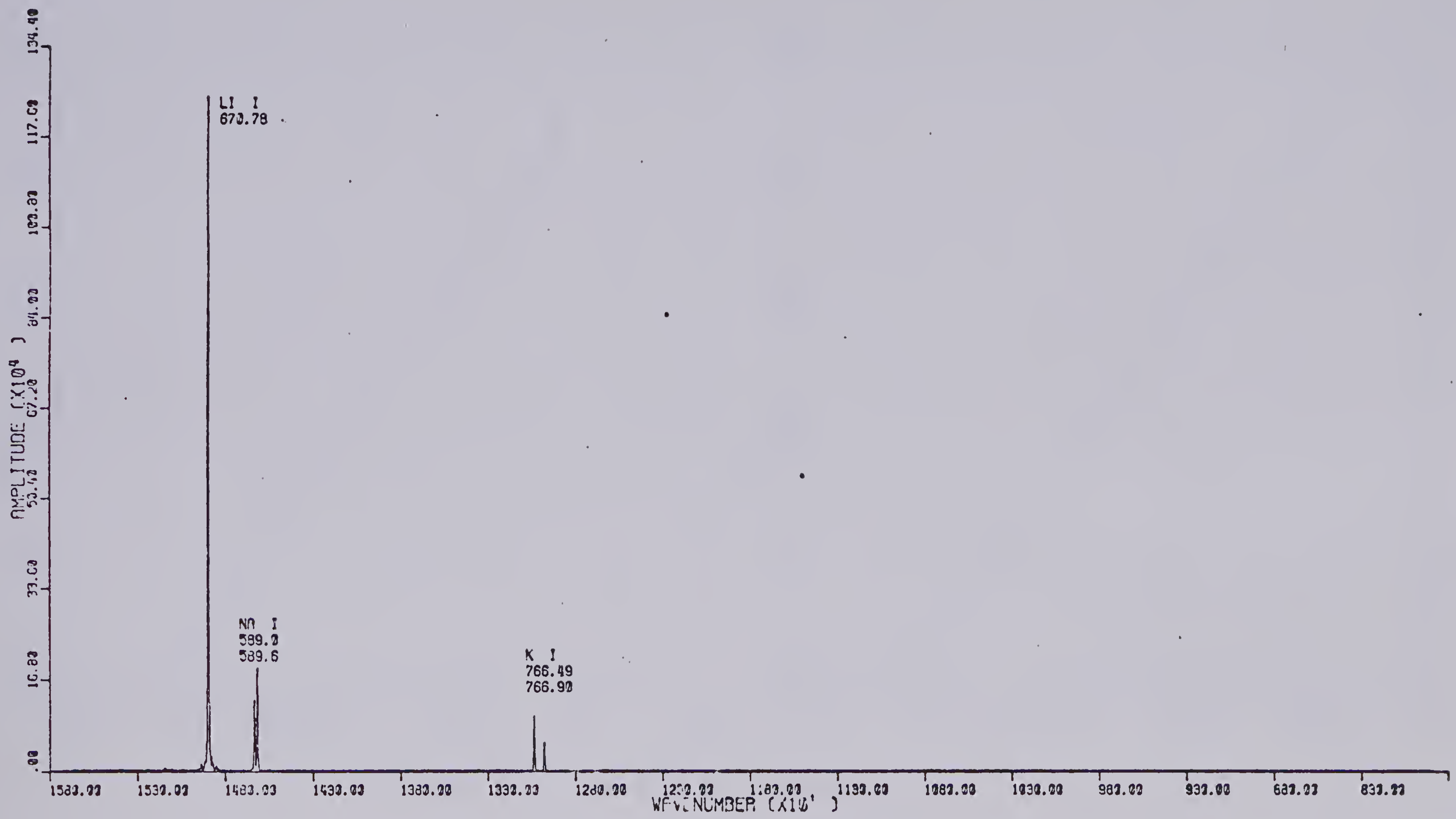

FIGURE 24. Flame emission spectrum of Li, Na, K.

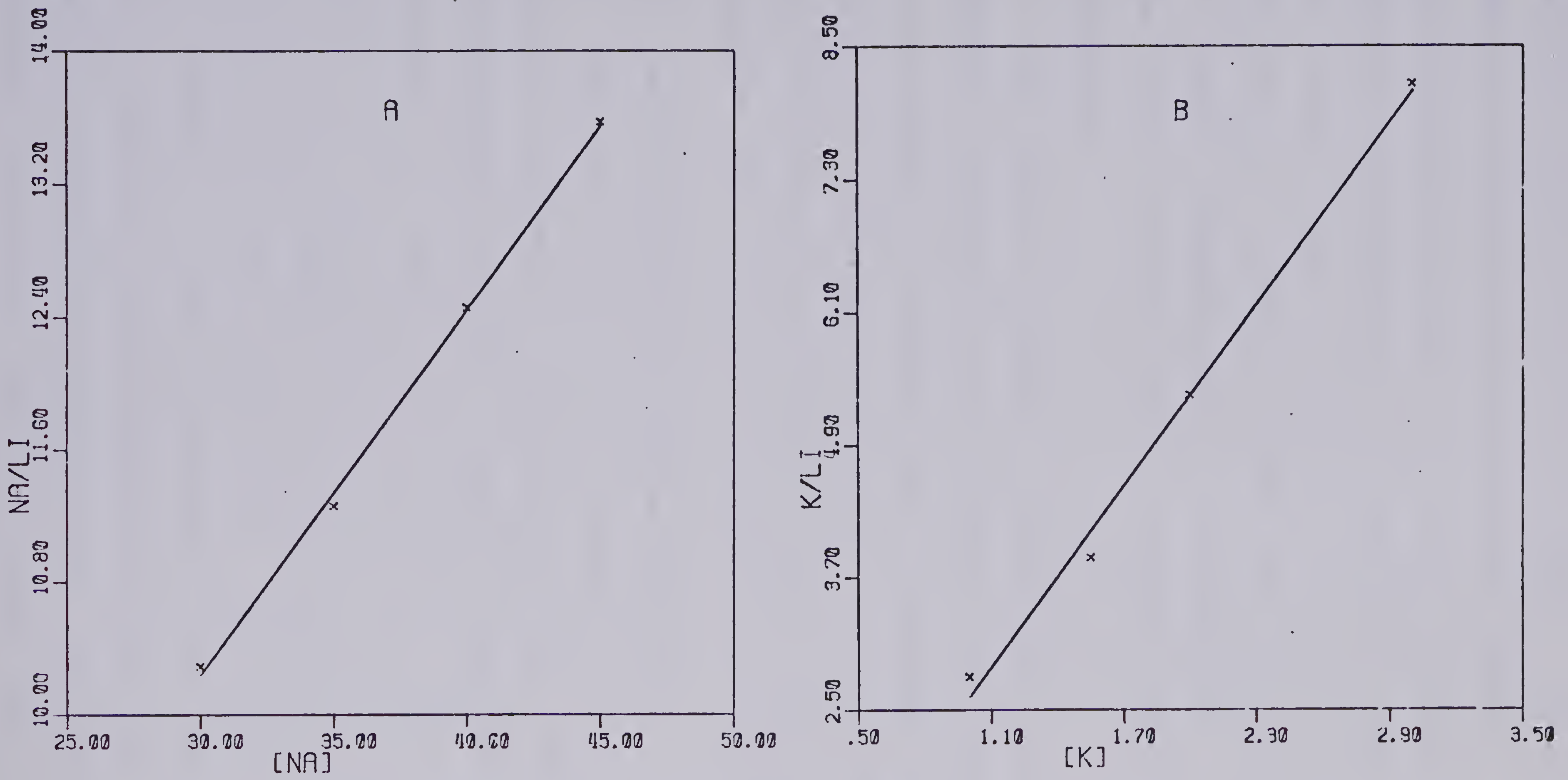

FIGURE 25. Analytical Curves

(A) sodium 30.0 to 45.0 ppm

(B) potassium 1.00 to 3.00 ppm

multiplex nature of the interferometer. The standard line must, of course, be within the spectral response range of the interferometer detector. An internal standard is often necessary with sources of low stability in order to account for changes in the analyte signal due to the source fluctuations. A word of caution must be noted in the use of internal standards with an interferometer. Do not allow the internal standard signal to become a dynamic range limitation.

The spectral response of the photodiode very quickly becomes a limitation if one wishes to simultaneously monitor a wide variety of elements such as magnesium, manganese, calcium and chromium to name a few. The spectral response of a 1P28 photomultiplier tube offers a much wider spectral coverage, particularly in the shorter wavelength regions.

3. The Photomultiplier Tube as a Detector

Further work with the air-acetylene flame emission involved the use of a photomultiplier tube (1P28) as the interferometer detector in order to extend the spectral response more towards the ultra violet. The spectral window now simultaneously available extends from 240 nm to 650 nm as opposed to the rather restricted range of the silicon photodiode in the visible. The lower spectral limit is a function of the interferometer rather than the detector. It is suspected that the germanium beamsplitter no longer acts as a beamsplitter below 240 nm. The photomultiplier tube was operated at 400.0 volts from a Heath EU-7-1-30 power

supply. Refer to Chapter II for details concerning the photomultiplier dynode chain modifications. A Princeton Applied Research Corporation low noise preamplifier was used for any further signal amplification necessary. The bandwidth of this preamplifier was set to isolate the frequency range 300 Hz to 10 KHz.

The air-acetylene flame background, as seen with this detector, is shown in Figure 26. Note the characteristic Swann Bands as labelled. As before, the flame background emission is not a limiting factor in quantitative work.

Calcium was chosen as an analyte to study with the flame interferometer system and the 1P28 detector, due to the presence of both broadband and neutral atom line emission within the spectral window available. Calcium will also provide a good element for inter-source comparison between the flames and the plasma due to its ability to undergo emission as an oxide, a neutral atom and an ion depending upon the energy available. The complete calcium emission spectrum in an air-acetylene flame is shown in Figure 27 for a 1000.0 ppm calcium nitrate aqueous solution. The large broadband CaO emission bands occur at 555.5 nm, 603.8 nm, 623.0 nm and 603.8 nm as labelled in the spectrum. The neutral atom emission line at 422.6 nm is also labelled. Note also the presence of a trace sodium contamination, at 589.0 nm and 589.6 nm, estimated to be in the range of one hundred parts per billion. Also present is an internal reference strontium emission line at 460.7 nm at the 10 ppm

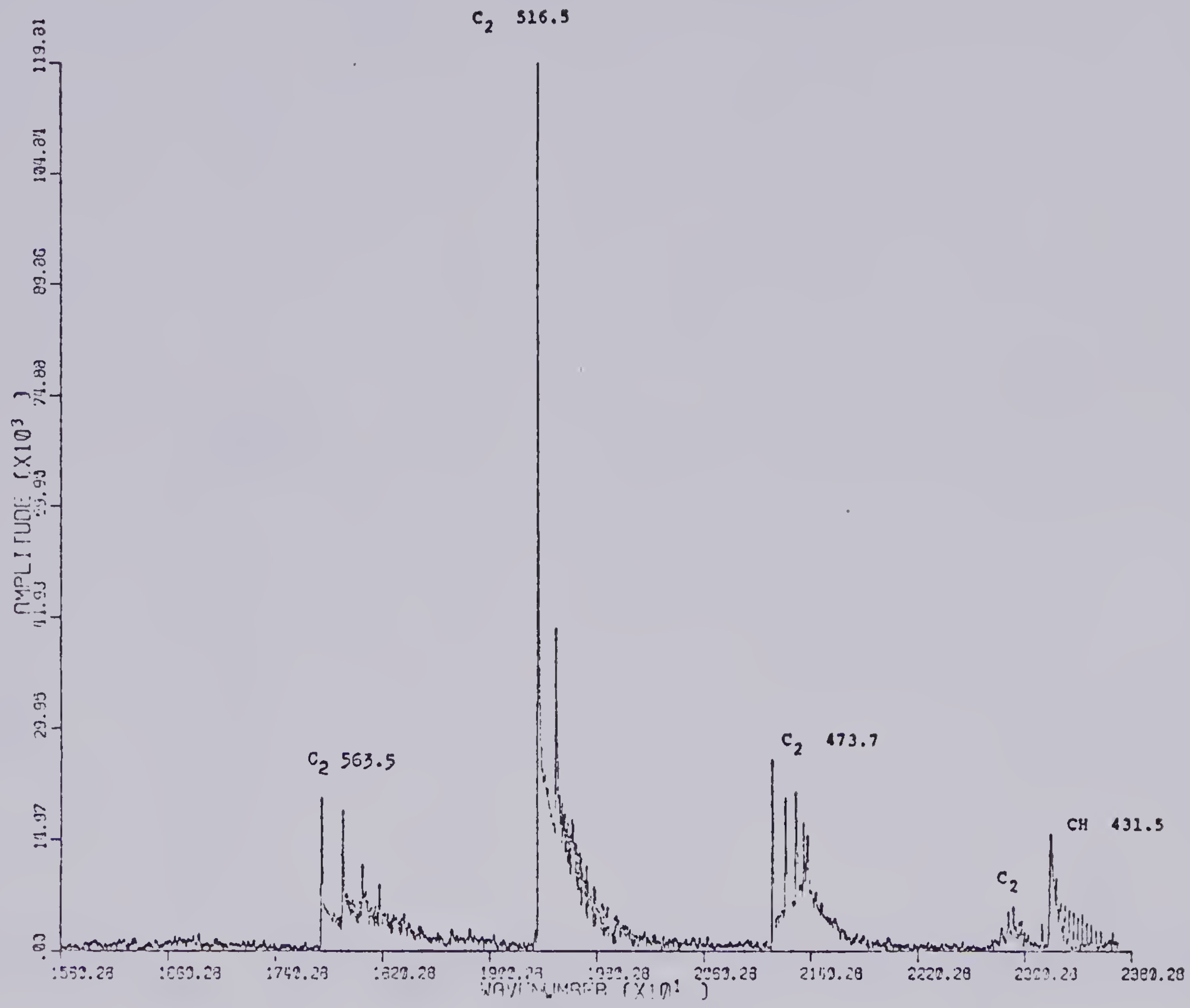

FIGURE 26. Air-acetylene flame background emission--1P28 P.M.T. detector

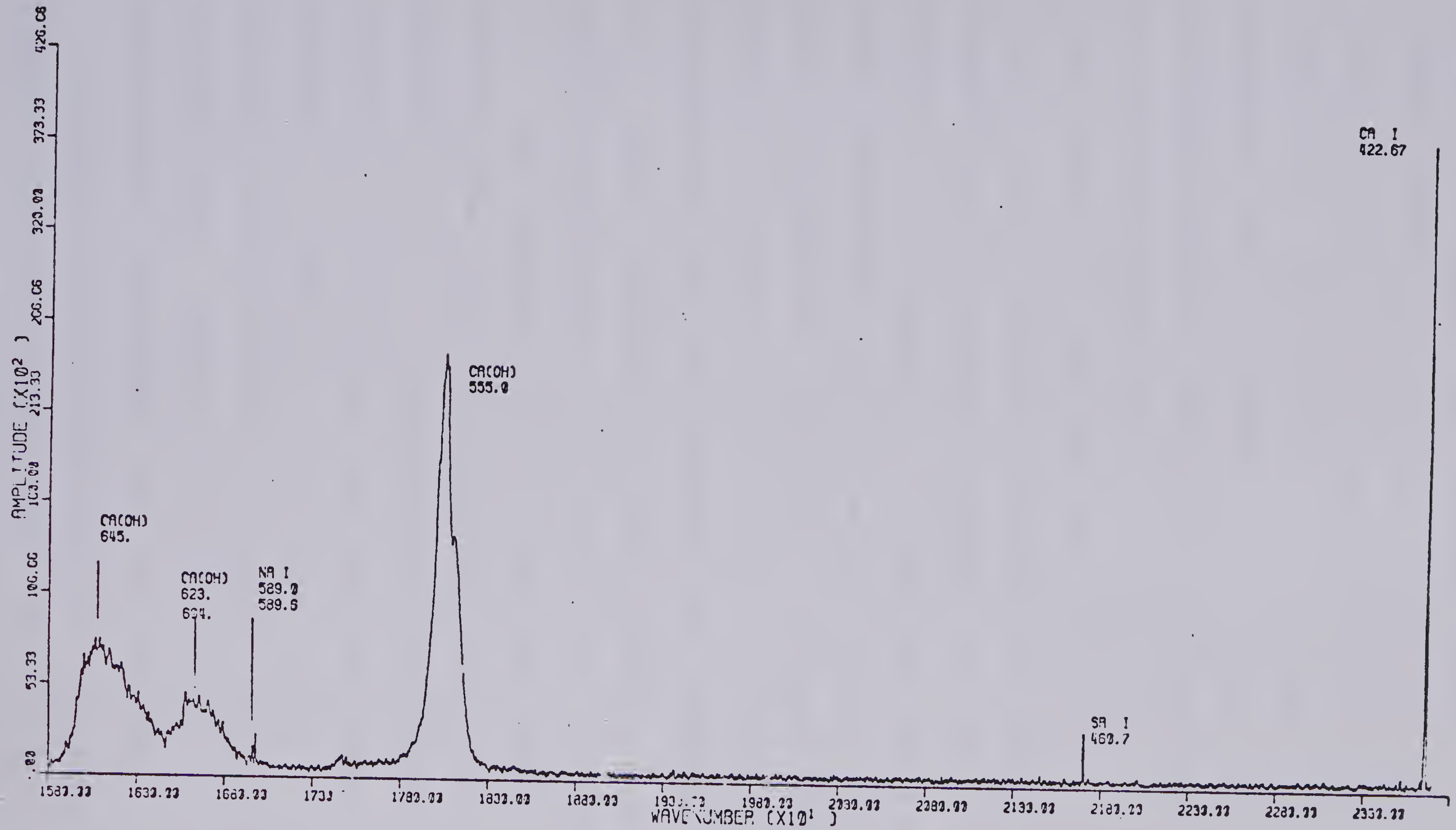

FIGURE 27. Air-acetylene flame emission spectrum of 1000.0 ppm Ca.

concentration level. The analytical curves for both the calcium neutral atom emission at 422.6 nm and the oxide emission at 555.5 nm are illustrated in Figures 28 and 29 respectively. The parabolic nature of the neutral atom analytical curve is evidence for the presence of the self absorption process. Cooler ground state neutral atom species on the outer limits of the flame absorb much of the neutral atom emission from the flame core. Due to the relatively low sensitivity for calcium in this flame and, therefore, the high concentrations that must be employed, the self absorption process is not unexpected. The analytical curve obtained using the broadband emission maximum has a slope of 1.05 ± 0.02 and an intercept of 1.29 ± 0.06 with an overall standard deviation of 0.0433 and a correlation coefficient of 0.9980. The detection limit for calcium in this flame was calculated to be 1 ppm. The detection limit is defined as the analyte concentration for which the signal to noise ratio is 2. The statistical basis for the data was six repetitions of twenty-five signal averaged interferograms at each concentration value. A log-log plot of the standard deviation of the oxide peak maximum versus the peak maximum is shown in Figure 30 indicating a little over an order of magnitude increase in noise with about two orders of magnitude increase in signal level. Again the multiplex theory concerning noise spectral distribution does not prove true in practice.

A similar study was undertaken for the emission of sodium in the air-acetylene flame. The complete emission

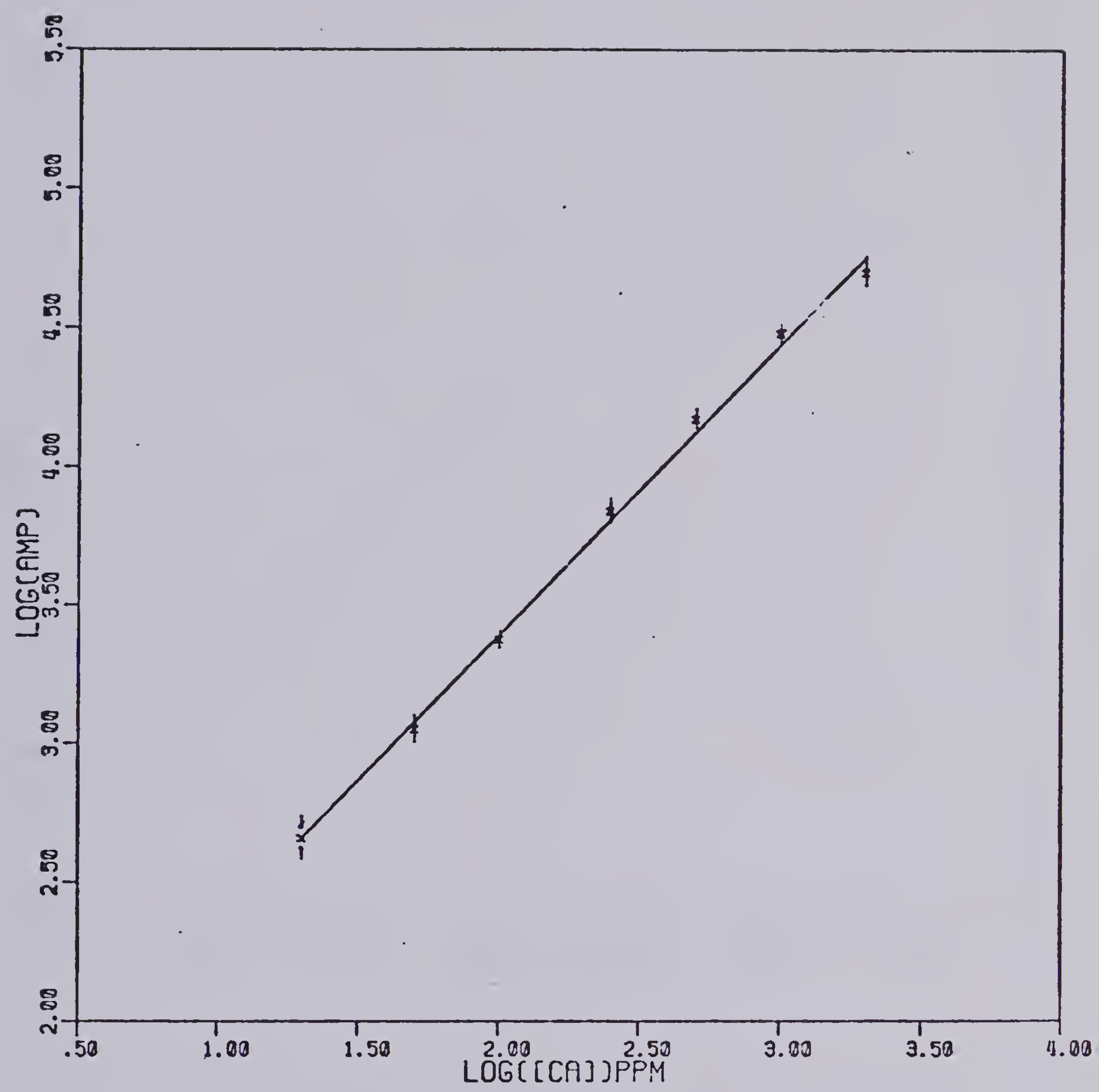

Figure 28 Ca analytical curve based on Ca(OH) 555.0 nm emission

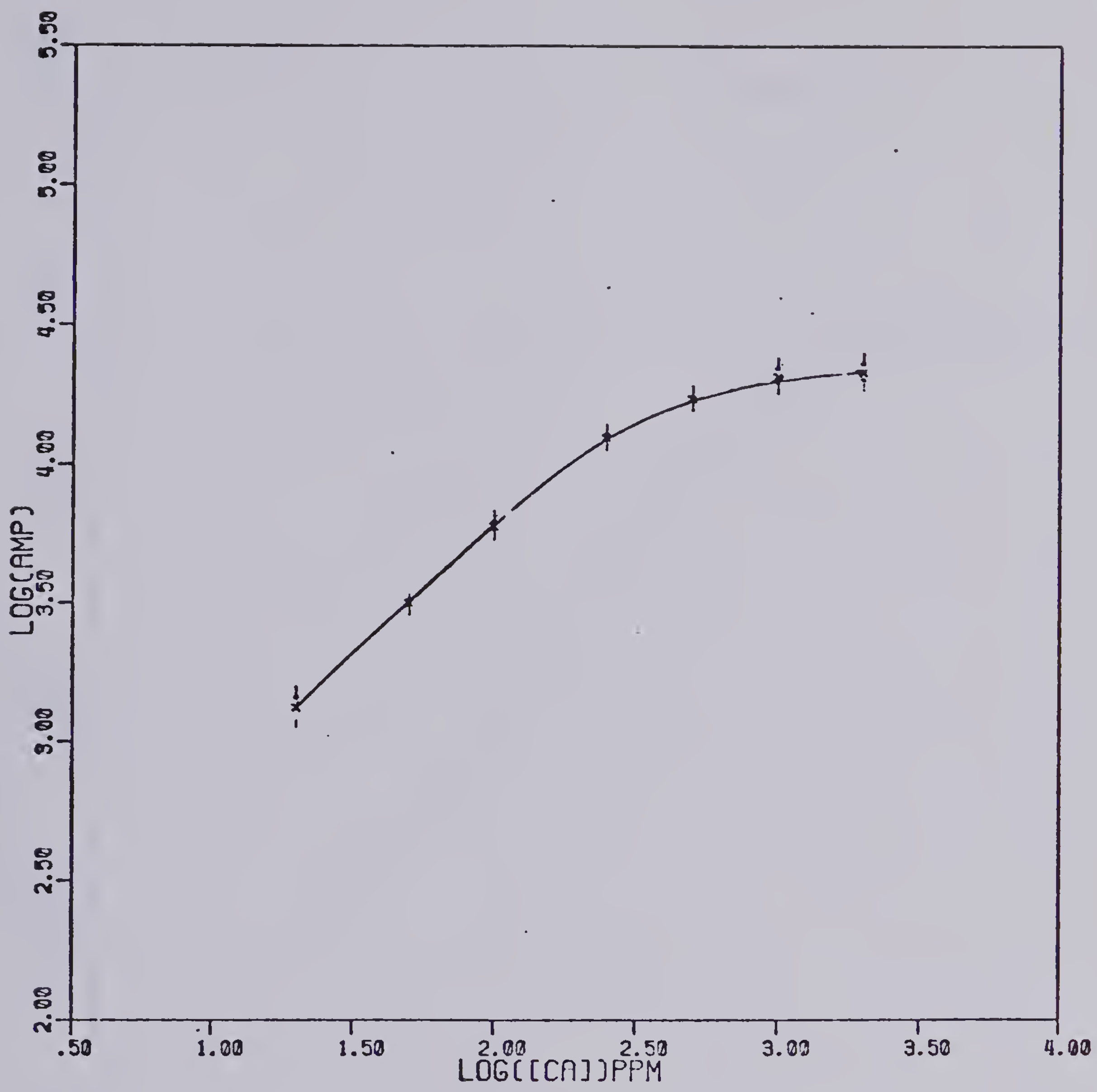

FIGURE 29. Ca analytical curve based on CaI 422.6 nm emission

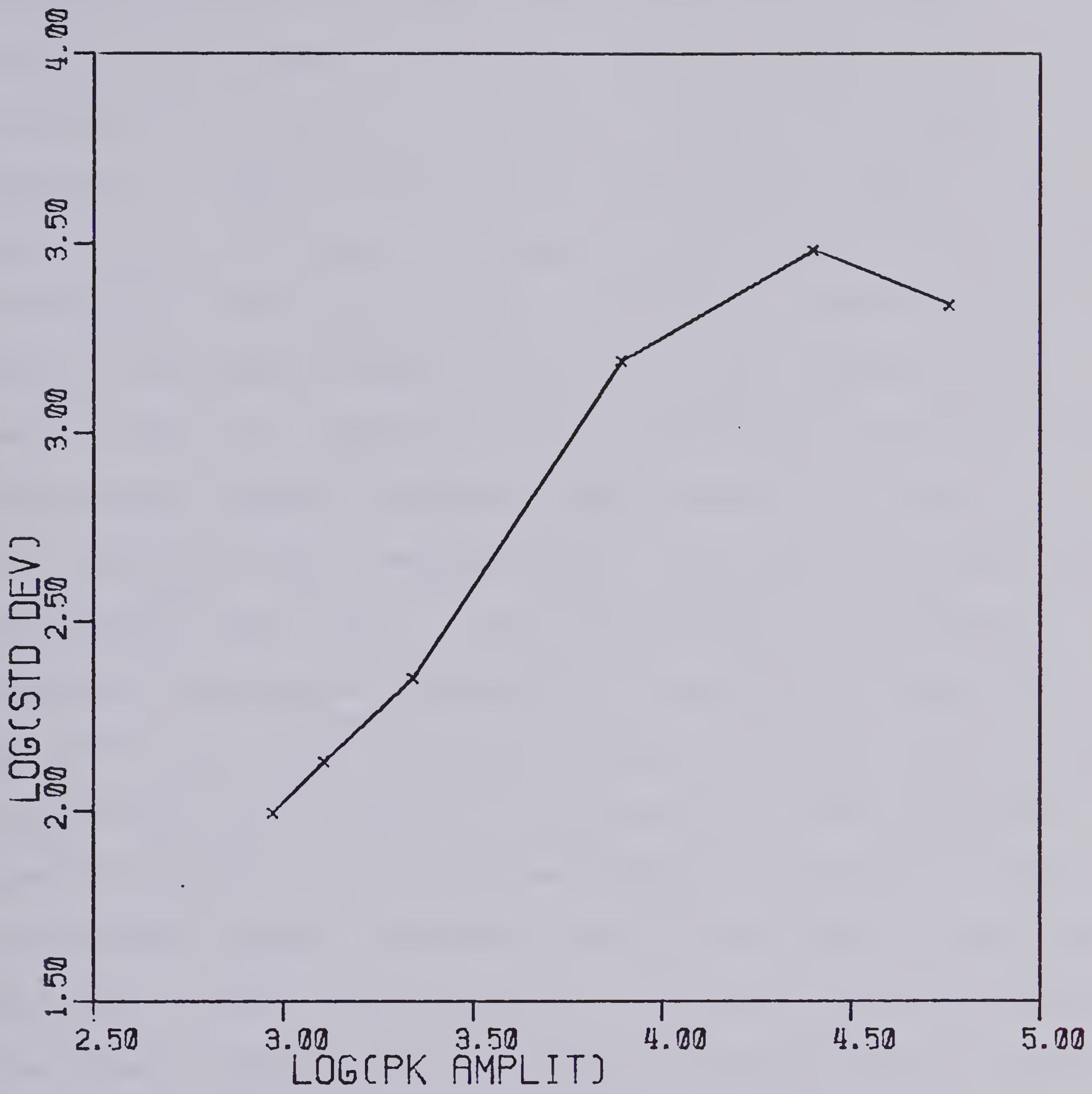

FIGURE 30. Ca standard deviation vs. Ca peak amplitude

spectrum resulting from a 1.0 ppm aqueous sodium chloride solution aspirated into the flame is shown in Figure 31. Provided for comparison with the lithium spectra in Figure 20, is Figure 32. The partial emission spectra for sodium emissions at the following concentrations are shown: 30.0 ppm, 1.0 ppm, 0.01 ppm. The analytical curve for the sodium emission at 589.6 nm over the concentration range of 0.01 ppm to 30.0 ppm is shown in Figure 33. The slope of the log-log plot is 0.908 ± 0.106 with an intercept of 4.491 ± 0.132. The overall standard deviation and correlation coefficient are 0.168 and 0.9910 respectively. The detection limit was calculated to be 3 ppb. A log-log plot of the standard deviation versus peak amplitude is contained in Figure 34. Curve "A" represents the peak standard deviation as a function of amplitude while curve "B" represents the mean baseline standard deviation of four wavelengths, some distance from the emission peaks. From this plot it may again be seen that the noise present indeed appears to be peak localized rather than equally distributed across the complete spectral range as the peak emission intensity increases. A similar plot is presented in Figure 35 for the mean baseline values again indicating no large increase in the baseline mean value as a function of emission intensity.

The atomic emission studies completed with lithium, sodium and calcium in the air-acetylene flame have indicated a different response to noise in the system than predicted with multiplex theory. In all three cases the noise generated by the presence of a high intensity emission signal

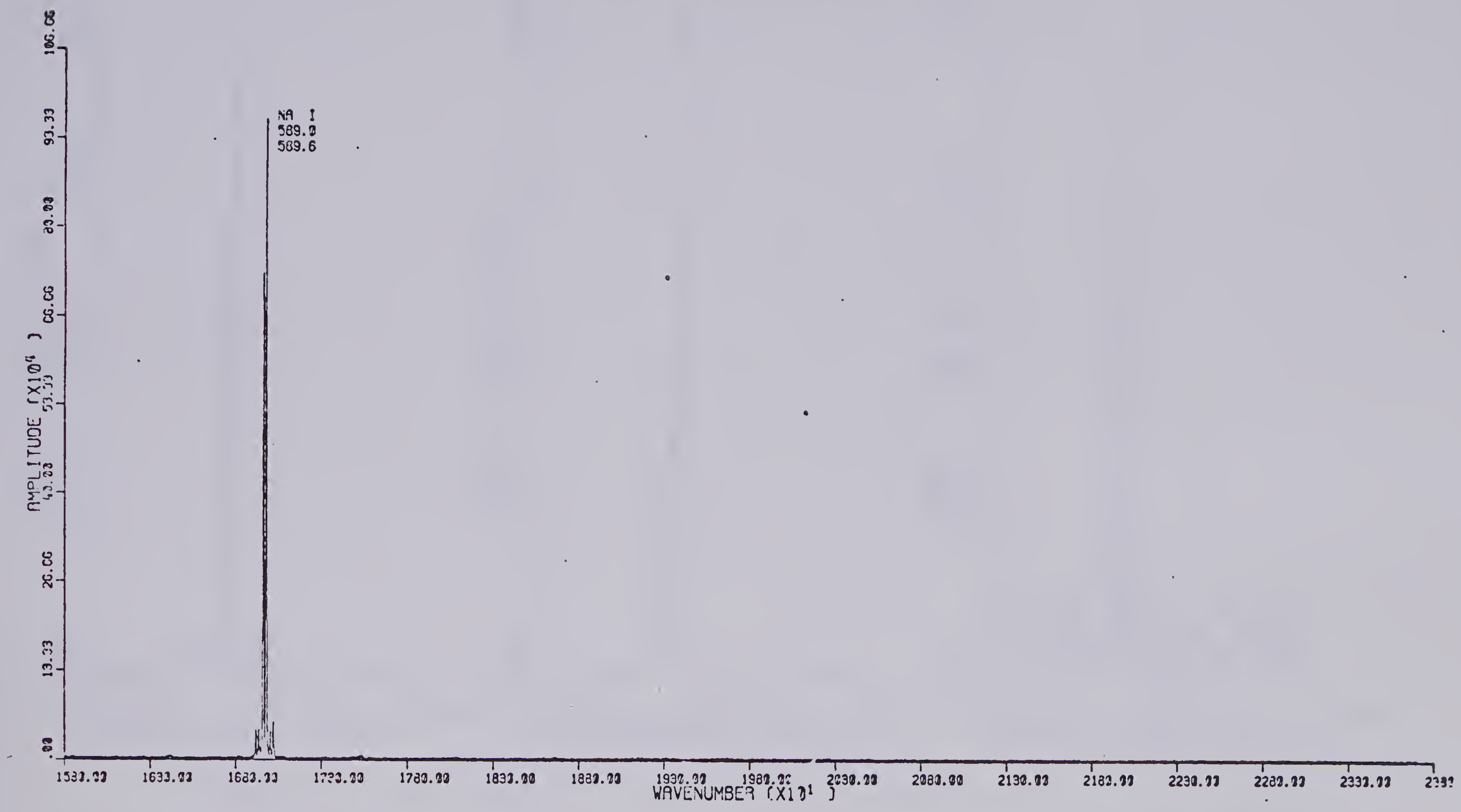

FIGURE 31. Air-acetylene flame emission spectrum of 1.0 ppm Na

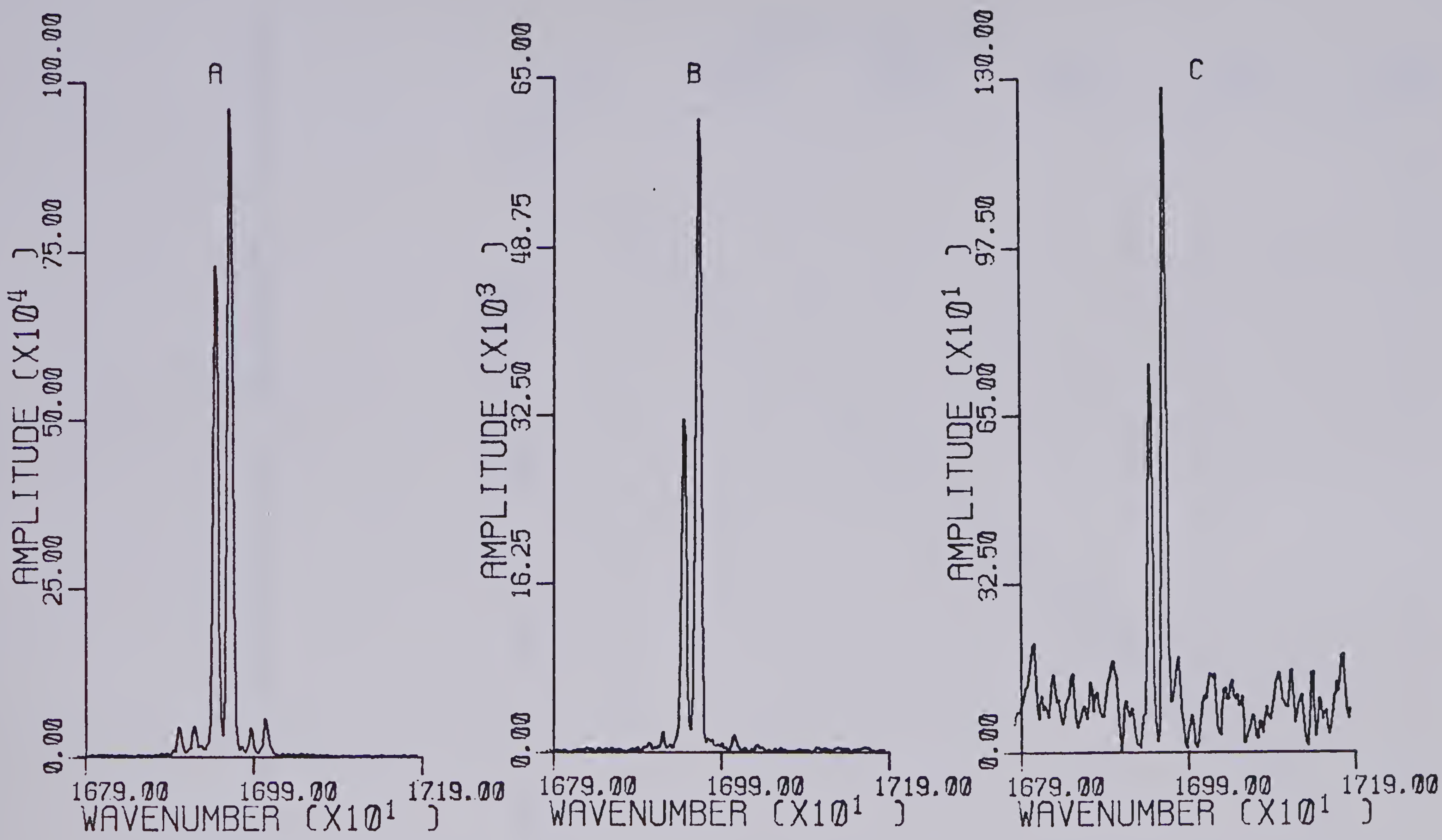

FIGURE 32. Air-acetylene flame emission spectrum of: (A) 30.0 ppm Na

(B) 1.0 ppm Na

(C) 0.01 ppm Na

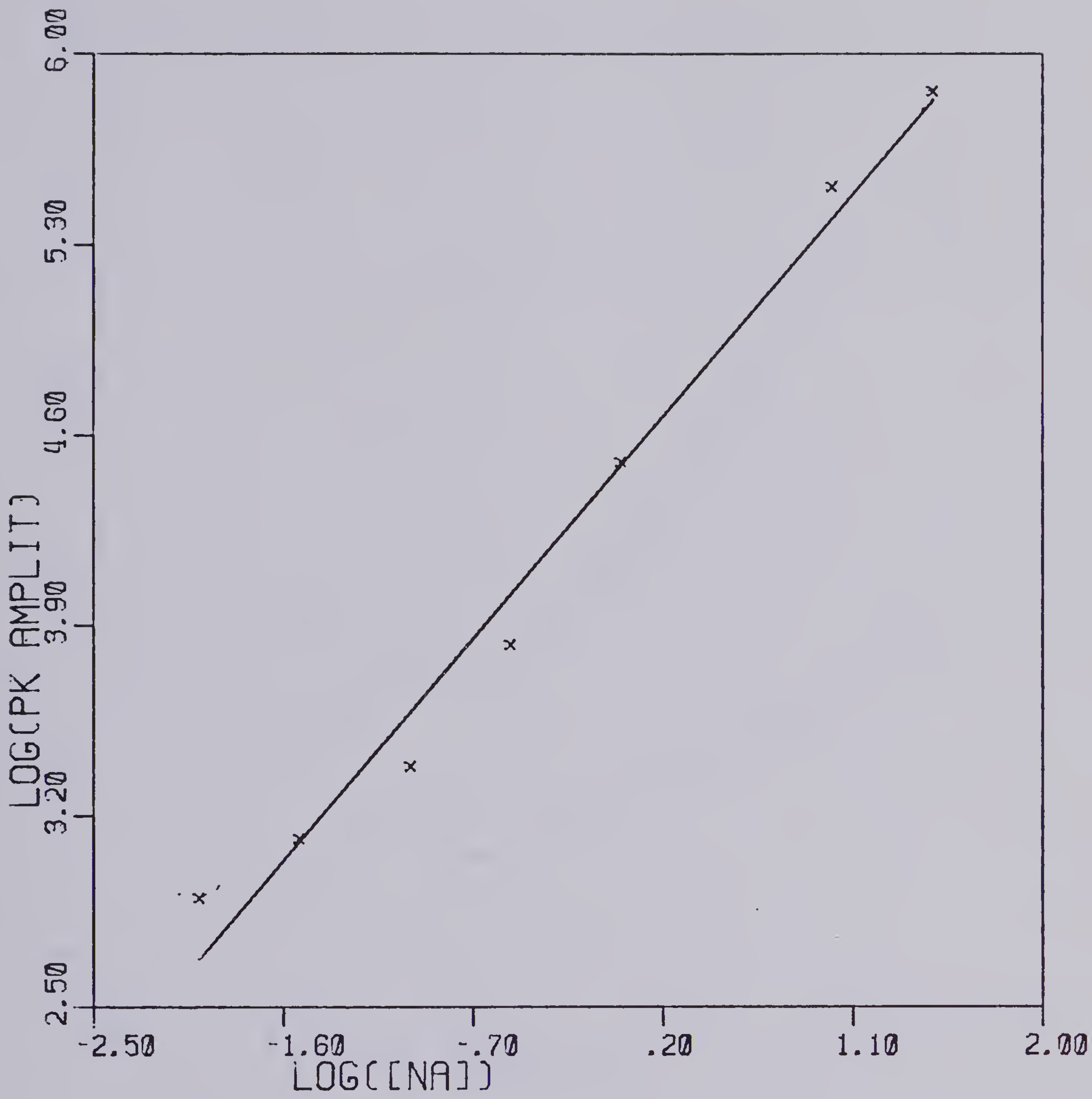

FIGURE 33. Analytical curve for Na 30.0 ppm to 0.01 ppm

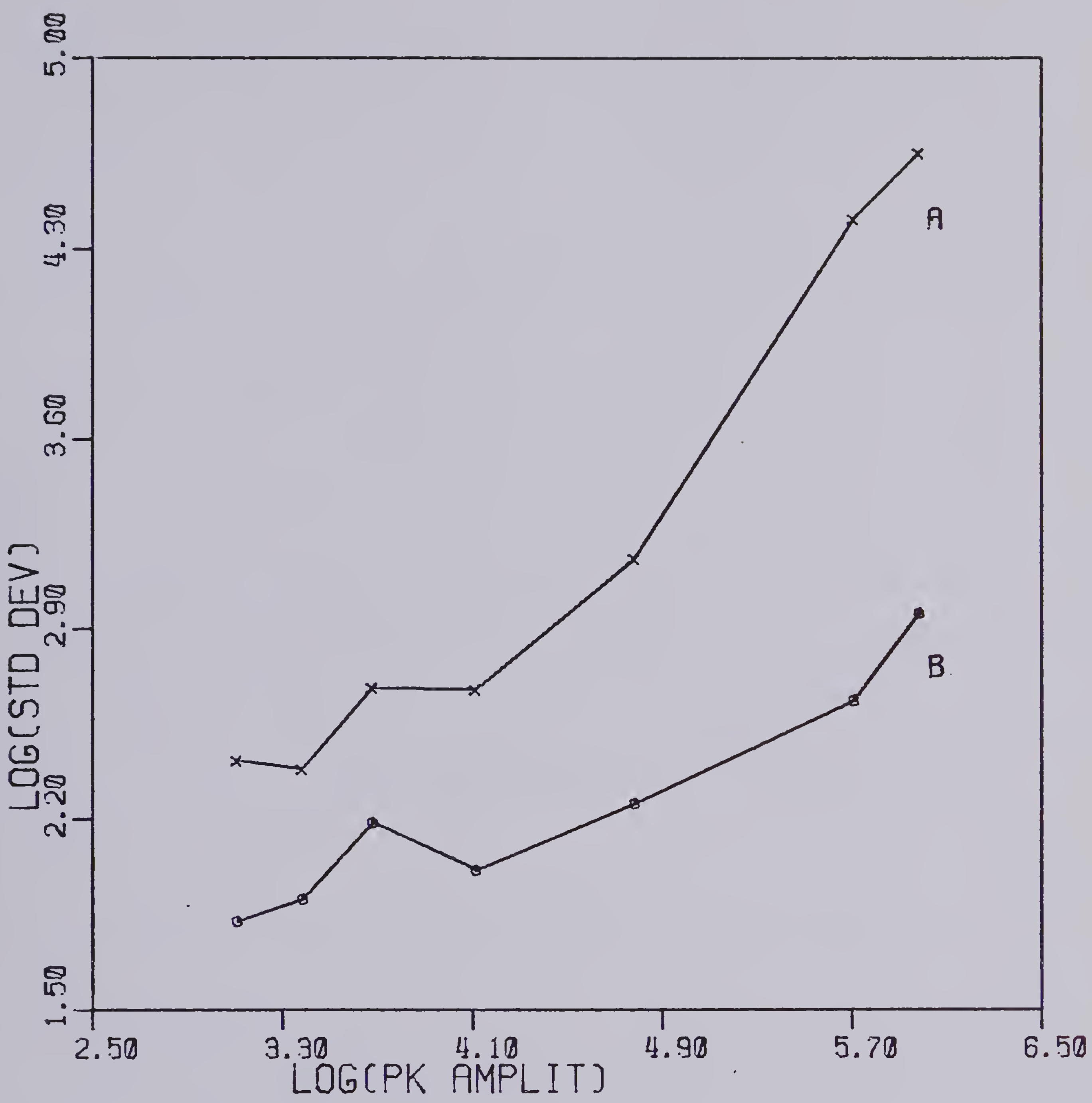

FIGURE 34.

A plot of standard deviation vs. Na peak amplitude

(A) Na peak standard deviation

(B) Baseline standard deviation

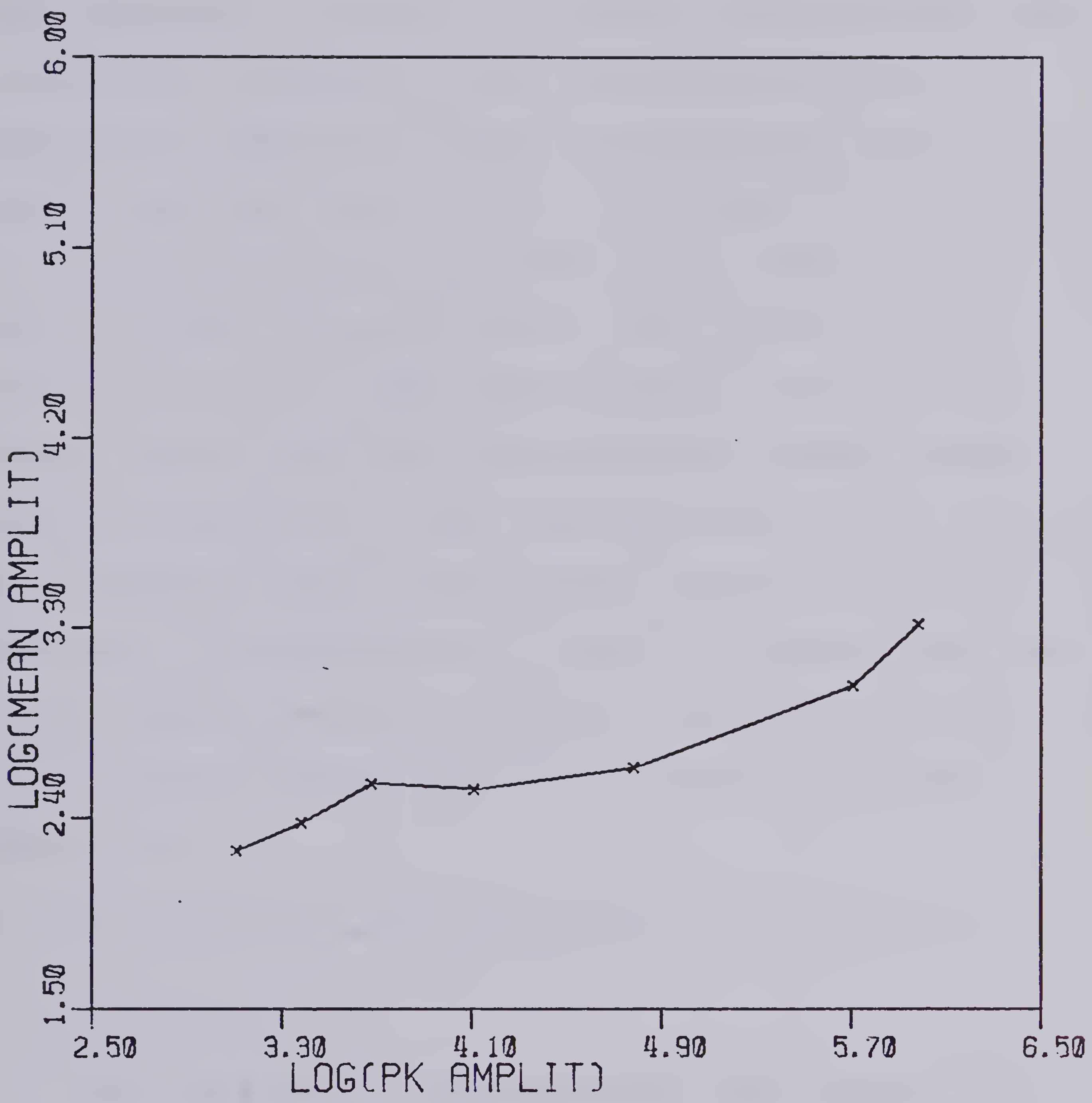

FIGURE 35. A plot of mean baseline amplitude vs. Na peak amplitude

has been found to be peak localized, a situation similar to that expected in the case of a scanning monochromator system. As discussed in Chapter I, the noise present should be distributed evenly with respect to wavelength across the complete spectral range. This is not borne out experimentally in the three situations mentioned above. Note also that the source of noise, whether detector shot noise or source fluctuation noise or some other intensity related noise source, is not important. Only the distributive aspects are being considered. Only noise generated after or during the transform process could account for such peak localized behaviour. The possibility of round off error accumulation in the computation stage does exist according to Foskett (76) but no detailed studies have been undertaken in this laboratory.

D. The Nitrous Oxide Acetylene Flame Emission Source

1. Introduction

Very few elements, excepting the alkali metals, have a high emission sensitivity in the air-acetylene flame due to several factors. The major source of excitation energy in flames has been established to be thermal in nature, implying that a higher temperature flame will provide a greater amount of energy for the excitation of atomic species than will a lower temperature flame (2). Thus the air-acetylene flame, at a temperature of about 2000°C, simply does not provide enough thermal energy for excitation of atomic species such

as the transition elements. The formation of refractory oxides is another source of decreased sensitivity for many elements, such as magnesium, in the air-acetylene flame. Interferences, such as phosphate and aluminum on the alkaline earth elements, also tend to decrease the level of neutral atom species available for excitation and therefore lower the sensitivity. The higher temperature, reducing atmosphere of the nitrous oxide acetylene flame overcomes both of these problems. Due to its higher temperature, about 3000°C, complex species, as in the phosphate interference, are broken apart releasing atomic species for potential excitation.

The nitrous oxide acetylene flame was first introduced analytically by Willis in 1965 (77). Since then many spectroscopic profiling studies have been completed by Willis and other writers (78-82) on this flame. A study of flame emission detection limits was completed by Christian and Feldmann (83) in 1971. Due to the high excitation energy available with this flame, and its freedom from interferences, it was decided to employ it as an atomic emission source in the interferometer based studies.

2. Applications with the F.T.S. System

The experimental system for use with the nitrous oxide acetylene flame involved changes only with the source. The 1P28 photomultiplier remained as the detector. The burner

head required for this flame has been previously described in this chapter. Gas flow rates were maintained at the following values throughout the experimental runs: acetylene at 4 litres per minute and nitrous oxide at 12 litres per minute. The characteristic red feather region was barely visible under these conditions.

The flame emission background spectrum is shown in Figure 36. Three spectral features predominate this spectrum. The first consists of a series of emission lines with a band head at 306.4 nm corresponding to the hydroxyl radical emission band. The band actually decreases in amplitude toward lower wavenumber (longer wavelength), but due to the presence of an aliasing point at 316.4 nm spectral overlapping by the higher frequency bands occur. The second feature located at 336.0 nm is the NH emission band. NH is a combustion by-product of this flame. The third feature is a rather more complex mixture of combustion products of this flame. These include the C_2 radical, CN and CH at approximately 380.0 nm. All of the above features were found to be continuously present at rather high emission levels when compared to the background emission of the air-acetylene flame. The hydroxyl band could be easily removed with optical filters (Corning CS 954, Ø-52 or 7-59) (66). The other two spectral features could not be easily removed due to their central location in a spectrally important region for atomic emission. Optical and electronic filtering was not possible and these bands created serious dynamic range limitations. This is

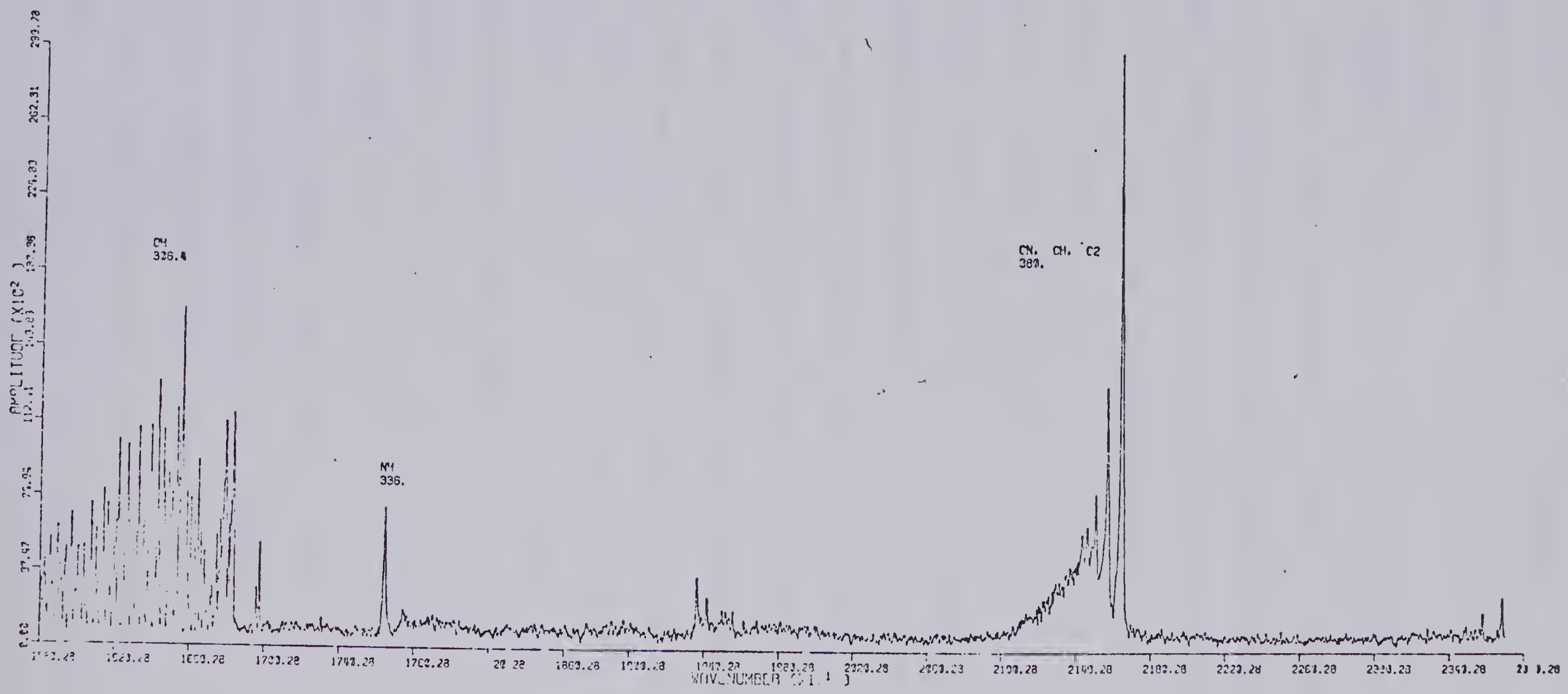

FIGURE 36. Nitrous oxide acetylene flame emission background

an excellent example of the situation discussed in Chapter I where the spectral background may severely limit the analyte dynamic range.

A second problem existed with the experimental system that severely limited the acquisition of valid quantitative emission data. In order to establish a statistical degree of confidence, many independent repetitions must be completed at each concentration value on an analytical curve. With the current interferometer system this may run into an inordinate amount of time, on the order of hours to complete a seven repetition, seven concentration point analytical curve. Each repetition consisted of 25 signal averaged interferograms. The actual observation time per scan is about one second or twenty-five seconds per repetition per concentration point or three minutes total per concentration point or twenty-one minutes of observation time for the complete analytical curve. The total experimental time is at least greater by a factor of five. Over this time period any source undergoes stability problems and they were especially prominent in the case of the nitrous oxide-acetylene flame. The narrow capillaries required to provide the high-flow velocity became very quickly obstructed with carbon, even with only water aspirating, eliminating any high salt concentrations. With the flow rates used, the flame would be considered full lean and no such carbonation should occur. Clogging of the capillaries most likely was initiated during the switch over from the very fuel rich air-

acetylene flame to the nitrous oxide acetylene flame. The manual gas flow control box used provided only limited flexibility in the gas mixtures and flows available since it was designed for the standard slotted nitrous oxide acetylene burner. Two possible solutions to this problem exist. First shorter length capillaries of the same diameter should be tried in the burner design. The capillaries are currently 4 cm long and provide a long distance of restricted flow over which clogging may easily occur. Caution must be used in this redesign to ensure adequate prevention of flashback. The second solution simply involves the design of a new gas flow control box especially suited to the burner design.

The experimental work completed with the nitrous oxide acetylene flame is qualitative in nature intending to illustrate the excitation potential available with this flame and the simultaneous multielement detection capabilities of the interferometer system. The spectrum in Figure 37 shows the emission lines of a 20 ppm aqueous solution of each of the following elements, Cr, Mn, Cu. Note that the copper doublet does not appear in its normally observed intensity ratio. The use of an optical filter, CS Ø-52, used to eliminate the hydroxyl band emission at 306.4 nm, has a slight attenuating effect upon the copper lines at 327.4 nm and 324.8 nm. A multielement spectrum containing Al, Mn, Cr, Cu, Fe and Ni, all at the 20.0 ppm concentration level, is shown in Figure 38. The observed and literature (65)

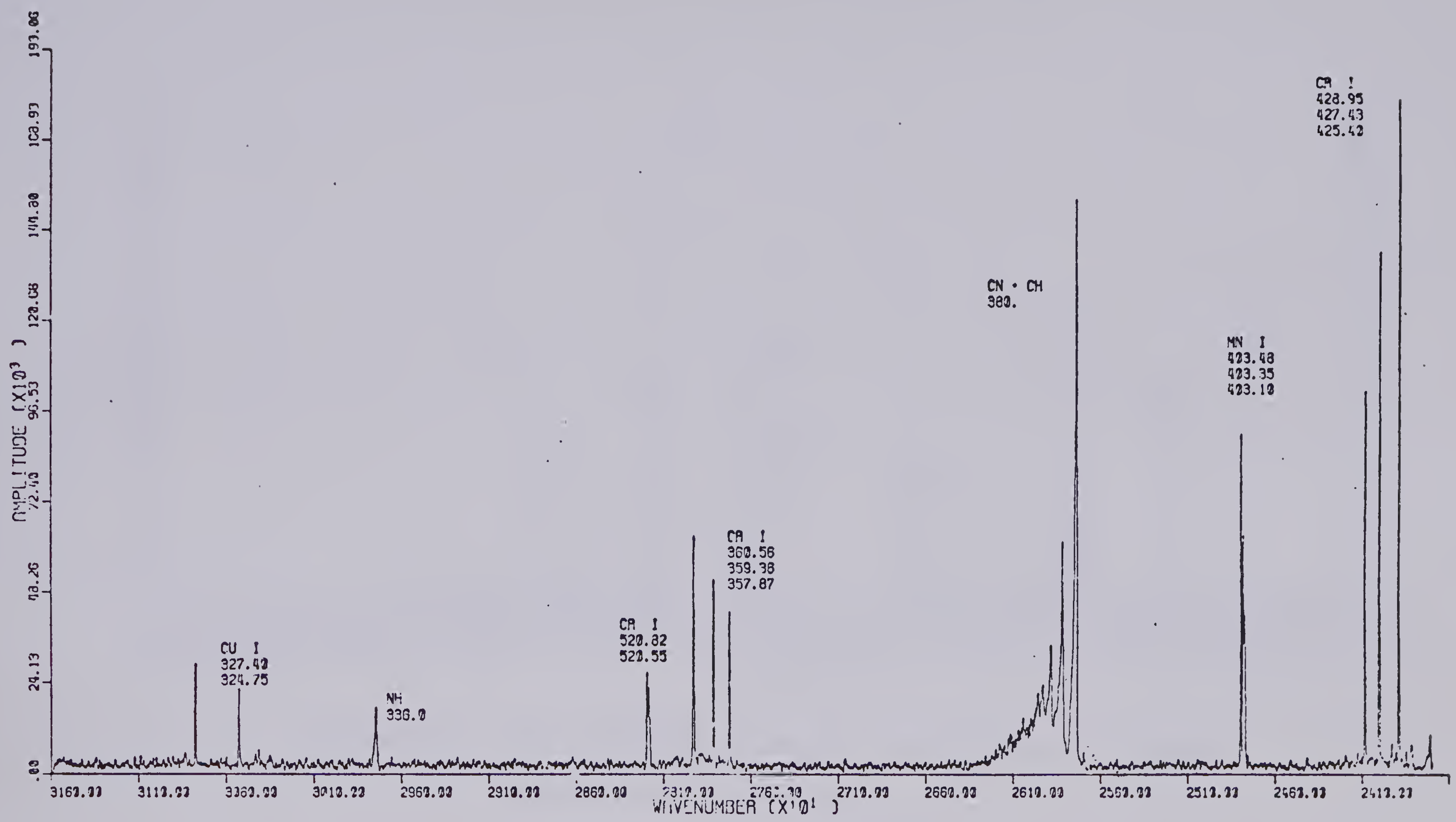

FIGURE 37. Cu, Mn, Cr nitrous oxide acetylene flame emission spectrum

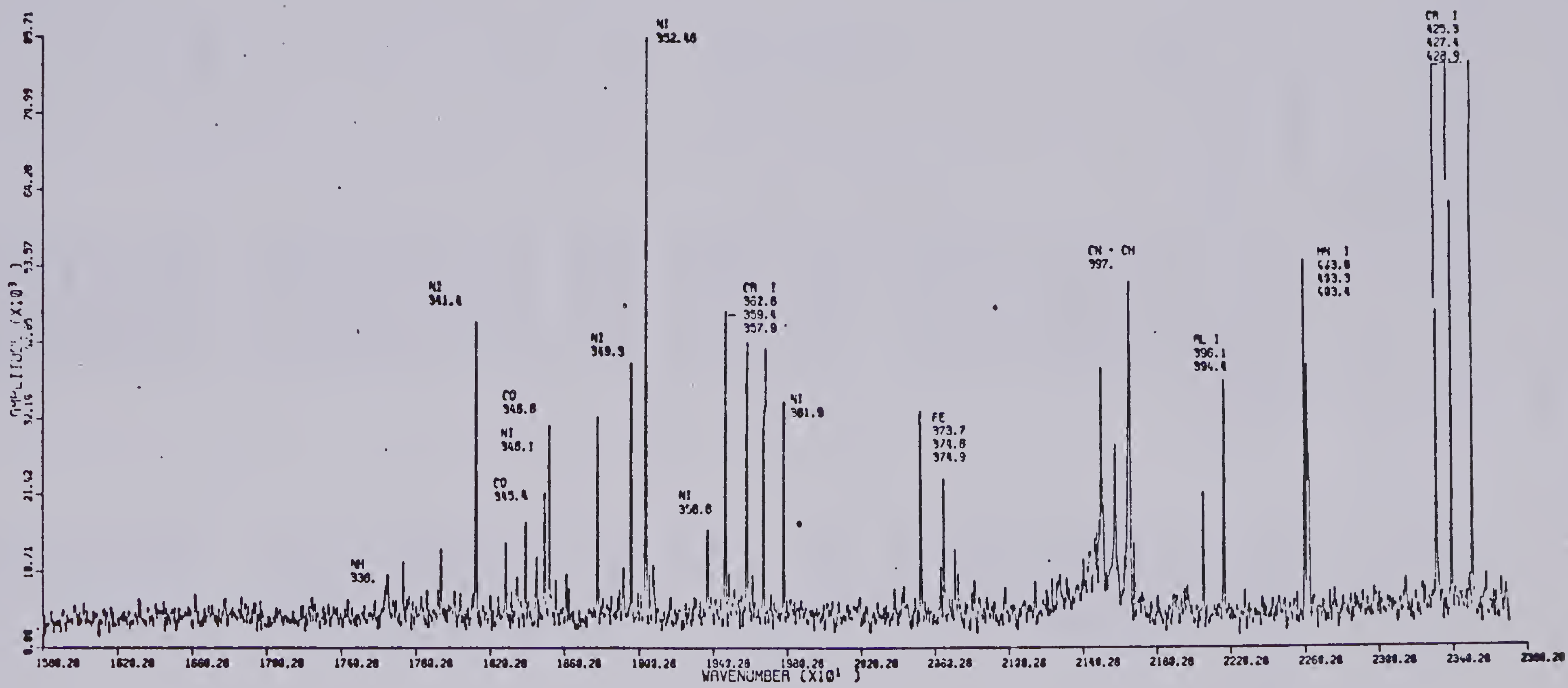

FIGURE 38. Multielement emission spectrum in a nitrous oxide acetylene flame

Table VII

Multielement Sample Emission Observed with the Nitrous Oxide-Acetylene Flame

Element	Observed Wavelength nm	Literature (65) Wavelength nm
Fe	358.44	358.47
	358.59	358.53
	358.88	358.86
	372.02	371.99
	373.50	373.50
	373.74	373.71
	374.58	374.56
	374.86	374.83
	376.35	376.34
Al	394.45	394.40
	396.20	396.15
Mn	403.10	403.08
	403.35	403.31
	403.48	403.45
Co	346.59	346.58
	345.37	345.35
Cr	420.82	420.84
	420.65	420.60
	--	420.45
	428.95	428.97
	427.43	427.48
	425.40	425.43
	360.56	360.53
	359.36	359.35
	357.87	357.87
Ni	361.97	361.94
	356.64	356.64
	352.46	352.45
	349.30	349.30
	346.18	346.17
	345.85	345.85
	344.64	344.64
	341.48	341.48

emission wavelengths are tablulated in Table VII for both of the above spectra.

A good indication of the relative amount of excitation energy available in this flame as compared to the air-acetylene flame, is given in the emission spectrum of calcium. The complete emission spectrum for a 10.0 ppm Ca aqueous solution aspirated into the flame is shown in Figure 39. Note the presence of the calcium ion lines at 393.3 nm and 396.8 nm as well as the neutral atom emission line at 422.6 nm. The majority of the emitting atoms are present as the neutral atom species but enough energy is present to both ionize and excite the calcium atoms. Note also the lack of any oxide species emission at all in the spectrum in contrast to the previous air-acetylene flame study.

The spectra presented above give a rather limited indication of the capability of the nitrous oxide acetylene flame for atomic emission. This is due, in the main, to instrumental design limitations as opposed to inherent characteristics of the flame. The simultaneous multielement detection capability of the interferometer system has been clearly demonstrated in the above spectra.

E. Conclusions

The results obtained in the preceding studies provided some interesting answers and raised some complex questions. The interferometer based system has proven itself as a viable

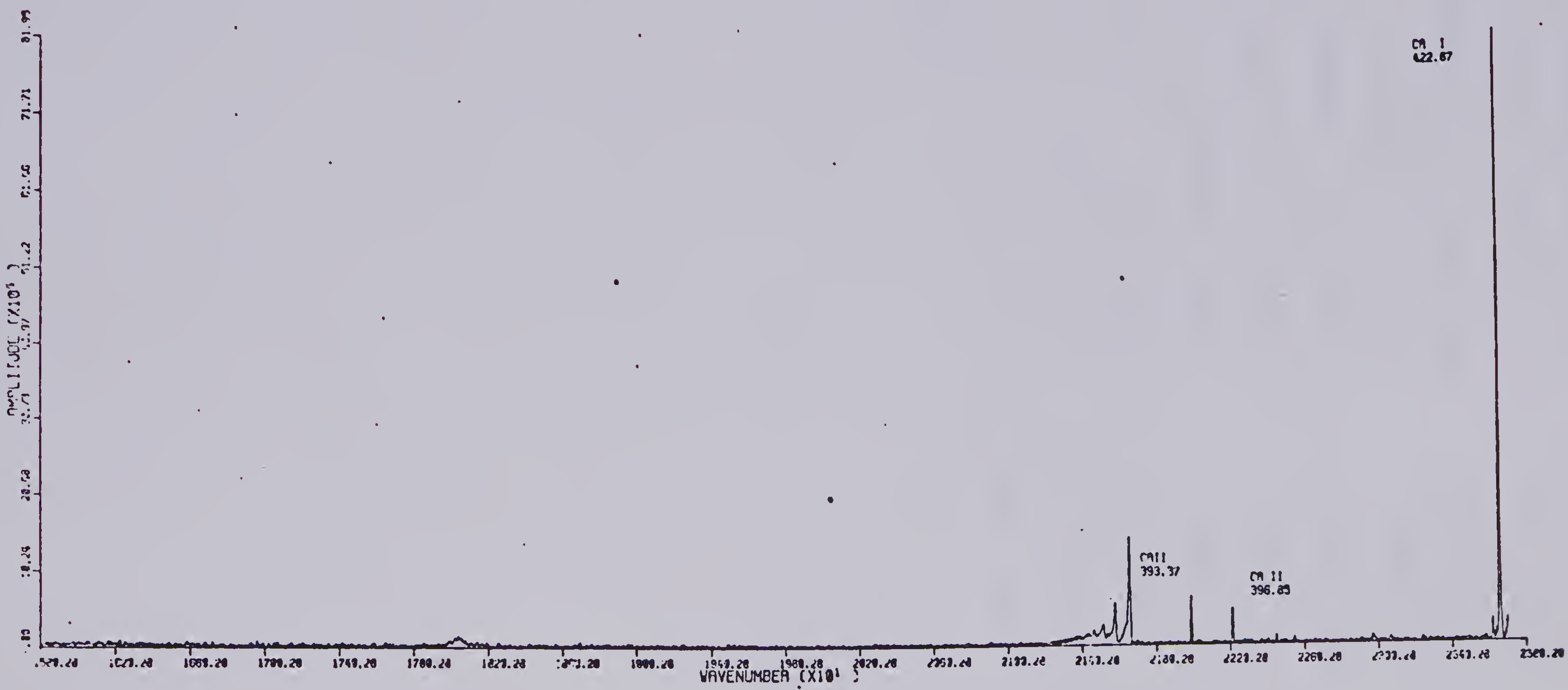

FIGURE 39. Emission spectrum of a 1.0 ppm Ca solution in a nitrous oxide acetylene flame

detection system, with restrictions, for flame atomic emission. The most evident problem is that of a limited dynamic range in the presence of other emitting species. Other than through the use of filters, if possible, no absolute solution exists for this problem. No clear explanation would be offered for the behaviour of the system with respect to the noise distribution question. The results indicate behaviour directly opposed to that predicted by theory. Further work is definitely needed in both of the areas mentioned above in order to fully utilize the multiplex, interferometer based spectrometer.

CHAPTER V

THE RADIO FREQUENCY-INDUCTIVELY COUPLED PLASMA AS AN ATOMIC EMISSION SOURCE FOR THE INTERFEROMETER

A. Introduction

A radio frequency inductively coupled argon plasma (R.F.-I.C.P.) was first utilized as an analytical atomic emission source in the late 1950's and early 1960's independently by two groups, Greenfield, Jones and Barry (84) and Wendt and Fassel (85). Over the last twenty years a great deal of both experimental and fundamental work have brought the R.F.-I.C.P. into the laboratory as an analytical spectroscopic tool for elemental determination. A great deal of work is still ongoing in order to characterize and fully utilize the plasma emission source (3,86,87). The R.F.-I.C.P. offers several major advantages as an atomic emission source. Firstly, the I.C.P. approaches very closely the ideal multielement spectroscopic emission source. It possesses a very large amount of energy, approximately 11.eV, for the excitation of ionic or atomic species, allowing elements previously not excited in flames to achieve emission. The larger amount of energy available also reduces the formation of inter-element complexes, thereby eliminating such interferences as aluminum on calcium (88). This greatly simplifies analyses on complex multielement mixtures where the matrix composition may be unknown. Secondly, the argon plasma does not suffer from severe background emission problems. As will

be shown later, the plasma background emission consists of an argon ion continuum emission, and various neutral atom argon emission lines. Thirdly, the plasma atomic emission source provides a very wide linear dynamic range for quantitative spectroscopic emission work. A linear range of at least five orders of magnitude is achievable, often limited by the detector response range. As well as the three major areas mentioned above, the plasma offers performance as good as, if not superior to, other atomic emission sources in the areas of precision, accuracy, and ease of sample preparation. As discussed in Chapter I, the plasma does suffer from spatial problems to a greater extent than the flames previously discussed in Chapter IV. Whether or not this is a serious limitation is an experimental study to be undertaken. An overall evaluation of the analytical capabilities of the plasma interferometer based atomic emission system will be undertaken in this chapter.

B. Instrumentation

The instrumentation for this system consisted of the Michelson interferometer based spectrometer described in Chapter II, a Plasma-Therm Inc. (Kreston, NJ) argon R.F.-I.C.P., and associated coupling optics. The I.C.P. specifications and normal operating parameters are listed in Table VII. The optical link between the plasma source and interferometer proved to be non trivial due to the combination of the collimated light input requirements of the interferometer and

Table VIII

I.C.P. Operating Conditions

Frequency:	27.12 MHz
Power:	1.5 Kw
Coolant Argon Flow:	18. l/min.
Nebulizer Argon Flow:	0.8 l/min.
Observation Height:	22 mm above load coil
Observation Aperture:	5.0 mm
Solar Blind P.M.T. Voltage:	600.0 volts
1P28 P.M.T. Voltage:	400.0 volts

the high degree of spatial resolution required on the plasma plume. Various authors have shown the influence of spatial effects when working with a plasma monochromator based system (55,88). Small changes in the nebulizer gas flow rate, coolant gas flow rate, and/or observation window result in very large changes in the analyte signal level. Refer to Edmonds and Horlick (55) for a detailed study. The following optical arrangement was found to provide adequate spatial selectivity for this preliminary work. Using a 5 cm diameter, 10.0 cm focal length quartz lens, an image of the plasma plume was projected on a 5 mm diameter aperture centered 22 mm above the load coil of the plasma torch assembly. A 12.5 cm focal length, 5 cm diameter quartz lens, placed 12.5 cm from the aperture and about 30.0 cm from the entrance aperture of the interferometer, provided the collimated light required. All three units, the plasma, lenses and interferometer were optically aligned using a He-Ne laser. An initial attempt was made to use the combination of an off axis parabolic mirror, 6.6" focal length, and a flat mirror, 3.5" × 4.0", to provide the optical interface. This combination proved extremely sensitive spatially on the plasma plume making system alignment and precision difficult to maintain. The presence of an easily accessible plasma plume image with the lens system was found to be very valuable in system alignment. Alignment was optimized on the calcium ion lines emission at 393.4 nm and 396.8 nm and maintained under those operating conditions. Spatial studies have shown that many element lines emit

strongly at this same position.

Another type of instrumental problem occurred with this system due to the nature of the radio frequency power source. As stated in Table VII, the source operates at a frequency of 27.12 MHz at a power level of 1.5 KW. The first problem occurred in the main interferometer signal channel pickup of high frequency multiples and sub-multiples of 27.12 MHz. Through careful isolation of the components and effective bandpass filtering this problem was eliminated. The pickup of high frequency signal components is especially serious for the interferometer system due to the possibility of aliasing these signals into the lower frequency spectral region. The second serious problem occurred in the signal channel pickup of a low frequency 240 Hz signal originating in the plasma power supply. Both bandpass filtering and notch filtering had to be employed to reduce, but still not eliminate the signal. An example of the spectral peak produced by this frequency is available in Figure 44 near the 31000 cm^{-1} region of the spectrum. Therefore, caution must be used when employing the plasma source in such an experimental configuration to ensure the complete elimination of such frequencies.

C. Results and Discussion

1. The 1P28 Photomultiplier Tube as a Detector

Experiments with the plasma interferometer combination were initiated using a 1P28 photomultiplier tube as a detector for the interferometer. The background emission

spectrum of the plasma with water aspirating into the plume is shown in Figure 40. The spectral range covered in this spectrum extends from 240 nm to 650 nm. Table IX lists some of the emission lines assigned for argon, hydrogen and hydroxyl radical emission found in this spectrum. The spectrum in Figure 41 illustrates the same plasma background emission under identical instrumental settings with the exception of no solution aspirating into the plasma plume. No central or analyte channel has been punched into the core of the plume. Note the absence of the strong hydrogen emission line at 486.1 nm and the smaller emission line at 434.0. In both spectra the hydroxyl radical emission appears only as a noisy baseline in the high wavenumber region of the spectrum. The lack of the characteristic tailing band shape of the hydroxyl radical emission is again accounted for with the phenomenon of aliasing. The aliasing point occurs in the center of the band emission causing it to fold over upon itself. An expansion over the last 2000 cm^{-1} region of the background emission spectrum is shown in Figure 42 illustrating the multiple, aliased argon neutral atom line emission covering the spectral range from 380 nm to 490 nm. This is a very important region analytically for the emission of various elements such as calcium, strontium, manganese and chromium and the argon emission lines could play a very important role in dynamic range limitations. A similar role must be considered for the hydrogen line emission at 486.1 nm.

Previous work with the I.C.P. has indicated a high level

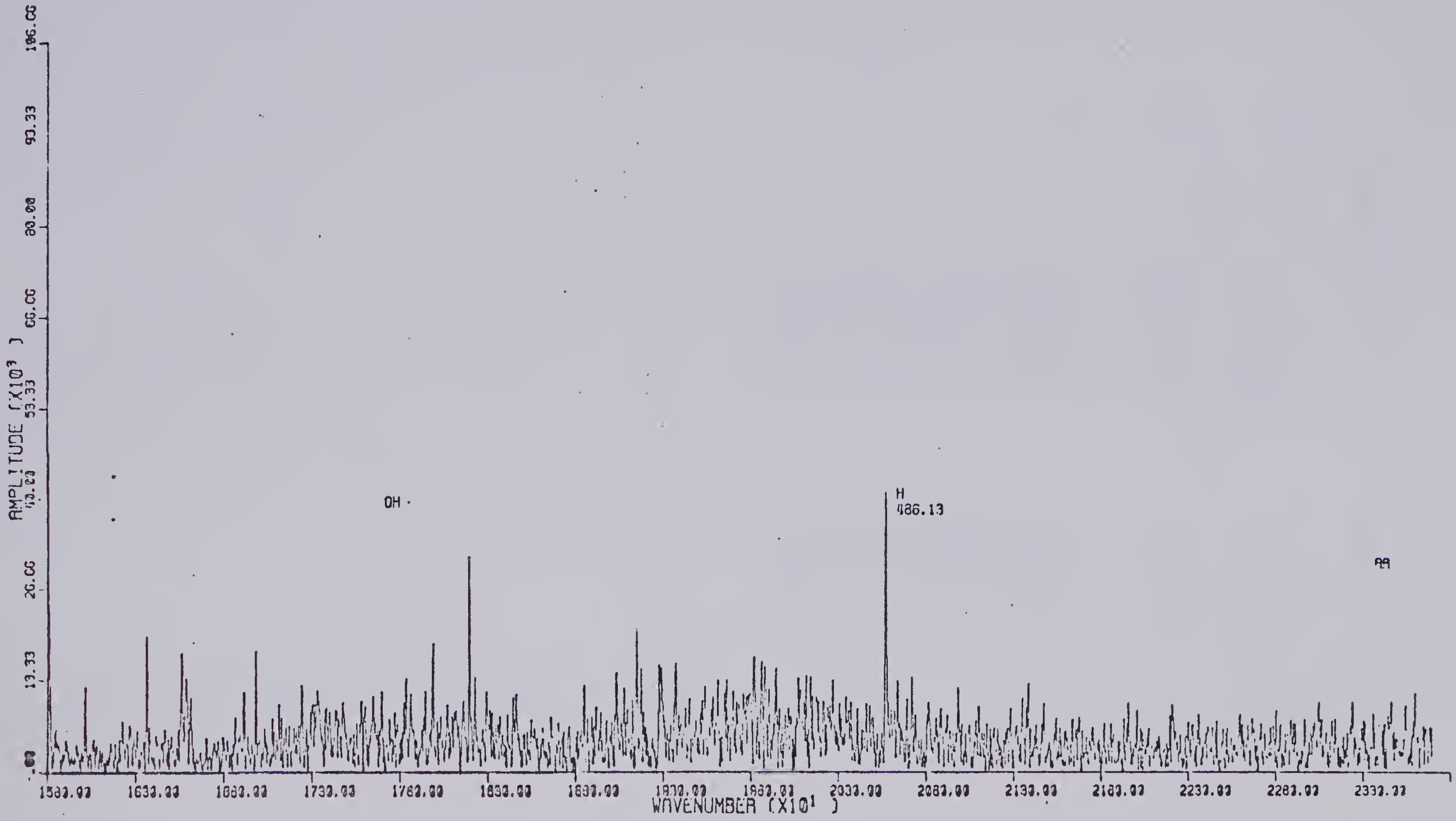

FIGURE 40. Argon plasma background emission spectrum, water aspirating

Table IX

Argon Plasma Source Emission Lines

Element	Observed Wavelength nm	Literature (65) Wavelength nm
H	486.13	486.08
	434.05	434.00
Ar	433.36	433.29
	429.95	430.01
	427.15	427.22
	426.55	426.63
	425.89	425.94
	420.09	420.07
	419.85	419.83
	419.10	419.10
	418.19	418.19
	416.41	416.42
	415.87	415.86
	404.45	404.42
OH	306.4	306.4 (bandhead)

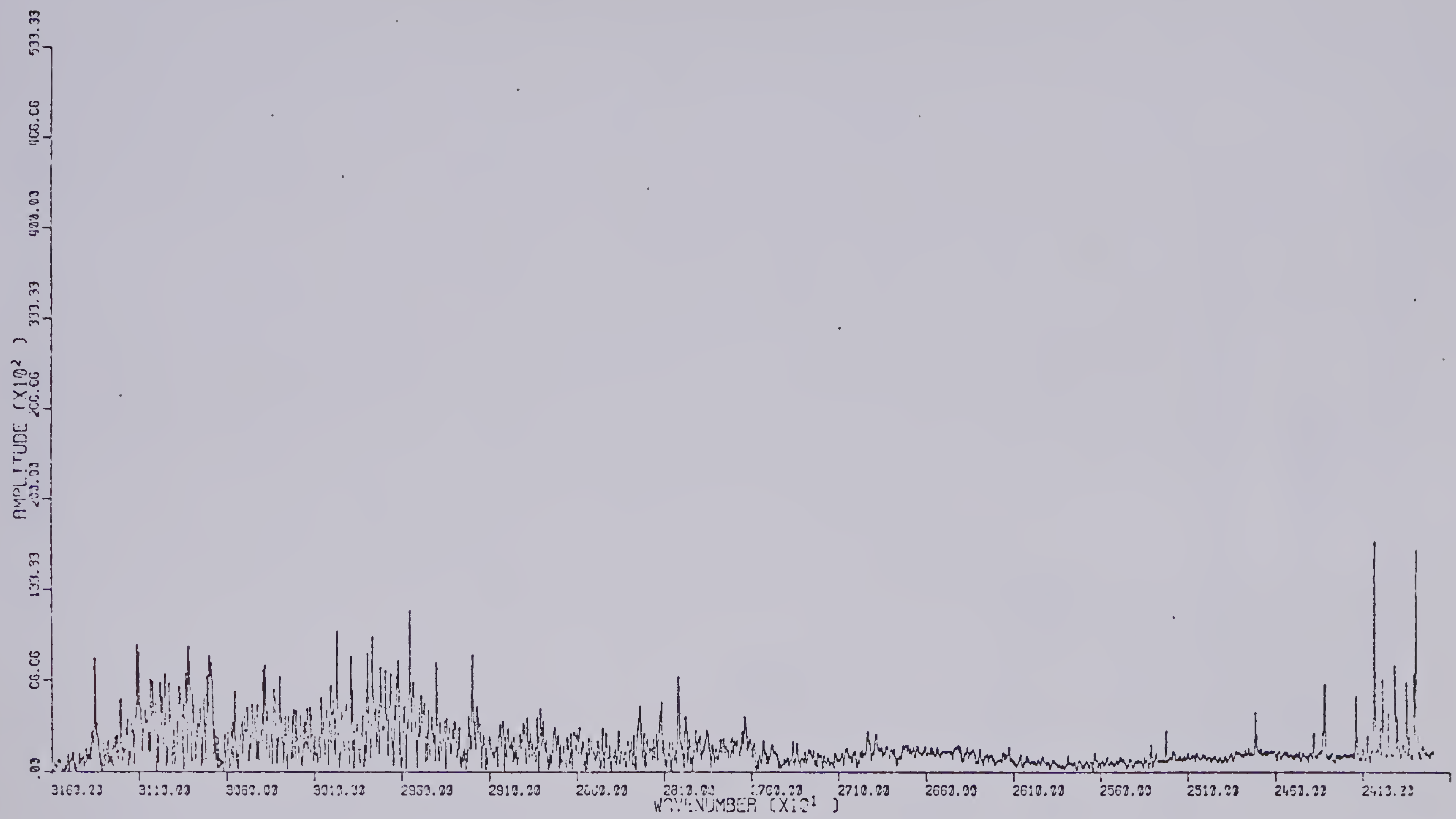

FIGURE 41. Argon plasma background emission spectrum, no water aspirating

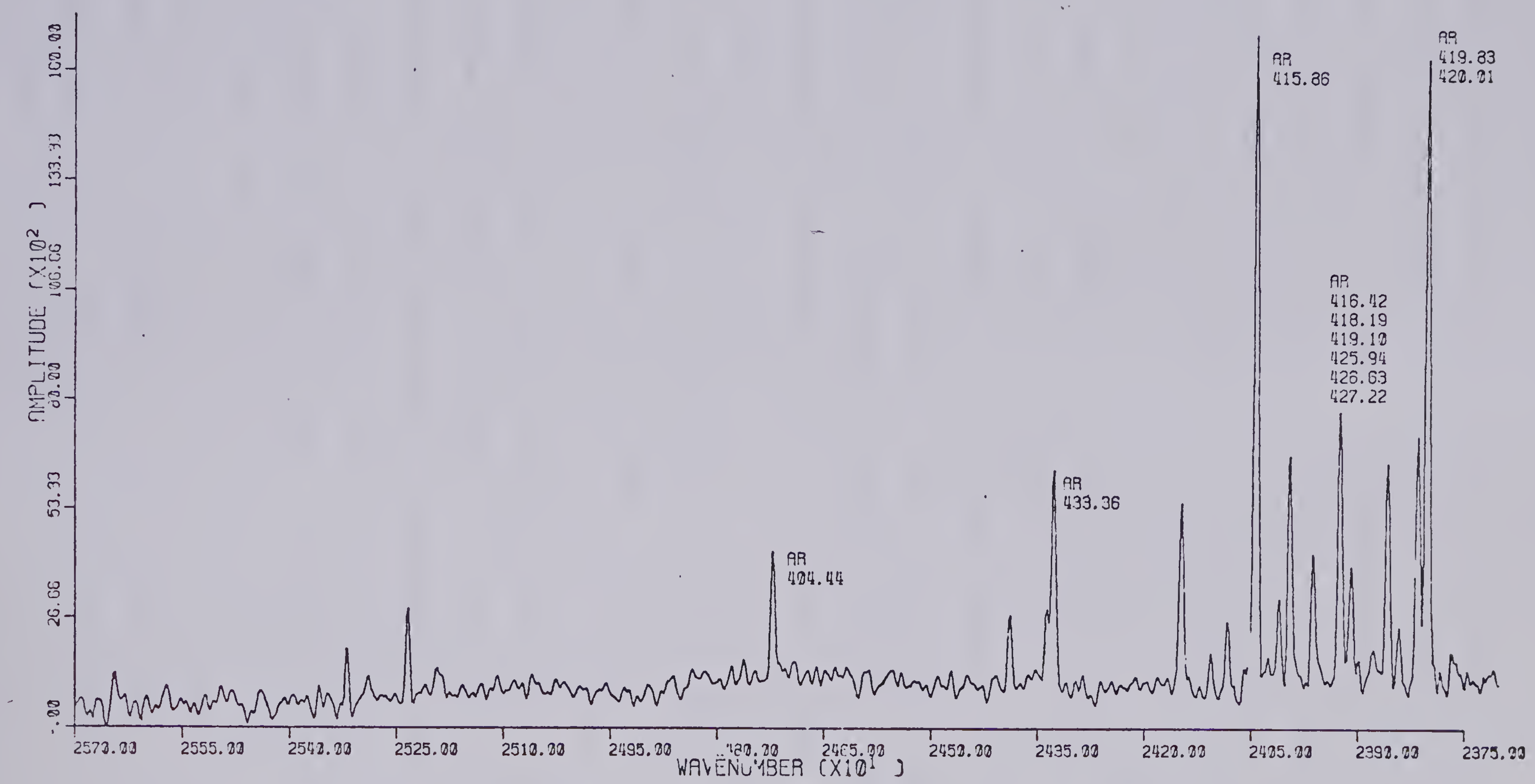

FIGURE 42. Expansion of the plasma emission near 400 nm

of energy available for atomic or ionic excitation. The neutral atom and ion emission lines of calcium provide a good indication of the energy available with respect to the flame sources discussed previously. The neutral atom calcium emission at 422.6 nm requires at least 2.93 eV for excitation to emission while the calcium ion emission lines at 396.9 nm and 393.4 nm require 3.12 eV and 3.15 eV, respectively, over and above their ionization potential of 6.1 eV. Thus a total of at least 9.22 eV must be available in the plasma emission source for calcium ion line emission to occur. The complete plasma emission spectrum for a 1.0 ppm aqueous solution of $Ca(NO_3)_2$ is shown in Figure 43. The corresponding emission spectrum for a 0.3 ppm $Ca(NO_3)_2$ aqneous solution under the same experimental settings is illustrated in Figure 44. Note the presence of only calcium ion line emissions at 396.9 and 393.4 nm as opposed to a mixture of ion and neutral atom line emission in the nitrous oxide flame. Note also the presence of the NH band at 336.0 nm due to the use of the nitrate salt of calcium. For the 1.0 ppm Ca solution the 393.4 nm emission line had a 0.6% relative standard deviation over eight repetitions of twenty-five signal averaged interferograms. Over a period of two and one half hours the percent relative standard deviation rose to 3.04%. An optical filter (Corning CS #7-59) was used to isolate the ion emission lines in both of the above spectra. This eliminated the strong hydrogen emission at 486.1 nm and most of the strong argon line emissions near 420 nm. The smaller hydroxyl band emissions were also removed with this filter.

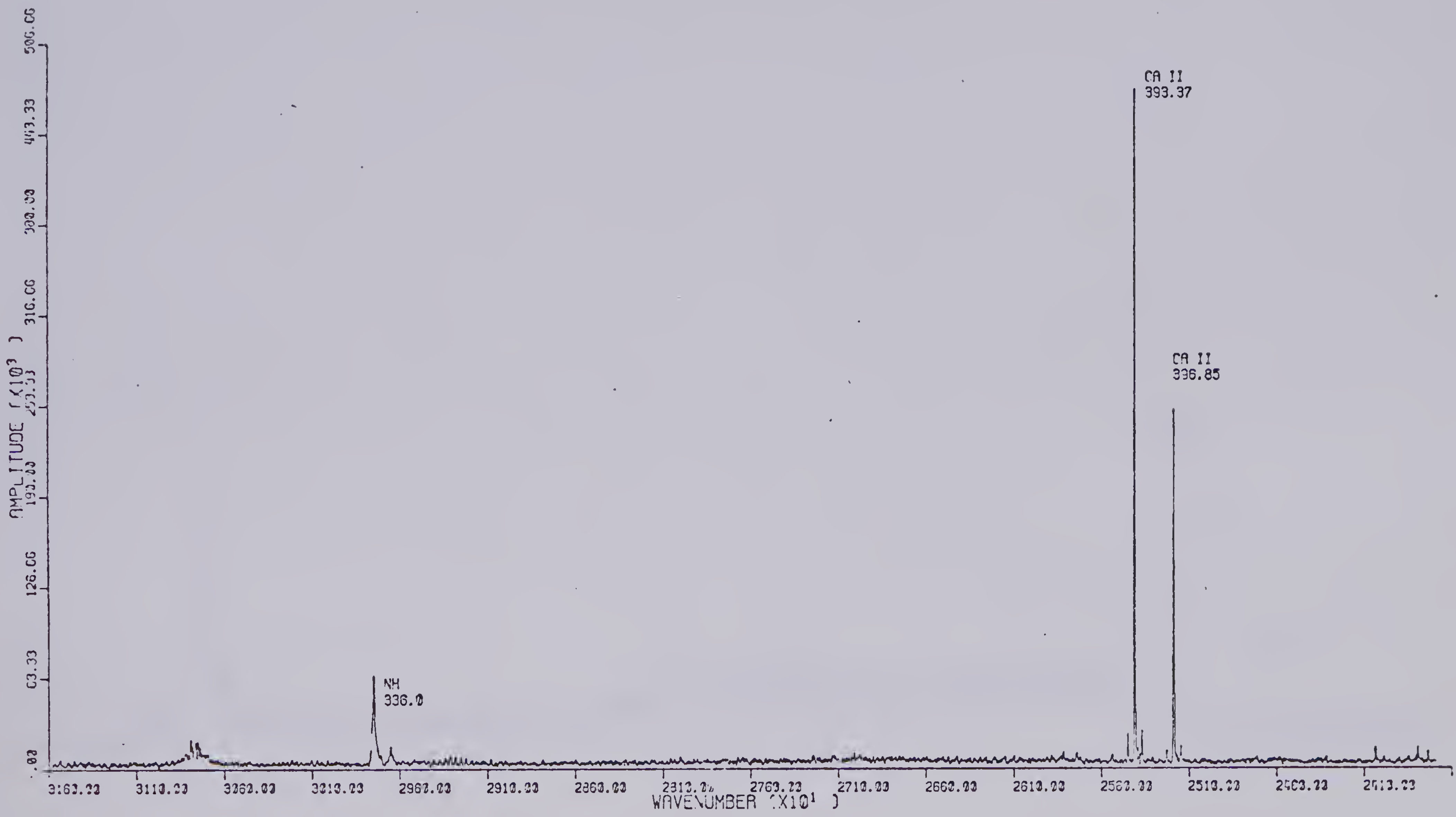

FIGURE 43. Plasma emission spectrum of 1.0 ppm $Ca(NO_3)_2$

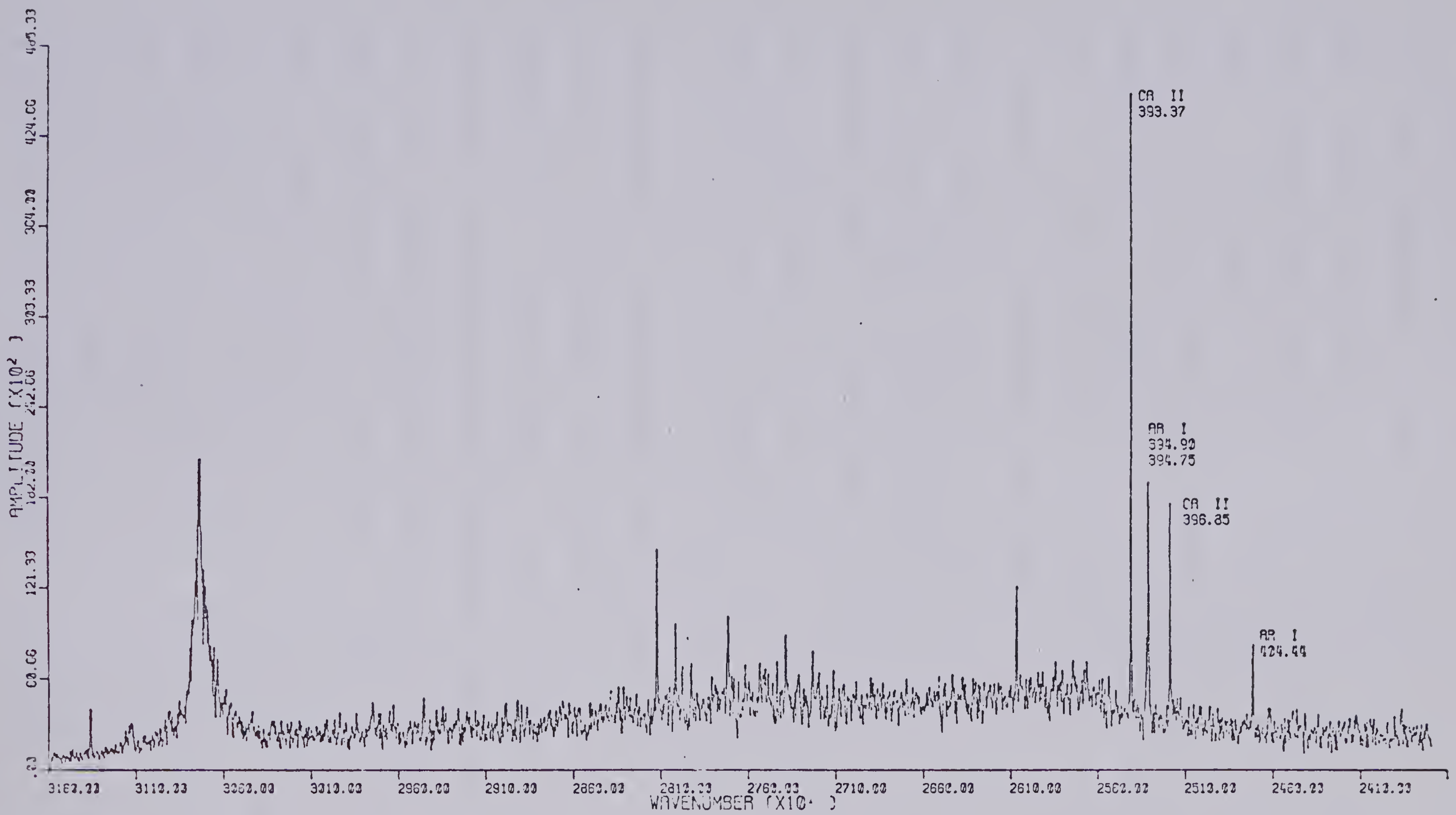

FIGURE 44. Plasma emission spectrum of 0.3 ppm $Ca(NO_3)_2$

Using the calcium emission spectra as an example system, a further comparison of the three atomic emission sources under study is warranted. How do the air acetylene flame, the nitrous oxide acetylene flame and argon R.F.-I.C.P. compare with respect to the amount of energy available for atomic excitation? The three partial calcium emission spectra shown in Figure 45 give an excellent indication. The spectral region from 390.0 nm to 430.0 nm has been isolated. In Figure 45 (A) note only the presence of neutral atom species emission at 422.6 nm. This emission was due to a 1000.0 ppm $Ca(NO_3)_2$ aqueous solution nebulized into the air acetylene flame. As described in Chapter IV the majority of the calcium is present as an oxide complex emitting broadband radiation in the 600 nm spectral range. This flame barely provides enough energy for the excitation of the neutral atom species of calcium and the ionic species emission need not even be considered. In Figure 45 (B) the corresponding portion of a 1.0 ppm $Ca(NO_3)_2$ aqueous solution emission spectrum in a nitrous oxide-acetylene flame is illustrated. All of the calcium emission occurs in this region since no oxide species exist in this flame. Note the presence of both the neutral atom and ion line emissions of calcium at 422.6 nm, 396.8 nm and 393.4 nm respectively. This flame, about 1000°C higher in temperature than the air-acetylene flame, provides enough energy for the partial ionization of the calcium atoms present. The major emission contribution is still from the calcium neutral atom species. Note the

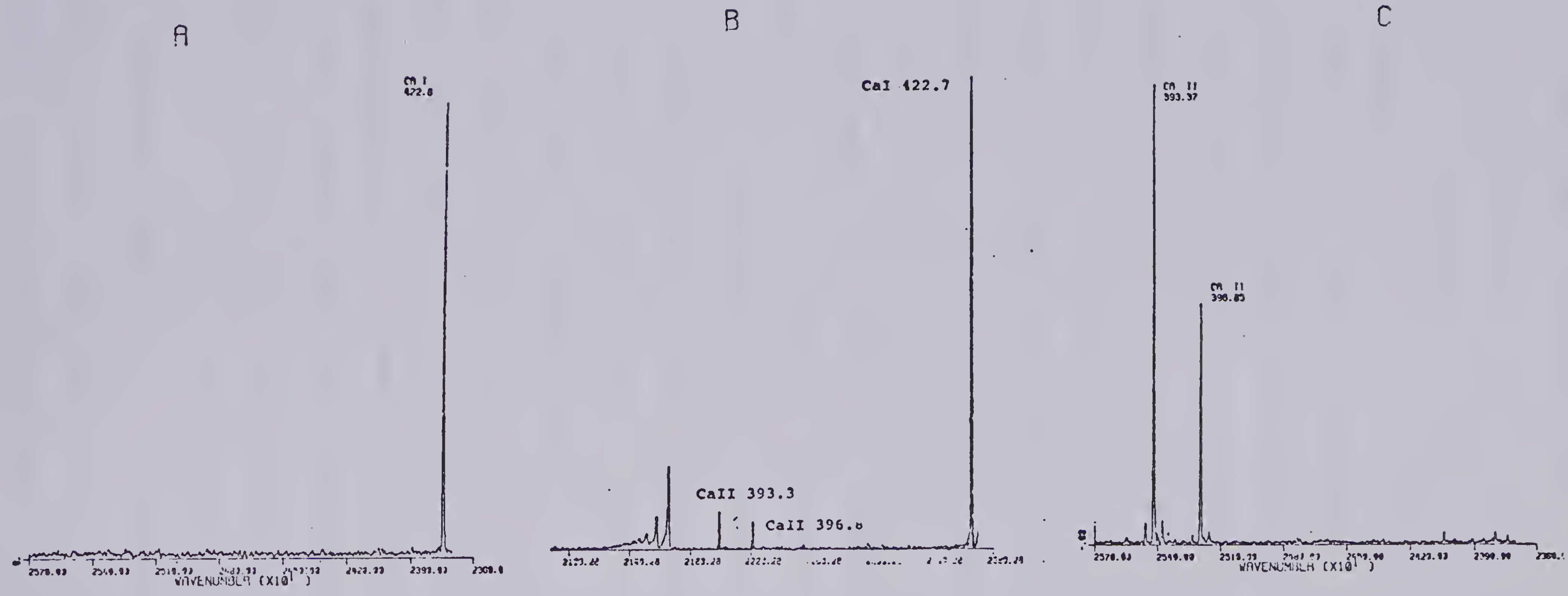

FIGURE 45. Ca emission

(A) air-acetylene flame

(B) nitrous oxide acetylene flame

(C) argon I.C.P.

proximity of the flame background emission band. In Figure 45 (C) the corresponding portion of the plasma emission spectrum of a 1.0 ppm aqueous $Ca(NO_3)_2$ solution is shown. No optical filtering could be used in order that any presence of a neutral atom species could be detected. As seen in the spectrum calcium now emits completely as an ionic species indicating that not only is enough energy available to ionize the calcium present, but also to excite a large proportion of the ionic species to emission. Thus the spectra in Figure 45 give a valuable quantitative indication of the relative amounts of excitation energy available in each of the three atomic emission sources under consideration.

The large amount of excitation energy provided by the plasma source not only affects the species of a particular element excited to emission but also the variety of elements capable of being excited. Many elements not excited to emission, with high sensitivity, in the flames previously discussed, now readily undergo emission in the plasma. The plasma thus naturally lends itself to multielement analysis very readily and, when coupled to an interferometer detection system, simultaneous multielement analysis is achievable. In Figure 46 the emission spectrum, obtained with the plasma-interferometer system, of a multielement mixture is shown. Table X presents a list of the observed and literature (65) elemental emission lines for the elements present as well as their concentrations. The spectrum presented is the result of eight averaged spectra each of twenty-five signal averaged

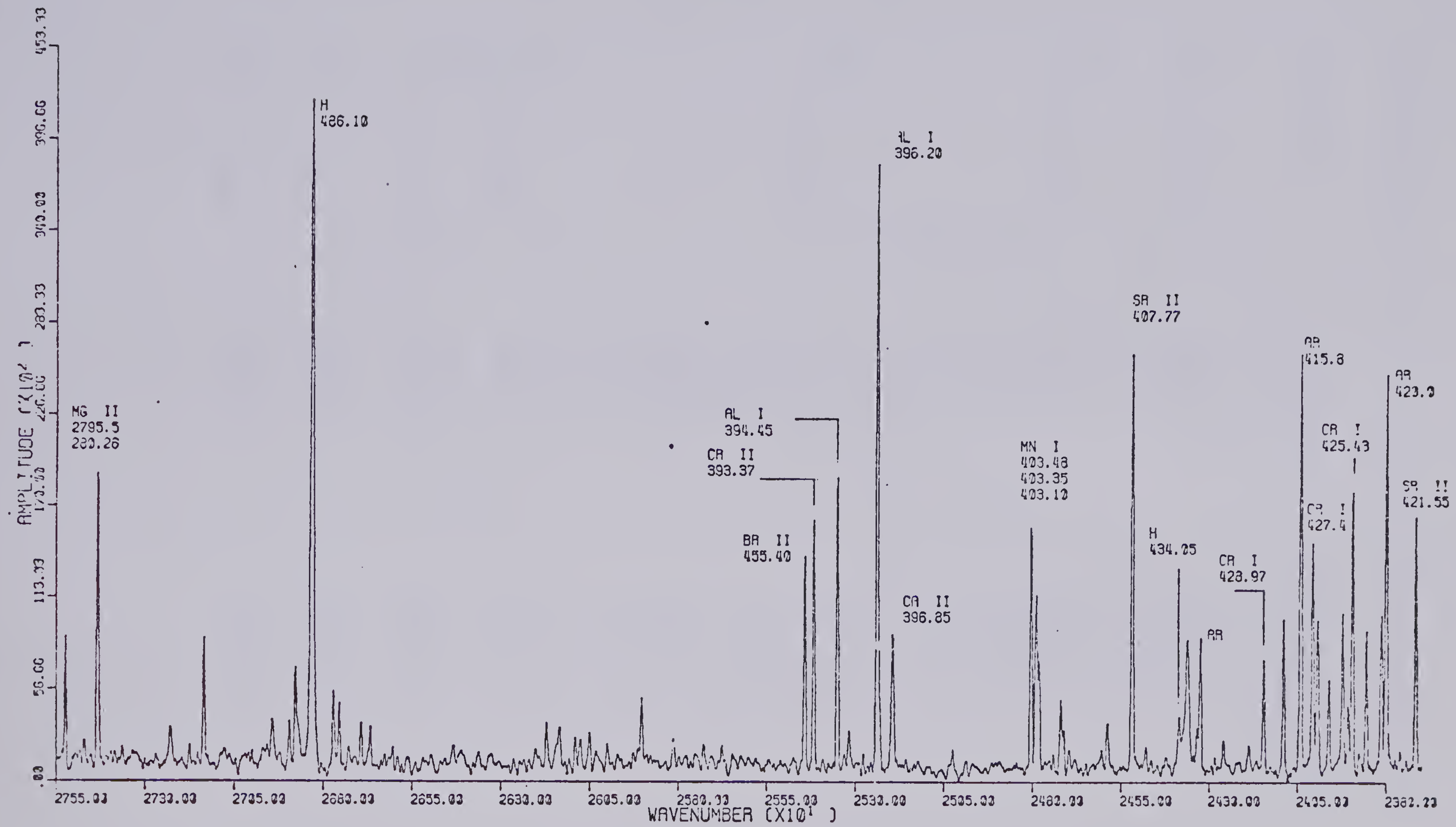

FIGURE 46. Multielement argon plasma emission spectrum

Table X

Multielement I.C.P. Emission with a 1P28 P.M.T.

Element		Observed Wavelength nm	Literature (65) Wavelength nm
Mg	I	285.18	285.21
(10.0 ppm)	II	280.25	280.26
	II	279.54	279.55
Mn	I	403.07	403.08
(30.0 ppm)	I	403.32	403.31
	I	403.47	403.45
	II	294.90	294.92
	II	293.92	293.93
	II	293.30	293.31
	II	260.55	260.57
	II	257.59	257.61
Fe	I	374.93	374.95
(50.0 ppm)		374.58	374.56
		373.71	373.71
		373.50	373.49
		371.99	371.99
		36.174	361.78
		358.11	358.12
		356.98	357.01
		356.71	356.74
		355.49	355.49
Al	I	309.24	309.28
(50.0 ppm)		308.20	308.22
Ba	I	553.46	553.55
(0.4 ppm)	II	493.35	493.41
	II	455.34	455.40
Sr	II	421.56	421.55
(0.2 ppm)		407.76	407.78
Ca	II	396.86	396.85
(0.1 ppm)		393.38	393.37

interferograms. This spectrum is an excellent example of the wide spectral coverage simultaneously available. For example, the manganese emission line at 259,5 nm and the barium emission line at 553.5 nm may be simultaneously monitored as well as all of the other spectral information present within the response range of the detector. In some cases, where the background or matrix emission is of much greater intensity than the analyte emission, a classic example of the limited dynamic range problem, previously discussed in Chapters I and IV, exists. Let us further consider this problem as it relates to the plasma emission source in the U.V.-VIS. spectral range.

Consider the case of trace aluminum determination in the presence of a high concentration calcium matrix. As illustrated in Figure 47, the aluminum neutral atom emission lines are very close to the calcium ion emission lines but differ greatly in sensitivity. According to Boumans (89) a factor of 250 exists in their plasma emission sensitivity. Optical or electronic filtering is out of the question due to their close proximity. The only alternative rests in the removal of calcium in a sample pre-analysis step adding one more source of experimental error if the dynamic range limiting emission line is the result of source background emission. Indeed this was found to be the case in attempting to obtain quantitative information on calcium emission in the form of an analytical curve extending over several orders of magnitude. Without the presence of optical filtering, the

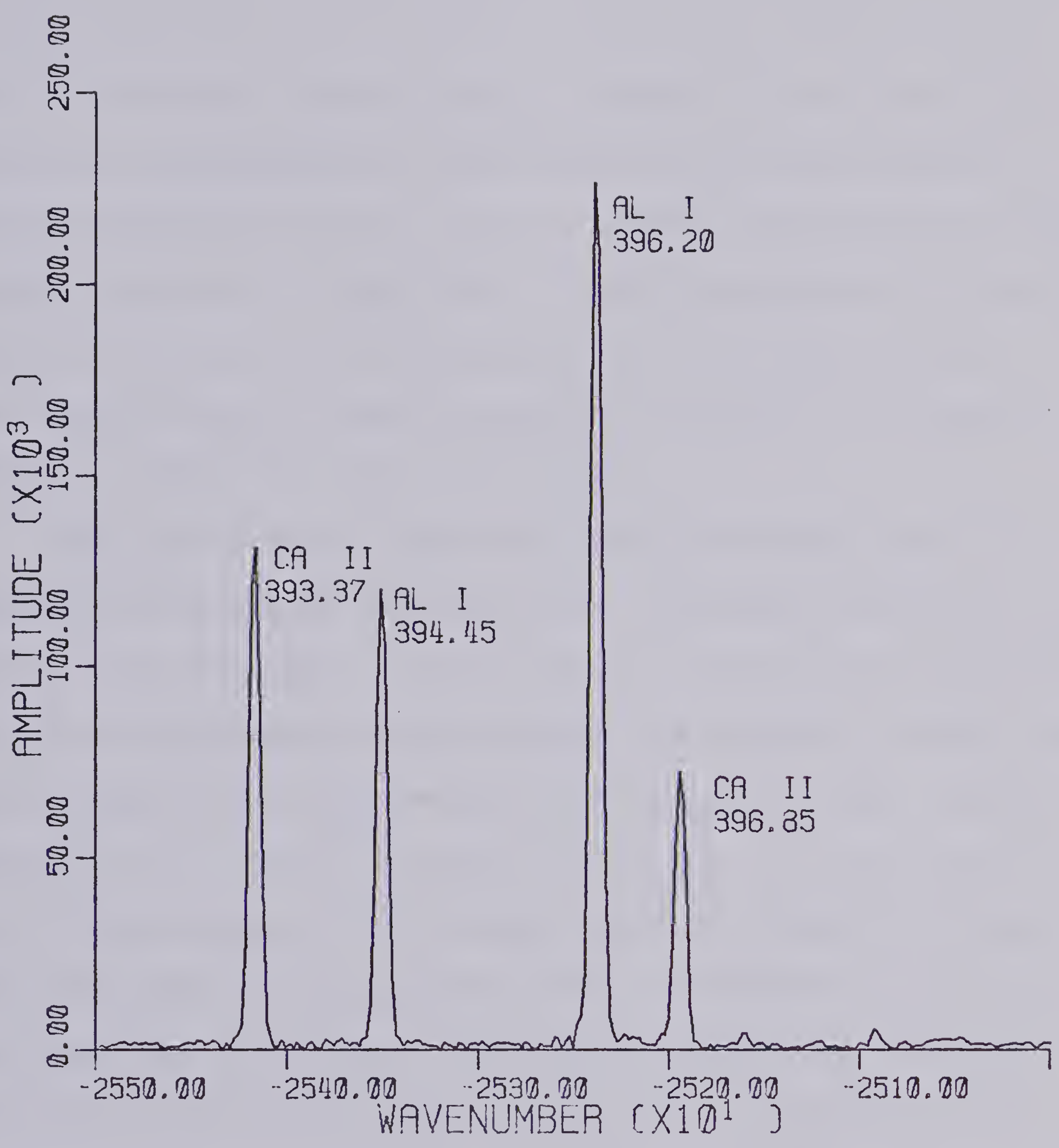

FIGURE 47. Emission spectrum of Ca and Al

486.1 nm hydrogen emission line quickly becomes a dynamic range limitation in the concentration range of 0.10 ppm calcium. After optical isolation of the calcium ion emission lines the argon line emission at 394.8 nm, midway between the ion emission lines, becomes a dynamic range limitation at calcium concentrations on the order of 0.01 ppm calcium. Typical detection limits using a plasma monochromator-based system are below 0.1 ppb (89). Thus the problem of dynamic range limitations may ultimately limit the sensitivity of the interferometer-based system for elements in a spectral position similar to that of calcium.

One quantitative study was completed using the 1P28 photomultiplier tube detector with the plasma emission source. Again some indication of the spectral distribution of noise in the interferometer-based system was sought. To gain this information one would ideally like to monitor the standard deviation of a small emission signal both in the presence of and in the absence of a larger amplitude emission signal. Normally this is accomplished using two separate solutions, one with and one without the high concentration species. A novel approach uses only one solution containing both analytes and employs the use of an optical filter that selectively eliminates emission from the high concentration species. Such an experiment was performed using the magnesium line emissions in the ultraviolet as the high intensity signal and the calcium ion line emissions in the visible as the low level signal. The magnesium was present at 100.0 ppm

and the calcium was present at 0.10 ppm. A Corning filter #Ø-54 was used, due to its 100% transmittance above 300 nm, to isolate the emission lines. Example spectra of the calcium ion emission lines at 393.4 nm and 396.8 nm with and without the magnesium emission present are shown in Figures 48 and 49. About a factor of ten exists between the Mg and Ca peak amplitudes. The variances of the 393.4 nm Ca ion emission line are presented in Table XI. Under a variance ratio F-test at $\alpha = 0.05$, the variances with and without the presence of Mg were found to be statistically equivalent. A similar test on the H 486.1 nm and Ar 420.1 nm emission lines also indicated no change in the peak variance due to the presence of Mg emission. This is definite evidence for the non uniform distribution of noise over the spectral domain, in direct contrast to the uniform distribution predicted by multiplex theory. Note that this is similar to the situation found for the flame emission sources.

The concept of internal standard use has been mentioned in Chapter IV with regard to flame analyte emission. The possibility of utilizing one of the argon or hydrogen lines as a plasma internal reference does seem tempting. With data from the experiment carried out above tests were carried out on the use of the 420.1 nm argon line emission or the 486.1 nm hydrogen line emission as internal reference standard lines. The precision of both the calcium ion emission line and the magnesium ion emission line (393.4 nm

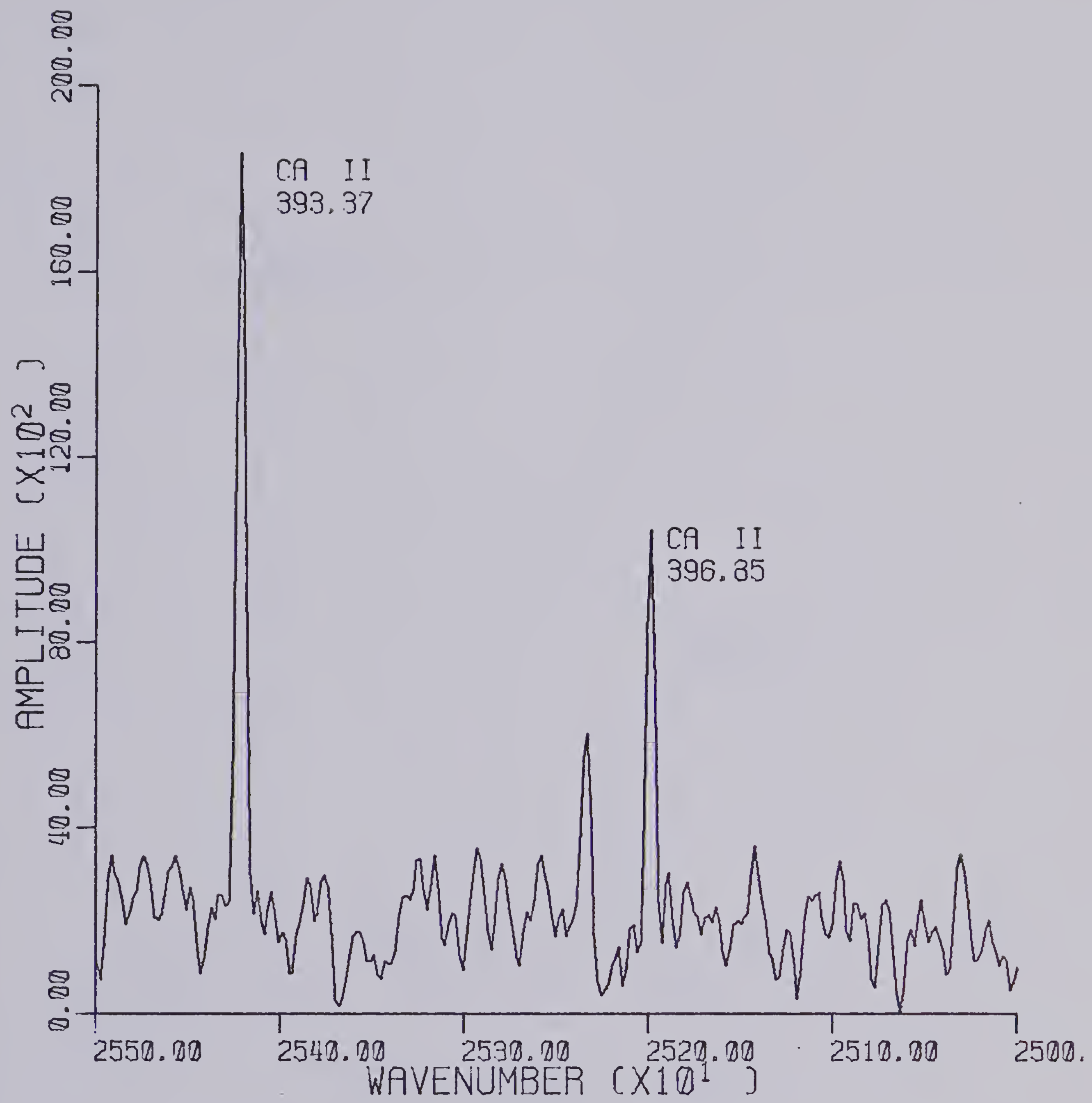

Figure 48.

Ca (0.1 ppm) ion emission lines in the presence of 100.0 ppm Mg, unfiltered.

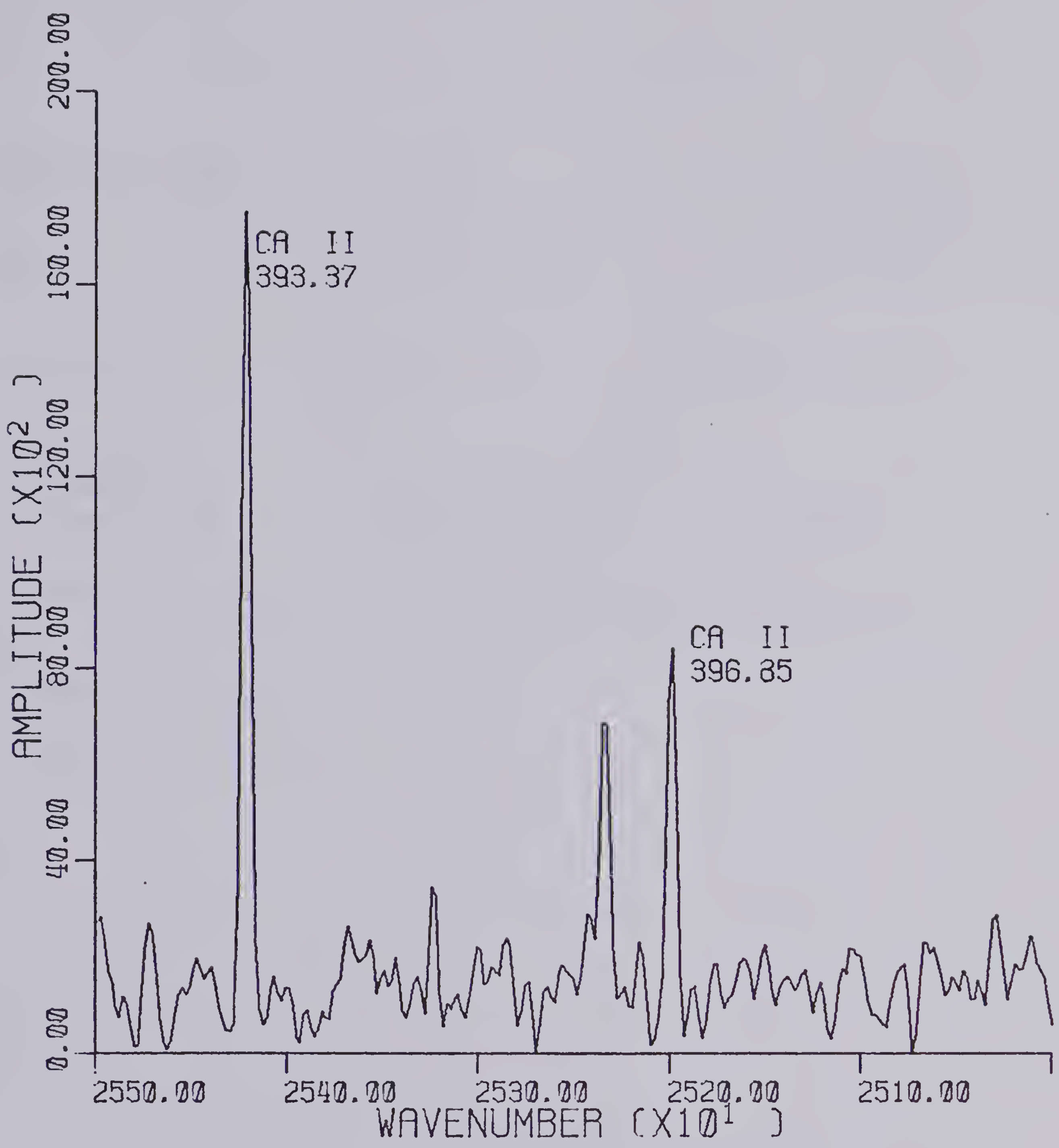

Figure 49.

Ca (0.1 ppm) ion emission lines in the presence of 100.0 ppm Mg, filtered.

Table XI

Variance Data for Ca-Mg Study

Ca 393.3 nm emission peak	Ca + Mg* no filter	Ca + Mg* + filter #0-54
Mean	1.97765×10^4	1.86731×10^4
Variance	1.0240×10^7	4.3482×10^6
% Relative Standard Deviation	16.19	11.16

*[Ca] = 0.1 ppm

[Mg] = 100.0 ppm

and 279.5 nm respectively) become worse upon internal referencing to either of these background emission lines. At least a 3.0% increase in relative standard deviation was noted in both cases. Further work needs to be done in this area of internal reference standards for the interferometer-based atomic emission instrument. The data base currently available was not felt to be large enough to draw any definite conclusions.

With the 1P28 photomultiplier detector dynamic range limiting factors have been rather serious and have prevented the acquisition of a large base of quantitative data. Let us now consider a more promising spectral region, that of the ultraviolet.

2. The Solar Blind P.M.T. as a Detector

A rather large variety of elements have sensitive spectral emission lines that fall in the spectral range from 200 nm to 300 nm. Chromium, manganese, cadmium, silicon, magnesium, boron, tin, lead, zinc and iron are among the elements falling into that classification. The current interferometer does not operate below a spectral limit of 240 nm, due to the germanium beamsplitter characteristics, and so eliminates several important spectral emission lines such as those of zinc at 213.9 nm and 206.2 nm and cadmium at 228.8 nm and 214.4 nm. In order to work in the spectral region 240.0 nm to 300.0 nm, without the dynamic range problems of the 1P28 PMT response, a solar blind photomultiplier tube (HTV-R166 Hamamatsu TV CO. Ltd.) (63) was employed as a

detector. The dynamic range limiting lines of hydrogen and argon will no longer be seen by this detector with a peak spectral response at 220 nm falling to 10% peak response at 180 nm and 300 nm. Note that the interferometer will not be operating in the optimal response region of this detector. The detector was operated at 600 volts with the same dynode chain as described in Chapter II. Refer to Chapter III for example spectra of hollow cathode lamps obtained with this solar blind tube.

The plasma emission background spectrum as seen by the solar blind tube is shown in Figure 50. This spectrum was obtained through the averaging of six spectra each consisting of twenty five signal averaged and transformed interferograms. No optical filters were used or were necessary. Note the absence of any distinguishing background emission features, providing an excellent region for analytical work. Both qualitative and quantitative studies were undertaken in this spectral region and the results from each study will now be presented.

Let us look first at the qualitative aspects of the plasma emission source in this spectral range. As mentioned in the introduction to this chapter many elements have spectral emission lines in this region. A multielement aqueous solution, containing tin, lead, chromium, boron, iron, silicon, magnesium, and manganese was aspirated into the argon plasma. The resulting emission spectrum is illustrated in Figure 51. The individual concentrations, observed

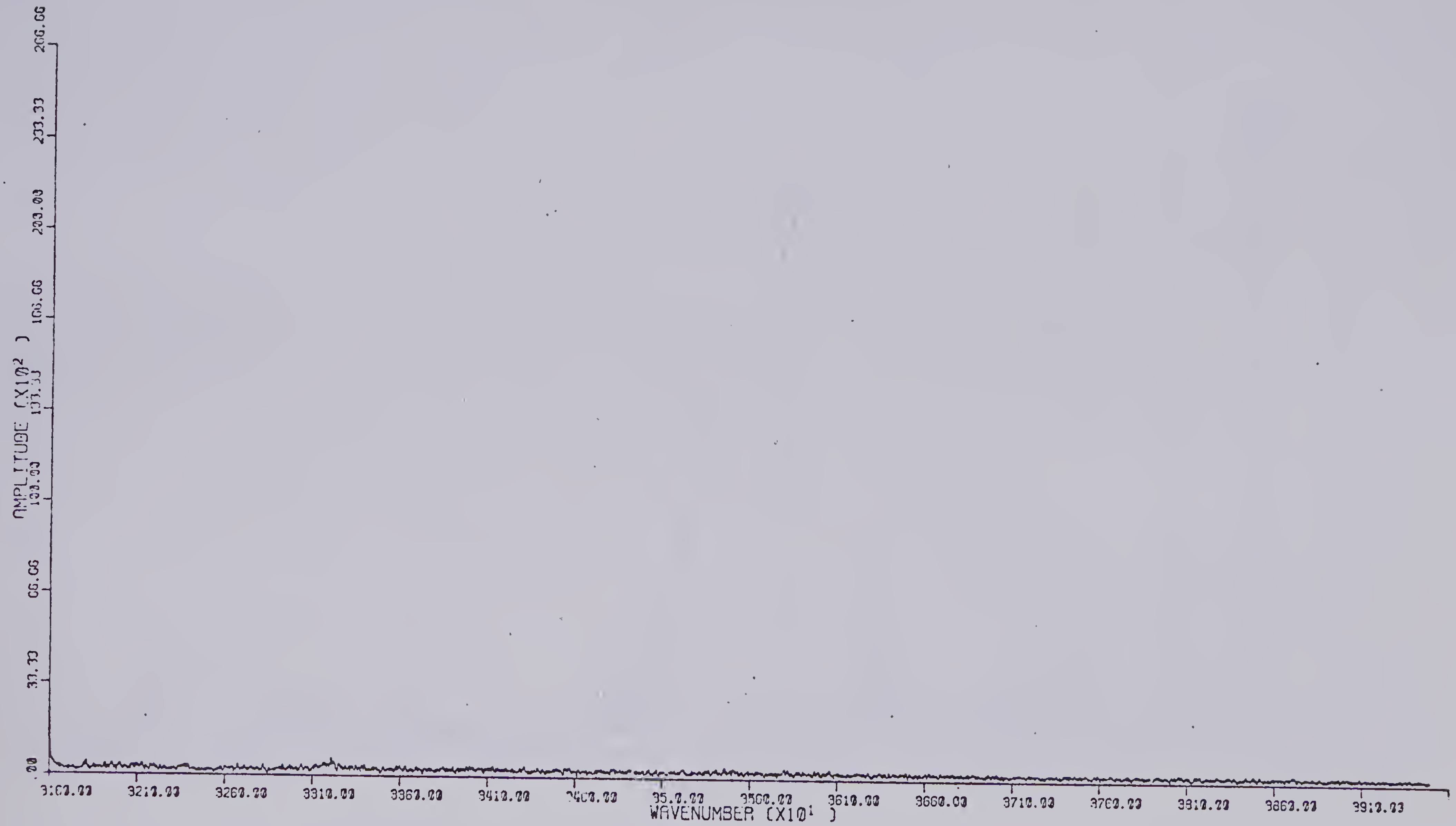

FIGURE 50. Argon plasma background emission as seen by the solar blind P.M.T.

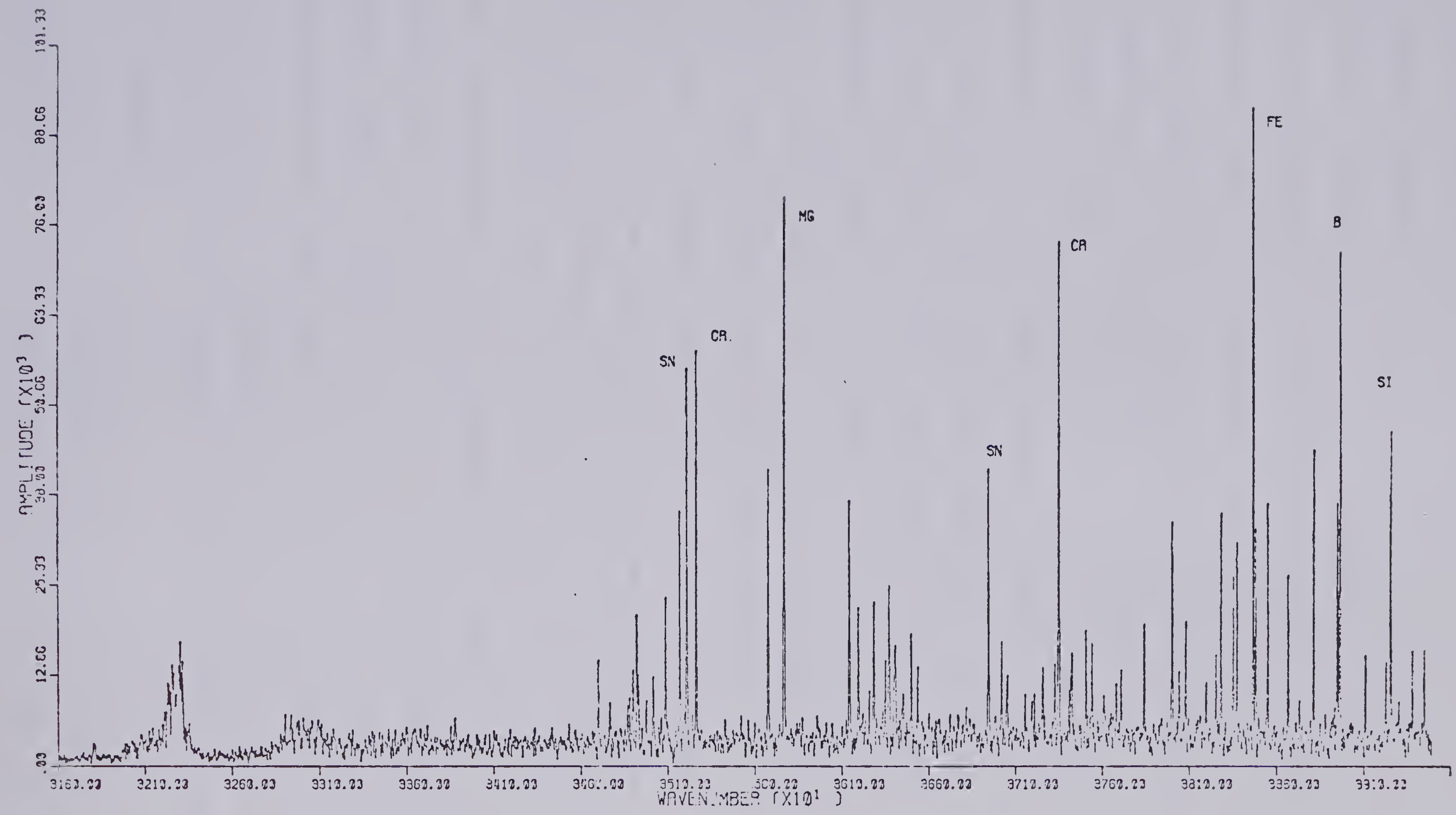

FIGURE 51. Multielement plasma emission spectrum--solar blind P.M.T. detector

emission wavelengths, and literature wavelengths (65) are listed in Table XII. The concentrations were chosen so as to provide a multielement sample emission spectrum and are in no way indicative of the detection limits available. The spectrum does give a qualitative indication of the relative concentrations that may be determined simultaneously. The experimental parameters were not optimized for any particular elemental emission but to yield the highest overall quality spectrum. An expanded version of the same spectrum is shown in Figure 52. Note the high resolution capability available in this spectral region, especially with respect to the boron doublet at 249.66 nm and 249.7 nm and the iron doublet at 259.84 nm and 259.94 nm. Even at this high resolution, 0.0483 nm, problems do occur with respect to the spectral overlap of aliased frequencies. For example the silicon emission line at 251.61 nm is aliased directly on top of the 254.66 nm emission line of tin. The silicon line aliases to 254.65 nm. With the current resolution, these peaks are not resolvable, but an increase by a factor of five in resolution, to 1.55 cm^{-1}, or .01 nm would adequately resolve these peaks. Aliasing may or may not be a serious problem depending upon the relative intensities of the two lines, their wavelength separation and whether or not any other analytically useful lines are available for the quantitative determination.

Since most of the quantitative work in this chapter will be done with manganese and magnesium, due to their

Table XII

Multielement I.C.P. Emission with a Solar Blind P.M.T.

Element	Observed Wavelength (nm)	Literature (65) Wavelength (nm)
Cr II	286.29	286.26
(20.0 ppm)	294.95	284.98
	283.53	383.56
	276.61	276.66
	276.22	276.26
	274.88	274.90
	267.67	267.72
B I	249.75	249.77
(100.0 ppm)	249.66	249.68
	239.54	239.51
Pb I	280.23	280.20
(200.0 ppm)	266.31	266.32
	261.35	261.42
Sn I	283.96	284.00
(200.0 ppm)	270.62	270.65
	254.55	254.66
	248.32	248.34
	242.93	242.95
	242.16	242.17
Si I	288.12	288.16
(250.0 ppm)	252.84	252.85
	252.39	252.41
	251.60	251.92
	251.43	251.43
	250.67	250.69
Fe II	275.54	275.57
(150.0 ppm)	274.62	274.65
	273.91	273.95
	263.08	263.11
	262.80	262.83
	262.53	262.55
	261.72	261.76
	261.14	261.18
	260.67	260.71
	259.90	259.94
	259.79	259.84
	258.55	258.59

Table XII

(Cont'd.)

Element	Observed Wavelength (nm)	Literature (65) Wavelength (nm)
Mn II	260.52	260.57
(10.0 ppm)	259.34	259.37
	257.57	257.61
Mg II	280.23	280.26
(4.0 ppm)	279.52	279.55

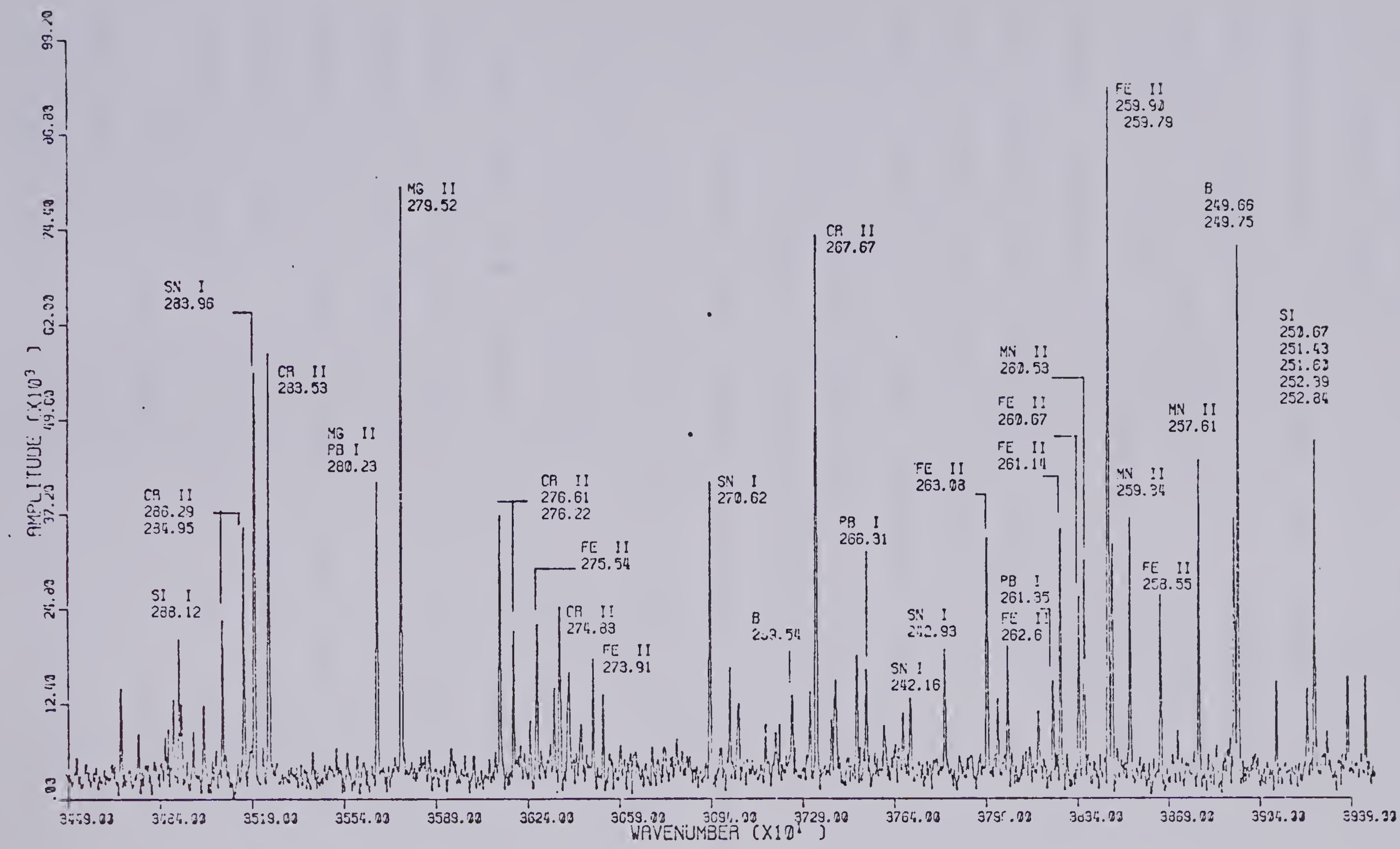

FIGURE 52. Expansion of multielement solar blind spectrum

relatively high emission sensitivity and simple spectra, let us examine their emission spectra. The spectrum in Figure 53 illustrates the emission resulting from the aspiration of an aqueous solution containing 20.0 ppm magnesium and 4.4 ppm manganese into the plasma. The emission lines, both observed and literature (65) are listed in Table XIII. Note also the presence of a carbon emission line in the spectrum. Its presence was due to a carbon dioxide or some other carbon based contaminant in the argon gas supply. Simply changing the supply tank eliminated the emission line. This may have some rather interesting aspects in that work is currently being done in our group and others (90) investigating the introduction of organics into the plasma directly or as aqueous mixtures. For interferometric analysis the presence of the carbon line, unless carefully filtered out, will create, again, a severe dynamic range problem. This would be expecially true in the case of direct introduction of organic solvents containing an analyte species of interest. A spectrum of an aqueous solution of 4.4 ppm manganese is shown in Figure 54, illustrating the loss of the carbon emission line and the presence of a third manganese emission triplet at 280 nm previously overlapped by the magnesium emission lines. The results from the quantitative emission study of manganese and magnesium will now be considered.

The first quantitative study involved the simultaneous determination of magnesium and manganese analytical curves. The magnesium concentration ranged from 100.0 ppm to 0.05 ppm,

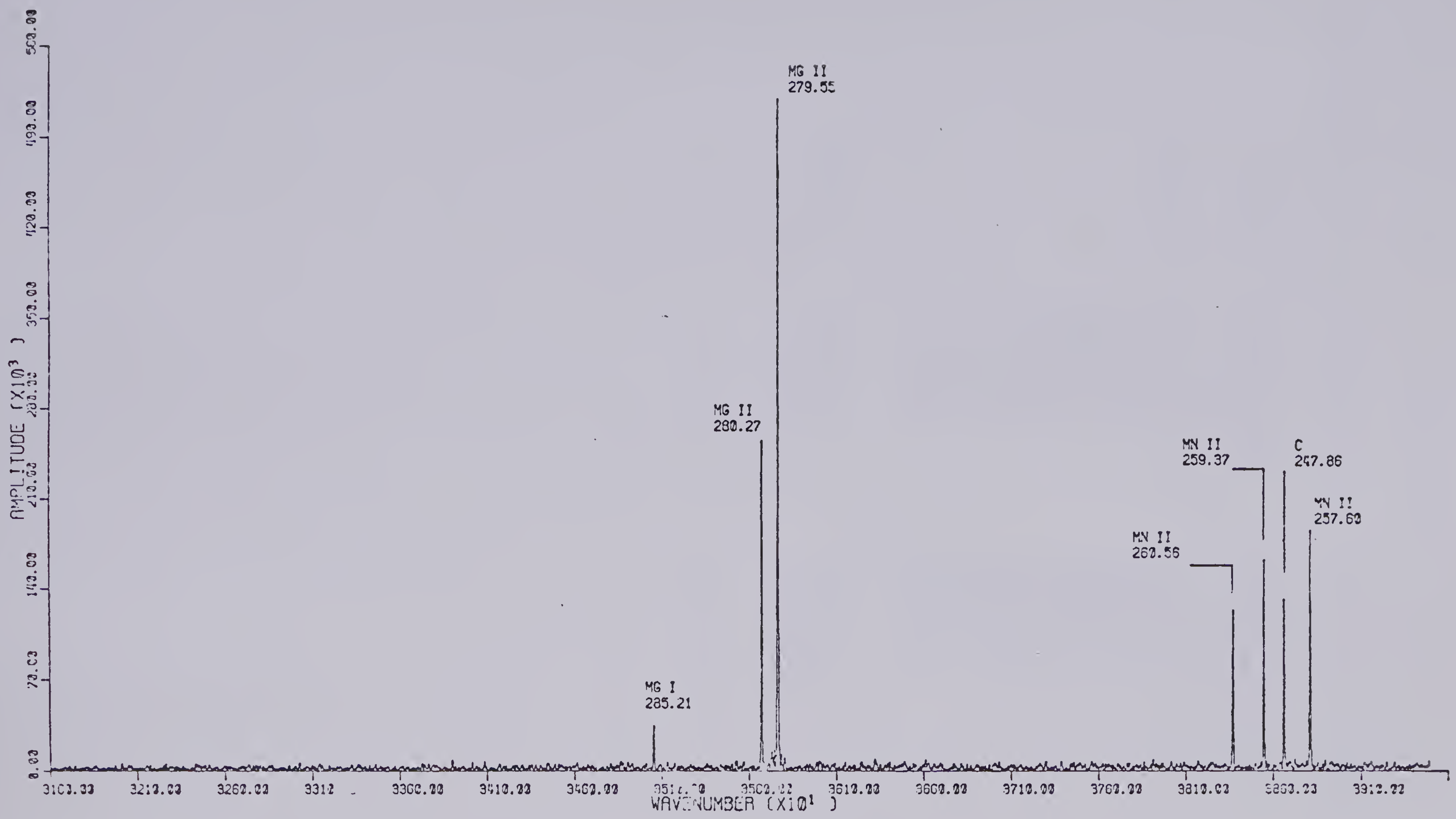

FIGURE 53. Emission of Mn and Mg with C line present

Table XIII

Emission Lines of Mn, Mg and C in the Ultra Violet Region

Element	Observed Wavelength nm	Literature (65) Wavelength nm
Mn II	294.92	294.92
	293.92	293.93
	293.30	293.31
	280.11	280.11
	279.79	279.83
	279.79	279.83
	279.45	279.48
	260.56	260.57
	259.37	259.37
	257.61	257.60
Mg I	285.21	285.21
II	280.27	280.26
II	279.55	279.55
C	247.86	247.86

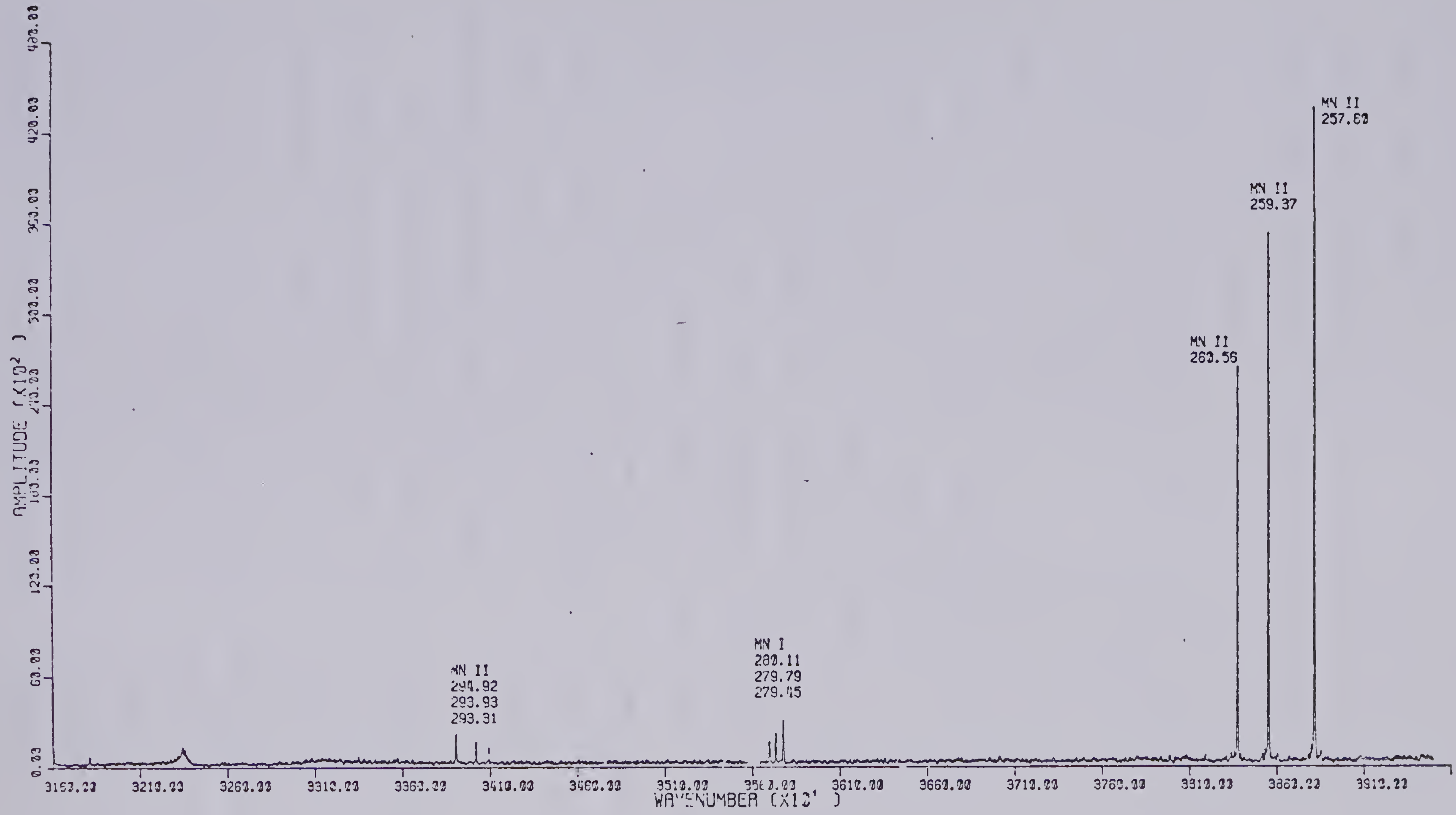

FIGURE 54. Plasma emission spectrum of a 4.4 ppm Mn solution-solar blind P.M.T.

as the manganese concentration was simultaneously varied from 300.0 ppm to 0.25 ppm. The analytical curve for the magnesium determination is presented in Figure 55, and is based upon the 279.5 nm peak emission amplitude. The data points each consist of six repetitions of twenty-five signal averaged interferograms. The slope of the curve is 0.979 ± 0.042 with an overall standard deviation of 0.059 and a correlation coefficient of 0.998. The simultaneously obtained data for the manganese analytical curve is shown in Figure 56 and is based upon the peak amplitude emission of manganese at 257.5 nm. The analytical curve has a slope of 0.970 ± 0.032 with an overall standard deviation and correlation coefficient calculated to be 0.127 and 0.993 respectively. For both manganese and magnesium, the analytical curves covering a three-order of magnitude concentration range have been achieved simultaneously. Although this is a very simple example, with no complicating factors such as dynamic range problems, the potential for simultaneous multielement determination has been identified.

The emission data obtained for the above study presents an excellent example to further study the noise spectral distribution characteristics of the interferometer system. The question still arises. Does the noise generated by a high intensity emission signal appear evenly distributed across the spectral range or will it be peak localized in the spectrum? A log-log plot of standard deviation versus magnesium peak amplitude (279.5 nm) is contained in Figure 57.

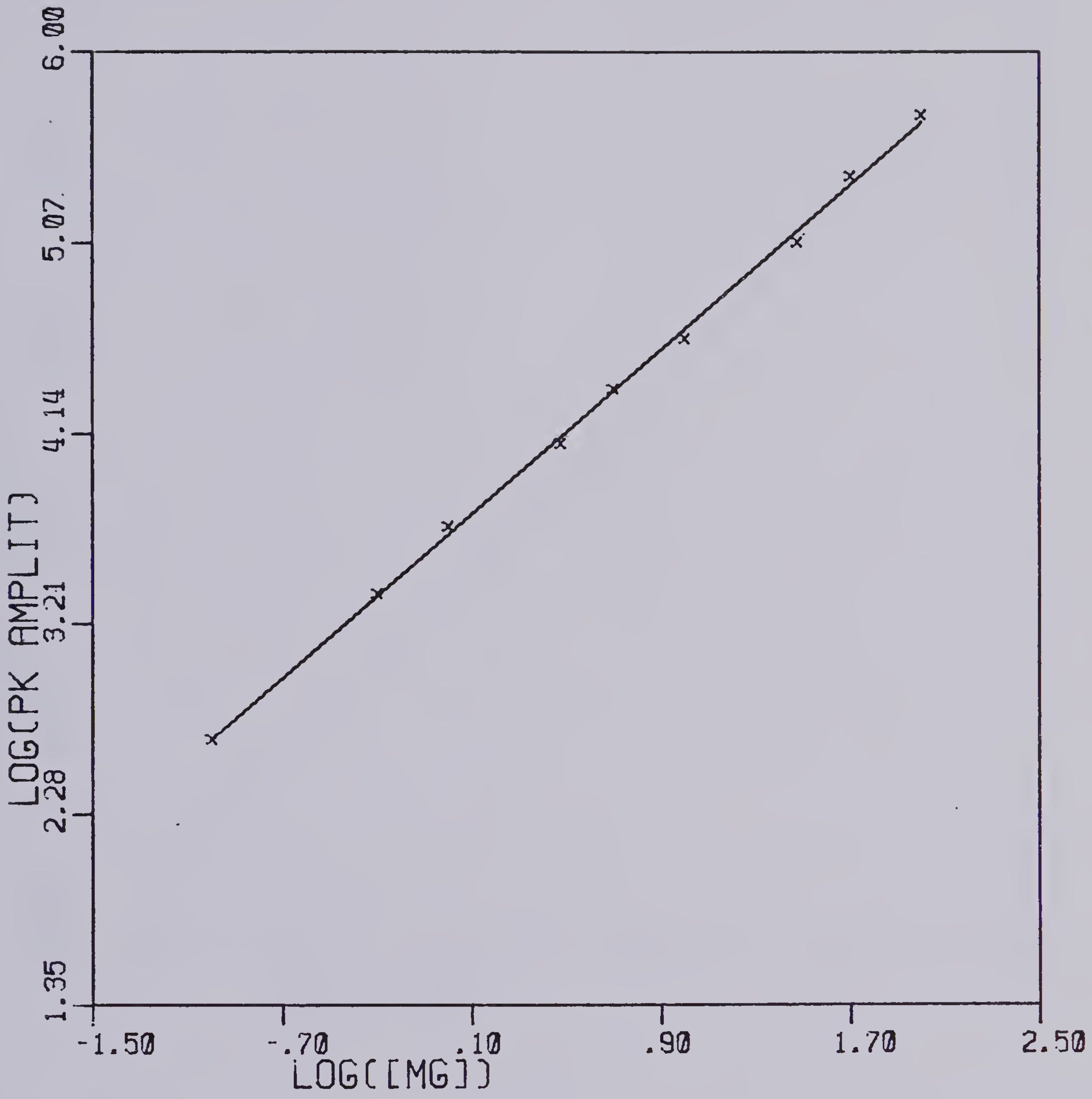

FIGURE 55. Mg analytical curve

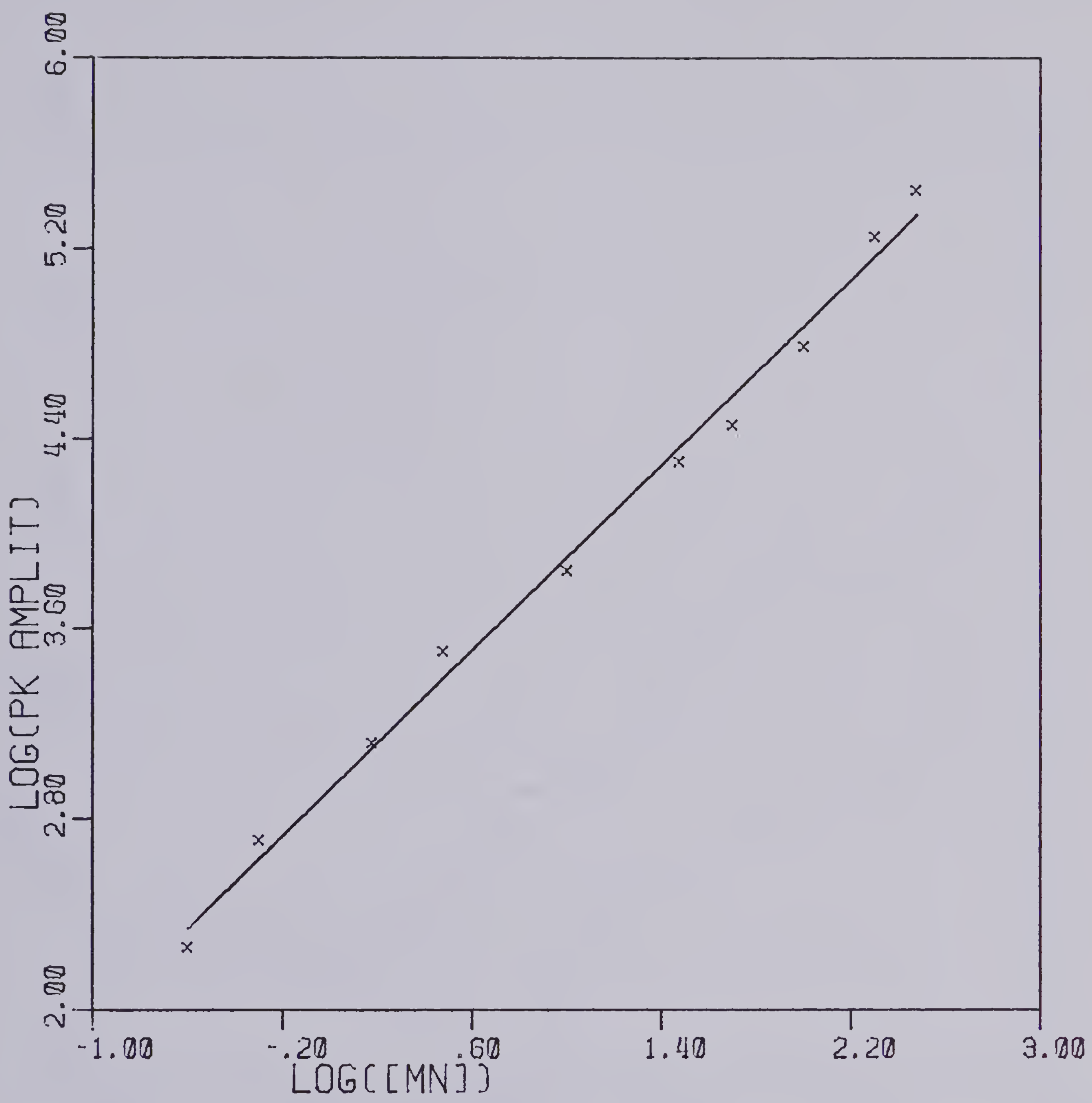

FIGURE 56. Mn analytical curve

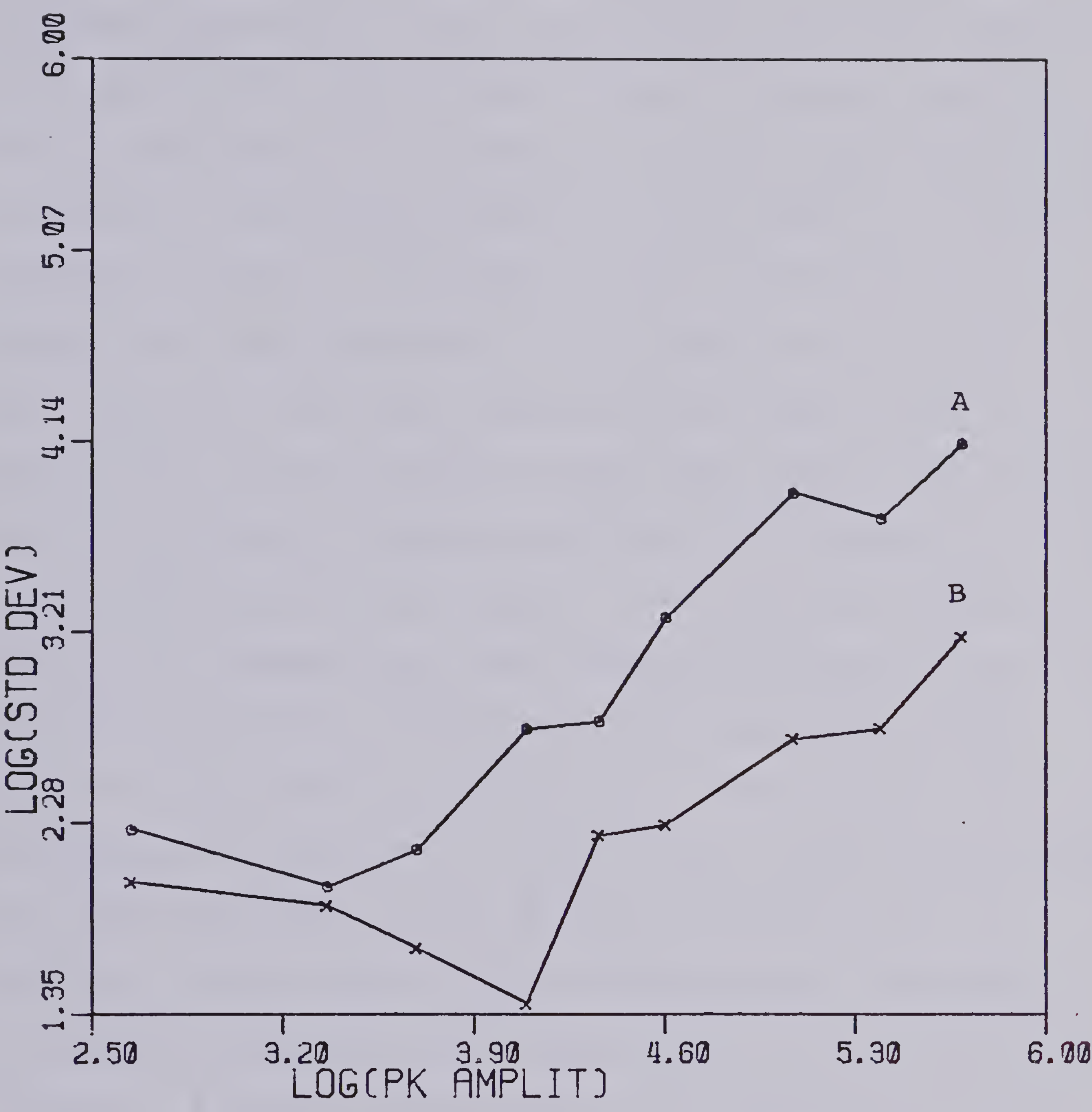

FIGURE 57.

Standard deviation plotted vs. 279.5 nm Mg peak amplitude

(A) 279.5 nm peak standard deviation

(B) 304.4 baseline point standard deviation

Curve 'A' is a plot of the magnesium peak standard deviation versus the peak amplitude and curve 'B' is the baseline standard deviation at 304.4 nm plotted versus the magnesium peak amplitude. Both curves 'A' and 'B' show a linearly increasing trend at the higher peak amplitudes, indicative of a source fluctuation noise limited system. In a shot noise limited situation a levelling effect would be present at higher peak amplitudes due to its square root relationship with emission intensity. Note that the same scale, as in the analytical curves of Figure 56 has been used on the vertical axis to provide a reference amplitude for comparison. Since the interferometer spectrometer is a multiplex technique, that is all signals are simultaneously observed, a plot of standard deviation versus total peak amplitude at each concentration would be appropriate. This would be true expecially in the case of a shot noise limited system where the noise amplitude varies directly with the signal intensity. In the case of the interferometer, the signal intensity consists of the algebraic sum of the interfering signals. A direct relationship exists between the sum of the peak amplitudes in the spectral domain and the maximum signal intensity that may be present in the time domain. Therefore the worst case possible for shot noise is taken into account. A log-log plot of standard deviation versus total peak amplitude at each concentration is presented in Figure 58. Curve 'A' and 'B' are the same as in the preceeding figure and the vertical axis is still scaled to the

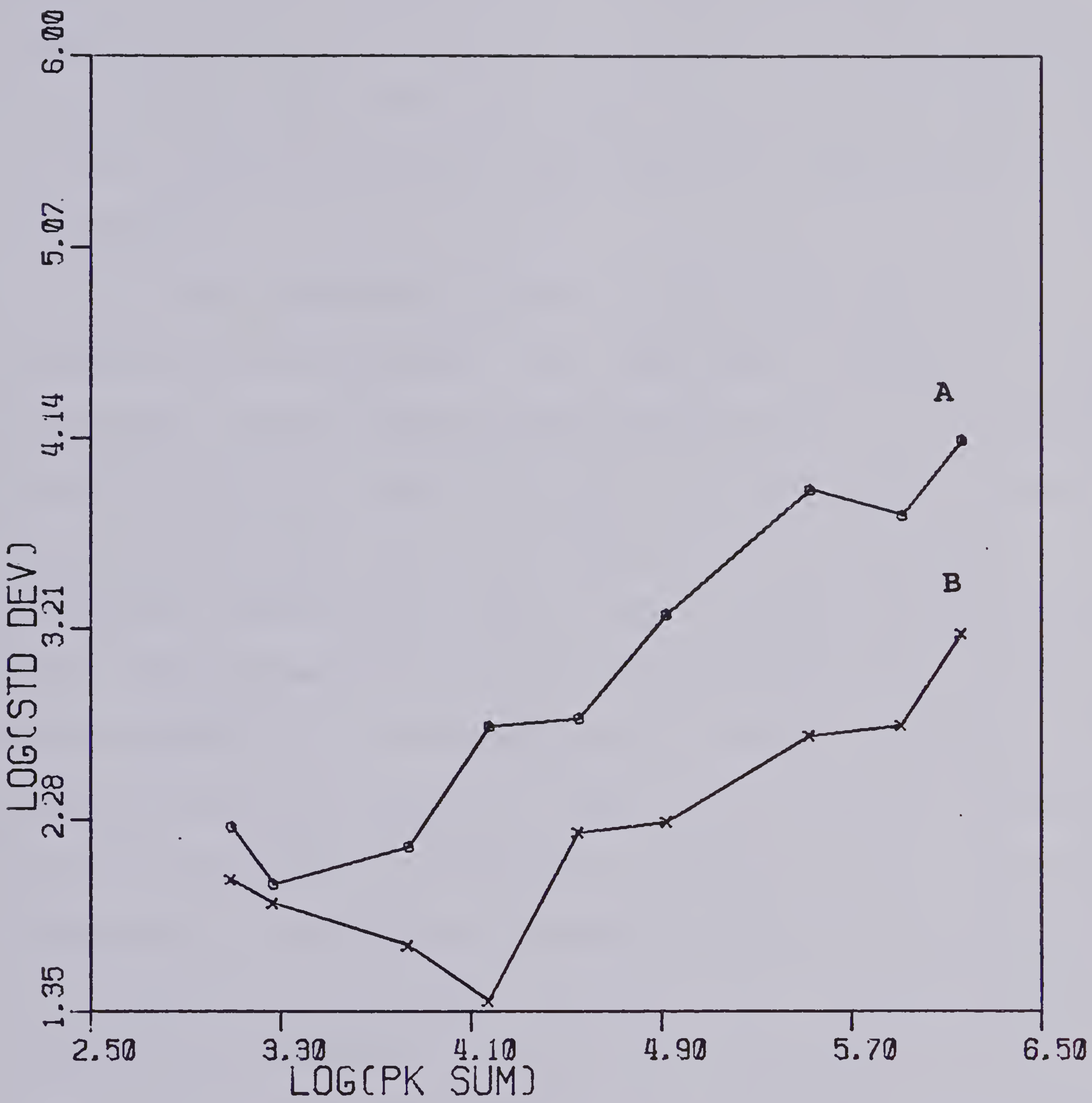

FIGURE 58. Standard deviation - total peak value plot.

(A) 279.5 nm Mg peak standard deviation.

(B) 304.4 baseline point standard deviation.

analytical curve axis for comparison purposes. Both curves still indicate an increasing standard deviation with increasing total peak intensity. Before any further comments or conclusions are made, the results of a further experiment on the system's behaviour with regard to noise will be considered.

In this experiment, again the manganese-magnesium emission lines were used. The experiment consisted of the following: observe the standard deviation of the manganese emission peaks at three different concentrations of magnesium ranging from 0.00 ppm to 20.0 ppm to 100.0 ppm. The manganese concentration was set at 4.40 ppm and held constant. The system input dynamic range was optimized for the 100.0 ppm magnesium and 4.40 ppm manganese aqueous solution plasma emission and held constant. The complete emission spectrum for this solution is presented in Figure 59. The standard deviation of the manganese triplet at 290.0 nm was monitored as a function of magnesium concentration. Partial spectra showing the manganese triplet at the three magnesium concentrations are shown in Figure 60. According to multiplex theory the standard deviation of this triplet, or any other spectral emission line, should vary directly with the magnesium emission intensity, assuming, of course, the predominant noise source is intensity related. The standard deviations of the manganese triplet, the magnesium doublet and a baseline point at 304.4 nm are tabulated in Table XIV. The baseline point is a rather interesting selection in that

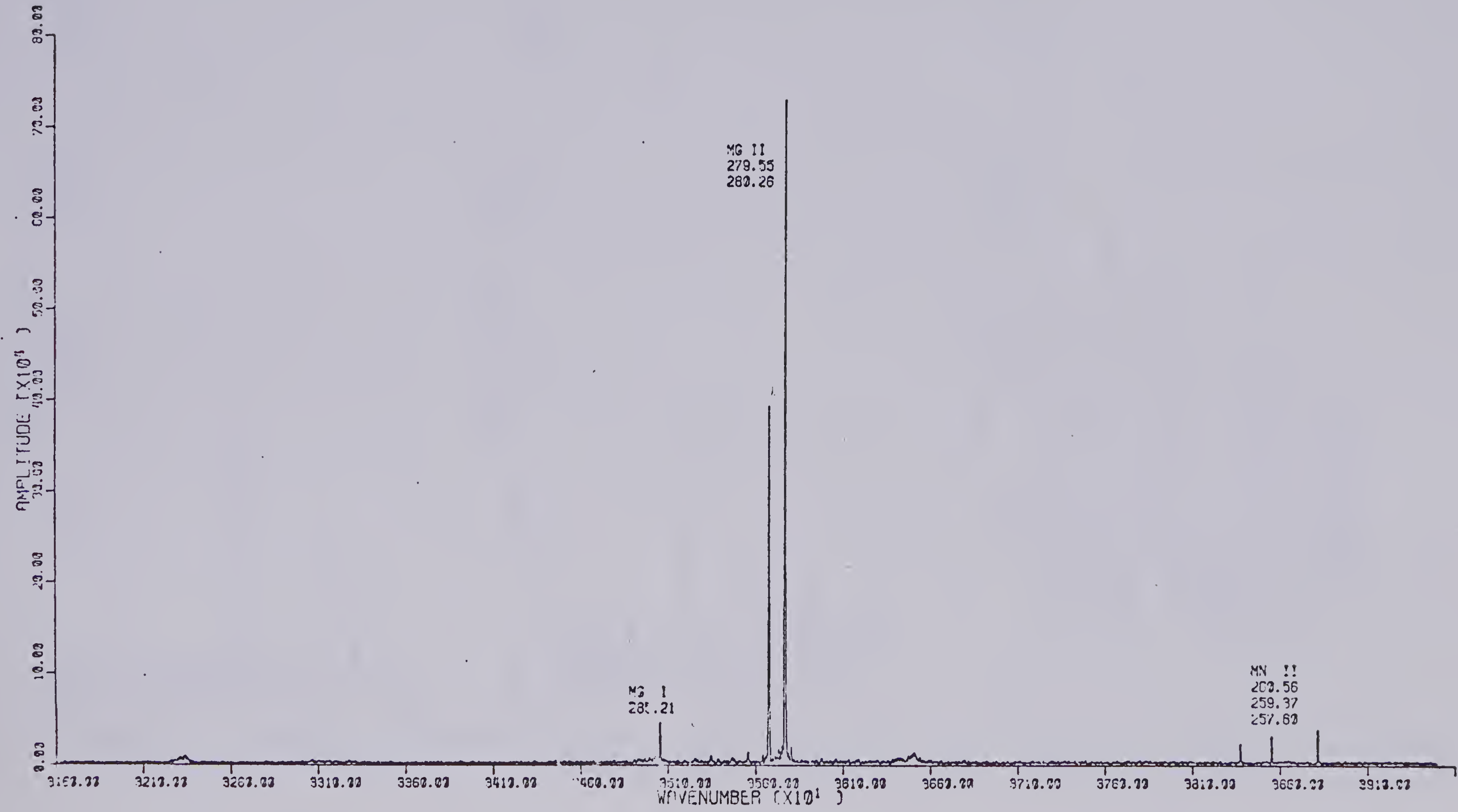

FIGURE 59. Plasma emission spectrum of 100.0 ppm Mg and 4.4 ppm Mn

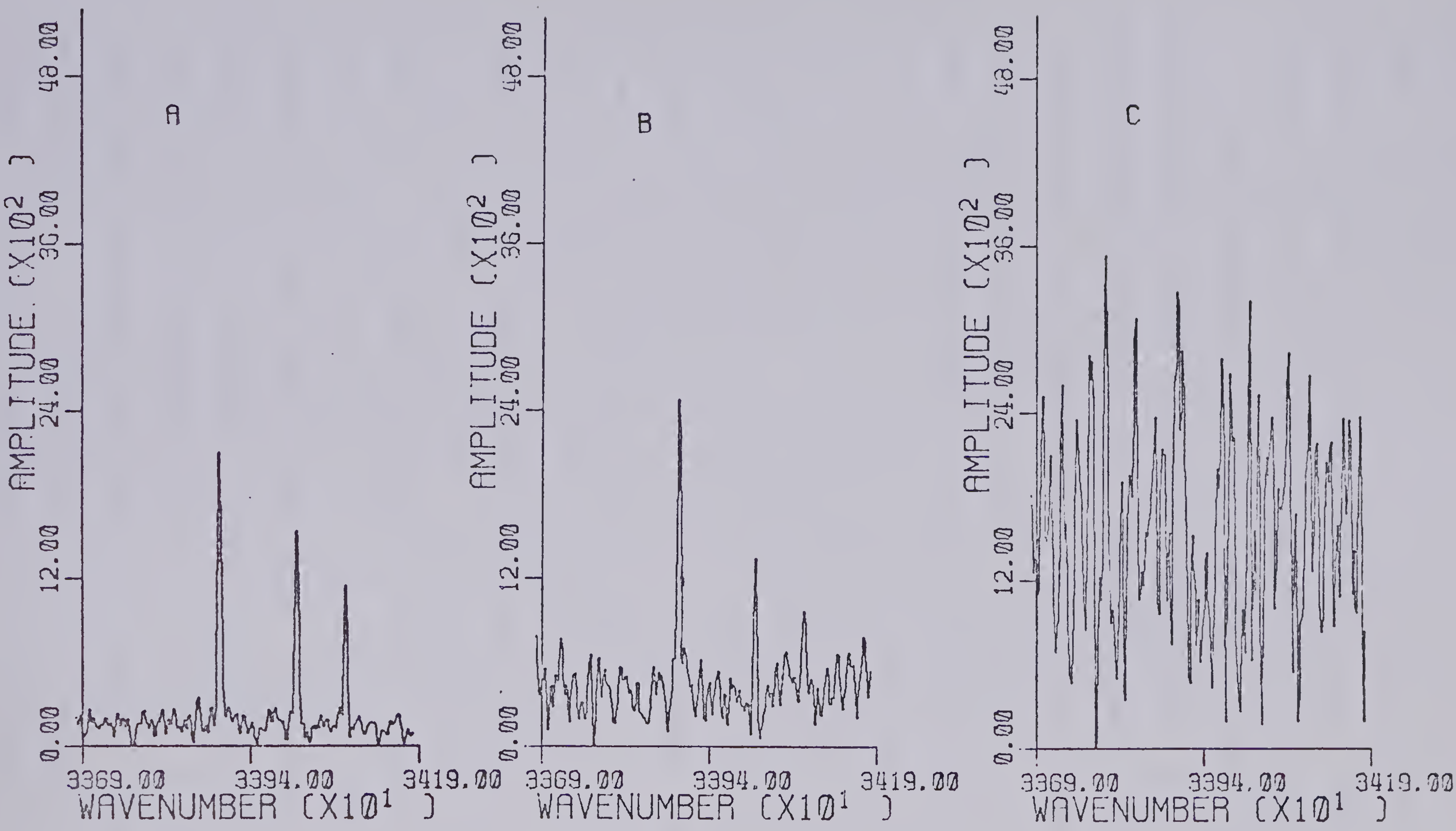

FIGURE 60. Mn triplet emission at 290.0 nm (A) 0.0 ppm Mg.

(B) 20.0 ppm Mg.

(C) 100.0 ppm Mg.

this wavelength is outside the spectral response range of the solar blind detector for both aliased and non-aliased spectral lines and so should provide a good indication of the spectral distributive properties of the noise present.

The interpretation of the results in Table XIV is not particularly straight forward. In general, upon increasing the magnesium emission signal intensity, all of the wavelengths monitored underwent an increase in variance of a statistically significant amount. A variance ratio F test (91) was employed at the $\alpha = 0.005$ confidence level. The only exceptions occurred for the two manganese peaks at 294.8 nm and 293.2 nm, upon increasing the magnesium from 0.0 ppm to 20.0 ppm. In trend, the multiplex theory appears correct, but if one considers the relative amplitudes of the standard deviations at the various wavelengths, there is no way in which the theory may be borne out experimentally. Since the noise is, in theory, equally spread across the spectral range, the standard deviations should at least be of the same order of magnitude. With simple reference to Table XIV, this was not found to be so. Again it is found that the noise is specifically restricted to the large spectral emission peak of magnesium. To further complicate matters, if one considers the standard deviation of the larger amplitude manganese peaks at 260 nm, no statistically significant increase was found as a function of magnesium concentration. It is very difficult to separate the amplitude related increases in noise from the distributive related

Table XIV

Variance study with Mn, Mg, 304.43 nm baseline point

Mg Conc. ppm	Mg Peak Amplitude 279.5 nm	Mn Variance ($\times 10^5$)			Mg Variance ($\times 10^5$)		304.43 nm
		294.8 nm	293.9 nm	293.2 nm	279.5 nm	280.2 nm	Variance ($\times 10^5$)
0.00	377.065	1.456	0.7940	0.7377	0.4311	0.5429	0.2357
20.00	92875.663	4.106	2.983	1.930	1712.	6380.	1.627
100.00	416028.61	15.78	13.00	8.260	15270.	48290.	8.281

increases in noise. For instance, the increase in standard deviation of the baseline point at 304.4 nm may simply be due to an amplitude increase in the baseline resulting from the presence of peak sidelobes of either manganese or magnesium. No tests were performed on the mean baseline values due to the t-test assumption of equal variances. It was already shown that the variances were unequal statistically. Therefore an absolute interpretation with regard to the noise spectral distributive properties is impossible.

3. The Silicon Photodiode as a Detector

In order to complete the spectral coverage from the ultra violet to the near infrared spectral range a silicon photodiode detector was installed in the interferometer. Specification have been given previously in Chapter IV. The plasma emission spectrum obtained with water aspirating into the plume is shown in Figure 61. Most of the emission lines are due to argon neutral atom emission in the near infrared, although two oxygen emission lines were found. Observed and literature (65) wavelength values for these lines are tabulated in Table XV. The intensities of these argon emission lines are very much greater in amplitude by several orders of magnitude, than the previously observed argon emission lines. For instance a 100.0 ppm sodium chloride solution was nebulized into the plasma and no evidence of the emission was present in the spectrum at all. This of course may have been due to spatial effects of the plasma emission. Not even barium, at 500.0 ppm, was observed to emit at 553.5 nm,

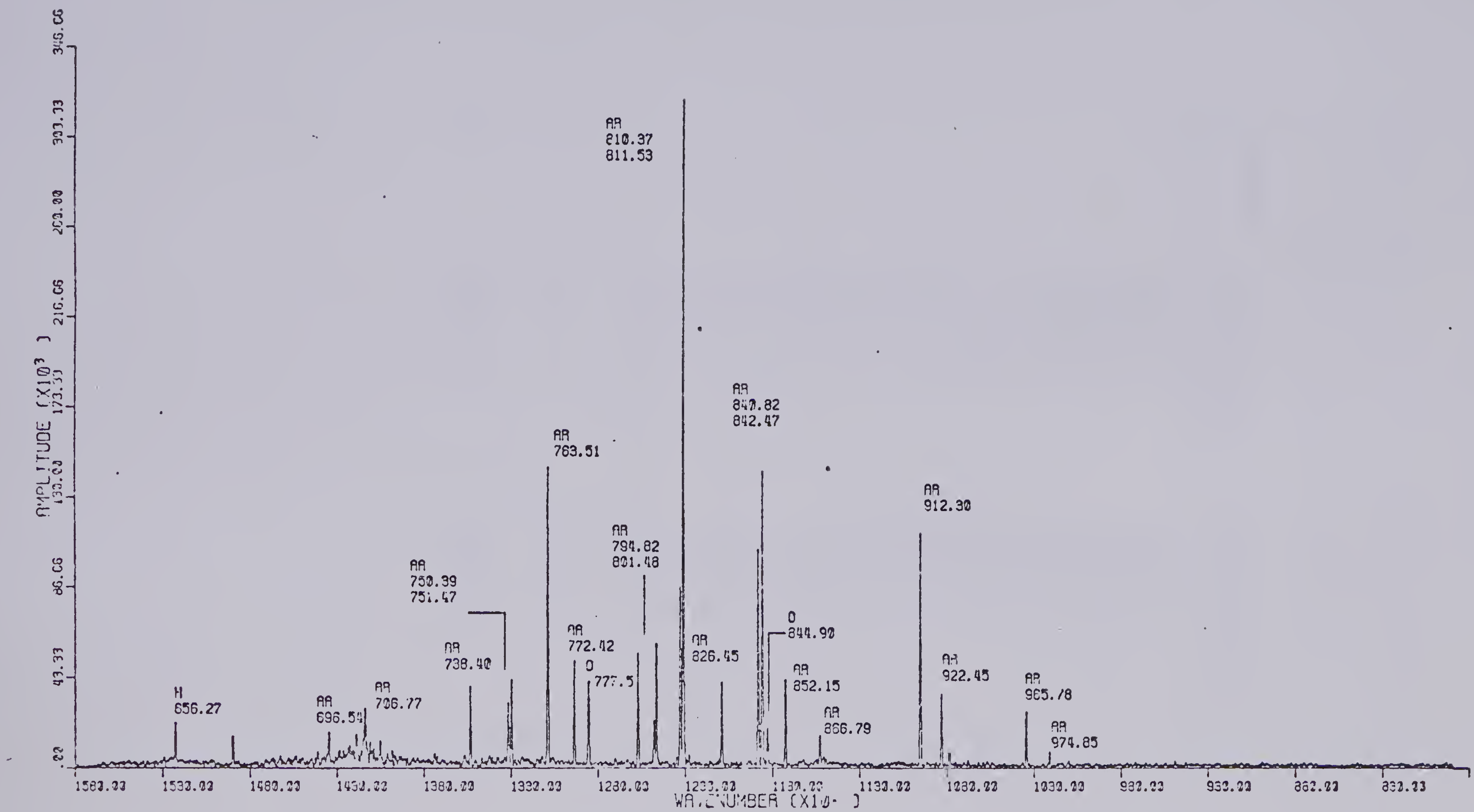

FIGURE 61. Plasma background emission spectrum--silicon photodiode detector

Table XV

Argon Plasma Background Emission as Observed with a Silicon Photodiode Detector

Element	Observed Wavelength	Literature (65) Wavelength
Ar I	696.59	696.54
	706.75	706.72
	738.48	738.40
	750.45	750.39
	751.54	751.47
	763.61	763.51
	772.49	772.42
	794.88	794.82
	801.64	801.48
	810.55	810.37
	811.69	815.53
	826.58	826.45
	840.93	840.82
	842.57	842.47
	852.27	852.15
	866.95	866.79
	912.43	912.30
	922.67	922.45
	966.01	965.78
	978.59	978.45
H	656.27	656.29
O	777.5	777.41
	844.90	844.64

a normally strong emission line for that element. Therefore, in the near infrared spectral region, the plasma-interferometer atomic emission instrument is rendered analytically useless due to dynamic range problems caused by intense plasma background emission.

D. Conclusions

The radiofrequency inductively coupled argon plasma, in combination with a Michelson interferometer based spectrometer has been assessed in a preliminary manner, as an analytically useful system in qualitative and quantitative elemental analysis. Although in certain spectral regions, such as the near infrared and the 400 nm region, the system suffers severly from dynamic range problems originating in the plasma, the advantage of simultaneous multielement analysis will warrant further research and development. With regard to the spectral distribution of noise the experimental evidence is inconclusive and further work is required before overall conclusions can be drawn.

CHAPTER VI

CORRELATION: A PARALLEL METHOD TO THE FOURIER TRANSFORM PROCESSING OF INTERFEROGRAMS

A. Introduction

The spectrochemical information available from a Michelson Interferometer detector is in the form of a time varying signal, termed the interferogram. In order to extract information from this interferogram it must first be decoded with respect to both the frequency and intensity domains. This is most commonly accomplished by transforming the interferogram from the amplitude-time domain into the amplitude-frequency domain through the use of Fourier Transform mathematics. The transformation is done on a computer using the Fast Fourier Transform (FFT) algorithm and the spectral information may be extracted from peak amplitudes in the normal manner.

An alternative method of information processing, correlation analysis, has been a long term research interest in this laboratory. For the most current applications refer to Betty (92) and for a general overall view of correlation analysis as applied to chemistry refer to the following references and the references contained therein (93,94). The correlation analysis previously done in this laboratory has been restricted to the spectral domain of information. Correlation analysis should work equally well in the interferogram domain, since the same amount of spectral information

is present in both domains. Through the specific properties of correlation analysis, especially in the low signal to noise ratio situation, several information extraction advantages may be present over Fourier analysis. In this chapter a comparison, based both mathematically and experimentally, between correlation and Fourier analysis applied to the extraction of atomic emission interferometrically detected information will be offered.

B. The Fourier Transform Process

1. Mathematical Definition

The Fourier Transformation, as mentioned in the preceeding section, transforms the information present in the amplitude-time domain, the interferogram, into the amplitude-frequency domain, the spectrum. Let us look further into the mathematics of this process. The interferogram resulting from a single frequency emission entering the interferometer may be expressed mathematically as a cosine wave.

$$I(x) = B(\bar{v}) \cos(2\pi\bar{v}x) \tag{1}$$

where $\bar{v}$ is the wavenumber of the emission line,

x is the distance in centimeters travelled by the mirror,

$B(\bar{v})$ is the amplitude of the emission intensity at wavenumber $\bar{v}$

$I(x)$ is the signal as a function of mirror movement in centimeters. i.e. the interferogram.

For a multiple frequency emission source the mathematics may be extended as follows:

$$I(x) = \int_{-\infty}^{+\infty} B(\bar{v}).\cos(2\pi\bar{v}x)d\bar{v} \qquad (2)$$

The Fourier Transformation is a reversible process in that information may be transferred in either direction between the two domains. Equation (2) is actually one half of a Fourier Transform pair. The second equation is shown in Equation (3) below.

$$B(\bar{v}) = \int_{-\infty}^{+\infty} I(x).\cos(2\pi x\bar{v})dx \qquad (3)$$

Equations (2) and (3) are referred to as a Fourier Transform pair. Equations (1) and (2) have both made the assumption that the output of the interferometer detector is a perfectly symmetrical or even function, about the zero path difference mark in mirror travel. Due to various optical and instrumental factors this is often not the case (23) and the output at the detector is a combination of even, $f(x) = f(-x)$, and odd, $f(x) = -f(-x)$, functions. In order to account for this character of the interferogram, the Fourier Transform pair must be expressed as follows:

$$B(\bar{v}) = \int_{-\infty}^{+\infty} I(x) . e^{-2\pi i\bar{v}x}dx \qquad (4)$$

and

$$I(x) = \int_{-\infty}^{+\infty} B(\bar{v})\ e^{2\pi i \bar{v} x} d\bar{v} \tag{5}$$

Euler's Rule states that

$$e^{2\pi i \bar{v} x} = \cos(2\pi\bar{v}x) + i\ \sin\ (2\pi\bar{v}x),$$

showing the presence of cosine and sine components in Equations (4) and (5). Since all of the data used in this thesis is the result of a digitization of a continuous analog signal, let us express Equations (4) and (5) in the discrete form

$$B(\bar{v}) = \sum_{x} I(x) e^{-2\pi i \bar{v}} \tag{6}$$

and $$I(x) = \sum_{\bar{v}} B(\bar{v}) e^{2\pi i \bar{v} x} \tag{7}$$

Note also the change in limits for both equations, since instrumental factors now play an important role. Data can only be acquired over a limited mirror drive distance -x to +x and the system is limited in its frequency response to $\bar{v}_o$ to $\bar{v}$. Details of the mathematical properties of the Fourier Transform are dealt with in several texts (95,24, 21) and will not be further considered in this thesis.

2. Historical Aspects of Interferogram Processing

The historical aspects of interferogram interpretation are rather interesting. Michelson invented the interferometer in 1880 and for the next thirty years, he and others were not able to fully decode the frequency information the

instrument provided. Using his eye as a detector, Michelson would sense the low frequency envelopes of the interferograms and termed them visibility curves. For example, from the visibility curve of the sodium doublet emission, he could tell the doublet was composed of two peaks separated by 0.6 nm, but he could not assign absolute frequencies to the signals. If more than two frequencies were present, the task of even the assignment of frequency separation became impossible. After the development of a radiometer detector in 1911, permanent detailed tracings, containing both of the interferogram's envelop and high frequency components could be obtained allowing more advanced processing techniques to be utilized. Rubens, Wood, Hollnagel and Michelson (96) performed the interpretation of interferograms in this manner. First, the frequency components most likely to be present were estimated. Then the sine and cosine values of each of these frequencies, corresponding to a particular point in mirror travel, were calculated and summed producing a mathematically generated interferogram. A detailed comparison of the features of the observed interferogram and the calculated interferogram then decided whether or not the predicted spectrum was the correct one. This may be termed the first "optical" interferogram correlation process. This method at least allowed a possible way of making an absolute frequency assignment to the multiple emission lines. Returning to the mathematics, the Fourier Transform pair had been recognized as the key to the complete interpretation

of the interferogram in 1892 by Lord Rayleigh, but mathematical techniques existing at the time did not allow implementation of the theory. The first numerical transformation was performed in 1949 by Fellgett (97). The interferogram could then be mathematically transformed into the more easily interpretable spectral domain. The classical Fourier Transform involves multiplying each point in the interferogram by a corresponding point in the cosine wave of the desired frequency and then summing the multiplications. A similar operation is performed with the same frequency sine wave. Finally a root sum of squares of the sine and cosine sums produces a single point in the frequency spectrum at the frequency of interest. The amplitude of this point is directly related to the amplitude of that frequency component in the interferogram and thus to the intensity of the emission signal entering the interferometer. Refer to Figure 62 for a graphical illustration of the transform process. For interferograms of any extended length, and for the determination of multiple frequencies, the classical transformation is a very cumbersome and time consuming process. Not until 1966, when Cooley and Tukey developed the Fast Fourier Transform (F.F.T.) algorithm, did the computation technique change. Their algorithm greatly increased the processing speed, at least by several orders of magnitude, while placing only a few minor limitations on the data format. Detailed descriptions and later modifications of the algorithm are readily available in the literature. An excellent collection of these papers is available in a text

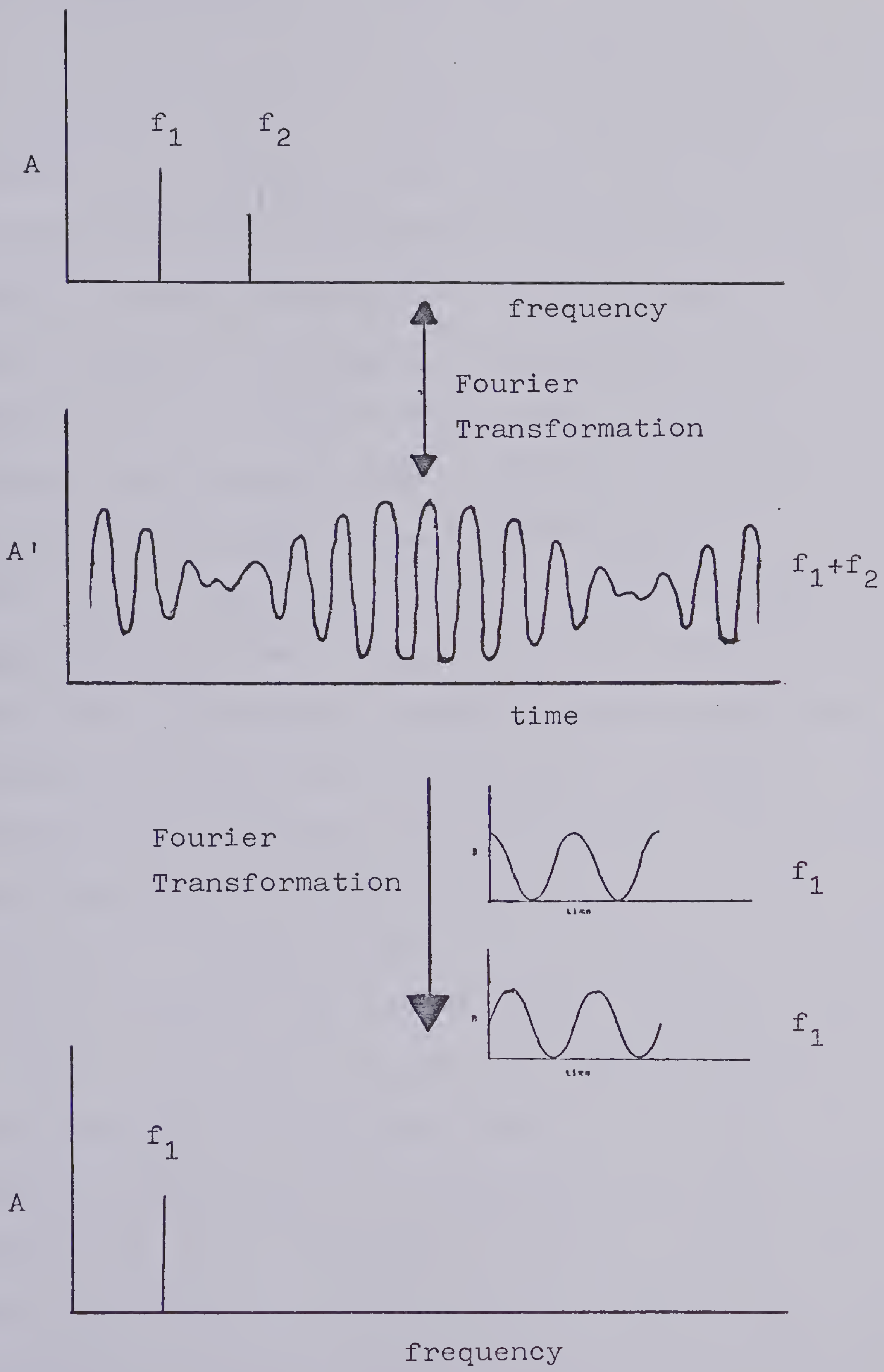

FIGURE 62. The FT illustrated graphically

by Liu (98).

3. Implementation of the F.F.T.

The F.F.T. algorithm is available in many language formats from Basic to Fortran to Macro Assembler. The Fortran version of a floating point format F.F.T. is currently used in this laboratory offering a computation accuracy of 23 bits. For most applications this accuracy is quite adequate. For a complete discussion of precision and accuracy in F.F.T. processing in interferometery refer to Foskett (76). The current minicomputer based system can process up to a 4096 point floating point format interferogram in core memory; that is, no swapping of data is required between the peripherals and memory during the F.F.T. routine execution. Once the interferogram length extends beyond 4096 points, the situation becomes more complex for our system. The minicomputer due to memory size limitations can no longer process the interferogram as one block of data with the current F.F.T. routine. A complex presorting routine must be employed in order to process the interferogram in several smaller blocks of data. It is not a matter of simply transforming the interferogram in successive 4096 point blocks. The presorting routine is referred to as decimation in time and has been well documented in the literature (99-101). Such a decimation in time routine was attempted with our system, but the software overhead development time was found to be to excessive in this situation. If necessary, the F.F.T. processing of very long

interferograms may be carried out on the larger central university computer. Currently a direct interface to this computer is being considered.

Considerations in the area of interferogram processing time have also been important. The current FFT routine requires on the order of two minutes to process a 4096 point interferogram. A second routine with less accuracy at sixteen bits performs the same transform in about 15 seconds. The latter routine is written in the Macro assembler code and employs a quarter wave sine/cosine look up table to account for its increased speed. It still suffers from the same interferogram size limitations as the Fortran FFT routine. In both cases further processing time is required to extract the specific peak information required. The time factor became very large when one considers that for the typical analytical curves of the previous chapters approximately a total of fifty interferograms had to be transformed. The time element often ran into several hours of processing. Since the data files were finally stored as interferograms a further transformation was required at a later date if the spectral information was to be re-examined. Due to the above mentioned implementation and time factors of the FFT routine, alternate data extraction in the form of correlation analysis was developed. As mentioned in the introduction correlation analysis in various forms has been an ongoing research interest of this group.

C. The Correlation Operation

1. Correlation and the Fourier Transformation

Upon examination of the mathematics of the classical Fourier Transform, Equations (6) and (7), similarities with the correlation operation may be detected. The correlation operation may be defined mathematically as follows:

$$Cab(\Delta x) = \lim_{X\to\infty} \frac{1}{2X} \int_{-X}^{+X} a(x).b(x\pm\Delta x)dx \qquad (8)$$

where a(x) and b(x) are arbitrary functions of x, Δx is the relative displacement of a(x) from b(x) in the x domain, and $Cab(\Delta x)$ is the correlation function of a(x) and b(x) at differing values of Δx. In the case of a digitized signal the correlation operation may be expressed in a discrete form as follows:

$$Cab(\Delta x) = \sum_{x} a(x).b(x\pm n\Delta x),\ n=0,\ 1,\ 2\ \ldots \qquad (9)$$

Let us now rewrite Equation 9 at the specific value of n=0, a single point in the correlation domain

$$Cab = \sum_{x} a(x).b(x) \qquad (10)$$

Let us now rewrite Equation (6) in its expanded form.

$$B(\bar{v}) = \sum_x I(x).(\cos(2\pi\bar{v}x) - i\sin(2\pi\bar{v}x))$$

$$= \sum_x I(x).\cos(2\pi\bar{v}x) - i\sum_x I(x)\sin(2\pi\bar{v}x) \qquad (11)$$

Thus the Fourier Transform may be separated into two parts, the cosine part dealing with symmetric functions of I(x) and the sine portion dealing with assymetric functions of I(x). Upon comparing the separate parts of Equation (11) and Equation (10) a similarity in the functional form may be noted. Furthermore at a single wavenumber $\bar{v}$ Equation (11) may be rewritten as follows:

$$B_1 = \sum_x I(x).C(x) - i\sum_x I(x)\cdot S(x) \qquad (12)$$

where $C(x) = \cos(2\pi\bar{v}x)$ and $S(x) = \sin(2\pi\bar{v}x)$. Upon performance of a root sum of squares operation of the two parts in Equation (12), B_1 corresponds to the amplitude in the spectral domain at wavenumber $\bar{v}$. Also note that the two portions of Equation (12) now are identical in form to the correlation operation of Equation (10). If a(x) from Equation (10) is set equal to I(x) of Equation (12) and b(x) is similarly set equal to S(x) or C(x), it is evident that the Fourier Transformation is actually a combination of two correlation operations. Remember the correlation operation is only performed at n=0. In order to obtain the spectral amplitude, B_1, at another frequency the value of $\bar{v}$ used in determining

S(x) and C(x) would have to be changed. The correlation operation is still performed at n=0. A flow diagram for the classical Fourier Transform or simple correlation is illustrated in Figure 62. The use of correlation to process a complete spectral range would offer no great advantage, in fact, it would be several orders of magnitude less efficient in processing time than the FFT. Why then should correlation processing even be considered as an alternate metnod of interferogram processing?

The processing of interferograms with the FFT provides all of the frequency information available over the complete spectral bandwidth of the interferogram. No small frequency bandwidth may be isolated for processing with the FFT at the interferogram stage. In the case of qualitative atomic emission spectroscopy, the presence of the complete spectral bandwidth in the frequency domain is necessary to provide an overall indicator of the elements present. In the case of repetitive quantitative information extraction concerning a single or small number of frequencies, the FFT is very inefficient. Why should 10,000 resolution elements be processed when at most only 10 resolution elements may be required? This is the point at which correlation processing becomes advantageous. With correlation those 10 selected frequencies or resolution elements may be individually processed in a fraction of the time required for a full FFT. This concept of selective frequency transformation is very important especially when dealing with the large amounts of data

present in high resolution work. It was shown in the previous section that, with a minicomputer-based data processing system the FFT to process long interferograms may be difficult to implement with a restricted memory size. This is not so, for correlation analysis. Since the correlation is simply a point by point multiplication and summation, no pre operation sort routine is required. The summation itself remains core resident as successive portions of the interferogram are swapped from disk into core, multiplied by the appropriate sine-cosine wave coefficients, and added into the summation. For interferometry the capability of processing large interferograms is exceedingly important in that the resolution varies directly as the length of the mirror drive over which data has been acquired. As mentioned in the previous chapter the presence of high resolution becomes important in the analysis of complex mixtures through the sorting of aliased or non-aliased overlapping emission lines. Higher resolution simply provides a higher degree of spectral selectivity, an important consideration.

Thus far in the discussion it has been assumed that only a single frequency analysis has been sought with each correlation performed C(x) and S(x) have been assumed to be single frequency cosine and sine waves respectively. In fact, these functions may contain multiple frequencies. Equation (12) may be rewritten as follows:

$$B_1' = \sum_x I(x) \cdot CC(x) - i \sum_x I(x) \cdot SS(x) \qquad (13)$$

where $CC(x) = \sum_{\bar{v}} \cos(2\pi x\bar{v})$ and

$SS(x) = \sum_{\bar{v}} \sin(2\pi x\bar{v})$

In the definition of CC(x) and SS(x) $\bar{v}$ need not be a continuous series but may take on any number of arbitrary values within the frequency bandwidth of the interferogram. Now through correlation the capability exists for selective, multiple frequency simultaneous transformation. The important point to note is that B_1' does not necessarily equal B_1. B_1' gives a quantitative indication of the total spectral amplitude of all frequencies present in CC(x) and SS(x). Therefore if 10 frequencies were present B_1' is equal to the summation of the spectral amplitudes of all 10 frequencies. This is best illustrated with reference to Figures 62 and 63. Let us now consider how correlation may be applied to interferometry.

2. Applications of Correlation to Interferometry

The interferometric experiment, utilizing a two beam Michelson Interferometer, is itself a correlation operation. The incoming light wave is autocorrelated as a function of the optical path difference between the two arms of the interferometer. The interferogram is actually the algebraic summation of the various autocorrelation functions of each frequency of light present. Correlation may also be used to decode the interferogram into its composite frequencies as discussed in the previous section. A different approach

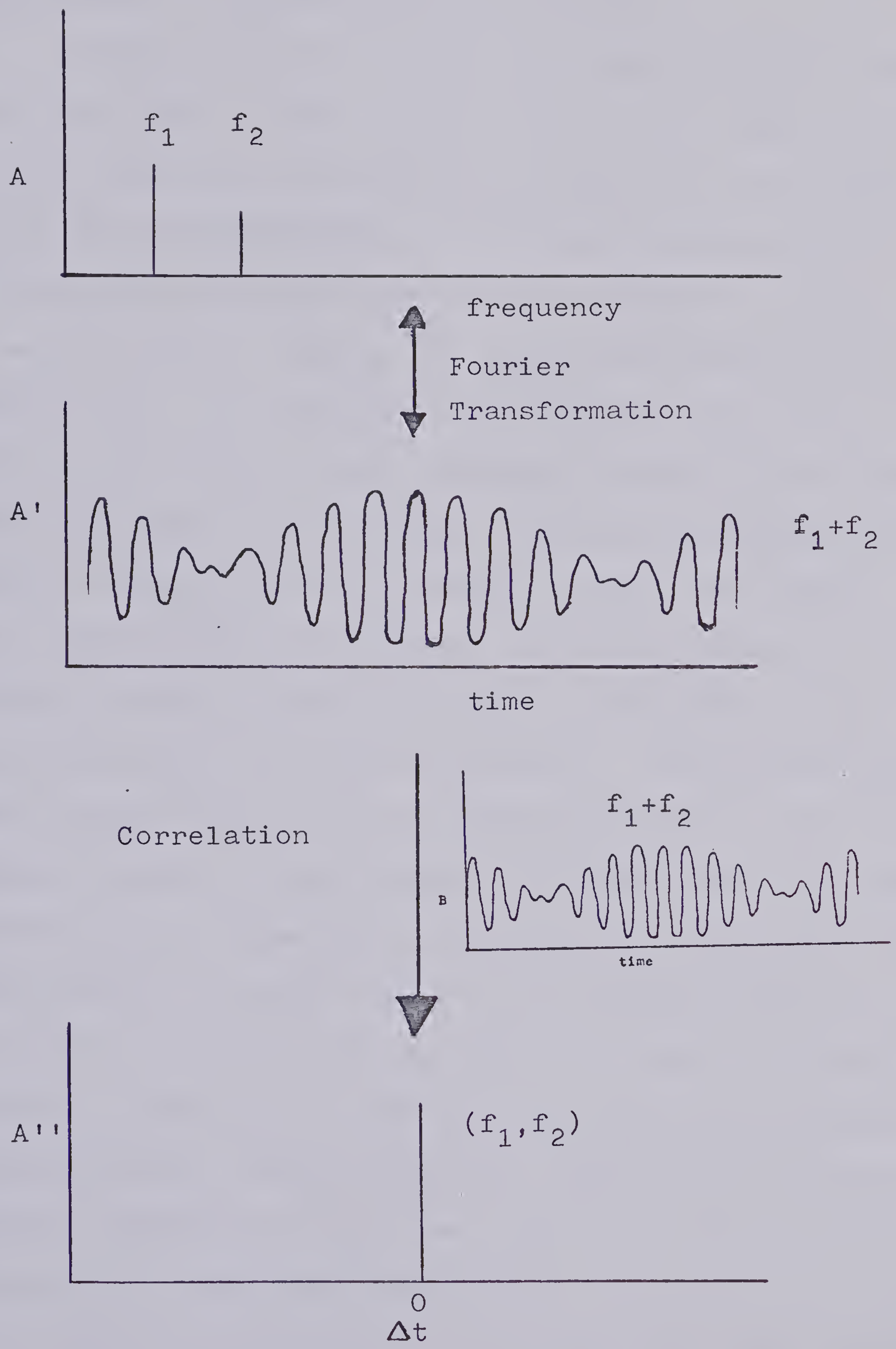

FIGURE 63. Correlation illustrated graphically

has been taken by various authors in the application of correlation in interferometric analysis.

Previous work has notably been done by Davis, Deck and Levy (102). Their approach was in the form of a hardware analog correlator requiring modifications to the basic Michelson interferometer. A reference interferogram containing the signals of interest was stored in analog form on a magnetic disk. During the sample interferogram data acquisition, the reference interferogram was read from the disk and fed into a phase sensitive detector simultaneously with the sample interferogram. The two interferograms were exactly synchronized with respect to the time domain. The D.C. level output of the phase sensitive detector, most likely a lock-in amplifier, gave an indication of the concentration of the species present. These experiments were carried out in the mid infrared spectral range utilizing gaseous samples. Other workers (103-106) have used the interferometer correlation technique for qualitative identification of species in the mid infrared spectral range. In order to test for the presence of a specific functional group on a molecule, a computer generated interferogram, containing only those frequencies specific to the functional group's absorbance bands, was stored on a disk. The experimentally generated interferogram containing the absorbance band frequencies specific to the sample was then acquired and stored. The correlation operation was then performed between the two interferograms with the resulting amplitude indicating

either the presence or absence of the functional group. The decision was dependent upon previously set confidence limits about the correlation amplitude. Other authors have also used only a small portion, 100 points of an interferogram, for similar correlation based analysis (105). How can such techniques be applied in the atomic emission experiment currently under study?

With a monochromator-based atomic emission instrument, quantitative information about an emitting species is obtained solely from the intensity information contained in a single frequency emission. Quantitative information may be obtained in a similar manner from the interferometer based instrument through the application of a classical Fourier transform or correlation at a single frequency or through the use of a single peak amplitude in the FFT generated spectrum. Since the drive is very often toward high precision, accuracy and sensitivity in the elemental determination, it would make sense to use all of the available element specific information. For example, in the case of chromium emission in a plasma, about twelve elemental emission frequencies are present. Unlike the scanning monochromator-based system, the interferometer simultaneously encodes and detects all of these frequencies. Correlation processing provides a technique whereby all of the information present in these twelve frequencies may be simultaneously extracted. In practice this may be accomplished by two methods.

The first method involves the computer generation of an interferogram containing only information specific to those

twelve frequencies. The second method involves the experimental generation of a high signal to noise ratio interferogram resulting from the atomic emission of a pure chromium sample. Either of these interferograms is stored on disk and is referred to as a chromium mask interferogram. Both of the masks suffers disadvantages. For example, the experimentally generated mask also contains information related to any spectral source background emission or any impurities present. The computer generated mask does not suffer from excess information present, but may suffer from the lack of information in the correct proportions. For example, the relative signal amplitudes for each of the frequencies present may not be exactly as in the experimentally generated interferogram. This would lead to error in analysis due to the incorrect weighting of the signals. In either case, the next step in the experiment involves the acquisition of the sample interferograms containing a wide variety of frequencies. A correlation at n=0, is then performed between the mask and sample interferograms. The amplitude of the correlation gives a direct indication of the amount of chromium, in our example, present in the sample. For an absolute value of the chromium concentration a correlation based analytical curve would have to be developed The extension of correlation into a multiple element mask situation can be easily observed. Through the previous determination of satisfactory confidence limits, several elements may be quantitatively monitored in one operation with the use of an interferometer and correlation techniques.

Let us now consider how these techniques operate in an experimental environment.

3. Experimental Results and Discussion

The mask interferogram correlation technique described in the previous section has been applied to various atomic emission examples outlined below. A comparison will be made to as large an extent as possible with the FFT data processing methods. All of the studies will be quantitative in nature and will attempt to show some of the advantages as well as the limitations in correlation processing of interferograms.

The first and most simple system used to test the correlation technique involved the simple frequency atomic emission of lithium at 670.78 nm. The same data files as used in Chapter IV for the emission of lithium in an air-acetylene flame provide the data basis for the correlation work. The lithium concentration ranged from 30.0 ppm to 0.03 ppm. One of the high concentration lithium emission interferograms was used as a mask interferogram for the correlation generated analytical curve in Figure 64(a). The FFT generated analytical curve is provided in Figure 64(b) for comparison and the regression analysis data are presented for both techniques in Table XVI. The slopes as well as the overall standard deviations are statistically equivalent at the 95% confidence levels for the two techniques. The regression correlation coefficients are also listed in the table and indicate a high positive dependence of the

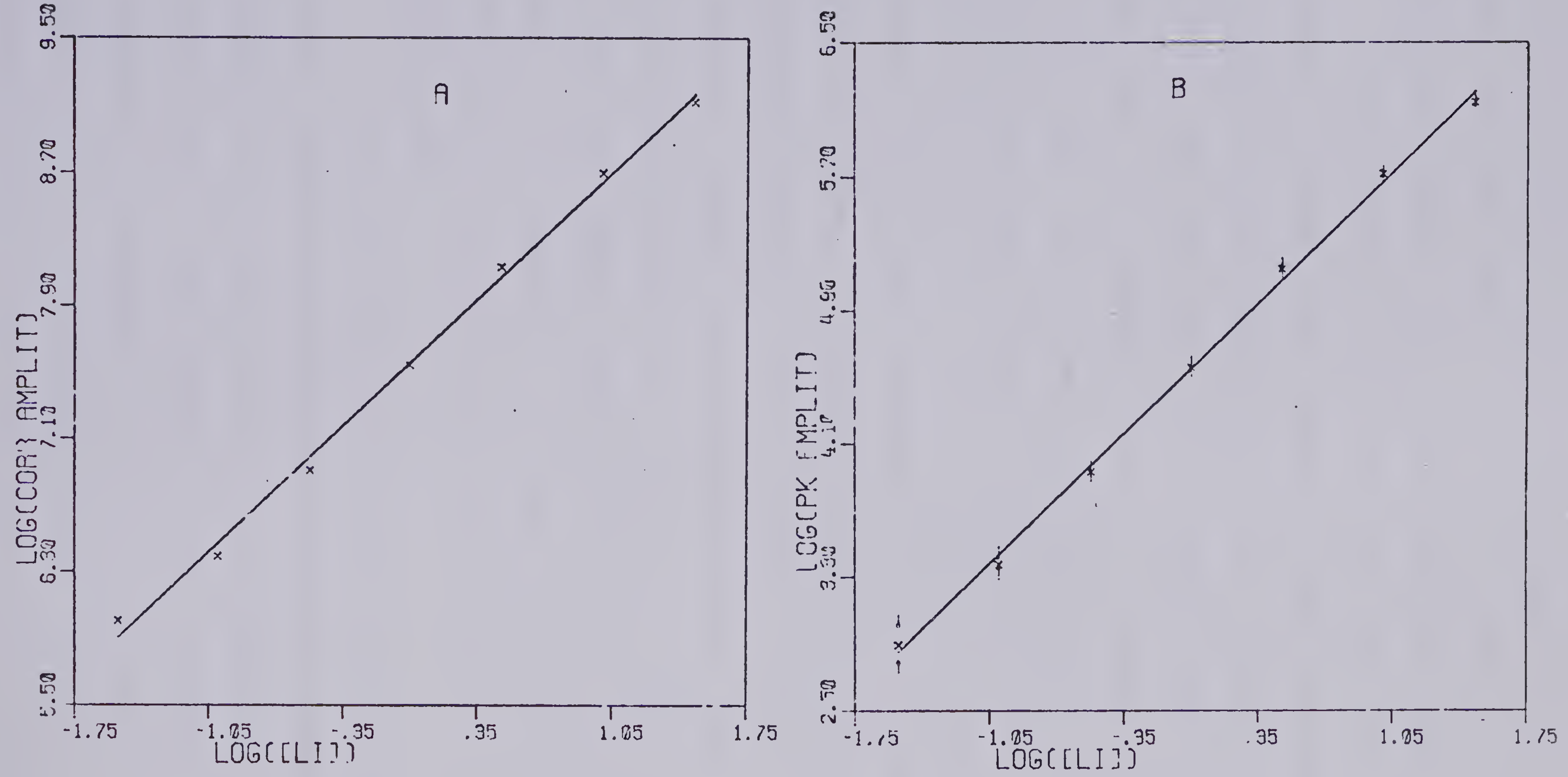

FIGURE 64. Li analytical curves

(A) FFT generated

(B) correlation generated

correlation peak amplitude upon concentration of the lithium. Thus for a very simple case the correlation and FFT processes produce statistically equivalent analytical curves.

The next model system that will test the correlation process involves a two frequency atomic emission source such as sodium, at 589.0 nm and 589.6 nm, in an air-acetylene flame. Again the same sodium emission data as in Chapter IV were used. The sodium concentration ranged from 30.0 ppm to 0.01 ppm. One of the high concentration sodium interferograms was again used as a correlation mask. The correlation generated analytical curve is presented in Figure 65. Table XVI also contains the regression analysis for both the correlation and FFT generated analytical curves. The FFT generated analytical curve is shown in Figure 65(b) for reference. Again the analytical curves, from the two processing techniques were found to be statistically equal in slope and overall standard deviation at the 95% confidence level. Both techniques, although using different amounts of information, have extracted the quantitative information equally well.

A more severe test for the correlation processing technique involves the air-acetylene flame emission of calcium. Present in the spectrum are both broadband molecular emissions and an atomic neutral atom line emission as previously illustrated in Chapter IV. The use of one of the 2000 ppm calcium emission interferograms as a mask for the correlation process resulted in the analytical curve illustrated in

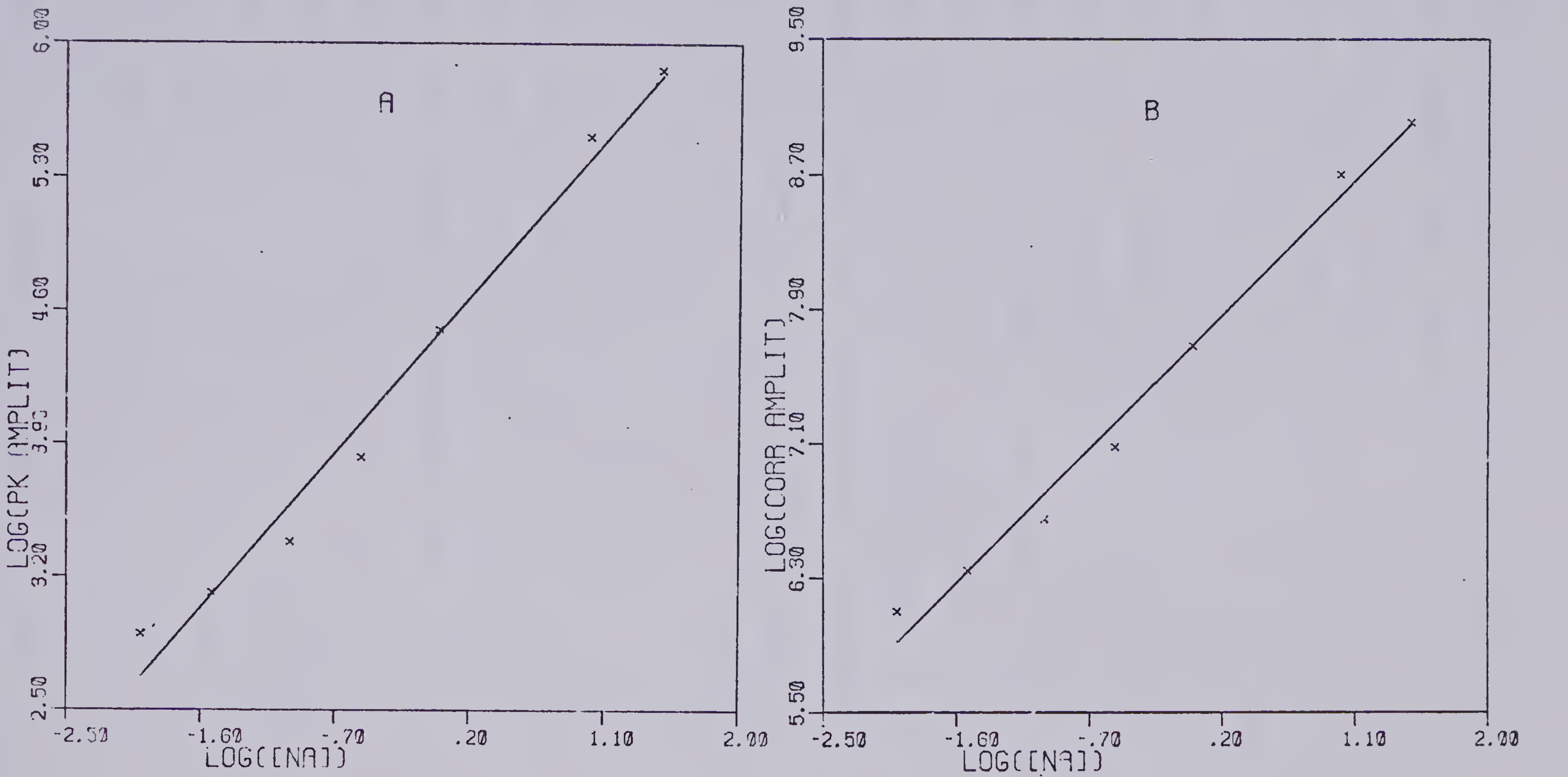

FIGURE 65. Na analytical curves

(A) FFT generated

(B) correlation generated

Figure 66(a). The concentrations ranged from 2000 ppm to 50 ppm calcium. For comparison purposes the FFT generated broadband emission analytical curve is presented in Figure 66(b). Refer to Chapter IV, Figure 29 for the neutral atom line emission analytical curve. The regression analysis data are contained in Table XVI. The three analytical curves are no longer statistically equivalent. The FFT generated CaO broadband analytical curve is very linear in nature while the neutral atom line emission curve is definitely parabolic in nature for the previously discussed reasons. Since the correlation process utilizes all of the information present in the mask interferogram including any non linear response lines, one would therefore expect the correlation analytical curve for calcium to be slightly parabolic in nature with a slope of approximately 0.8. This was not found to be the case in the present example. The slope of the correlation analytical curve showed a positive deviation from linearity indicating the presence of positive non linear responses greater in amplitude than the negative non linear response of the neutral atom emission line. The possibility exists that one of the other smaller broadband emissions around 600 nm, see Figure 27, deviates from linearity in a highly positive manner. This is an excellent example of a case where the utilization of all the available spectral information is a definite disadvantage. The correlation mask must be very carefully planned therefore, in order to include only those signals with a linear response over the con-

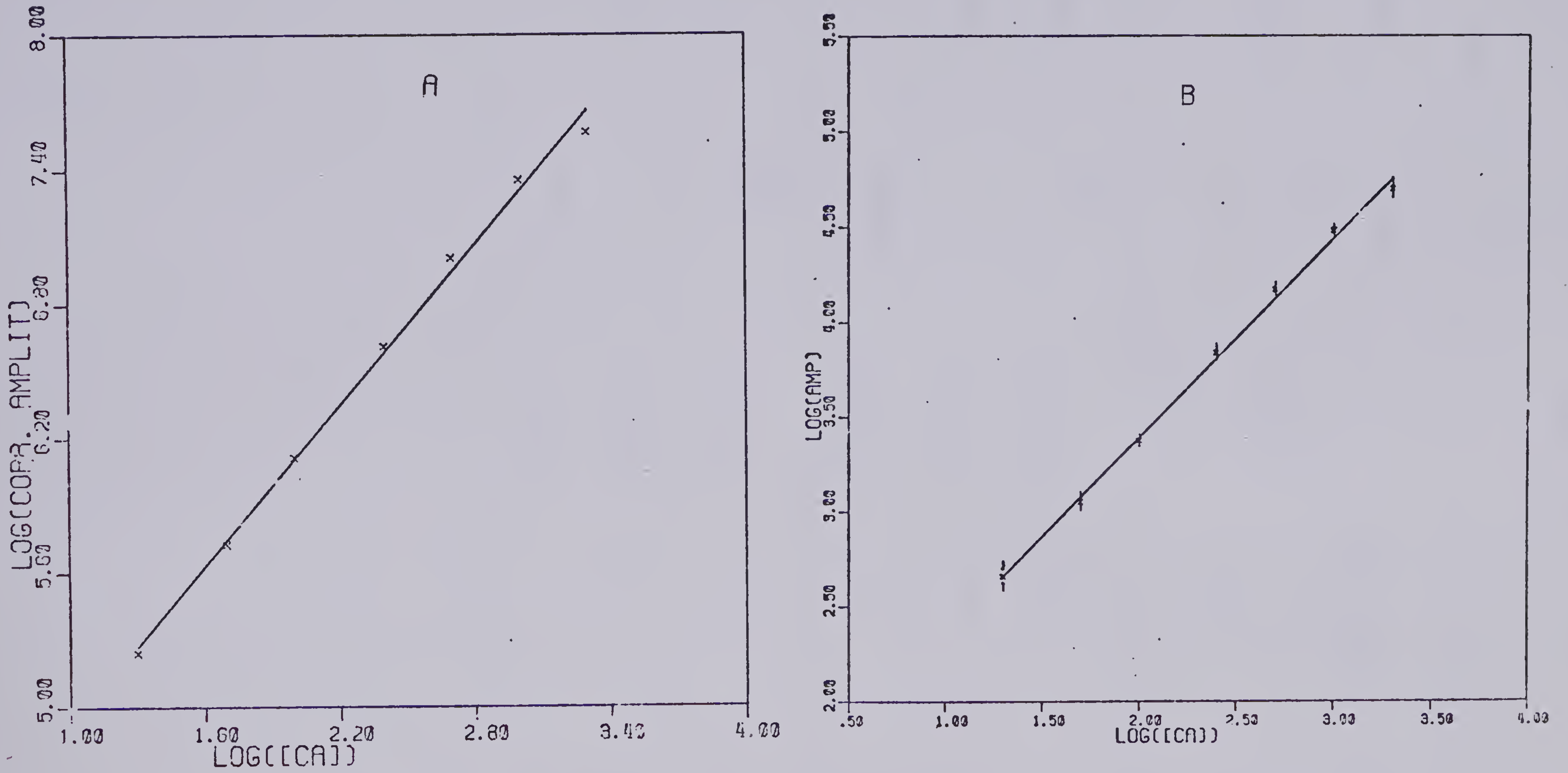

FIGURE 66. Ca analytical curves

(A) FFT generated

(B) correlation generated

Table XVI

Regression Data for Li, Na, Ca Analytical Curves

Element	Method	Slope	Overall Std. Dev.	Correlation Coefficient
Li (670.7)	FFT	1.118 ±0.022	0.0730	0.9980
	Correl.	1.086 ±0.027	0.0874	0.9968
Na	FFT			
(589.0)		0.878 ±0.084	0.132	0.9940
(589.6)		0.908 ±0.106	0.168	0.9910
	Correl.	0.891 ±0.034	0.125	0.9933
Ca	FFT			
(555.0)		1.047 ±0.021	0.0433	0.9980
(422.6)		0.592 ±0.030	0.117	0.9512
	Correl.	1.192 ±0.0230	0.0640	0.9966

centration range under study. It must be remembered that changes with regard to the frequency composition of the interferogram are very difficult to implement once the interferogram has been digitized.

Thus far, the correlation studies have been limited to the interferograms produced by a single emitting element, although multiple emission lines may have been present. The correlation studies now turn to the extraction of quantitative information from a multiple element, multiple line emission source. In order to decrease the effect of any source background emission signal, the ultra violet spectral range of the plasma atomic emission source was chosen. Both magnesium and manganese have suitable sensitivities and number of emission lines in this spectral region. Refer to Chapter V for details concerning the background and elemental emission lines as detected by a solar blind photomultiplier tube for magnesium and manganese emission in this spectral region.

The following study is based upon the simultaneous determination of magnesium and manganese analytical curves over the concentration ranges from 100.0 ppm to 0.05 ppm and 300.0 ppm to 0.25 ppm respectively. The same data base, as used in Chapter V, provided the interferograms for the correlation produced analytical curve for magnesium, shown in Figure 67(a), and manganese, shown in Figure 68(a). Also shown as (b) in each of the above figures are the FFT generated analytical curves for manganese and magnesium. The

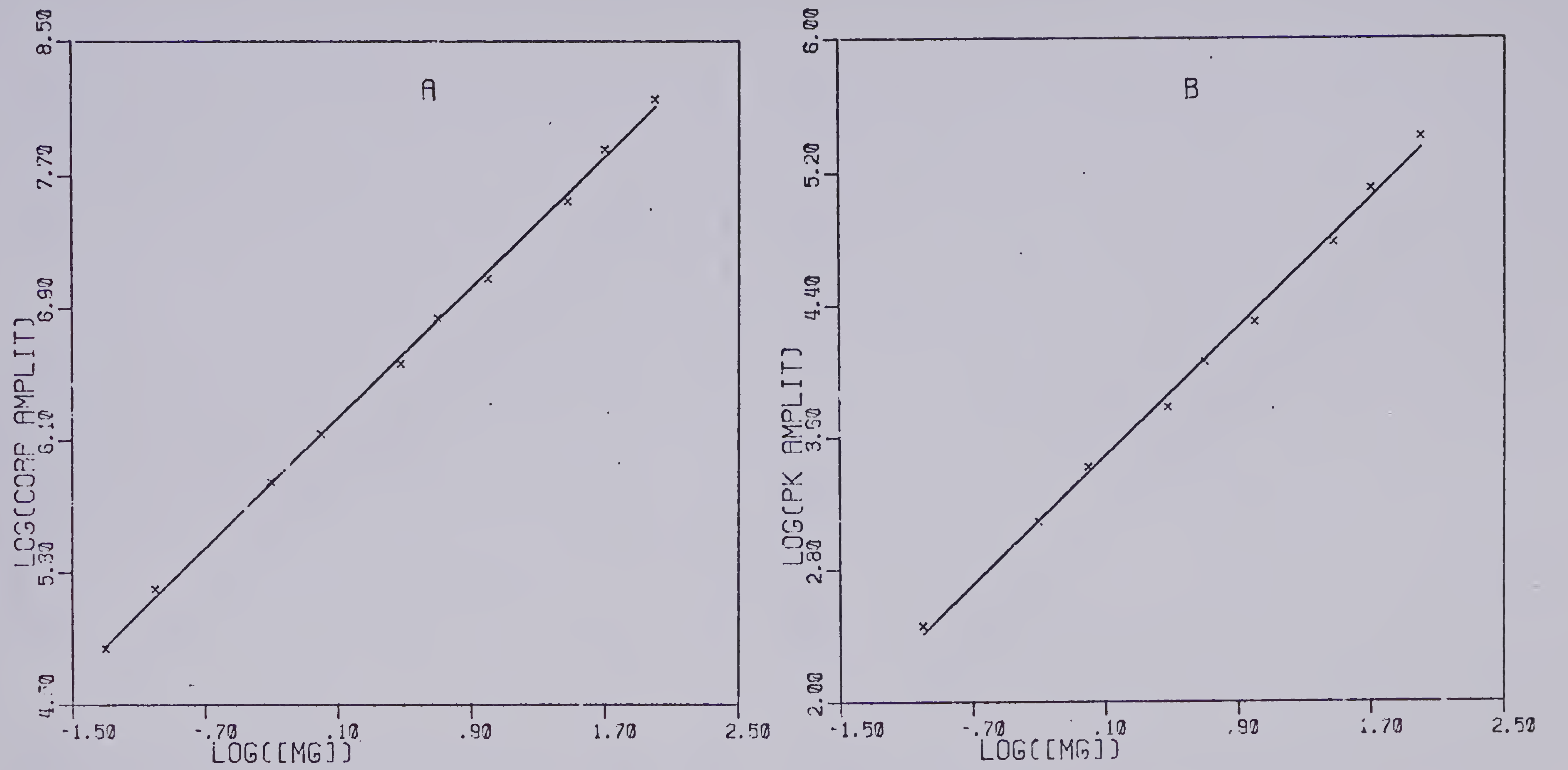

FIGURE 67. Mg analytical curves

(A) FFT generated

(B) correlation generated

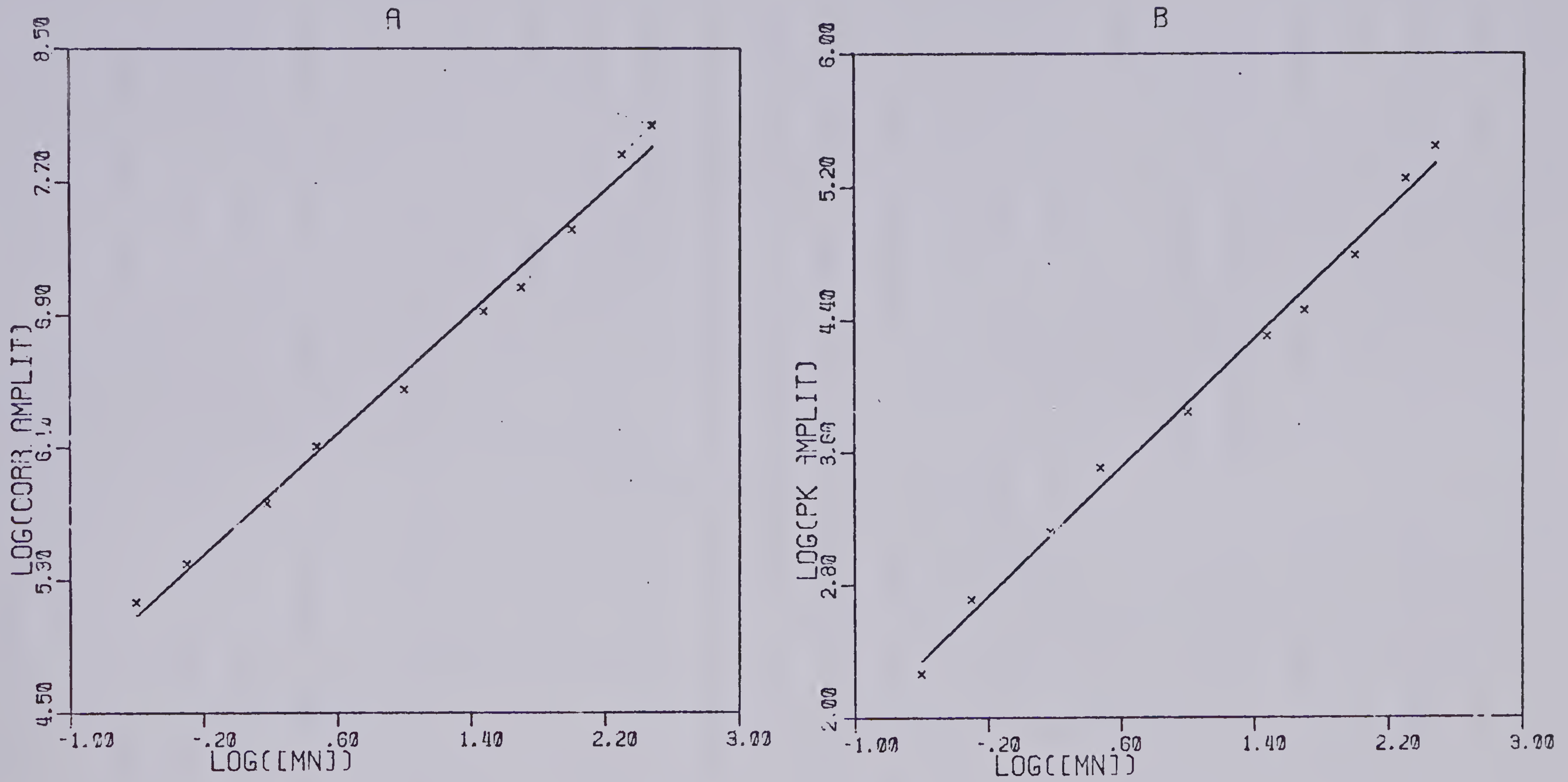

FIGURE 68. Mn analytical curves

(A) FFT generated

(B) correlation generated

corresponding regression analysis data is presented in Table XVII. Note that the analytical curves have been generated using both of the magnesium emission peaks at 280.3 nm and 279.5 nm, and using three of the manganese emission peaks at 260.6 nm, 259.4 nm and 257.6 nm. Let us first consider the magnesium analytical curves. Both of the FFT produced analytical curves show a high degree of linearity over the concentration range tested with the analytical curve obtained from the 279.5 nm peak emission showing a lower overall standard deviation. The correlation generated analytical curve has a slope statistically equivalent at the 95% confidence level to the 279.5 nm peak analytical curve slope. Note the lower standard deviation of the slope present in the correlation produced curve. In the simultaneous determination of manganese, the best combination of lowest standard deviation and highest linearity of slope occurs for the analytical curve based upon the 259.3 nm peak amplitude emission of manganese. Refer to Table XVII for the regression analysis data based on all three manganese peaks centered at 260 nm. The correlation processed analytical curve is much poorer both in respect to slope linearity and overall standard deviation than the individual FFT peak amplitude generated analytical curves. These results are in contrast to those of the magnesium data discussed above and illustrate an important factor in the utilization of correlation processing of interferograms. Further discussion will follow below.

The spectrum in Figure 54 illustrates the three triplet

Table XVII

Regression Data for Mg and Mn Analytical Curves

Element (nm)	Method	Slope	Overall Std. Dev.	Regression Correlation Coefficient
Mg	FFT			
(280.2)		0.935 ±0.042	0.169	0.9868
(279.5)		0.979 ±0.042	0.590	0.9984
	Correl.	0.960 ±0.042	0.0743	0.9979
Mn	FFT			
(260.5)		0.927 ±0.070	0.116	0.9943
(259.3)		0.981 ±0.052	0.0851	0.9972
(257.6)		0.970 ±0.032	0.127	0.9928
Sum of Peak Amplitudes		0.959 ±0.052	0.0863	0.9970
	Correl.	0.914 ±0.028	0.112	0.9970

emission system of manganese emission in the ultraviolet spectral range. The relative amplitudes of the triplets present a problem for correlation processing. The three peak emissions centered at 280 nm are just above the background emission level, close to the dynamic range limitations of the data acquisition system, while in contrast, the three peaks centered at 260 nm are close to the maximum amplitude allowed within the system's dynamic range. The third triplet emission, centered at 294 nm is of intermediate emission amplitude. For the determination of both manganese and magnesium through correlation processing a high signal to noise ratio single emission element, either manganese or magnesium, mask interferogram was used. If the spectrum of the manganese mask interferogram is inspected, in Figure 56, the spectral peaks of all nine manganese emission peaks may be discerned. The frequency information from all of these peaks is therefore present in the mask interferogram. The problem occurs in that the frequency information from all nine emission signals may or may not be present in the sample interferograms depending upon the relative concentrations of manganese and magnesium and the dynamic range of the data acquisition system. Consider for example the situation where the magnesium emission intensity accounts for about one-half of the total emission intensity thereby halving the intensity dynamic range available for the manganese emission signals. Obviously, the triplet emission of manganese at 280 nm will no longer be seen by the analog to

digital converter due to its small intensity in comparison to the overall intensity entering the data acquisition system. At lower manganese concentrations and/or higher magnesium concentrations, the manganese triplet emission at 294 nm may also disappear from the analog to digital converter's dynamic range leaving only the manganese triplet emission at 260 nm to provide quantitative information about the manganese present. Remember that the mask interferogram has been determined under high signal to noise ratio conditions and contains frequency information from all nine of the manganese emission lines. By performing a correlation between this manganese mask and the sample interferogram that would be obtained from the above example, we are effectively seeking a correlation between six signals present in the mask and absent in the sample. Only three frequencies are common to both interferograms. Such a correlation leads to a general degradation of the quantitative information available. In the more common case of correlation in the spectral domain between two emission spectra, this problem would be eliminated by setting an amplitude threshold in the mask spectrum. The amplitude of the threshold determines the number of peaks to be used in the correlation since all amplitude values below the threshold are no longer considered. Through the use of a variable threshold the optimum number of spectral peaks for correlation may be chosen. A similar threshold value may not be imposed in the interferogram domain due to the interferogram's multiplex nature. Once the interferogram

has been acquired it is nearly impossible to selectively eliminate specific frequencies. Therefore any selective filtering, equivalent to the setting of thresholds in the spectral domain, must be accomplished before the interferogram is digitized. Selective optical or electronic signal filtering does offer one solution for the generation of an optimal mask interferogram, as well as the selection of appropriate concentrations and amplifications with reference to the sample interferogram conditions. A high concentration, high signal to noise ratio interferogram that completely fills the system's imput dynamic range may be far from the optimal mask interferogram when sample experimental conditions are considered. An easy solution, in the case of a single element sample, is to use one of the high concentration analytical curve interferograms as a mask interferogram. This worked well in the lithium, sodium and calcium situations presented earlier. A great deal of caution must be used in selecting a mask interferogram in order to use correlation processing to its fullest advantage.

Thus far in the discussion only quantitative information concerning a single emitting species has been extracted through correlation analysis. The question arises as to correlation's ability to simultaneously monitor several elements undergoing concentration changes. As a simple example again consider the case of magnesium and manganese discussed in the previous section. Both analytical curves have been separately determined, but it is possible to follow the

concentration changes of both elements simultaneously using a manganese-magnesium mixture mask interferogram. The analytical curve for such a simultaneous determination is shown in Figure 70. The slope is 0.991 ± 0.036 with an overall standard deviation of 0.112 and a regression correlation coefficient of 0.9939. The concentration axis is expressed in terms of magnesium concentration since both elements undergo similar concentration changes. The interferometer system offers great potential in combination with correlation processing in the area of simultaneous data acquisition and simultaneous processing of spectral information. A great deal more work is warranted in this area.

To this point in the discussion, the precision of the correlation and FFT processes have been considered only with respect to the overall analytical curve. Let us further consider the precision within a group of repetitions such as would be at a single concentration point on an analytical curve. Does the correlation method at least match the precision of the FFT single spectral peak method of determining an element's concentration ratio? As previously discussed, the use of all of the available spectral information may not be the most precise or accurate method for quantitative determinations. Consider for example the second set of manganese-magnesium data used in Chapter V. The manganese concentration was held constant at 4.40 ppm while the magnesium concentration ranged from 0.00 ppm to 20.0 ppm to 100.0 ppm. Twelve repetitions at each magnesium concentration

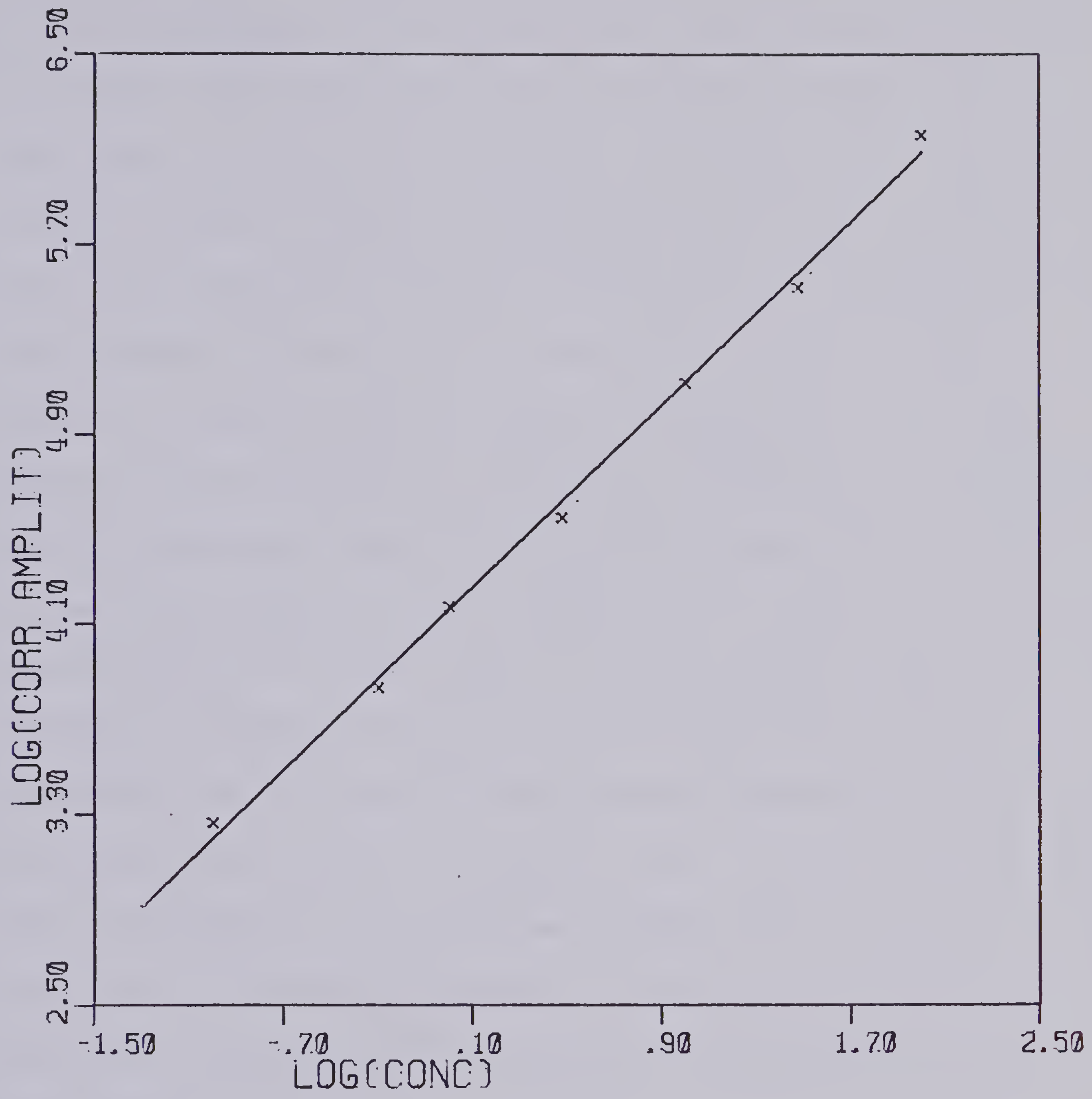

FIGURE 69. Analytical curve for Mn and Mg simultaneously detected

were available. A separate mask interferogram was generated for both manganese and magnesium and the correlations were performed. The resulting data is listed in Table XVIII, along with the corresponding FFT generated data. Comparisons between the two processing techniques are very difficult to make since the quantitative information is obtained from two very different domains and involves the use of different amounts of data to obtain similar information. The only possible value that may be used for comparison, is the percent relative standard deviation of the peak amplitude, whether the peak amplitude is in the spectral or correlation domain. With reference to Table XVIII,it can be easily seen that no significant difference exists in the relative standard deviations, at any specific magnesium concentration, between the correlation and FFT generated data. This trend was also found throughout all of the experimental work carried out in this study. Neither processing technique offerred any particular advantage with respect to the precision of a measurement.

D. Future Correlation Applications

The correlation operation, thus far, has been assumed to be only an alternate method of achieving a Fourier Transformation, In part this is true, the correlation operation when performed at a shift of zero does provide equivalent results, at one point in the spectral domain, with the Fourier Transformation. One must not forget that correlation

Table XVIII

Correlation and F.F.T. Precision Comparison

Mg concentration ppm		100.0	20.0	0.0
Element	Method	%R.S.D.	%R.S.D.	%R.S.D.
Mn	Correl.	15.0	13.5	10.3
(257.5 nm)	F.F.T.	17.0	13.8	10.0
Mg	Correl.	4.92	17.0	29.4
(279.5 nm)	F.F.T.	8.96	14.0	48.9
(280.2 nm)		9.39	14.1	55.1

analysis is a very powerful technique on its own, especially in the area of pattern recognition (94). This leads to some very interesting possibilities for the analysis of interferograms.

Many times throughout this thesis, the existence of a dynamic range problem has been experimentally demonstrated or theoretically discussed. This problem is a serious limitation for the interferometer based atomic emission system when dealing with real samples such as lithium in blood serum situation previously cited in Chapter III. Correlation may, in fact, provide a solution to this problem. It must be remembered that interferometry is a multiplex based technique, that is, all of the information available is present in each interferogram data point. Let us look at the situation of a small signal in the presence of a large signal. Initially due to the limited dynamic range the analog to digital converter can see only the large signal. What happens if the interferogram is allowed to clip at the input limits of the converter? Clipping refers to the assignment of minimum or maximum values of the input dynamic range to signals exceeding that dynamic range through excessive amplification. Let us consider the case of an interferogram that has had one half of its points clipped. Remember that the remaining one half of the points will still contain all of the information present and will now be seen at a higher resolution than in the previous unclipped situation. The smaller amplitude signal may now be seen by

the analog to digital converter and its information will be present in the interferogram unclipped portions. Through the proper selection of a correlation mask, this information should be extractable along with the large amplitude peak information. This is an application of correlation vs. a pattern recognition technique. Only very preliminary work has been carried out on computer generated interferograms and so no definite conclusions can be drawn on its application in practical situations. The results were promising but incomplete at this time. A great deal more work should be done in this area of correlation analysis.

E. Conclusions

The objective of this chapter was to provide a comparison of the Fourier Transform and correlation methods of information extraction from an interferogram. The techniques have been compared on a mathematical basis and on an experimental basis with respect to relative accuracy and precision and ease of implementation. Both techniques offer advantages and disadvantages in specific areas, but overall appear to be equivalent in their capability for the extraction of the quantitative spectral information in this experiment. Further work and expansion of the correlation analysis technique applied to interferometry needs definitely to be done to fully exploit this analysis technique.

CHAPTER VII

SUMMARY

The combination of atomic emission sources with an interferometer-based detection system shows great potential as a simultaneous multielement analysis unit. Three atomic emission sources, the air-acetylene and nitrous oxide-acetylene flames, and the argon R.F.-I.C.P., have been considered in combination with the Michelson interferometer built in our laboratory. The answers to two problems inherent in the interferometer detection system were sought in this study. Firstly, does the multiplex disadvantage become prevalent under conditions commonly encountered in atomic emission spectroscopy? Secondly, does the noise distribution character of a multiplex based system, operating in a detector shot noise or source fluctuation noise limited situation, play a dominant role in a practical analysis situation? An answer to the question of overall system feasibility was also sought. Finally, consideration was given to the correlation processing of system generated interferograms as an alternative to FFT processing.

Let us first consider the question of the multiplex disadvantage or dynamic range limitation imposed by the interferometer. The system was indeed found to have dynamic range problems due to source and/or sample matrix background emission signals. Source background emission is especially evident in the case of the plasma emission in the near infrared

spectral range. Similar problems were encountered with the nitrous oxide acetylene flame. Such dynamic range limiting emissions must be eliminated through either optical or electronic notch or bandpass filtering.

The second question brought out some very interesting experimental results. The experiments definitely show a "peak localization" of intensity related noise. Distribution of noise across the spectral domain was not observed as predicted by multiplex theory. The noise obviously has a narrow bandwidth spectral frequency distribution about the peak signal emission frequency, uncharacteristic of either detector shot noise or source fluctuation noise. The noise distribution behaviour is very similar to that of a scanning monochromator.

The question of practical feasibility is complex. The system operates well under the restricted condition of a non-dynamic range limited situation. Whether this is a commonly encountered situation, is purely dependent upon the sample being analyzed and the source spectral region observed.

The correlation processing of interferometer generated data was found to be equivalent to that of the FFT in both precision and accuracy of the analytical curve. Advantages in the software and time overhead of the computer system were noted due to the spectral selectivity available with correlation processing. Correlation processing may also provide a partial solution to the dynamic range problem through its pattern recognition capabilities.

Future work, with the current system, would involve further exploration into correlation processing as a solution to the dynamic range problem and as a general, flexible processing technique. An improved interferometer-emission source optical interface needs to be developed, making the system less susceptible spatially. Extension of the current mirror drive length to provide higher resolution, ~1 cm^{-1} would be adequate for most atomic emission work, is definitely warranted. This would also involve a general update of the system's electronics and software. Extension of the system spectral response to 200 nm or lower would also be a great asset for atomic emission work.

In conclusion, the atomic emission source-interferometer based detection system for simultaneous elemental analysis shows great potential, if and only if, the dynamic range problem can be controlled or managed.

Bibliography

1. H.A. Strobel, "Chemical Instrumentation", (Addison Wesley Pub. Co., 1973).
2. G.M. Hieftje and T.R. Copeland, Anal. Chem., 50 (5), 300R (1978).
3. R. Mavrodineanu and H. Boiteux, "Flame Spectroscopy", (J. Wiley and Sons Inc. N.Y., 1965).
4. J.A. Dean and T.C. Rains eds., "Flame Emission and Atomic Absorption Spectrometery", Vol. 1, (Decker, N.Y., 1969).
5. R. Herrmann and C.T.J. Alkemade, "Chemical Analysis by Flame Photometry", 2nd ed., (Interscience, New York, 1963).
6. V.A. Fassel, Science, 202, 181 (1978).
7. L.P.P. Buttler, H.G.C. Human and R.H. Scott, "Handbook of Spectroscopy", Chapt. XIV, 816.
8. A.F. Ward, American Laboratory, 10, 79 (1978).
9. J.D. Winefordner, J.J. Fitzgerald and S. Omenetto, Appl. Spectrosc., 29, 5, 369 (1975).
10. Jarrell-Ash Co., 590 Lincoln St., Waltham MA.
11. EG & G Reticon, 345 Potrero Ave., Sunnyvale, California.
12. RCA, Harrison, New Jersey.
13. G. Horlick, Appl. Spectrosc., 30, 2, 113 (1976).
14. Princeton Applied Research Co., Princeton, New Jersey.
15. J.A. Decker, Anal. Chem., 44, 127A (1972).
16. M. Harwit, Appl. Opt., 10, 1415 (1971).

17. M. Harwit, "Transform Techniques in Chemistry", P.R. Griffiths ed., Chapt. 7, (Plenum Press, N.Y., 1978).

18. J.A. Decker, "Spectrometric Techniques", Vol. L, G.A. Vanasse ed., Chapt. 5, (Academic Press, N.Y., 1977).

19. "Aspen International Conference on Fourier Spectroscopy 1970", AFCRL-71-0019, G.A. Vanasse, A.T. Stair Jr., D.J. Baker, editors.

20. G.A. Vanasse, "Fourier Spectroscopy: A Critical Review", CRC Critical Reviews in Solid State Sciences, 4, (1973).

21. P.R. Griffiths, ed., "Transform Techniques in Chemistry", Chapts. 1-6, (Plenum, New York, 1978).

22. H. Sakai, "Spectrometric Techniques," G.A. Vanasse ed., Chapt. 1, (Academic Press, N.Y., 1977).

23. P.R. Griffiths, "Chemical Infrared Fourier Transform Spectroscopy", (Wiley Interscience, 1975).

24. R.J. Bell, "Introductory Fourier Transform Spectroscopy", (Academic Press, N.Y., 1972).

25. W.H. Steel, "Interferometers for Fourier Spectroscopy", reference 19.

26. G. Horlick and W.K. Yuen, Anal. Chem., 47, 775A (1975).

27. W.K. Yuen and G. Horlick, Anal. Chem., 49, 1446 (1977).

28. G. Horlick and W.K. Yuen, Appl. Spectrosc., 32, 38 (1978).

29. G. Horlick, Ph.D. Thesis, Univ. of Illinois, Urbana, Illinois (1970).

30. W.K. Yuen, Ph.D. Thesis, Univ. of Alberta, Edmonton Alberta, (1978).

31. P.R. Griffiths, H.J. Sloane and R.W. Hannah, Appl. Spectrosc., 31, 485 (1977).

32. M.I.T. Wavelength Tables (M.I.T. Press, Cambridge Mass., 1969).

33. D.J. Johnson, F.W. Plankey and J.D. Winefordner, Can. J. Spectrosc., 19, 151 (1974).

34. E. Cordos and H.V. Malmstadt, Anal. Chem., 45, 425 (1973)

35. Nicolet Instrument Corporation, 5225 Verona Road, Madison Wisconsin.

36. H. Sakai, "Consideration of the Signal to Noise Ratio in Fourier Spectroscopy", reference 19.

37. G.W. Chantry and J.W. Fleming, Infrared Physics, 16, 655 (1976).

38. R.H. Morton and R. Beer, J. Opt. Soc. Am., 66, 259 (1976).

39. E.G. Codding and G. Horlick, Appl. Spectrosc., 27, 2 (1973).

40. J.O. Lephardt, Chapt. 11, reference 21.

41. Y. Talmi, R. Crosmun and N.M. Larson, Anal. Chem., 48, 326 (1976).

42. L. Mertz, J. Opt. Soc. Am., 51, 4 (1961).

43. J.D. Winefordner, R. Avni, T.L. Chester, J.J. Fitzgerald, L.P. Hart, D.J. Johnson, F.W. Plankey, Spectrochemica Acta, 31B, 1 (1976.

44. T. Hirschfeld, Appl. Spectrosc., 30, 68 (1976).

45. M.H. Tai and M. Harwit, Appl. Opt., 15, 2664 (1976).

46. M. Harwit and M.H. Tai, Appl. Opt., 16, 3071 (1977).

47. R.R. Treffers, Appl. Opt., 16, 3103 (1977).

48. T. Hirschfeld, Appl. Opt. 16, 3070 (1977).

49. F.D. Kahn , Astrophys. J., 129, 518 (1959).

50. A.S. Filler, J. Opt. Soc. Am., 63, 589 (1973).

51. T.L. Chester, J.J. Fitzgerald and J.D. Winefordner, Anal. Chem., 48, 793 (1976).

52. R.F. Knacke, Appl. Opt., 17, 684 (1978).

53. P. Luc and S. Gerstenkorn, Appl. Opt., 17, 1327 (1978).

54. T.E. Edmonds and G. Horlick, Appl. Spectrosc., 31, 536 (1977).

55. W.H. Steel, J. Opt. Soc. Am., 54, 2 (1964).

56. Reference 24, Chapt. 11, pg 141.

57. H. Sakai, "Spectrometric Techniques", Vol. 1, G.A. Vanasse ed., (Academic Press, 1977).

58. EMI Photomultiplier Tube Catalogue, EMI Gencom Inc., 80 Express St., Plainsview New York, 11803.

59. F.E. Lytle, Anal. Chem., 46, 545A (1974).

60. J.J. Harris, F.E. Lytle and T.C. McCain, Anal. Chem., 48, 2095 (1976).

61. LPS11-S Laboratory Peripheral System User's Guide, DEC Manual #DEC-11-HLPGA-C-D.

62. LPS11-S Laboratory Peripheral System Maintenance Manual, DEC manual # DEC-11-HLPMA-B-D.

63. H.T.V.-R166 P.M.T., Hamamatsu TV Co. Ltd., 456 Ebitsuka Cho, Hamamatsu City, Japan.

64. 1P28, S5 Response P.M.T., RCA, Electronic Components, Lancaster, Penn. 17604.

65. A.N. Zaidel, V.K. Prokof'ev, S.M. Raiskii, V.A. Slavnyi, E. Ya. Schreider, "Table of Spectral Lines", 3rd edition, (IFI/Plenum Publishers, 1970).

66. Corning Glass Works, Corning, New York.

67. E.E. Pickett and S.R. Koirtyohann , Anal. Chem., 41, 28A (1969).

68. K.M. Aldous, R.F. Browner, R.M. Dagnall and T.S. West, Anal. Chem., 42, 939 (1970).

69. G.M. Hieftje, Appl. Spectrosc., 25, 6 (1971).

70. J.A. Fiorino, R.N. Kniseley, and V.A. Fassel, Spectrochemica Acta, 23B, 413 (1968).

71. G.M. Hieftje and R.I. Bystroff, Spectrochemica Acta, 30B, 187 (1975).

72. G.F. Kirkbright and S. Vetter, Spectrochemica Acta, 26B, 505 (1971).

73. ENL Laboratories Inc., 115 Independence Drive, Menlo Park, Calif. 94025.

74. E. Berman, Appl. Spectrosc., 29, 1 (1975).

75. K.W. Busch, N.G. Howell and G.H. Morrison, Anal. Chem., 46, 1231 (1974).

76. C.T. Foskett, Appl. Spectrosc., 30, 431 (1976).

77. J.B. Willis, Nature, 207, 715 (1965).

78. M.D. Amos and J.B. Willis, Spectrochemica Acta, 22, 1325 (1966).

79. E.E. Pickett and S.R. Koirtyohann, Spectrochemica Acta, 23B, 235 (1968).

80. G.R. Kornblum and L. de Galen, Spectrochemica Acta, 28B, 139 (1973).

81. J.O. Rasmusson, V.A. Fassel and R.N. Kniseley, Spectrochemica Acta, 28B, 365 (1973).

82. V.A. Fassel, J.D. Rasmusson, R.N. Knisely and T.G. Cowley, Spectrochemica Acta, 25B, 559 (1970).

83. G.D. Christian and F.J. Feldman, Appl. Spectrosc., 25, 660 (1971).

84. S. Greenfield, I.L. Jones and C.T. Berry, Analyst, 89, 713 (1964).

85. R.H. Wendt and V.A. Fassel, Anal. Chem., 37, 920 (1965).

86. R.L. Dahlquist and J.W. Knoll, Appl. Spectrosc., 32, 1 (1978).

87. S.S. Berman and J.W. McLaren, Appl. Spectrosc., 32, 372 (1978).

88. P.W.J.M. Boumans and F.J. de Boer, Spectrochemica Acta, 30B, 309 (1975).

89. P.W.J.M. Boumans and M. Bosveld, Spectrochemica Acta Part B, in press.

90. D.L. Windsor and M.B. Denton, Appl. Spectrosc., 32, 366 (1978).

91. J.E. Fruend, "Mathematical Statistics", 2nd ed., (Prentice Hall Inc., N.J., 1971).

92. G. Horlick and K.R. Betty, Appl. Spectrosc., 32, 31 (1978).

93. H.V. Malmstadt, C.G. Enke, S.R. Malmstadt and G. Horlick, "Optimization of Electronic Measurements", (Benjamin, Menlo Park, Calif., 1974).

94. G. Horlick and G.M. Hieftje, "Contemporary Topics in Analytical and Clinical Chemistry, Vol. 3", D.M. Hercules, G.M. Hieftje, L.R. Snyder and M.A. Evenson editors, Chapter 4, 153, (Plenum Publishing Co., 1978).

95. R. Bracewell, "The Fourier Transform and its Applications", (McGraw Hill, 1965).

96. H. Rubens and R.N. Wood., Phil. Mag., 21, 249 (1911).

97. P. Fellgett, J. Phys. Radium., 19, 187 (1958).

98. B. Liu, "Digital Filters and the Fast Fourier Transform", (Halsted Press, 1975).

99. J. Connes, "Computing Problems in Fourier Spectroscopy", reference 19.

100. G. Guelachvili and J.P. Maillard, "Fourier Spectroscopy from 10^6 Samples", reference 19.

101. J.W. Cooper, Chapt. 4, reference 21.

102. R. Dick and G. Levy, "Correlation Interferometry", reference 19.

103. J.H. Davies, Anal. Chem., 42, 101A (1970).

104. R.C. Wieboldt et al., Pittsburgh Conference, Cleveland, Ohio, paper #369, March 5-9, 1979.

105. G.W. Small et al., Pittsburgh Conference, Cleveland, Ohio, paper #370, March 5-9, 1979.

106. J.A. de Haseth and T.L. Isenhour, Anal. Chem., 49, 1977 (1977).

Appendix A

Fellgett's Advantage (Multiplex Advantage)

This appendix develops mathematically the signal to noise ratio advantage offered by a multiplex interferometer based detection system over a scanning monochromator based system under two conditions: a detector noise limited or photon noise limited system. The total observation time for the two systems was assumed equal.

Let the observation time be T seconds.

Let the spectral range covered be $\bar{v}_2-\bar{v}_1$ cm^{-1}.

Let the resolution be Δv cm^{-1}.

Let the detector generated noise be 'a'.

Let the source generated noise be 'b'.

Let $I(\bar{v})$ be the spectral intensity distribution function.

Let $M = \Delta v/(\bar{v}_2-\bar{v}_1)$ be the number of spectral resolution elements.

Let S be the signal at the detector output.

Let N be the noise at the detector output.

Let E be an interferometer efficiency factor.

1. Scanning Monochromator

$$S = I(\bar{v}).\Delta v.T/M$$

$$N = (I(\bar{v}).\Delta v.T/M)^{1/2}$$

$$N_{TOT} = (a^2.T/M + b^2.I(v).\Delta\bar{v}.T/M)^{1/2}$$

$$= (T/M(a^2 + b^2.I(\bar{v}).\Delta\bar{v}))^{1/2}$$

$$S.N.R._{SC} = S/N_{TOT}$$

$$= \frac{I(\bar{v}).\Delta v.T/M}{(M^{\frac{1}{2}}(a^2+b^2.I(\bar{v}).\Delta v)^{\frac{1}{2}}}$$

$$= \frac{I(\bar{v}).\Delta v.T}{(M^{\frac{1}{2}}(a^2+b^2.I(\bar{v}).\Delta v)^{\frac{1}{2}}}$$

2. Multiplex Interferometer

$$S = I(\bar{v}).\Delta v.T/E$$

$$N = (\frac{T}{E}\int_{\bar{v}_1}^{\bar{v}_2} I(\bar{v})\,dv)^{\frac{1}{2}}$$

$$N_{TOT} = (\frac{T}{E}(a^2+b^2 \int_{\bar{v}_1}^{\bar{v}_2} I(\bar{v})\,d\bar{v})^{\frac{1}{2}}$$

$$S.N.R._{FT} = S/N_{TOT}$$

$$= \frac{I(\bar{v}).\Delta v.T}{E^{\frac{1}{2}}(T(a^2+b^2 \int_{\bar{v}_1}^{\bar{v}_2} I(\bar{v})\,d\bar{v})^{\frac{1}{2}}}$$

$$= \frac{I(v).\Delta v.T}{E^{\frac{1}{2}}((a^2+b^2 \int_{\bar{v}_1}^{\bar{v}_2} I(\bar{v})\,d\bar{v})^{\frac{1}{2}}}$$

3. $$\frac{SNR_{FT}}{SNR_{SC}} = \frac{M^{\frac{1}{2}}(a^2+b^2 I(\bar{v}).\Delta v)^{\frac{1}{2}}}{E^{\frac{1}{2}}(a^2+b^2 \int_{\bar{v}_1}^{\bar{v}_2} I(\bar{v})\,d\bar{v})^{\frac{1}{2}}}$$

In a detector limited situation 'a' predominates leading to

$$\frac{SNR_{FT}}{SNR_{SC}} = \left(\frac{M}{E}\right)^{1/2}$$

Thus the number of spectral resolution elements present plays a determining role in any signal to noise ratio advantage.

In a photon noise limited situation a<<b leading to

$$\frac{SNR_{FT}}{SNR_{SC}} = \frac{(M.I(\bar{v}).\Delta v)^{\frac{1}{2}}}{(E.\int_{\bar{v}_1}^{\bar{v}_2} I(\bar{v})d\bar{v})^{\frac{1}{2}}}$$

$$= \left[\frac{I(\bar{v})}{\frac{E}{\bar{v}_2-\bar{v}_1} . \int_{\bar{v}_1}^{\bar{v}_2} I(\bar{v})d\bar{v}}\right]^{\frac{1}{2}}$$

Thus both the intensity of the emission line of interest and the intensity over the total spectral range covered lead to the determination of any signal to noise ratio advantage present.

Appendix B

D.C. Level Studies

By definition, the interferogram consists only of the modulated or A.C. portion of the signal at the interferometer detector output. It is well known that a D.C. level also exists at the output and is of no consequence in a detector noise limited situation. For work in a detector shot noise or source fluctuation noise limited environment the unmodulated light present may have a definite effect upon the amplitude of the noise present. In both the shot and fluctuation noise limited situation, the noise amplitude increases with the total light intensity present.
Thus the peak to peak interferogram amplitude does not necessarily give a true indication of the total light intensity present at the photocathode and responsible for the generation of detector shot noise or carrying source fluctuation noise. An experiment was performed with this system to obtain an indication of the relative amounts of modulated and unmodulated light typically present.

The emission of a 30.0 ppm aqueous sodium chloride solution in an air-acetylene flame was used as a model system for the D.C. level studies. The 1P28 photomultiplier tube was used as a detector tube was used as a detector, both with and without the dynode chain modifications outlined in Chapter II.

The experimental results typically indicate a modulation

efficiency on the order of 7% with the linear dynode chain, Modulation efficiency is defined as the A.C. signal peak to peak amplitude divided by twice the D.C. signal and then a factor of 100 applied. Upon making the dynode chain changes outlined in Chapter II the modulation efficiency increased to 20%. This appears to be a direct result of the increased electrostatic focussing capability of the last two dynodes. In both cases only a small portion of the light intensity hitting the photocathode is ultimately used as a source of spectral information while the shot or fluctuation noise present is actually due to a much higher light level at the photocathode. In this way, the absolute values of the noise intensity relationship may never be obtained, if only the interferogram is considered. It is possible for the D.C. level to increase to a greater extent than the interferogram peak to peak amplitude, thereby giving false information about the spectral peak amplitude-noise relationship. Caution must be used in interpreting such results.

Appendix C

Accurate Start Pulse Generation

The lack of an accurate start pulse is one of the basic design problems with this interferometer system. The data processing system currently utilizes double sided interferograms; that is, an equal number of data points on each side of the zero path difference point in mirror travel. A third interferometer in the system utilizing a white light broadband source, and the same mirror as the sample channel and laser reference channel, now provides a zero path difference reference signal. For complete details see Yuen (30). There is, therefore, no way of determining accurately the starting point for the data acquisition routine prior to the zero path difference position. If a single scan of the mirror provided a very high signal to noise ratio interferogram, a large amount of data on both sides of the zero path difference point could be acquired and the correct 4096 points could be extracted (2048 per side). The problem occurs in that the interferograms must be signal averaged in real time, requiring that an accurate reference point, preferably the first data point in the interferogram, be present from scan to scan. This is easily accomplished in a three mirror (white light, laser, sample) interferometer by optically offsetting the white light mirror causing the zero path difference point of the white light interferogram to occur before the zero path difference point

of the sample channel. This is done by decreasing the optical path in the moving arm of the interferometer for the white light beam. Such a system provides a reproducible reference point occuring a specified number of points, such as 2048, before the main channel zero path difference point and serves as an accurate start pulse for the data acquisition system. The current interferometer, due to the fact that all three interferometers, laser, white light and sample beam share the same mirror, cannot utilize such an offset system. The alternative method is to lengthen the optical path travelled by the white light beam in the stationary mirror arm of the interferometer. This would produce a similarly offset accurate start pulse.

Just such a technique was tested on the current system. A fused quartz optical flat was placed in the white light beam in the stationary mirror interferometer arm. It was calculated that a thickness of 6.0 mm would provide an offset of 9671 data points before the zero path difference reference point on the main channel. This would serve quite adequately as an accurate start pulse. Such a system did not work in practice for the following reasons. The quartz flat extends the optical path due to its higher refractive index than the surrounding air, 1.46 as compared to 1 respectively. The assumption of no variation of refractive index with wavelength was made. In fact, for fused quartz the refractive index varies from 1.46690 at 434.047 nm to 1.45517 at 706.520 nm a change of 0.01183. This results in a different optical

offset for each wavelength of light present in the white light source, and therefore different positions of zero path difference for each wavelength. This results in a chirped or spread out maximum at the zero path difference reference point, rendering it useless as an accurate start pulse source. No maximum at zero path difference was even detectable. If the mathematics are worked out for such a system, a variation in refractive index of no more than 5×10^{-5} is allowable over the emission band of the white light source. This is an impossible criterion for almost any substrate to meet. A description of the system currently used is given by Yuen (30). It envolves the use of an accurate stop pulse in combination with software and hardware data manipulation in order to provide signal averaging capability.

Appendix D

Software Developed for the Interferometer System

A. Introduction

This appendix will provide a description of the software programs used to interface the interferometer-minicomputer system and to mathematically process the interferogram data. The programming was done on a DEC PDP 11/10 16 bit mini-computer system under the RT11 02C operating system using Fortran 01C and Macro 01C programming languages. An overall program sequencing flow chart will be presented as well as a brief description of each program outlining any unique features used. Detailed documentation will be provided within the program listing. Refer to the DEC manuals for further information.

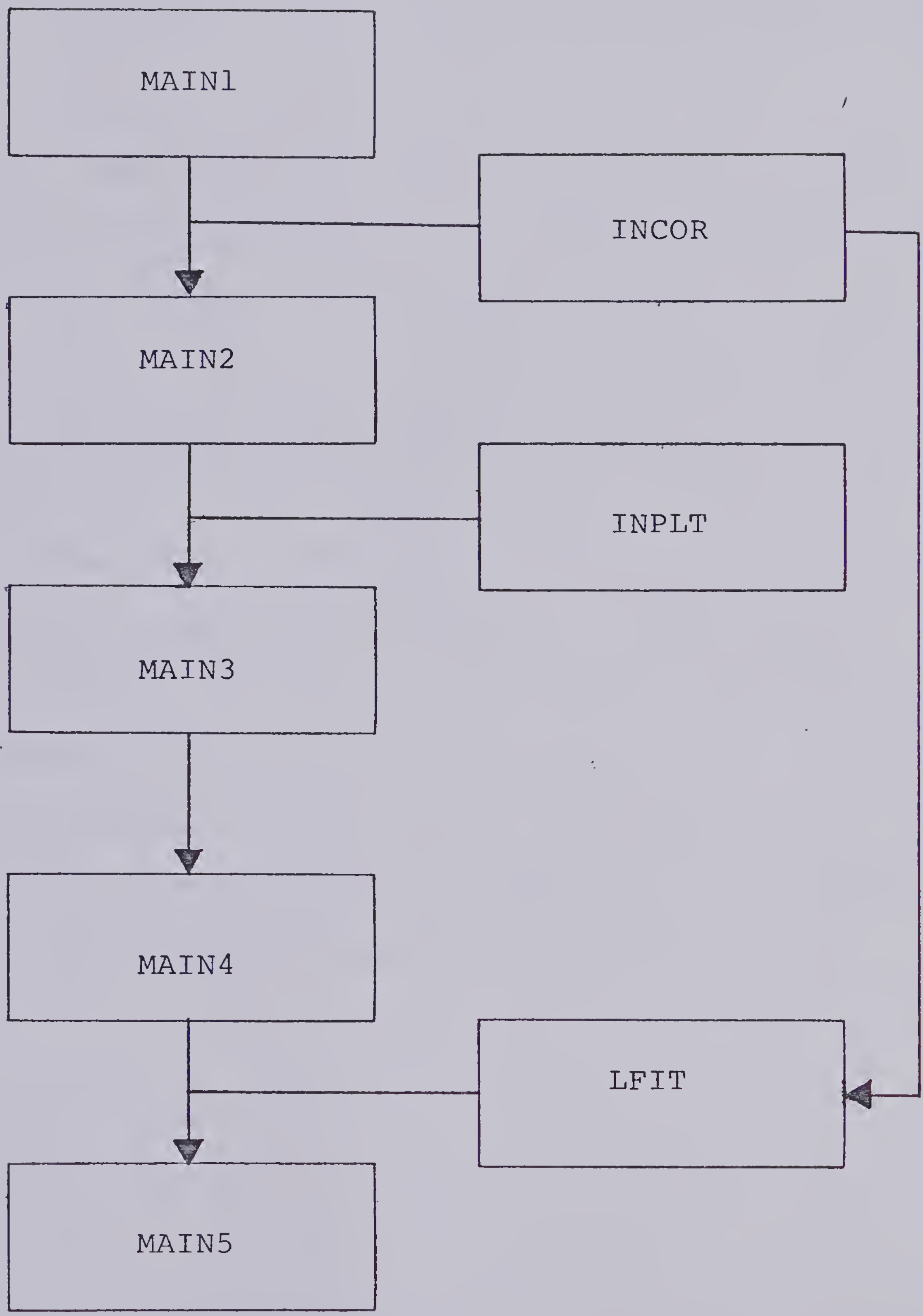

FIGURE 70. Software Flow Diagram.

B MAIN1 - Data Acquisition Routine

1. Purpose: This routine provides the timing and sequencing interface to the interferometer, signal averaging capability and storage of interferograms on the disk under user defined names.

2. Operation: The operator is required to input a title (12 characters) and the desired number of interferograms to be acquired and averaged. The program accesses the system date automatically. After acquisition the central 1024. points of the interferogram are displayed on the VT11 screen for 15 seconds. The operator then has the option of storing the interferogram as a named data file or returning to the start of the program or exiting to the monitor. This routine currently acquires a 4096. point double sided interferogram. Note also the use of an accurate stop pulse and the resulting software complications. This program also makes use of "common block" arrays between an assembler subroutine and a Fortran program. See the program listings for further details.

```
C
C
C                              MAIN1.FOR
C
C
C       THIS PROGRAM IN COMBINATION WITH 'MAIN1A.MAC' PROVIDES THE
C       INTERFACE BETWEEN THE INTERFEROMETER AND DATA ACQUISITION
C       SYSTEM. USE IS MADE OF THE LPS11-S DATA ACQUISITION SYSTEM
C       ACCESSED AT THE MACRO LEVEL. FOR DETAILS SEE 'MAIN1A.MAC'
C       DOCUMENTATION. THIS PROGRAM ACCEPTS A SAMPLE NAME OF 12
C       CHARACTERS IN LENGTH AND ACCESSES THE SYSTEM DATE. BOTH ARE
C       PERMANENTLY STORED WITH THE INTERFEROGRAM ON THE DISK ALONG
C       WITH THE NUMBER OF SCANS ,MIN,MAX,(AND SUBSCRIPTS) AND THE
C       INTERFEROGRAM AMPLITUDE RANGE. THE FILE IS NAMED USING THE
C       CALL ASSIGN COMMAND. NOTE THE USE OF A NAMED COMMON BLOCK
C       IN ORDER TO PUT ARRAYS IN COMMON WITH THE MACRO ROUTINE ARRAYS.
C       NOTE ALSO THAT FORTRAN DOES NOT SUPPORT INTEGER*4 FUNCTIONS.
C
C       THIS ROUTINE WAS WRITTEN IN 1976 AND LATER MODIFIED IN 1978
C       BY R.H.HALL.
C
C
C       THIS PROGRAM REQUIRES THE MAIN1A.OBJ,VTLIB.OBJ,LPSLIB.OBJ,
C       SYSLIB.OBJ/F FILES AT THE LINKING STAGE.
C
C
        DIMENSION TITLE(3),DAT(3),IA(4600),IB(8192)
C
C       COMMON BLOCK NAME MUST MATCH .CSECT NAMED SECTION IN MAIN1A
C
        COMMON  /RHH/IB,IA,N,N2
        DATA    DAT/3*0.0/
        CALL DATE(DAT)
        WRITE(7,121)DAT
121     FORMAT(' ',3A4)
51      WRITE(7,103)
103     FORMAT(' ','INPUT SAMPLE NAME  3A4')
        READ(5,104) TITLE
104     FORMAT(3A4)
        WRITE(7,11)
11      FORMAT(' ','INPUT # SCANS I5')
        READ(5,73) N
73      FORMAT(I5)
        N2=4096
C
C       CALL THE MACRO SUBROUTINE MAIN1A.MAC
C       ENTRY PT IS 'GDATA'
        CALL GDATA
C
C
        XLL=FLOAT(N2)
        AN=0.
        ANN=FLOAT(N)
C
C       CONVERSION FROM DOUBLE WORD INTEGER TO FLOATING POINT
C       SEE 'MAIN1A' FOR DETAILS
        DO 22 I=1,N2*2,2
        XL=(FLOAT(IB(I))+FLOAT(IB(I+1))*32768.)/ANN
        IA((I+1)/2)=INT(XL)
22      AN=AN+XL
```

```
C
C
C       CALCULATION OF THE MIN AND MAX VALUES WITH THEIR
C       SUBSCRIPTS
C
C
        IA(N2+1)=N
        AN=AN/XLL
        IA(N2+2)=-30000
        IA(N2+3)=30000
        IA(N2+4)=30000
        IA(N2+5)=-30000
        DO 23 I=1,N2
        IA(I)=IA(I)-AN
        IF(IA(N2+2).LT.IA(I))IA(N2+2)=IA(I)
        IF(IA(N2+2).EQ.IA(I))IA(N2+3)=I
        IF(IA(N2+4).GT.IA(I))IA(N2+4)=IA(I)
23      IF(IA(N2+4).EQ.IA(I))IA(N2+5)=I
        IA(N2+6)=IA(N2+2)-IA(N2+4)
C
C       VT11 GRAPHICS DISPLAY OF THE CENTRAL 1000 POINTS OF THE
C       INTERFEROGRAM FOR 15 SECONDS. MIN AND MAX ARE ALSO PRINTED.
C
        CALL INIT(IB,5000)
        CALL SCROL(10,100,5)
        CALL SCAL(0.,-2048.,1023.,2048.)
        CALL APNT(0.,0.,-1,6,-1,1)
        XL=0.
        DO 24 I=1,1024
        XLL=FLOAT(IA(I+1536))-XL
        XL=FLOAT(IA(I+1536))
24      CALL LVECT(1.,XLL)
        WRITE(7,77) (IA(N2+I),I=2,6)
77      FORMAT(' ','MAX=',I6,2X,'SUB=',I6,//' MIN=',I6,2X,'SUB=',
     1  I6,//' RANGE=',I6)
        CALL TIME(15*60)
1       CALL TIMR(IE)
        IF(IE.NE.0)GO TO 1
        CALL TIME(0)
        CALL SCROL(-1,-1,-1)
        CALL INIT
        CALL FREE
C
C       OPTIONS OFFERRED FOR SAVING OR REJECTING THE DATA.
C
61      WRITE(7,70)
70      FORMAT(' ','RETURN=1,SAVE=2,EX=3    I2')
        READ(5,6)I
6       FORMAT(I2)
        GO TO(51,53,123),I
53      CONTINUE
        WRITE(7,122)
122     FORMAT(' ','INPUT FILENAM FOR OUTPUT',/)
        CALL ASSIGN(1,'DK0:FTN1.DAT',-1,'NEW','NC',1)
        WRITE(1)N2
        WRITE(1)(DAT(I),I=1,3)
        WRITE(1)(TITLE(I),I=1,3)
        WRITE(1)(IA(I),I=1,N2+6)
        ENDFILE 1
        CALL CLOSE(1)
        CALL ASSIGN(1)
        GO TO 61
123     STOP
        END
```

```
        .TITLE INTERFACE TO INTERFEROMETER
;
;
;
;       THIS SUBROUTINE PROVIDES THE TIMING AND SEQUENCING
;       INTERFACE TO THE INTERFEROMETER. THREE DIGITAL INPUT
;       LINES ARE USED AS FLAGS FOR THE START,CLOCK AND STOP
;       PULSE SIGNALS GENERATED BY THE INTERFEROMETER. DOUBLE
;       WORD (32 BIT) SIGNAL AVERAGING IS USED IN ORDER TO
;       PROVIDE AN ADEQUATE DYNAMIC RANGE. THE ARRAYS DEFINED
;       .CSECT /RHH/ ARE IN COMMON WITH FORTRAN DEFINED ARRAYS
;       OF THE SAME NAME AND LENGTH. NOTE THAT FORTRAN DOES NOT
;       SUPPORT DOUBLE WORD INTEGER FUNCTIONS AND AN ALGORITHM
;       IS INCLUDED TO TAKE THIS INTO ACCOUNT BEFORE CONTROL IS
;       RETURNED TO THE FORTRAN PROGRAM. THIS ROUTINE MUST BE
;       LINKED TO 'MAIN1.OBJ' TO OPERATE CORRECTLY.
;
;
;       THIS ROUTINE WAS WRITTEN INITIALLY IN 1976 AND LATER
;       MODIFIED IN 1978 BY R.H.HALL
;
;
;
        .MCALL  ..V2..,.REGDEF
        ..V2..
        .REGDEF
        .GLOBL  GDATA
                                        ; SET ADDRESS REGISTERS
        ADB=170402                      ; A/D DATA BUFFER
        ADSR=170400                     ; A/D STATUS REGISTER
        DIBUF=170412                    ; DIGITAL INPUT BUFFER
;
;
GDATA:  MOV     N,R1                    ; ENTRY POINT FROM FORTRAN
        MOV     N2,R2
        MOV     #IB,R0
        ADD     R2,R2
LP1:    CLR     (R0)+                   ; ZERO CORE LOCATIONS
        DEC     R2                      ; TO INITIALIZE SYSTEM
        BNE     LP1
        MOV     #IA,R0
        MOV     N2,R2
        ADD     #500.,R2
LP1A:   CLR     (R0)+
        DEC     R2
        BNE     LP1A
;
;       START THE ACTUAL ACQUISITION OF DATA
;       USING DIGITAL INPUT BUFFER AS START,CLOCK AND STOP
;
LP4:    MOV     N2,R2                   ; SET WINDOW FOR POINTS
        ADD     #500.,R2
        MOV     #IA,R0                  ; SET UP ARRAY IA
        MOV     DIBUF,R4                ; CLEAR DIGITAL INPUT BUFFER
        MOV     R4,DIBUF
LP2:    MOV     DIBUF,R4
        BIT     #1,R4                   ; TEST FOR START FLAG ON BIT 0
        BEQ     LP2
LP3:    CLR     ADSR
LP3A:   MOV     DIBUF,R4                ; TEST FOR CLOCK FLAG ON BIT 3
```

```
                BIT     #10,R4
                BEQ     LP3A
                INC     ADSR                    ; START ADC
                DEC     R2
                BEQ     LP4                     ; CHECK FOR TOO MANY PTS
                MOV     R4,DIBUF
        LP5:    TSTB    ADSR                    ; TEST FOR A/D DONE FLAG
                BPL     LP5
                MOV     ADB,(R0)+               ; SAVE A/D BUFFER IN IA
                BIT     #2,R4                   ; CHECK FOR STOP FLAG
                BEQ     LP3
                SUB     #500.,R2                ; CHECK FOR TOO FEW POINTS
                BGT     LP4
;
; DOUBLE WORD ADD ROUTINE
;
                MOV     #IB,R3                  ; START OF DOUBLE WORD ADD
                MOV     N2,R2                   ; FORM ARRAY IA TO IB
        LP6:    ADD     -(R0),(R3)+             ; NOTE LAST POINT FIRST
                ADC     (R3)+
                DEC     R2
                BGT     LP6
;
; LOAD LEDS WITH SCAN COUNTER
;
                MOV     R1,LEDSV1               ; PUT # SCANS LEFT ON LEDS
                DEC     LEDSV1                  ; N.B. OCTAL DOWN COUNTER
                MOV     #6,CNTLED
                CLR     LEDSV3
        LP9:    MOV     LEDSV1,LEDSV2
                BIC     #177770,LEDSV2
                MOVB    LEDSV3,LEDSV2+1
                MOV     LEDSV2,ADB
                ASR     LEDSV1
                ASR     LEDSV1
                ASR     LEDSV1
                INC     LEDSV3
                DEC     CNTLED
                BGT     LP9
                DEC     R1
                BGT     LP4
;
; START OF ROUTINE FOR CONVERSION TO FORTRAN
; FLOATING POINT FORMAT
; NOTE THAT DIVISION FOR AVERAGE IS DONE IN FORTRAN
;
                MOV     #IB,R1
                MOV     N2,R4
        LP16:   MOV     (R1),R2
                MOV     2(R1),R3
                ASL     R3
                ROL     R2
                ADC     R3
                CLC
                ROR     R2
                MOV     R2,(R1)+
                MOV     R3,(R1)+
                DEC     R4
                BNE     LP16
;
```

```
;
                RTS     PC                  ; TRANSFER TO FORTRAN
;
; DEFINITION OF VARIABLES
;
                .EVEN
        LEDSV1: .WORD   0
        LEDSV2: .WORD   0
        LEDSV3: .WORD   0
        CNTLED: .WORD   0
;
; COMMON BLOCK
;
                .CSECT  RHH                 ; NOTE THAT THE LABEL 'RHH'
                .EVEN                       ; MUST MATCH THE COMMON BLOCK
        IB:     .BLKW   8192.               ; LABEL
        IA:     .BLKW   4600.
        N:      .WORD   0
        N2:     .WORD   0
;
; END OF NAMED BLOCK
;
                .CSECT
        END:    .END    GDATA
```

C MAIN2 - Concatenation and Apodization

1. Purpose: This routine accesses the files generated under MAIN1 individually and forms a single concatenated file of length determined by the operator. The program then performs either a Gaussian or Boxcar apodization as defined by the operator. The output file (FTN2.DAT) is a single file containing multiple apodized interferograms ready for access by the FFT algorithm (MAIN3).

2. Operation: The operator is required to input the number of files and the individual file names as requested. If the number of files is positive the apodization will be Gaussian with FAC = 2.5 centered at point 2048. If the number of files is negative the apodization will be Boxcar (i.e. no apodization applied by the program). For further details see the program listing.

```
C
C
C                       MAIN2.FOR
C
C
C       THIS ROUTINE ACCEPTS INTERFEROGRAMS GENERATED FROM
C       MAIN1 AND PLACES  THEM INTO A LONG CONCATENATED FILE
C       READY FOR APODIZATION AND TRANSFORMATION AS A STRING OF
C       FILES. APODIZATION IS EITHER GAUSSIAN OR BOXCAR IN THIS
C       ROUTINE. THE OUTPUT DATA FILE (FTN2.DAT)IS READY TO BE
C       ACCESSED BY THE FFT (MAIN3.FOR) ROUTINE.
C
C
C       THIS ROUTINE WAS WRITTEN BY R.H.HALL IN 1978.
C
C
C       ROUTINES NECESSARY FOR LINKING ARE: SYSLIB,LPSLIB/F
C
C
        DIMENSION IX(4105),TITL(3),DAT(3),ABUFF(4105)
C
C       GENERATION OF A SCRATCH FILE OF LENGTH NFF
C
        CALL ASSIGN(1,'DK0:FTN1.DAT',0,'SCR','NC',1)
        WRITE(7,7)
7       FORMAT(' ','INPUT # OF FILES , GAUSS.>0,BXCR<0     I5')
        READ(5,11)NFF
11      FORMAT(I5)
        NF=IABS(NFF)
        DO 10 K=1,NF
27      WRITE(7,50)
50      FORMAT(' ','ENTER NAME FOR INPUT FROM DK',/)
        CALL ASSIGN(2,'DK0:DAT.DAT',-1,'OLD','NC',1)
        CALL LED(K,'I5')
        READ(2)NP
        READ(2)(DAT(I),I=1,3)
        READ(2)(TITL(I),I=1,3)
        READ(2)(IX(I),I=1,NP+6)
        ENDFILE 2
        CALL CLOSE(2)
        WRITE(1)(DAT(I),I=1,3)
        WRITE(1)(TITL(I),I=1,3)
        WRITE(1)(IX(I),I=1,NP)
10      CONTINUE
C
C       GENERATION OF THE OUTPUT FILE (FTN2.DAT) AND
C       APODIZATION OF THE INTERFEROGRAMS.
C
        CALL ASSIGN(2,'DK0:FTN2.DAT',0,'NEW','NC',1)
        WRITE(2)NF
        REWIND  1
        DO 21 K=1,NF
        CALL LED(K,'I5')
        READ(1)(DAT(I),I=1,3)
        READ(1)(TITL(I),I=1,3)
        READ(1)(IX(I),I=1,NP)
        IF(NFF.LT.0)GO TO 215
C
C       N.B. FAC=2.5 AND Z=2048. FOR GAUSSIAN APOD.
C
```

```
      Z=2048.
      FAC=2.5
      SUM=0.
      DO 60 I=1,NP
      DUM=ABS(FLOAT(I)-Z)/(FLOAT(NP)-Z)
      DUM1=EXP(-FAC*DUM**2)
      ABUFF(I)=FLOAT(IX(I))*DUM1
60    SUM=SUM+ABUFF(I)
      SUM=SUM/FLOAT(NP)
      DO 213  I=1,NP
213   ABUFF(I)=ABUFF(I)-SUM
      GO TO 217
215   CONTINUE
      DO 216  I=1,NP
216   ABUFF(I)=FLOAT(IX(I))
217   CONTINUE
      WRITE(2)(DAT(I),I=1,3)
      WRITE(2)(TITL(I),I=1,3)
      WRITE(2)(ABUFF(I),I=1,NP)
21    CONTINUE
      ENDFILE 1
      CALL CLOSE (1)
      ENDFILE 2
      CALL CLOSE (2)
      STOP
      END
```

D MAIN3 - The FFT Algorithm

1. Purpose: This program contains the FFT algorithm adapted from Horlick (29). Data in the amplitude-time domain is transformed into the amplitude frequency domain. This transforms the interferogram domain data into spectral domain data.

2. Operation: The program automatically accesses and transforms all of the files in FTN2.DAT outputing them as concatenated spectral files in PLOT.DAT. This allows for unattended operation once FTN2.DAT has been formed by MAIN2.

```
C
C
C                        MAIN3.FOR
C
C       THIS ROUTINE CONTAINS THE FFT ALGORITHM AS USED BY
C       HORLICK AND YUEN (PH.D. THESES), THE ROUTINE IS CURRENTLY
C       SET UP TO PERFORM A SEQUENCE OF FFTS WITH THE NUMBER
C       DETERMINED BY THE NUMBER OF FILES DEFINED IN MAIN2.FOR.
C       IT CURRENTLY PERFORMS A 4096 POINT FFT INCLUDING ONE LEVEL
C       OF ZERO FILLING. THE ROOT SUM OF SQUARES OF THE REAL
C       ('X' ARRAY) AND THE IMAGINARY ('Y' ARRAY) IS OUTPUT AS THE
C       AMPLITUDE SPECTRUM IN 'PLOT.DAT' READY FOR ACCESS BY 'MAIN4'.
C
C       THE FILES NECESSARY AT THE LINKING STAGE ARE!SYSLIB,LPSLIB/F
C
C
        DIMENSION X(4100),Y(4100),L(20),DAT(3),TITL(3)
        NP=4096
        REWIND 2
        READ(2)NIF
        CALL    ASSIGN(4,'DKO!PLOT.DAT',0,'NEW','NC',1)
        DO 187  JJK=1,NIF
        CALL LED((NIF-JJK),'I5')
        READ(2)(DAT(I),I=1,3)
        READ(2)(TITL(I),I=1,3)
        READ(2)(X(I),I=1,NP)
        NPT=NP/2
        N=NP
        DO 2 I=1,NPT
        X(I)=X(I*2-1)
2       Y(I)=X(I*2)
        DO 3 I=NPT+1,NP
        Y(I)=0.0
3       X(I)=0.0
        N2POW=12
        NTHPOW=2**N2POW
        N4POW=N2POW/2
        IF(N4POW)60,63,60
60      DO 61 IPASS=1,N4POW
        NXTLTH=2**(N2POW-2*IPASS)
        LENGTH=4*NXTLTH
        SCALE=6.2831853/FLOAT(LENGTH)
        DO 61 J=1,NXTLTH
        ARG=FLOAT(J-1)*SCALE
        C1=COS(ARG)
        S1=SIN(ARG)
        C2=C1*C1-S1*S1
        S2=C1*S1+C1*S1
        C3=C1*C2-S1*S2
        S3=C2*S1+S2*C1
        DO 61 ISQLOC=LENGTH,NTHPOW,LENGTH
        J1=ISQLOC-LENGTH+J
        J2=J1+NXTLTH
        J3=J2+NXTLTH
        J4=J3+NXTLTH
        R1=X(J1)+X(J3)
        R2=X(J1)-X(J3)
        R3=X(J2)+X(J4)
        R4=X(J2)-X(J4)
        FI1=Y(J1)+Y(J3)
```

```
C
C
      FI2=Y(J1)-Y(J3)
      FI3=Y(J2)+Y(J4)
      FI4=Y(J2)-Y(J4)
      X(J1)=R1+R3
      Y(J1)=FI1+FI3
      IF(J-1)64,62,64
64    X(J3)=C1*(R2+FI4)+S1*(FI2-R4)
      Y(J3)=-S1*(R2+FI4)+C1*(FI2-R4)
      X(J2)=C2*(R1-R3)+S2*(FI1-FI3)
      Y(J2)=-S2*(R1-R3)+C2*(FI1-FI3)
      X(J4)=C3*(R2-FI4)+S3*(R4+FI2)
      Y(J4)=-S3*(R2-FI4)+C3*(R4+FI2)
      GO TO 61
62    X(J3)=R2+FI4
      Y(J3)=FI2-R4
      X(J2)=R1-R3
      Y(J2)=FI1-FI3
      X(J4)=R2-FI4
      Y(J4)=R4+FI2
61    CONTINUE
63    IF(N2POW-2*N4POW)65,66,65
65    DO 67 J=1,NTHPOW,2
      R1=X(J)+X(J+1)
      R2=X(J)-X(J+1)
      FI1=Y(J)+Y(J+1)
      FI2=Y(J)-Y(J+1)
      X(J)=R1
      Y(J)=FI1
      X(J+1)=R2
67    Y(J+1)=FI2
66    DO 68 J=1,13
      L(J)=1
      IF(J-N2POW)69,69,68
69    L(J)=2**(N2POW+1-J)
68    CONTINUE
      IJ=1
      L1=L(13)
      NTHPOW=L(12)
      ISQLOC=L(11)
      J=L(10)
      N2P1=L(9)
      N2=L(8)
      NP2MJ=L(7)
      L8=L(6)
      N2POW=L(5)
      N4POW=L(4)
      LENGTH=L(3)
      NXTLTH=L(2)
      IPASS=L(1)
      DO 601 J1=1,L1
      DO 601 J2=J1,NTHPOW,L1
      DO 601 J3=J2,ISQLOC,NTHPOW
      DO 601 J4=J3,J,ISQLOC
      DO 601 J5=J4,N2P1,J
      DO 601 J6=J5,N2,N2P1
      DO 601 J7=J6,NP2MJ,N2
      DO 601 J8=J7,L8,NP2MJ
      DO 601 J9=J8,N2POW,L8
```

```
C
C
      DO 601 J10=J9,N4POW,N2POW
      DO 601 J11=J10,LENGTH,N4POW
      DO 601 J12=J11,NXTLTH,LENGTH
      DO 601 JI=J12,IPASS,NXTLTH
      IF(IJ-JI)610,610,601
610   R=X(IJ)
      X(IJ)=X(JI)
      X(JI)=R
      FI=Y(IJ)
      Y(IJ)=Y(JI)
      Y(JI)=FI
601   IJ=IJ+1
      ARG=3.1415927/FLOAT(N)
      C1=COS(ARG)
      S1=-SIN(ARG)
      C1JX=1.
      S1JX=0.
      N2=N/2
      N2P1=N2+1
      DO 70 J=2,N2P1
      NP2MJ=N+2-J
      SORR1=X(J)+X(NP2MJ)
      SORI1=Y(J)-Y(NP2MJ)
      R=C1JX
      C1JX=C1JX*C1-S1JX*S1
      S1JX=R*S1+S1JX*C1
      SORR2=X(J)-X(NP2MJ)
      SORI2=Y(J)+Y(NP2MJ)
      SORR3=C1JX*SORR2-S1JX*SORI2
      SORI3=C1JX*SORI2+S1JX*SORR2
      Y(J)=0.5*(SORI1-SORR3)
      X(J)=0.5*(SORR1+SORI3)
      IF(J-N2P1)71,70,71
71    Y(NP2MJ)=0.5*(-SORI1-SORR3)
      X(NP2MJ)=0.5*(SORR1-SORI3)
70    CONTINUE
      X(1)=X(1)+Y(1)
      Y(1)=0.
      DO 311  I=1,NP
      X(I)=SQRT(X(I)*X(I)+Y(I)*Y(I))
311   CONTINUE
      WRITE(4)(DAT(I),I=1,3)
      WRITE(4)(TITL(I),I=1,3)
      WRITE(4)(X(I),I=1,NP)
187   CONTINUE
      ENDFILE  4
      CALL CLOSE(4)
      STOP
      END
```

E MAIN4 - Spectral Analysis

1. Purpose: This program provides the statistical analysis and spectral averaging of the spectra contained in PLOT.DAT.

2. Operation: The operator is required to input the spectral range (from 15802.8 cm^{-1} to 23704.2 cm^{-1}), the number of spectra to be averaged, and a threshold value to be used in the peak search section. The output consists of statistical information for any peaks greater in amplitude than the threshold over the spectral range defined. There is also the option of a spectral listing of all points over the range defined. The output file (SPAVE.DAT) contains the average spectrum over the complete spectral range irregardless of the defined spectral range. A peak is defined as a maximum surrounded by three decreasing amplitude points (i.e. a seven point peak). See the listing for further details.

```
C                        MAIN4.FOR
C
C
C       THIS ROUTINE ACCEPTS DATA FILES OUTPUT FROM MAIN3 (PLOT.DAT)
C       AND ALLOWS SIGNAL AVERAGING IN THE SPECTRAL DOMAIN. THE ROUTINE
C       ALSO HAS A PEAK LOCATE AND A THRESHOLD VALUE CAPABILITY.
C       STATISTICS SUCH AS THE STANDARD DEVIATION AND THE MEAN AMPLITUDE
C       OF A PEAK VALUE OVER A SELECTED NUMBER OF SPECTRA ARE ALSO
C       AVAILABLE.THE SPECTRAL WINDOW OVER WHICH THESE STATISTICS ARE
C       AVAILABLE IS OPERATOR DEFINED. NOTE THAT THIS PROGRAM MUST BE
C       EXECUTED BEFORE 'MAIN5' CAN BE EXECUTED. THIS ROUTINE IS RESTRICTED
C       IN OPERATION TO THE SPECTRAL RANGE 15802.8 TO 23704.2 CM-1 BUT
C       PROVIDES A PRINTOUT OF THE POSSIBLE ALIASED WAVELENGTHS FOR
C       EACH PEAK FOUND. ALSO NOTE THAT THE FILES ARE SEQUENTIALLY
C       ACCESSED IN 'PLOT.DAT'.
C
C       THIS ROUTINE WAS WRITTEN BY R.H.HALL IN 1978.
C
C       THIS ROUTINE REQUIRES ONLY SYSLIB/F AT THE LINKING STAGE.
C
        DIMENSION X(4096),Y(4096),TITLE(36),DATE(36),A(7),SSQ(525),IP(75)
        CALL ASSIGN(4,'DK0:PLOT.DAT',0,'OLD','NC',1)
        DATA SSQ/525*0./
        DATA Y/4096*0.0/
        DATA DATE/36*0./
        DATA TITLE/36*0./
        AK=4095./7901.4
C
C       DEFINE: THE SPECTRAL RANGE 15802.8 TO 23704.2 CM-1
C               THE NUMBER OF SPECTRA TO BE AVERAGED
C               THE PEAK THRESHOLD VALUE
C
        WRITE(7,1)
1       FORMAT(' ','ENTER WAVE # LIMITS ,#SPECTRA,THRESHOLD VALUE 4F8.1')
        READ(5,2)AN1,AN2,ANS,THRES
2       FORMAT(4F8.1)
        N3=ANS
        N1=(-8189.+AN1*AK)
        N2=(-8189.+AN2*AK)
        IFF=0
        DO 200 IJ=1,N3
        IJK=3*(IJ-1)
        READ(4)(DATE(I+IJK),I=1,3)
        READ(4)(TITLE(I+IJK),I=1,3)
        READ(4)(X(I),I=1,4096)
        WRITE(7,33)(TITLE(I+IJK),I=1,3),(DATE(I+IJK),I=1,3),THRES
33      FORMAT(' ',/,'  SAMPLE: ',3A4,2X, ' DATE: ',3A4,2X,'THRESHOLD = '
     1  ,F12.3)
        IF(THRES.EQ.0.)GO TO 729
C
C       DETERMINE THE PRESENCE OF ANY 7 PT PEAKS WITHIN THE
C       SPECTRAL RANGE CHOSEN AND PRINT OUT THE INDIVIDUAL VALUES
C       FROM EACH SPECTRUM AS WELL AS KEEP TRACK OF THE STATISTICS
C       FOR THE PEAK OVER THE DEFINED NUMBER OF SPECTRA.
C       THE STATS ARE PRINTED OUT AT THE END OF THE INDIVIDUAL VALUES.
C       NOTE THAT ONLY THOSE PEAKS DEFINED IN THE FIRST SPECTRUM WILL
C       BE KEPT TRACK OF FOR STATS. ANY OTHER PEAKS FOUND IN LATER
C       SPECTRA WILL HAVE INDIVIDUAL VALUES PRINTED BUT NO STATS.
C       NOTE THAT A THRESHOLD OF ZERO MAY BE USED IF NO STATS ARE
C       REQUIRED.
```

```
C
      DO 108 I=N1,N2
      IF(THRES.EQ.0)GO TO 112
      IF(X(I).LT.THRES) GO TO 112
      IF(X(I).LT.X(I+1).OR.X(I).LT.X(I-1)) GO TO 112
      IF(X(I).LT.X(I+2).OR.X(I).LT.X(I-2)) GO TO 112
      IF(X(I).LT.X(I+3).OR.X(I).LT.X(I-3)) GO TO 112
      IF(IJ.EQ.1)IP(IFF+1)=I
      IF(IJ.EQ.1)IFF=IFF+1
      A(1)=FLOAT(I+8189)/AK
      YX=23704.2-A(1)
      A(2)=1.E08/A(1)
      A(3)=1.E08/(23704.2+YX)
      A(4)=1.E08/(39507.-YX)
      A(5)=1.E08/(39507.+YX)
      WRITE(7,705)X(I),A(1),(A(IN),IN=2,5)
705   FORMAT(' ','MAXIMUM AMPL:',F12.4,'  AT WAVE #: ',F12.4,
     1 '     ANGSTROMS: ',4F12.2)
112   CONTINUE
108   CONTINUE
      DO 712 KL=1,IFF
      K=IP(KL)
      DO 713 IL=1,7
713   SSQ((KL-1)*7+IL)=SSQ((KL-1)*7+IL)+X(K+IL-4)*X(K+IL-4)
712   CONTINUE
729   CONTINUE
      DO 711  I=1,4096
711   Y(I)=Y(I)+X(I)
200   CONTINUE
      DO 201 I=1,4096
      X(I)=Y(I)/ANS
201   Y(I)=X(I)
      ENDFILE 4
      CALL CLOSE(4)
      IF(THRES.EQ.0) GO TO 99
      IF(ANS.EQ.1.)GO TO 99
      DO 109 J=1,IFF
      K=IP(J)
      KJ=(J-1)*7
      DO 110 IK=1,7
      D=SSQ(KJ+IK)-X(K+IK-4)*X(K+IK-4)*ANS
      SSQ(KJ+IK)=SQRT(D/(ANS-1.))
110   A(IK)=FLOAT(8185+K+IK)/AK
      WRITE(7,111) A,(X(K+IK-4),IK=1,7),(SSQ(KJ+IK),IK=1,7)
111   FORMAT(' ',//,'WAVE #   :',7(F12.3,3X),/' MEAN AMP:',7(F12.3,3X),
     1 /,' STD DEV :',7(F12.3,3X))
      WRITE(7,113)((SSQ(KJ+IK)/X(K+IK-4)*100.),IK=1,7),(X(K+IK-4)/
     2 SSQ(KJ+IK),IK=1,7)
113   FORMAT(' ','%REL S D:',7(F12.3,3X),/,' S.N.R.   :',7(F12.3,3X)//)
109   CONTINUE
C
C     THIS SECTION PROVIDES A PRINTOUT OF THE MEAN AMPLITUDE VALUE
C     OVER THE DEFINED SPECTRAL RANGE. ALL POINTS ,NOT ONLY PEAKS,ARE
C     INCLUDED.
C
99    WRITE(7,4)
4     FORMAT(' ','PRINT Y=1,N=0    I2')
      READ(5,5)NN3
5     FORMAT(I2)
      IF(NN3.EQ.0)GO TO 60
```

```
C
C
        WRITE(7,206)
206     FORMAT(' ',' WAVE #            MEAN AMPL.          WAVE #        MEAN
     1 AMPL.        WAVE #            MEAN AMPL.')
        DO 204  I=N1,N2,3
        DO 720  J=1,3
        A(2*J-1)=FLOAT(8189+I+J)/AK
720     A(2*J)=Y(I-1+J)
        WRITE(7,205)(A(IK),IK=1,6)
205     FORMAT(' ',6(F12.3,3X))
204     CONTINUE
60      CONTINUE
C
C       THE OUTPUT DATA FILE IS SPAVE.DAT AND MAY BE ACCESSED BY MAIN5
C       NOTE THE ALL POINTS IN THE SPECTRUM HAVE BEEN AVERAGED NO MATTER
C       WHAT THE DEFINED SPECTRAL RANGE HAS BEEN.
C
        CALL ASSIGN(3,'DK0:SPAVE.DAT',0,'NEW','NC',1)
        WRITE(3)(DATE(I),I=1,24)
        WRITE(3)(TITLE(I),I=1,24)
        WRITE(3)(X(I),I=1,4096)
        ENDFILE 3
        CALL CLOSE(3)
        STOP
        END
```

F MAIN5 - Graphics and Plotting Routine for Averaged Spectra

1. Purpose: This routine provides graphics and incremental plotter output facilities for the averaged spectra produced by MAIN4 in file SPAVE.DAT.

2. Operation: This routine requires a filename input to access a file of the form of SPAVE.DAT. The operator must then enter a spectral window to be plotted and the number of spectra used to obtain the average spectrum. The program then outputs the title and date information of each component spectrum. If a greater than 2000 cm^{-1} window is defined, only the first 2000 cm^{-1} will be displayed on the graphics screen, but the complete range will be output to the plotter. For further details see the program listing.

```
C
C
C                              MAINS.FOR
C
C
C       THIS ROUTINE PROVIDES THE VT11 GRAPHICS  AND
C       INCREMENTAL PLOTTER DISPLAY OF THE SPECTRUM CONTAINED IN
C       SPAVE.DAT OR A USER DEFINED FILE OF THE SAME FORMAT.
C       NOTE THAT ONLY A 2000 CM-1 REGION MAY BE DISPLAYED ON
C       THE GRAPHICS SCREEN. IF THE DEFINED WAVENUMBER RANGE
C       EXCEEDS THIS VALUE ONLY THE FIRST 2000 CM-1 WILL BE SHOWN
C       BUT THE COMPLETE SPECTRAL RANGE MAY BE PLOTTED ON THE
C       INCREMENTAL PLOTTER. NOTE THAT THE PLOTTER DOES NOT HANDLE
C       NEGATIVE INCREMENTS ON THE AXIS.THE SPECTRAL REGIONS THAT MAY
C       BE USED WITH THIS PROGRAM ARE: -15802.8 -- -7901.4
C                                      15802.8 -- 23704.2
C                                      -31605.6 -- -23704.2
C                                      31605.6--39507.0
C
C
C       THIS ROUTINE WAS WRITTEN BY R.H.HALL IN 1978.
C
C
C       THE FOLLOWING ROUTINES ARE NECESSARY AT THE LINKING STAGE
C       ARE:    SYSLIB,VTLIB,LPSLIB,XYLIB/F
C
C       NOTE, DUE TO SPACE LINITATIONS DO NOT USE THE /U OPTION
C       AT THE COMPILER STAGE
C
C
        DIMENSION X(4097),Y(1027),IX(1050),TITLE(24),DATE(24)
        DATA TITLE/24*0./
        DATA DATE/24*0.0/
10      CONTINUE
        WRITE(7,17)
17      FORMAT(' ',' INPUT FILE NAME FOR PLOTTING',/)
        CALL ASSIGN(11,'DK0:SPAVE.DAT',-1,'OLD','NC',1)
        READ(11)(DATE(I),I=1,24)
        READ(11)(TITLE(I),I=1,24)
        READ(11)(X(I),I=1,4096)
        ENDFILE 11
        CALL CLOSE(11)
        WRITE(7,1)
1       FORMAT(' ','ENTER WAVE# LIMITS , #SPECTRA  3F10.1')
        READ(5,2)AN1,AN2,ANS
2       FORMAT(3F10.1)
        NS=INT(ANS)
        AK=4095./7901.4
        ANUM=8189.
        IF(AN1.LT.0.)ANUM=16381.
        IF(ABS(AN1).LT.15802.8)ANUM=8191.
        IF(AN1.GE.31605.6)ANUM=16379.
        N1=ABS(-ANUM+ABS(AN1)*AK)
        N2=ABS(-ANUM+ABS(AN2)*AK)
        IF(N1.EQ.0)N1=1
        N11=N1
        IF(AN1.LT.0)N11=-N1
        AN12=(FLOAT(N11)+ANUM)/AK
        IF(AN1.LT.0)AN12=-AN12
        AN13=FLOAT(INT(AN12/10.))*10.
```

```
        DO 100  I=1,NS
        II=3*(I-1)
        WRITE(7,33)(TITLE(II+IK),IK=1,3),(DATE(II+IK),IK=1,3)
33      FORMAT(' ',' SAMPLE: ',3A4,2X, ' DATE: ',3A4)
100     CONTINUE
        AMAX=-1.E+20
        AMIN=1.E+20
        DO 3 I=N1,N2
        IF(AMAX.LT.X(I))AMAX=X(I)
        IF(AMAX.LE.X(I))IMAX=I
3       IF(AMIN.GT.X(I))AMIN=X(I)
        N3=N2-N1
        N4=N3
        IF(N3.GT.1024) N3=1024
        IF(N3.LT.20)N3=20
        DO 38 I=N1,N1+N3
38      Y(I-N1+1)=X(I)
C
C       GRAPHICS DISPLAY SECTION
C
        CALL INIT(IX,1050)
        CALL APNT(1.0,1.0,-1,5,-1,1)
        CALL SCAL(1.,AMIN,1024.,AMAX)
        CALL YGRA(1024.0/FLOAT(N3),Y,N3)
        FLAG=0
        BMAX=(ANUM+FLOAT(IMAX))/AK
        WRITE(7,117)AMAX,BMAX
117     FORMAT(' ','MAXIMUM AMPLITUDE =',F12.3,'   AT ',F10.1,' WAVE #')
6       WRITE(7,4)
4       FORMAT(' ','RETURN=1,PLOT=2,EXIT=3')
        READ(5,5)N3
5       FORMAT(I2)
        IF(N3.LT.1.OR.N3.GT.3) GO TO 6
        IF(FLAG.EQ.1)GO TO 21
        CALL INIT
        CALL FREE
        FLAG=1
21      CONTINUE
        GO TO (10,11,13),N3
        GO TO 6
C
C       INCREMENTAL PLOTTER DISPLAY SECTION
C       NOTE THE COMPLETE SPECTAL RANGE MAY BE DISPLAYED
C
11      WRITE(7,103)
103     FORMAT(' ',' INPUT PLT HT, WAVE#S PER INCH, AMAX 3F8.1')
        READ(5,104)PLTHT,AN6,AMAX
104     FORMAT(3F8.2)
        WRITE(7,105)
105     FORMAT(' ','INPUT TITLE FOR PLOT   24A4')
        READ(5,106)TITLE
106     FORMAT(24A4)
        N3=1024
        IF(N4.LT.1024)N3=N4
        FL=1
        XS=0.
        XSS=0.
        XNS=X(1025)
        XNSS=X(1026)
        XNSSS=X(1027)
```

```
99      CONTINUE
        DO 12 I=N1,N1+N3
        IF(FL.NE.2)GO TO 27
        X(1027)=XNSSS
        X(1025)=XNS
        X(1026)=XNSS
27      Y(I-N1+1)=(X(I)-AMIN)/(AMAX-AMIN)*PLTHT
12      X(I-N1+1)=FLOAT(I-N1)/AK/AN6
        AN4=ABS((AN1-AN2)/AN6)
        X(N3+2)=(AN12-AN13)/AN6
        X(N3+3)=1.
        Y(N3+2)=0.
        Y(N3+3)=1.0
        IF(FL.GT.1)GO TO 118
        AX=AMAX/PLTHT
        CALL PLOTST(0.005,'IN')
118     CALL PLOT(XS,0.,-3)
        CALL LINE(X,Y,(N3+1),1,0,0)
        XS=X(N3+1)
        N3=N4-1024*FL
        IF(N3.LT.0)GO TO 98
        IF(N3.GT.1024)N3=1024
        FL=FL+1
        N1=N1+1024
        XSS=XSS+XS
        GO TO 99
98      CONTINUE
        CALL PLOT(-XSS,0.0,-3)
        CALL AXIS(0.0,0.0,10HWAVENUMBER,-10,AN4,0.0,AN13,AN6)
        CALL PLOT(0.0,0.0,+3)
        CALL AXIS(0.0,0.0,9HAMPLITUDE,9,PLTHT,90.,0.0,AX)
        CALL SYMBOL((AN4/4),(PLTHT+0.5),0.14,TITLE,0.0,40)
        IF(AN4.LE.8.)AN4=8.5
        IF(AN4.GT.8.5.AND.AN4.LE.16.)AN4=17.
        IF(AN4.GT.17..AND.AN4.LE.24.)AN4=25.5
        CALL PLOT((AN4),0.0,-3)
        GO TO 6
13      CALL PLOTND
        STOP
        END
```

G INPLT - Interferogram Plot

1. Purpose: This routine provides for the plotting and display of the apodized interferogram contained in FTN2.DAT as output by MAIN2.

2. Operation: The complete or partial interferogram scaled between the minimum and maximum amplitude present may be displayed on the graphics screen or plotted on the incremental plotter. Note that only the first 1024 points may be displayed graphically but the complete interferogram may be output to the incremental plotter. The user is required to input N1 and N2 referring to the first and last point of the interferogram range to be plotted. See the program listing for further details.

```
C
C
C                         INPLT.FOR
C
C
C       THIS ROUTINE PROVIDES CAPABILITY FOR INTERFEROGRAM PLOTTING
C       BOTH ON THE GRAPHICS SCREEN AND ON THE INCREMENTAL PLOTTER.
C       THE GRAPHICS SCREEN SHOWS ONLY A 1000 PT REGION WHILE THE
C       PLOTTER CAN PLOT THE COMPLETE INTERFEROGRAM. DATA FILES ARE
C       ACCESSED AS FTN2.DAT BY DEFAULT AS THE OUTPUT OF 'MAIN2',
C       THEREFORE THE INTERFEROGRAM MAY BE APODIZED OR UNAPODIZED
C       WHEN PLOTTED. THE USER MUST DEFINE THE POINT RANGE OVER
C       WHICH THE INTERFEROGRAM IS TO BE PLOTTED.
C
C       THIS ROUTINE WAS WRITTEN IN 1976 AND MODIFIED IN 1978
C       BY R.H.HALL.
C
C       ROUTINES  REQUIRED AT THE LINKING STAGE: SYSLIB,XYLIB/F
C
C
        DIMENSION X(4097),Y(1027),IX(1050),TITLE(3),DATE(3)
10      CONTINUE
        NP=4096
        CALL ASSIGN(11,'DK0:FTN2.DAT',0,'OLD','NC',1)
        READ(11)I
        READ(11)(DATE(I),I=1,3)
        READ(11)(TITLE(I),I=1,3)
        READ(11)(X(I),I=1,NP)
        ENDFILE 11
        CALL CLOSE(11)
        WRITE(7,1)
1       FORMAT(' ','ENTER N1,N2,2F8.1')
        READ(5,2)AN1,AN2
2       FORMAT(2F8.1)
        N1=AN1
        N2=AN2
        AMAX=-1.E+20
        AMIN=1.E+20
        DO 3 I=N1,N2
        IF(AMAX.LT.X(I))AMAX=X(I)
        IF(AMAX.LE.X(I))IMAX=I
3       IF(AMIN.GT.X(I))AMIN=X(I)
        N3=N2-N1
        N4=N3
        IF(N3.GT.1024) N3=1024
        IF(N3.LT.20)N3=20
        DO 38 I=N1,N1+N3
38      Y(I-N1+1)=X(I)
C
C       VT11 GRAPHICS DISPLAY SECTION
C
        CALL INIT(IX,1050)
        CALL APNT(1.0,1.0,-1,5,-1,1)
        CALL SCAL(1.,AMIN,1024.,AMAX)
        CALL YGRA(1024.0/FLOAT(N3),Y,N3)
        FLAG=0
        WRITE(7,120)TITLE,DATE
120     FORMAT(' ',' SAMPLE: ',3A4,' DATE: ',3A4)
        WRITE(7,117)AMAX,IMAX
117     FORMAT(' ','MAXIMUM AMPLITUDE =',F12.3,'    AT POINT # ',I4)
```

```
C
C
6       WRITE(7,4)
4       FORMAT(' ','RETURN=1,PLOT=2,EXIT=3')
        READ(5,5)N3
5       FORMAT(I2)
        IF(N3.LT.1.OR.N3.GT.3) GO TO 6
        IF(FLAG.EQ.1)GO TO 21
        CALL INIT
        CALL FREE
        FLAG=1
21      CONTINUE
        GO TO (10,11,13),N3
        GO TO 6
C
C       INCREMENTAL PLOTTER DISPLAY SECTION
C
11      WRITE(7,67)
67      FORMAT(' ','INPUT POINTS PER INCH   F8.1')
        READ(5,45)AN6
45      FORMAT(F8.1)
        N3=1024
        IF(N4.LT.1024)N3=N4
        FL=1
        XS=0.
        XSS=0.
        XNS=X(1025)
        XNSS=X(1026)
        XNSSS=X(1027)
99      CONTINUE
        DO 12 I=N1,N1+N3
        IF(FL.NE.2)GO TO 27
        X(1027)=XNSSS
        X(1025)=XNS
        X(1026)=XNSS
27      Y(I-N1+1)=(X(I)-AMIN)/(AMAX-AMIN)*8.
12      X(I-N1+1)=FLOAT(I-N1)/AN6
        AN4=ABS((AN1-AN2)/AN6)
        X(N3+2)=0.
        X(N3+3)=1.
        Y(N3+2)=0.
        Y(N3+3)=1.0
        IF(FL.GT.1)GO TO 118
        AX=(AMAX-AMIN)/8.
        CALL PLOTST(0.005,'IN')
118     CALL PLOT(XS,0.,-3)
        CALL LINE(X,Y,(N3+1),1,0,0)
        XS=X(N3+1)
        N3=N4-1024*FL
        IF(N3.LT.0)GO TO 98
        IF(N3.GT.1024)N3=1024
        FL=FL+1
        N1=N1+1024
        XSS=XSS+XS
        GO TO 99
98      CONTINUE
        CALL PLOT(-XSS,0.0,-3)
        CALL AXIS(0.0,0.0,10HPOINT NUM.,-10,AN4,0.0,AN1,AN6)
        CALL PLOT(0.0,0.0,+3)
        CALL AXIS(0.0,0.0,9HAMPLITUDE,9,8.0,90.,AMIN,AX)
```

```
C
C
      CALL SYMBOL((AN4/4),9.,0.14,DATE,0.0,12)
      CALL SYMBOL((AN4/4),8.5,0.14,TITLE,0.0,12)
      IF(AN4.LE.8.)AN4=8.5
      IF(AN4.GT.8.5.AND.AN4.LE.16.)AN4=17.
      IF(AN4.GT.17..AND.AN4.LE.24.)AN4=25.5
      CALL PLOT((AN4),0.0,-3)
      CALL PLOTND
      GO TO 6
13    STOP
      END
```

H INCOR - Interferogram Correlation

1. Purpose: This routine performs the correlation operation between a user defined mask interferogram and a series of user defined sample interferograms.

2. Operation: This routine requires the following inputs: 1) The number of sample files, 2) the mask and sample Gaussian apodization factors (MFAC and SFAC, normally 2.5), and 3) the number of Δt shift values for each correlation (normally 3 shifts are adequate to define the correlation maximum). The user is also required to input the mask and sample data file names. The printout consists of the correlation maximum for each data file over the Δt range defined. See the program listing for further details.

```
C                         INCOR.FOR
C
C        THIS PROGRAM PERFORMS THE CORRELATION OPERATION BETWEEN THE MASK
C        AND SAMPLE INTERFEROGRAMS. THE NUMBER OF POINTS SHIFTED FROM THE
C        0 T  POSITION MAY BE DEFINED AT THE INPUT. I.E. #SHIFTS = 3
C        MEANS THAT A CORRELATION WILL BE PERFORMED 7 TIMES FROM T=-3 TO
C        T=3. THE APODIZATION FUNCTION MAY ALSO BE SEPARATELY DEFINED FOR
C        THE MASK AND THE SAMPLE,MFAC AND SFAC RESPECTIVELY. THE
C        APODIZATION IS GAUSSIAN AND UNDER NORMAL CONDITIONS MFAC=SFAC=2.5.
C        THE CORRELATION DATA IS PRINTED OUT AT THE END OF EACH SEQUENCE
C        OF CORRELATIONS. NO DATA IS STORED ON DISK. THE ROUTINE IS
C        SET UP TO ACCESS THE OUTPUT FILES OF MAIN1.SAV BY NAMEAS DEFINED
C        AT EXECUTION TIME.
C
C        THIS PROGRAM WAS WRITTEN BY R.H.HALL IN 1978
C
C        LPSLIB.OBJAND SYSLIB.OBJ ARE REQUIRED AT THE LINKING STAGE.
C
C

         DIMENSION M(4108),IS(4108),CM(15),DAT(3),DUM1(4096),CMM(250),DM(3)
         DATA     CM/15*0.0/
         DATA CMM/250*0./
         WRITE(7,10)
10       FORMAT(' ','INPUT # SAMPLE INTEFEROGRAMS,MFAC,SFAC,#SHIFTS,4F5.1')
         READ(5,11)ANS,FAC,FAC2,SP
11       FORMAT(4F5.1)
         WRITE(7,1)
1        FORMAT(' ','ENTER MASK FILE',/)
         CALL ASSIGN(2,'DK0:DAT.DAT',-1,'OLD','NC',1)
         READ(2)NP
         READ(2)(DAT(I),I=1,3)
         READ(2)(DM(I),I=1,3)
         READ(2)(M(I),I=1,NP)
         ENDFILE 2
         CALL CLOSE(2)
         Z=2048.
         ISP=INT(SP)
         DO 299 I=1,NP
299      M(NP+ISP-I+1)=M(NP+1-I)
         DO 300 I=1,NP
         DUM=ABS(FLOAT(I)-Z)/(FLOAT(NP)-Z)
         DUM2=EXP(-FAC*DUM**2)
         DUM1(I)=EXP(-FAC2*DUM**2)
300      M(I+ISP)=INT(FLOAT(M(I+ISP))*DUM2)
         DO 30 I=1,ISP
         M(I)=M(NP+I)
30       M(NP+ISP+I)=M(ISP+I)
         NSS=INT(ANS)
         JK=1
         DO 4 J=1,NSS
         CALL LED(J,'I4')
         WRITE(7,2)
2        FORMAT(' ','ENTER SAMPLE FILE',/)
         CALL ASSIGN(2,'DK0:DAT.DAT',-1,'OLD','NC',1)
         READ(2)NP
         READ(2)(DAT(I),I=1,3)
         READ(2)(DAT(I),I=1,3)
         READ(2)(IS(I),I=1,NP+6)
         ENDFILE 2
```

```
C
C
      CALL CLOSE(2)
      DO 3 I=ISP+1,NP+ISP
      ABC=FLOAT(IS(I-ISP))*DUM1(I-ISP)
      DO 26 JJ=1,2*ISP+1
26    CM(JJ)=ABC*FLOAT(M(I+JJ-(ISP+1)))+CM(JJ)
3     CONTINUE
      CMM(JK+3)=-100000.
      DO 27 IK=1,3
27    CMM(JK+IK-1)=DAT(IK)
      DO 25 JJ=1,2*ISP+1
      IF(CMM(JK+3).LT.CM(JJ))CMM(JK+3)=CM(JJ)
      IF(CMM(JK+3).EQ.CM(JJ))CMM(JK+4)=ISP+1-JJ
25    CM(JJ)=0.
4     JK=JK+5
      PAUSE 'TYPE CR FOR PRINTOUT OF DATA'
      WRITE(7,23)(DM(I),I=1,3)
23    FORMAT(' ',' MASK FILE: ',3A4,/,'  CORRELATION MAX. T= 0')
      DO 80 I=1,5*NSS,5
      WRITE(7,22)(CMM(I+J-1),J=1,3),CMM(I+3),CMM(I+4)
22    FORMAT(' ',' SAMPLE: ',3A4,2X,' CORR. MAX.:',F14.2,2X,' AT T= '
     1 ,F8.2)
80    CONTINUE
      STOP
      END
```

I LFIT - Regression Analysis Program

1. Purpose: This routine performs a linear least squares regression analysis on data points entered by the operator at the terminal.

2. Operation: The user may enter up to 32 repetitions each of 45 abscissa values. The number of repetitions at each abscissa value is also variable. To exit from the data entry routine, enter a -1 for the number of repititions. The user has the option of a log-log or linear plot and may change but not add or delete data points before the statistical analysis section. The regression curve is shown on the graphics screen and may also be plotted on the incremental plotter in various formats. For complete details of the information printed out and the plotting options, please see the program listing.

```
C
C
C                        LFIT.FOR
C
C
C       THIS ROUTINE PERFORMS A LINEAR LEAST SQUARES REGRESSION
C       ANALYSIS UPON THE DATA ENTERED AT THE TERMINAL. THE
C       REGRESSION STATISTICS ARE PRINTED OUT AND THE REGRESSION
C       CURVE IS DISPLAYED ON THE GRAPHICS SCREEN. AN OPTION EXISTS
C       FOR OUTPUT TO THE INCREMENTAL PLOTTER OR TO RETURN TO THE
C       ORIGINAL DATA. THE PLOT MAY BE LINEAR OR LOG IN FORMAT AND
C       THE DATA POINTS MAY BE CHANGED BUT NOT DELETED OR ADDED TO
C       IN NUMBER. A MAXIMUM OF 45 ABSCISSA POINTS WITH 32 REPEATS
C       EACH ARE AVAILABLE. NOTE ALSO THE CAPABILITY FOR CURVE
C       EXTRAPOLATION AND THE PLOTTING OF ONLY THE POINTS AND NOT
C       THE LINE. FOR FURTHER DETAILS REFER TO THE LISTING.
C
C       THIS ROUTINE WAS WRITTEN IN 1978 BY R.H.HALL.
C
C       THE ROUTINES NECESSARY AT THE LINKING STAGE ARE: SYSLIB
C                                                        LPSLIB
C                                                        XYLIB
C                                                        VTLIB/F
C
C
        DIMENSION X(45),Y(45,32),YP(45),XAXIS(6),YAXIS(6),IX(1000)
        DIMENSION YAVE(45),YSS(45),NR(45),YPE(45),STAT(11),TITP(6)
        DIMENSION XGT(350),YGT(350),XS(45),YS(45,32)
        DATA STAT/12.706,4.303,3.182,2.776,2.571,2.447,2.365,2.306
     1  ,2.262,2.228,1.960/
1       WRITE (5,500)
500     FORMAT (' ','LINEAR LEAST SQUARES FIT TO Y=AX + B ')
        WRITE (5,502)
502     FORMAT (' ','TO TERMINATE DATA INPUT ENTER NRPTS<0',//)
504     FORMAT (I2)
C
C       DATA ENTRY LOOPS
C
        DO 130 JJ=1,45
        WRITE(7,117)
117     FORMAT(' ','  INPUT #REPTS PER X VALUE ')
        READ(5,504)NRPTS
        IF(NRPTS.LT.0)GO TO 131
        N=JJ
        NR(JJ)=NRPTS
        WRITE(7,149)
149     FORMAT(' ',' INPUT X VALUE ')
        READ(5,121)XS(JJ)
        DO 120 IJ=1,NRPTS
        CALL LED(IJ,'I4')
        WRITE(7,159)
159     FORMAT(' ',' INPUT Y VALUE')
        READ(5,121)YS(JJ,IJ)
121     FORMAT(F14.3)
120     CONTINUE
130     CONTINUE
C
C       END OF DATA ENTRY
C       START OF STATISTICAL ANALYSIS
C
```

```
C
131     WRITE(7,505)
505     FORMAT(' ','LOG-LOG PLOT? Y=1,N=0')
        READ(5,504)JG
        DO 139 I=1,N
        YAVE(I)=0.
        YSS(I)=0.
139     YPE(I)=0.
        YTOT=0.
        NTOT=0
        SYS=0.0
        YT=0.0
        E=0.
        F=0.
        C=0.
        YSD=0.
        NT1=0
        DO 140 I=1,N
        KK=NR(I)
        X(I)=XS(I)
        IF(JG.EQ.1)X(I)=ALOG10(X(I))
        DO 129  J=1,KK
        Y(I,J)=YS(I,J)
        IF(JG.EQ.1)Y(I,J)=ALOG10(Y(I,J))
        YAVE(I)=Y(I,J)+YAVE(I)
        F=F+X(I)*Y(I,J)
        C=C+X(I)
        E=E+X(I)*X(I)
129     YSS(I)=YSS(I)+Y(I,J)*Y(I,J)
        YT=YT+YAVE(I)
        YAVE(I)=YAVE(I)/FLOAT(NR(I))
        NTOT=NR(I)+NTOT
        SYS=SYS+YSS(I)
        IF(NR(I).EQ.1)GO TO 89
        YPE(I)=YSS(I)-(YAVE(I)**2*NR(I))
        YTOT=YPE(I)+YTOT
        YPE(I)=SQRT(YPE(I)/FLOAT(NR(I)-1))
        YSS(I)=(YPE(I))/(YAVE(I))*100.
        NT1=NR(I)-1+NT1
89      CONTINUE
140     CONTINUE
        IF(NT1.EQ.0)NT1=1
        XA=YTOT/FLOAT(NT1)
        IF(XA.EQ.0)XA=1.
        AN=FLOAT(NTOT)
        G=0.0
        ANX=(AN*E-C*C)
        A=(AN*F-C*YT)/ANX
        B=(E*YT-C*F)/ANX
        WRITE(7,703)
703     FORMAT(' ','    N          X(I)',7X,'Y(I)...')
        DO 702 II=1,N
        KK=NR(II)
        WRITE(7,501)II,X(II),(Y(II,JJ),JJ=1,KK)
501     FORMAT(' ',I5,8(F14.4,X))
702     CONTINUE
C
C       OPTION FOR DATA CHANGE
C
C
```

```
C
      WRITE(7,800)
800   FORMAT(' ',' CHANGE X OR Y VALUES  Y=1,N=0')
      READ(5,504)NJ
      IF(NJ.EQ.0)GO TO 801
      WRITE(7,803)
803   FORMAT(' ','SPECIFY X(I),Y(I,K) TO CHANGE  2I3')
      READ(5,804)I,J
804   FORMAT(2I3)
      WRITE(7,805)
805   FORMAT(' ','INPUT X AND Y VALUES   2F12.4')
      READ(5,605)X(I),Y(I,J)
      XS(I)=X(I)
      YS(I,J)=Y(I,J)
      GO TO 131
C
C     STATISTICAL ANALYSIS PRINTOUT
C
801   WRITE (5,508)
508   FORMAT (' '//,3X,'N',7X,'X',10X,'YAVE',6X,'YSTDDEV',4X,'% REL S.D.
     1',3X,'YCALC',9X,'DIFF.',7X,'S/N')
      NJ=0
      AMVT=-1000000.
      ANVT=100000.
      XMIN=100000.
      XMAX=-100000.
      DO 13 I=1,N
      YP(I)=A*X(I)+B
      Q=YAVE(I)-YP(I)
      NN=NR(I)
      DO 113 J=1,NN
      NJ=NJ+1
      XGT(NJ)=X(I)
      IF(XMAX.LT.X(I))XMAX=X(I)
      IF(XMIN.GT.X(I))XMIN=X(I)
      YGT(NJ)=Y(I,J)
      IF(AMVT.LT.YGT(NJ))AMVT=YGT(NJ)
      IF(ANVT.GT.YGT(NJ))ANVT=YGT(NJ)
      QQ=Y(I,J)-YP(I)
113   G=G+QQ*QQ
      IF(NR(I).EQ.1)YSS(I)=-1.
      WRITE (5,509) I,X(I),YAVE(I),YPE(I),YSS(I),YP(I),Q,(100./YSS(I))
509   FORMAT (I4,7(F12.3,X))
13    CONTINUE
      SO=G/(AN-2.0)
      DO=SQRT(SO)
      SA=SO*AN/ANX
      DA=SQRT(SA)
      SB=SO*E/ANX
      DB=SQRT(SB)
      IF((NTOT-2-NT1).EQ.0)NT1=2
      XC=(G-YTOT)/FLOAT(NTOT-2-NT1)
      R=(AN*F-C*YT)/((SQRT(ANX))*(SQRT(AN*SYS-YT*YT)))
      WRITE (5,510) A,B
510   FORMAT ('0','THE BEST FIT LINEAR EQUATION IS Y=',F12.3,' X +'
     1,F12.6)
      WRITE (5,511) DA,ABS((DA/A*100.))
511   FORMAT (' ','THE STANDARD DEVIATION OF A=',F12.6,3X,'%= ',F8.3)
      WRITE (5,512) DB,ABS((DB/B*100.))
512   FORMAT (' ','THE STANDARD DEVIATION OF B=',F12.6,3X,'%= ',F8.3)
```

```
C
C
      WRITE (5,513) DO
513   FORMAT (' ','OVERALL STANDARD DEVIATION =',F12.6)
C     WRITE(5,155)XA,XC,XC/XA
C155  FORMAT(' ','P.E. ',F13.4,'  L.OF.FIT ',F13.4,'  F TEST <1',F10.5)
      WRITE (5,514) R
514   FORMAT (' ','CORRELATION COEFFICIENT, R=',F10.6)
C
C     GRAPHICS DISPLAY OF REGRESSION CURVE
C
      CALL INIT(IX,1000)
      CALL SCROL(5,1020,5)
      CALL APNT(1.,1.,-1,5,-1,-1)
      CALL SCAL(XMIN,ANVT,XMAX,AMVT)
      YPN=1.E20
      YPM=-1.E20
      DO 215  JJ=1,N
      IF(YPM.LT.YP(JJ))YPM=YP(JJ)
      IF(YPN.GT.YP(JJ))YPN=YP(JJ)
215   CONTINUE
      DO 115 JJ=1,NTOT
      XX=XGT(JJ)
      YY=YGT(JJ)
      CALL APNT(XX,YY)
115   CONTINUE
      YP1=YPN
      XP1=XMIN
      YPN=YPM-YP1
      XPN=XMAX-XMIN
      CALL APNT(XP1,YP1,-1,3,-1,1)
      CALL LVECT(XPN,YPN)
      CALL APNT(XMIN,AMVT)
      CALL LVECT(0.,-(AMVT-ANVT))
      CALL LVECT((XMAX-XMIN),0.)
      WRITE (5,520)
520   FORMAT ('0','DO YOU WISH A PLOT? Y=1,N=0')
      READ (7,504) JS
      IF (JS .NE. 1) GO TO 19
C
C     INCREMENTAL PLOTTER SECTION
C
65    WRITE (5,600)
600   FORMAT (' ','ENTER TITLE FOR X AXIS, 3A4')
      READ (7,601) XAXIS
601   FORMAT (6A4)
      WRITE (5,602)
602   FORMAT (' ','ENTER TITLE FOR Y AXIS, 3A4')
      READ (7,601) YAXIS
      WRITE(7,711)
711   FORMAT(' ','INPUT TITLE FOR PLOT  3A4')
      READ(5,601)TITP
      WRITE (5,604)
604   FORMAT (' ','ENTER STARTING & FINISHING POINTS FOR X AXIS,2F12.4')
      READ (7,605) XMIN, XMAX
605   FORMAT (2F12.4)
      WRITE (5,606)
606   FORMAT (' ','ENTER STARTING & FINISHING POINTS FOR Y AXIS,2F12.4')
      READ (7,605) YMIN, YMAX
      WRITE (5,607)
```

```
607     FORMAT (' ','ENTER LENGTH OF X&Y AXIS IN INCHES,MAX=7.0, 2F12.4')
        READ (7,605) XLONG, YLONG
        X(N+1)=XMIN
        YAVE(N+1)=YMIN
        X(N+2)=(XMAX-XMIN)/XLONG
        YAVE(N+2)=(YMAX-YMIN)/YLONG
        WRITE (5,608)
608     FORMAT (' ','ENTER LINE START & FINISH X VALUES X1=X1 NO LINE,2F')
        READ (5,605) XA,XB
        IF(XA.EQ.XB)GO TO 675
        IF (XA .GE. XMIN .AND. XA .LT. XMAX) GO TO 60
        XA=XMIN
60      IF (XB .GT. XMIN .AND. XB .LE. XMAX) GO TO 61
        XB=XMAX
61      YA=A*XA + B
        YB=A*XB + B
        IF (YA .GE. YMIN .AND. YA .LT. YMAX) GO TO 62
        YA=YMIN
62      IF (YB .GT. YMIN .AND. YB .LE. YMAX) GO TO 63
        YB=YMAX
        XA=(YA-B)/A
        XB=(YB-B)/A
63      CONTINUE
        XGT(1)=XA
        XGT(2)=XB
        XGT(3)=X(N+1)
        XGT(4)=X(N+2)
        YGT(1)=YA
        YGT(2)=YB
        YGT(3)=YAVE(N+1)
        YGT(4)=YAVE(N+2)
675     CONTINUE
        DO 811 IK=1,N
        KK=NR(IK)
        IF(KK.EQ.1)GO TO 677
        NKK=KK-1
        IF(NKK.GT.10) NKK=11
        ST=YPE(IK)*STAT(NKK)/SQRT(FLOAT(KK))
        YSS(IK)=YAVE(IK)+ST
811     YPE(IK)=YAVE(IK)-ST
        WRITE(7,987)
987     FORMAT(' ',' THE 95 % CONFIDENCE INTERVAL ABOUT  THE MEAN')
        WRITE(7,989)(YSS(I),I=1,N)
        WRITE(7,989)(YAVE(I),I=1,N)
        WRITE(7,989)(YPE(I),I=1,N)
989     FORMAT(' ',10F12.4,/)
        YSS(N+1)=YMIN
        YSS(N+2)=YAVE(N+2)
        YPE(N+1)=YMIN
        YPE(N+2)=YAVE(N+2)
677     CALL PLOTST (0.005,'IN')
        CALL PLOT (0.0,0.0,-3)
        CALL AXIS (0.0,0.0,XAXIS,-24,XLONG,0.0,X(N+1),X(N+2))
        CALL AXIS (0.0,0.0,YAXIS,+24,YLONG,90.0,YAVE(N+1),YAVE(N+2))
        CALL PLOT (0.0,YLONG,+3)
        CALL PLOT (XLONG,YLONG,+2)
        CALL PLOT (XLONG,0.0,+2)
        CALL PLOT (0.0,0.0,+3)
        IF(XA.EQ.XB) GO TO 678
        CALL LINE (XGT,YGT,2,1,0,0)
```

```
678     CALL PLOT (0.0,0.0,+3)
        IF(KK.EQ.1)GO TO 676
        CALL LINE(X,YSS,N,1,-1,17)
        CALL PLOT(0.,0.,3)
        CALL LINE(X,YPE,N,1,-1,18)
        CALL PLOT(0.,0.,3)
676     CALL LINE(X,YAVE,N,1,-1,4)
        CALL PLOT (XLONG/4.,YLONG+0.5,3)
        CALL SYMBOL((XLONG/4.),(YLONG+0.5),0.14,TITP,0,24)
        CALL PLOT (8.5,0.0,-3)
        CALL PLOTND
C
C       OPTION FOR EXIT OR RETURN TO START OF ROUTINE
C
19      WRITE (5,518)
518     FORMAT (' ','TYPE 0 TO REPEAT CALCULATION OR 1 TO EXIT')
        READ (7,504) JK
        CALL SCROL(-1,-1,-1)
        CALL INIT
        CALL FREE
        IF (JK .EQ. 0) GO TO 131
        STOP
        END
```

B30261